RHODIUM CATALYSIS IN ENANTIOSELECTIVE HYDROGENATIVE TRANSFORMATIONS: FROM THE DESIGN OF NEW LIGANDS TO REACTIONS OF ATYPICAL SUBSTRATES

Joan Ramon Lao Mulinari

UNIVERSITAT ROVIRA i VIRGILI

Rhodium Catalysis in Enantioselective Hydrogenative Transformations: From the Design of New Ligands to Reactions of Atypical Substrates

Joan R. Lao Mulinari

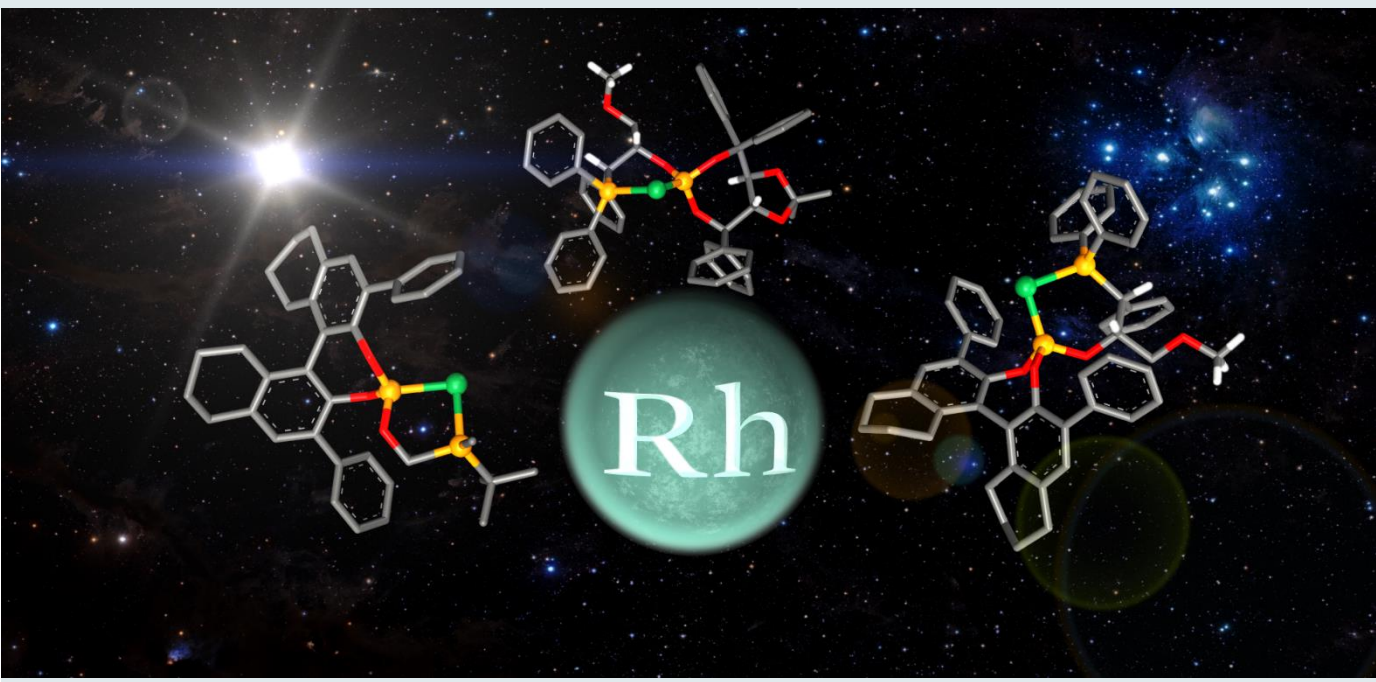

DOCTORAL THESIS

2017

UNIVERSITAT ROVIRA I VIRGILI
RHODIUM CATALYSIS IN ENANTIOSELECTIVE HYDROGENATIVE TRANSFORMATIONS: FROM THE DESIGN OF NEW LIGANDS TO REACTIONS OF ATYPICAL SUBSTRATES
Joan Ramon Lao Mulinari

UNIVERSITAT ROVIRA I VIRGILI
RHODIUM CATALYSIS IN ENANTIOSELECTIVE HYDROGENATIVE TRANSFORMATIONS: FROM THE DESIGN OF NEW LIGANDS TO REACTIONS OF ATYPICAL SUBSTRATES
Joan Ramon Lao Mulinari

UNIVERSITAT ROVIRA I VIRGILI
RHODIUM CATALYSIS IN ENANTIOSELECTIVE HYDROGENATIVE TRANSFORMATIONS: FROM THE DESIGN OF NEW LIGANDS TO REACTIONS OF ATYPICAL SUBSTRATES
Joan Ramon Lao Mulinari

Joan R. Lao Mulinari

Rhodium Catalysis in Enantioselective Hydrogenative Transformations: From the Design of New Ligands to Reactions of Atypical Substrates

Doctoral Thesis

Supervised by Prof. Dr. Anton Vidal i Ferran

Institute of Chemical Research of Catalonia (ICIQ)

UNIVERSITAT ROVIRA i VIRGILI

Tarragona 2017

UNIVERSITAT ROVIRA I VIRGILI
RHODIUM CATALYSIS IN ENANTIOSELECTIVE HYDROGENATIVE TRANSFORMATIONS: FROM THE DESIGN OF NEW LIGANDS TO REACTIONS OF ATYPICAL SUBSTRATES
Joan Ramon Lao Mulinari

ICIQ
Institut Català d'Investigació Química

UNIVERSITAT ROVIRA I VIRGILI
DEPARTAMENT DE QUIMICA ANALITICA I QUIMICA ORGANICA
C/ Marcel.lí Domingo s/n
Campus Sescelades
43007 Tarragona

Prof. Dr. Anton Vidal Ferran, Group Leader of the Institute of Chemical Research of Catalonia (ICIQ) and Research Professor of the Catalan Institution for Research and Advanced Studies (ICREA),

CERTIFY that the present Doctoral Thesis entitled: "*Rhodium Catalysis in Enantioselective Hydrogenative Transformations: From the Design of New Ligands to Reactions of Atypical Substrates*" that Joan R. Lao Mulinari presents to obtain the PhD degree in chemistry, has been carried out under my supervision, in the corresponding research group at the Institute of Chemical Research of Catalonia (ICIQ).

Tarragona, September 2017

PhD Thesis Supervisor

Prof. Dr. Anton Vidal i Ferran

UNIVERSITAT ROVIRA I VIRGILI
RHODIUM CATALYSIS IN ENANTIOSELECTIVE HYDROGENATIVE TRANSFORMATIONS: FROM THE DESIGN OF NEW LIGANDS TO REACTIONS OF ATYPICAL SUBSTRATES
Joan Ramon Lao Mulinari

ACKNOWLEDGEMENTS

En primer lloc vull donar les gràcies al Prof. Anton Vidal per haver-me donat l'oportunitat de realitzar la tesi doctoral al seu grup d'investigació, per tot els coneixements que m'ha transmès durant els transcurs de la tesi, per tota la dedicació que ha destinat a la meva formació científica i sobretot per la confiança que sempre ha depositat en mi. Moltes gràcies.

També m'agradaria agrair a tots els membres del grup (antics i no tant antics) per tots els bons moments que hem passat durant tot aquest temps: Héctor Fernández, José Luís Nuñez, Nacho Mon, Pablo Etayo, Balakrishna Bugga, Laura Rovira, Lucas Carreras, Mónica Vaquero, Alícia Martínez, Nuria Llorente, Rajesh Pudi i Ester Iniesta. M'agradaria mencionar especialment les persones amb les que he compartit més temps i experiències: a Balakrishna Bugga (alias *Bagga*), per tot el que m'ha ensenyat d'una cultura completament diferent, per ser una persona impressionant i sobretot per la seva incalculable hospitalitat; a José Luís Nuñez (alias *Pepelu* o *Don José*), per aguantar-me (o aguantar-lo jo a ell) com a company d'oficina durant tant de temps, per explicar-me tantes curiositats (explicades "a la seva manera") i per les milions de converses profundes/surrealistes que hem tingut; a Héctor Fernández (alias *HFP* o *el Señor de la Barba*), per tot el que he gaudit treballant amb ell, per tots el moments que hem rigut plegats i pel seu suport personal als moments més difícils de la tesi; i a Lucas Carreras (alias *Lucky Boy*), pel suport i comprensió propi d'un gran amic i sobretot per fer-me plorar de riure dia rere dia.

Altres figures que vull agrair són la meva colla d'amics de Matadepera (AAVC) i la colla d'amics de la universitat per tot el suport que m'han donat durant aquests últims 5 anys; a la Dra. Carme Brossa, per ser una gran professora i una bellíssima persona; i a altres persones que també han format part de la meva vida i que injustament ens han deixat (Cristina Ragués, Nuria Roy i Carme Tort).

La part més important dels agraïments va destinada a la meva família. En primer lloc als meus pares, els quals han sigut els responsables de despertar i potenciar (des de ben petit) la meva curiositat innata per a la ciència. Sóc molt afortunat de tenir-vos com a pares i tot el que sóc és gràcies a vosaltres. En segon lloc, a les meves germanes Nuri i Vanesa; per la confiança que han dipositat sempre en mi i pel seu incalculable suport en tots els àmbits de la vida. En tercer lloc, als meus dos nebots (Jepi i Pau) i al meu cunyat (Santi) per escoltar-me (i sobretot per no dormir-se) quan he "intentat" explicar el curiós fenomen de la quiralitat i les bases de la catàlisi asimètrica.

Finalment vull agrair a l'Adaia, la meva companya de vida que ha estat sempre al meu costat i que m'ha recolzat inqüestionablement en totes les decisions importants. Gràcies per haver-me aguantat durant tot aquest temps i per l'amor que em segueixes donant cada dia. T'estimo.

The research work developed in the present PhD thesis has been possible thanks to the ICIQ Foundation for a predoctoral fellowship (ICIQ-03/12-5), and the financial support provided by the ICIQ Foundation, MINECO (CTQ2011-28512 and CTQ2014-60256P) and Severo Ochoa Excellence Accreditation (SEV-2013-0319).

UNIVERSITAT ROVIRA I VIRGILI
RHODIUM CATALYSIS IN ENANTIOSELECTIVE HYDROGENATIVE TRANSFORMATIONS: FROM THE DESIGN OF NEW LIGANDS TO REACTIONS OF ATYPICAL SUBSTRATES
Joan Ramon Lao Mulinari

Als meus pares, germanes
i a l'Adaia

UNIVERSITAT ROVIRA I VIRGILI
RHODIUM CATALYSIS IN ENANTIOSELECTIVE HYDROGENATIVE TRANSFORMATIONS: FROM THE DESIGN OF NEW LIGANDS TO REACTIONS OF ATYPICAL SUBSTRATES
Joan Ramon Lao Mulinari

"Somewhere, something incredible is waiting to be known"

- Carl Sagan

UNIVERSITAT ROVIRA I VIRGILI
RHODIUM CATALYSIS IN ENANTIOSELECTIVE HYDROGENATIVE TRANSFORMATIONS: FROM THE DESIGN OF NEW LIGANDS TO REACTIONS OF ATYPICAL SUBSTRATES
Joan Ramon Lao Mulinari

LIST OF PUBLICATIONS

The research work performed within this PhD thesis lead to the following publications:

- "Catalytic enantioselective reductive desymmetrization of achiral and *meso* compounds" Férnandez-Pérez, H.; Etayo, P.; Lao, J. R.; Núñez-Rico, J. L.; Vidal-Ferran, A., *Chem. Commun*. **2013**, *49*, 10666-10675.

- "1,1-P–OP Ligands with P-Stereogenic Phosphino Groups in Asymmetric Hydrogenations and Hydroformylations" Lao, J. R.; Benet-Buchholz, J.; Vidal-Ferran, A. *Organometallics* **2014**, *33*, 2960-2963.

- "Hydrogenative Kinetic Resolution of Vinyl Sulfoxides" Lao, J. R.; Fernández-Pérez, H.; Vidal-Ferran, A. *Org. Lett.* **2015**, *17*, 4114-4117.

- "Stereoselective Rh-Catalyzed Hydrogenative Desymmetrization of Achiral Substituted 1,4-Dienes" Fernández-Pérez, H.; Lao, J. R.; Vidal-Ferran, A. *Org. Lett.* **2016**, *18*, 2836-2839.

At the moment of writing the present document, the manuscript corresponding to the contents described in Chapter III is under preparation, and will be submitted in due time:

- "Exploiting Substrate's Diversity for Preparing Synthetically Valuable Sulfoxides via Asymmetric Hydrogenative Kinetic Resolution" Lao, J. R.; Vidal-Ferran, A.

UNIVERSITAT ROVIRA I VIRGILI
RHODIUM CATALYSIS IN ENANTIOSELECTIVE HYDROGENATIVE TRANSFORMATIONS: FROM THE DESIGN OF NEW LIGANDS TO REACTIONS OF ATYPICAL SUBSTRATES
Joan Ramon Lao Mulinari

TABLE OF CONTENTS

LIST OF ACRONYMS AND ABBREVIATIONS

The acronyms and abbreviations used in this manuscript are in accordance with the recommendations given by the American Chemical Society.

[http://pubs.acs.org/paragonplus/submission/joceah/joceah_abbreviations.pdf, ACS guidelines for authors (accessed July 2017)]

$[\alpha]$	specific rotation [expressed without units; the units, (deg·mL)/(g·dm), are understood]
Å	angstrom(s)
Ac	acetyl
acac	acetylacetonate
aq	aqueous
Ar	aryl
atm	atmosphere
BINOL	1,1'-bi-2-naphtol
Bn	benzyl
bp	boiling point
br	broad (spectral)
Bz	benzoyl
°C	degrees, Celsius
calcd	calculated
cat	catalytic, catalyst
CIF	Crystallographic Information Framework
cm	centimeter(s)

cm^{-1}	wavenumber(s)
COSY	correlation spectroscopy
m-CPBA	*meta*-chloroperbenzoic acid
Cy	cyclohexyl (group), cyclohexane (solvent)
δ	chemical shift in ppm
d	day(s), doublet (spectral)
DABCO	1,4-diazabicyclo[2.2.2]octane
DEPT	Distortionless Enhancement by Polarization Transfer
ΔG	Gibbs free energy
DKR	Dynamic Kinetic Resolution
dm	decimeter(s)
DMAP	4-(*N*,*N*-dimethylamino)pyridine
DME	1,2-dimethoxyethane
dr	diastereomeric ratio
EI	Electron Impact
equiv	equivalent(s)
ESI	electrospray ionization
Et	ethyl
FID	Flame Ionization Detector, Free Induction Decay
g	gram(s)
GC	Gas Chromatography
h	hour(s)
HMBC	Heteronuclear Multiple Bond Correlation

HPLC	High Performance Liquid Chromatography
HRMS	High Resolution Mass Spectrometry
Hz	herz
IR	infrared
J	coupling constant [expressed in Hz]
K	kelvin(s) (absolute temperature)
KR	Kinetic Resolution
L	liter(s)
LiHMDS	lithium bis(trimethylsilyl)amide
lit.	literature value
μ	micro (prefix)
m	multiplet (spectral), milli- (prefix)
M	molar (moles per liter), parent molecular ion
MALDI	Matrix Assisted Laser Desorption Ionization
max	maximum
Me	methyl
MHz	megahertz
min	minute(s); minimum
mol	mole(s), molecular
mp	melting point
MS	Mass Spectrometry
MTBE	methyl *tert*-butyl ether
MW	Molecular Weight

m/*z*	mass-to-charge ratio
nbd	norbornadiene
NBS	*N*-bromosuccinimide
nm	nanometer(s)
NMR	Nuclear Magnetic Resonance
NOE	Nuclear Overhauser Effect
NOESY	nuclear Overhauser effect spectroscopy
ORTEP	Oak Ridge Thermal Ellipsoid Plot Program
PCC	pyridinium chlorochromate
Ph	phenyl
ppm	part(s) per million
Pr	propyl
*i*Pr	isopropyl
q	quartet (spectral)
rel	relative
rt	room temperature
s	singlet (spectra), second(s), selectivity factor (kinetic resolutions)
t	triplet (spectral)
t	time
T	temperature
TADDOL	(α,α,α,α-tetraaryl-1,3-dioxolane-4,5-dimethanol)
THF	tetrahydrofuran
TLC	Thin Layer Chromatography

TMS	tetramethylsilane, tetramethylsilyl
t_R	retention time (chromatography)
TS	Transition State
UV	ultraviolet
vis	visible
v/v	volume-to-volume ratio
wt	weight
w/w	weight-to-weight ratio

UNIVERSITAT ROVIRA I VIRGILI
RHODIUM CATALYSIS IN ENANTIOSELECTIVE HYDROGENATIVE TRANSFORMATIONS: FROM THE DESIGN OF NEW LIGANDS TO REACTIONS OF ATYPICAL SUBSTRATES
Joan Ramon Lao Mulinari

INTRODUCTION

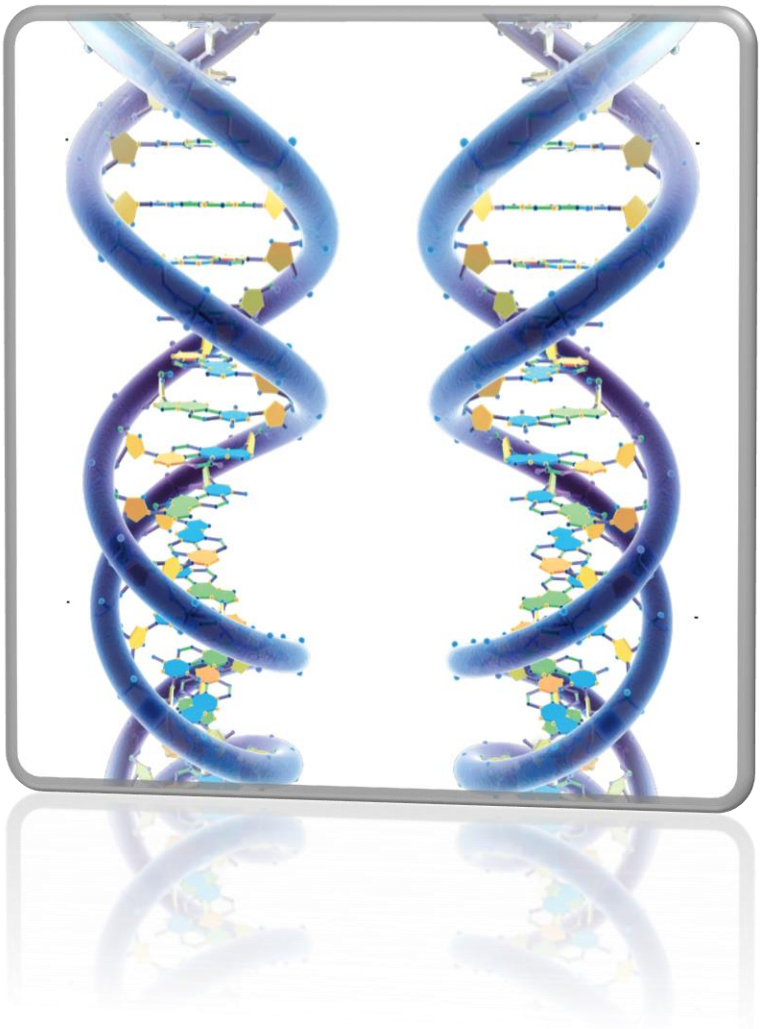

UNIVERSITAT ROVIRA I VIRGILI
RHODIUM CATALYSIS IN ENANTIOSELECTIVE HYDROGENATIVE TRANSFORMATIONS: FROM THE DESIGN OF NEW LIGANDS TO REACTIONS OF ATYPICAL SUBSTRATES
Joan Ramon Lao Mulinari

GENERAL INTRODUCTION

The term *chirality* is defined as the property of an object to be non-superimposable on its mirror image. This particular property can be expressed in terms of symmetry elements: an object or the arrangement of atoms in a molecule is said to be chiral when it does not possess any improper rotation-reflection axes S_n.[1,2] The evidence of this omnipresent phenomenon can be found from the smallest objects that constitute matter (e.g., in elementary particles) to the largest objects present in the universe, such as galaxies.[3] The two mirror images of a given arrangement of atoms in a molecule are called *enantiomers* [4] although one might encounter old or ill-defined synonyms like (optical) antipodes and optical isomers.[5] Biological systems like human beings exist in a chiral environment and the most crucial macromolecular architectures of life (i.e. proteins and nucleic acids) are almost entirely constituted by L-aminoacids and D-carbohydrates, respectively, whilst life based on the opposite enantiomeric forms (D-aminoacids and L-carbohydrates) is practically non-existent on Earth.[6] This natural selectivity is known as *biological homochirality* (Figure 1).

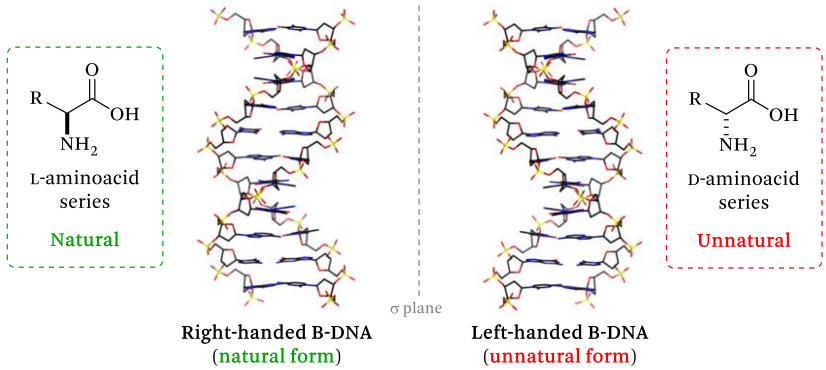

Figure 1. Structures of natural and unnatural aminoacids and nucleic acids.

(1) Mirror planes (σ) and inversion centers (*i*) are included in this statement as they can be considered as S_1 and S_2 rotation-reflection axes, respectively.
(2) Eliel, E. L; Wilen, S. H.; Mandel, L. N. *Stereochemistry of Organic Compounds*, John Wiley & Sons: USA, 1994.
(3) Wagnière, G. H. *On Chirality and the Universal Asymmetry: Reflections on Image and Mirror Image,* Wiley-VCH Verlag GmbH & Co. KGaA: Weinheim, 2008.
(4) One refers to *enantiomorphs* when macroscopic objects are involved.
(5) Mislow, K. *Chirality* **2002**, *14*, 126-134.
(6) *Chirality in Natural and Applied Science*, Lough, W. J., Wainer, I. W., Eds.; Blackwell: Oxford, 2002.

Although the two enantiomeric forms or *enantiomers* are equivalent in terms of composition and physical properties, they may differ in terms of their biological properties.[7] This phenomenon is extremely important in drug design and different scenarios are encountered when a *racemic*[8] biologically active compound is employed as a pharmaceutically active agent (Figure 2):[9] (i) both enantiomers have the same activity (type I, see Iclaprim as a selected example), (ii) the two enantiomers have qualitatively the same biological effects but their intensities are different (type II, see Citalopram as a selected example), (iii) one enantiomer is responsible for the therapeutic action while the other is substantially inactive at normal doses (type III, see TMC207 as a selected example) or (iv) one enantiomer is responsible for the therapeutic effect while the other can cause severe adverse effects (type IV, see Thalidomide[10] as a selected example).

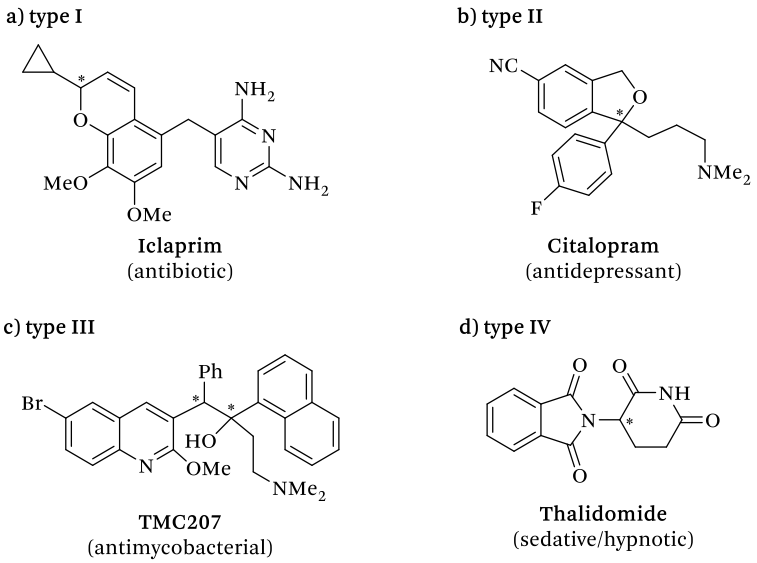

Figure 2. Selected examples of optically active pharmaceutical active compounds with different situations in terms of the biological activity of the two enantiomers.[9]

(7) *Chirality in Drug Design and Development*, Reddy, I. K., Mehvar, R., Eds; Marcel Dekker Inc: New York, 2004.
(8) The term *racemic* or *racemate* refers to a mixture composed in equal parts by the two enantiomers.
(9) (a) Scott, A. K. *Drug Saf.* **1993**, *8*, 149-159. (b) Cossy, J. R. Comprehensive Chirality. In *Introduction: The Importance of Chirality in Drugs and Agrochemicals*; Carreira, E. M, Yamamoto, H., Eds.; Elsevier Science: France, 2012, Vol. 1, pp 1-7.
(10) For more detailed information about the Thalidomide tragedy, see: McCredie, J. *J. Med. Imaging Radiat. Oncol.* **2009**, *53*, 433-441.

The important role of enantiomeric purity in the pharmaceutical industry has been one of the main driving forces in the development of new synthetic methodologies with a better control of the stereochemical outcome of the reaction.[9b,11] For that purpose, organic chemists have developed numerous methods for preparing compounds as single enantiomers, which can be mainly classified in the following categories:

1. Chiral pool approach: This strategy entails the conversion or derivatization of readily available enantiomerically pure natural compounds. The scope of the applicability is obviously limited, as the repertoire of compounds from natural sources is limited (Figure 3).

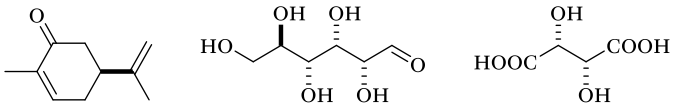

(+)-carvone D-glucose (linear form) L-tartaric acid

Figure 3. Selected examples of optically active building blocks from the chiral pool.[12]

2. Separation of racemic mixtures: The resolution of racemic mixtures into their pure enantiomers by preferential[13] or *diastereoisomer*[14] crystallization was one of the first methods to be used and it still is probably the most important method for industrial preparation of pure enantiomers (Scheme 1).[15] Selected examples of *resolving agents*[16] are shown in Figure 4. Whilst theoretical yields of 100% are accessible for both crystallization

(11) Mohan, S. J.; Mohan, E. C.; Yamsani, M. R. *Int. J. Pharm. Sci. Nanotechnol.* **2009**, *1*, 309-316.
(12) Hoffmann, R. W. *Elements of Synthesis Planning*; Springer-Verlag: Heidelberg, 2009.
(13) Preferential crystallization of crystalline conglomerates into one pure enantiomer is a less common strategy, as less than 10% of the crystalline mixtures of enantiomers form conglomerates, see: Anderson, N. G. Chiral Syntheses. In *Practical Process Research & Development*. Academic Press: USA, 2000; pp 329-344.
(14) In contrast to *enantiomers*, *diastereomers* are not related as non-superimposable mirror images and they usually differ in their physical properties.
(15) Lorenz, H.; Seidel-Morgenstern, A. *Angew. Chem., Int. Ed.* **2014**, *53*, 1218-1250.
(16) The term *resolving agent* is referred to an enantiomerically pure reagent that interacts with a racemic mixture (either by covalent or non-covalent interactions) to form a separable mixture of diastereomeric compounds, complexes or salts. For a more detailed explanation, see the following book: *Handbook of Chiral Chemicals*; Ager, D., Ed.; Taylor & Francis: FL, 2006.

techniques in some particular cases (i.e., spontaneous in situ racemization and diastereomer interconversion for preferential and diastereomer crystallization, respectively), most of the cases result in theoretical yields of only 50%, which constitutes the main drawback of this strategy unless the "undesired" enantiomer can be racemized and recycled, or there is a demand for both enantiomers.

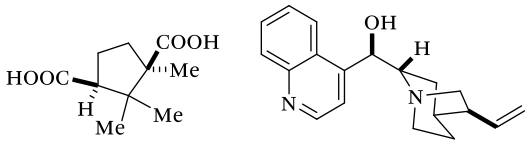

(+)-camphoric acid Cinchonidine

Figure 4. Selected examples of resolving agents.

More recently, large-scale chromatographic separation techniques (e.g., simulated moving bed (SMB) chromatography) are emerging as important preparation methods for active pharmaceutical ingredients (APIs), especially at the early phases of product development or even for the whole production process (Scheme 1).[17]

Scheme 1. Strategies for the separation of racemic mixtures

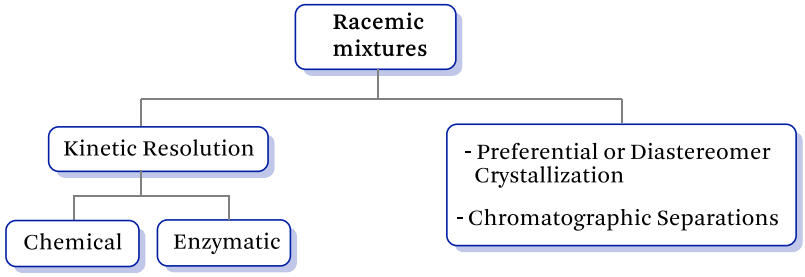

Kinetic resolutions can also be considered an efficient method for obtaining enantiopure compounds from racemic mixtures. Kinetic resolution[18] (KR) is defined as the process in which one of the enantiomers constituting a racemic mixture is more readily transformed to a product than is the other enantiomer. Moreover, KRs can be generally coupled with all methods that stereoselective catalysis offers (i.e., stereoselective non-natural or enzymatic reagents in stoichiometric or in catalytic amounts; see Scheme 1). In the simplest version of a kinetic resolution, the two enantiomers of the starting material (or substrate) interact with an enantiopure reagent or catalyst to

(17) Rajendran, A.; Paredes, G.; Mazzotti, M. *J. Chromatogr. A.* **2009**, *1216*, 709-738.
(18) Kagan, H. B.; Fiaud, J. C. Kinetic Resolution. In *Topics in Stereochemistry*; Eliel, E. L., Wilen, S. H., Eds.; John Wiley & Sons: USA, 1988, Vol. 18, pp 249-330.

generate two diastereomeric products or transition states, respectively. The conversion of the reaction and the energy gap between the free energies of those diastereomeric species determine the product distribution after the KR (for a representation of an ideal catalytic kinetic resolution, see Figure 5). The ideal situation in a kinetic resolution is that in which the difference in the reaction rates of the individual substrate enantiomers (S_S and S_R in Figure 5) is high enough so that only one enantiomer reacts ($k_{fast} >> k_{slow}$, see Figure 5). Under such circumstances, the reaction proceeds until the reacting enantiomer of the substrate (S_S in Figure 5) is completely consumed (i.e. at 50% of conversion) and the other enantiomer of the substrate remains unaltered. Thus, a mixture of enantiopure resolved product (P_S) and enantiopure non-reacting substrate (S_R) are obtained (Figure 5).

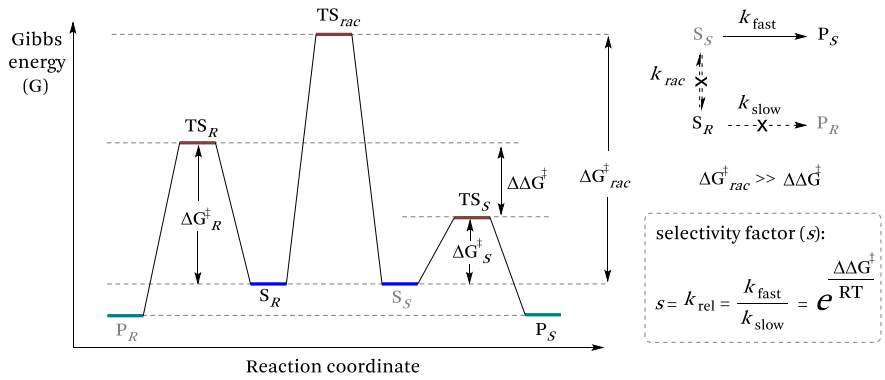

Figure 5. Simplified free energy vs. reaction coordinate diagram in an ideal catalytic KR of the two enantiomers of a substrate (S = substrate, P = product, ΔG = free energy, TS = transition state). Products marked in grey are not observed at the end of an ideal KR (i.e., S_S as the reacting enantiomer of the substrate and P_R as the product derived from the non-reacting enantiomer of the substrate).

As shown in Figure 5, the requirement for being able to perform such a kinetic resolution is that the free energy of the interconversion between enantiomers ($\Delta G^{\ddagger}_{rac}$) is much higher than that for the transformation of the slow-reacting substrate enantiomer ($\Delta G^{\ddagger}_{rac} >> \Delta G^{\ddagger}_{R}$, see Figure 5).[19] Under these circumstances, interconversion between the two enantiomers of the

(19) If $\Delta G^{\ddagger}_{rac} << \Delta G^{\ddagger}_{R}$ and racemization of the substrate occurs at faster rate than that for the catalytic reaction of the slow-reacting enantiomer ($k_{rac} >> k_{fast}$) the process is referred to as a *Dynamic Kinetic Resolution* (DKR). In this particular case, the substrate can be stereoselectively converted into a highly enantioenriched (or even enantiomerically pure) product with a 100% of theoretical yield. As a selected review for DKRs, see for example: Pellissier, H. *Tetrahedron* **2011**, *67*, 3769-3802.

substrate does not take place. The *selectivity factor* (*s*) in a kinetic resolution is a widely used parameter to describe the stereoselectivity of the resolution process and is defined as the quotient of the rate constant of the fastest reacting enantiomer into that of the slowest one (Figure 5). From the practical point of view, selectivity factor values above 50 are required in order to obtain a product with a high enantiomeric purity in useful yield.[20] Selected examples of pharmaceutically relevant products that have been synthesized via catalytic kinetic resolution are shown in Figure 6.

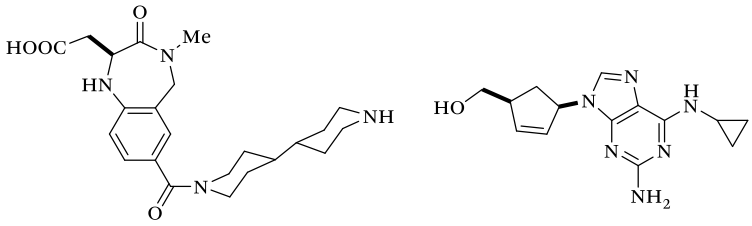

Lotrafiban
(antiplatelet agent)

Abacavir
(antiretroviral agent)

Figure 6. Examples of relevant biologically active compounds obtained in large scale by a catalytic kinetic resolution step.[21]

3. Stereoselective synthesis: Organic synthesis introducing in a controlled manner one or more new and desired stereogenic elements in a molecule is referred to as stereoselective synthesis, which implies the transformation of a substrate prostereogenic's element into a stereogenic center, plane, axis or helix. This strategy provides the most general entry to the preparation of enantiomerically enriched products. The use of chiral reagents or auxiliaries[22] allow for the preparation of highly complex enantioenriched compounds, although stoichiometric amounts of those reagents are required, which represents the main drawback of this approach. Among all the possible approaches that stereoselective synthesis offers, enantioselective catalysis is, by far, the most advantageous method: this method, in which one molecule of enantioselective catalyst produces many molecules of enantioenriched product, is a priori the most elegant approach for synthesizing enantiopure compounds. Moreover, the advantages of enantioselective catalytic methods, such as atom economy, simplicity in large-scale reactions and minimal

(20) Keith, J. M.; Larrow, J. F.; Jacobsen, E. N. *Adv. Synth. Catal.* **2001**, *343*, 5-26.
(21) Gawronski, J. *Acta Pol. Pharm.* **2006**, *63*, 333-351.
(22) The *chiral auxiliary* term refers to an optically active compound that is reversely incorporated into an organic substrate. For a more detailed information, see: Roos, G. *Key Chiral Auxiliary Applications*, 2nd Ed., Academic Press: USA, 2014.

formation of by-products are also well-known.[23] The use of the catalyst often makes product isolation also easier, since there is less unwanted material to remove at the end of the reaction.[24] Figure 7 illustrates the general principle of a transition-metal catalyzed transformation. The key step in the catalytic event resides in the formation of a supramolecular complex around the metal including an enantiopure ligand, which is generally bound to the metal center through several functional groups, and the substrate(s). In this supramolecular complex, the catalytic metal is the responsible for providing a low-energy reaction pathway while the enantiopure ligand enables the preferential recognition of the corresponding enantiotopic element in the substrate molecule.

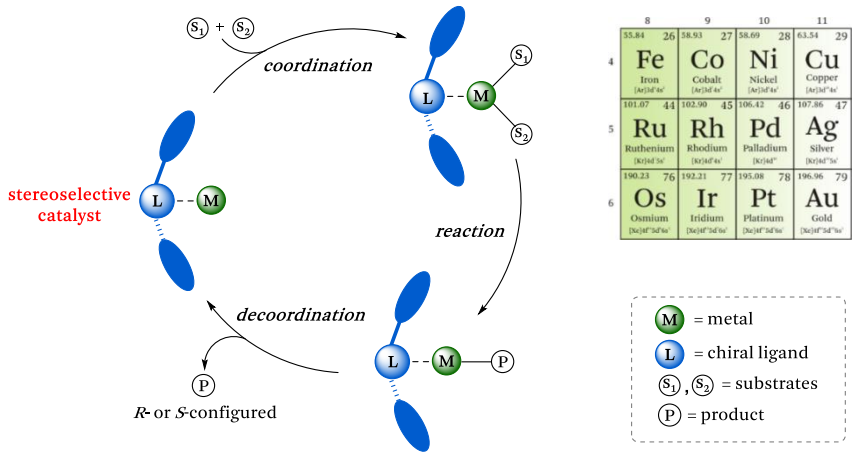

Figure 7. Schematic representation of an enantioselective catalytic process.

The great potential of enantioselective catalysis has been widely exploited in topologically diverse arrays of substrates via myriad chemical transformations.[23] It falls beyond the scope of the introduction of this PhD thesis to categorize the different types of substrates that have been employed in asymmetric catalysis. However, achiral and *meso*[25] substrates deserve special mention. When these substrates are subjected to a synthetic operation that breaks the symmetry of the molecule by selectively transforming one of the possible enantiotopic elements, an optically active product is formed. Enantiotopic element selection (for instance, the choice of one enantiotopic

(23) Noyori, R. *Angew. Chem., Int. Ed.* **2002**, *41*, 2008-2022.
(24) (a) *Catalysis in Asymmetric Synthesis*; Coxon, J., Bailey, P., Gladysz, J., Parsons, P., Stang, P., Eds.; John Wiley & Sons, Inc.: Hoboken, 2009. (b) *Catalytic Asymmetric Synthesis;* Ojima, I., Ed.; John Wiley & Sons, Inc.: Hoboken, 2010.
(25) According to ref. 2, the *meso* stereodescriptor refers to an achiral member of a set of diastereoisomers that includes at least one chiral member.

atom or functional group over the others) is provided by a chiral reagent or catalyst (Figure 8).

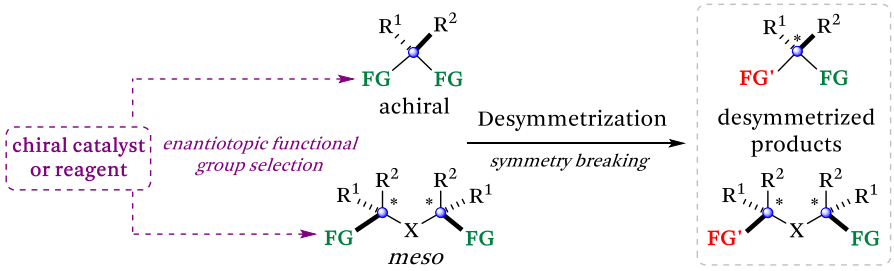

Figure 8. Schematic representation of the desymmetrization reaction of a general achiral or *meso* compound by enantiotopic functional group selection.

This synthetic operation, referred to as *desymmetrization*, has become an extremely powerful tool for synthesizing enantioenriched (or enantiopure) compounds,[26] and has been widely explored in a broad range of achiral and *meso* substrates (Figure 9) through myriad chemical transformations,[26] which mainly comprise: (i) C–X bond (X = C, O, N, S or halogen) formation reactions through nucleophilic ring-opening of *meso* anhydrides, epoxides, aziridines and their respective vinylogous analogs, (ii) desymmetrization of *meso* difunctional compounds such as diols, diamines, dithiols, dicarboxylic acid derivatives and bisallylic alcohols derivatives by diverse well-stablished functional group transformations, (iii) oxidative desymmetrization transformations (e.g., Sharpless asymmetric epoxidations, dihydroxylations, iodolactonizations and Baeyer-Villiger reactions, among others), (iv) various inter- and intra-molecular desymmetrization reactions involving C–C bond formation (e.g., Robinson annulation, Wittig olefination, olefin metathesis, cyclopropanations, ene-reactions, etc.) and (v) stereoselective deprotonation of achiral or *meso* compounds by using various chiral bases.

While catalytic desymmetrizations of achiral and *meso* compounds involving reductive transformations have been studied, the reported examples are scarce and did not offer in some cases satisfactory solutions in terms of catalytic efficiencies and/or stereoselectivities.[27]

(26) For selected reviews on this topic, see: (a) Fernández-Pérez, H.; Etayo, P.; Lao, J. R.; Núñez-Rico, J. L.; Vidal-Ferran, A. *Chem. Commun.* **2013**, *49*, 10666-10675. (b) Borissov, A.; Davies, T. Q.; Ellis, S. R.; Fleming, T. A.; Richardson, M. S. W.; Dixon, D. J. *Chem. Soc. Rev.* **2016**, *45*, 5474-5540. (c) Zeng, X.-P.; Cao, Z.-Y.; Wang, Y.-H.; Zhou, F.; Zhou, J. *Chem. Rev.* **2016**, *116*, 7330-7396. (d) Merad, J.; Candy, M.; Pons, J.-M.; Bressy, C. *Synthesis* **2017**, *49*, 1938-1954.
(27) See ref. 26a, and the references cited therein.

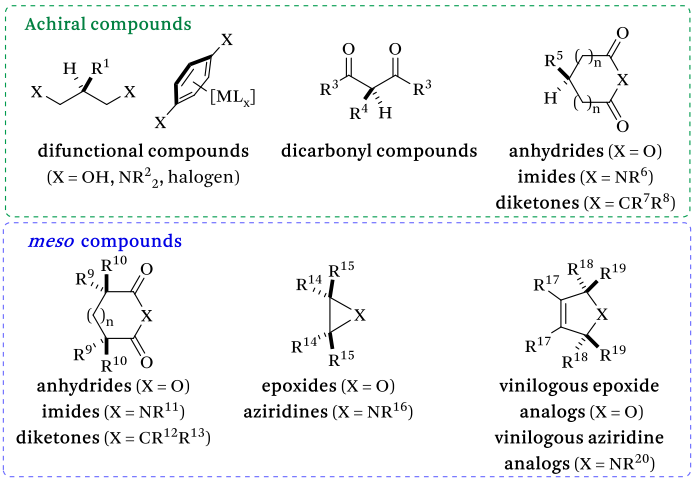

Figure 9. General structures of commonly used achiral (top) and *meso* (bottom) compounds used for desymmetrization reactions.

The development and evolution of enantiopure phosphorus-derived ligands is strongly related to the development of asymmetric hydrogenation.[28,29] In 1968 Knowles accomplished the first homogeneous asymmetric hydrogenation of prochiral C=C-moieties by a Rh-catalyst derived from the optically enriched CAMP ligand.[28] Later on, in the early 70's, Kagan made an important breakthrough with the development of the DIOP ligand,[30] a bidentate C_2-symmetric bisphosphine derived from enantiomerically pure tartaric acid. This discovery led to a remarkable advance in this field and significant progress has been made since then by developing high performing bidentate ligands for rhodium-mediated enantioselective hydrogenations. For instance, DIPAMP,[31] BINAP[32] and DUPHOS[33] ligands, among other

(28) Knowles, W. S.; Sabacky, M. J. *Chem. Commun.* **1968**, 1445-1446.
(29) (a) Korpiun, O.; Lewis, R. A.; Chickos, J.; Mislow, K. *J. Am. Chem. Soc.* **1968**, *90*, 4842-4846. (b) Horner, L.; Siegel, H.; Büthe, H. *Angew. Chem., Int. Ed. Engl.* **1968**, *7*, 942. (c) Naumann, K.; Zon, G.; Mislow, K. *J. Am. Chem. Soc.* **1969**, *91*, 7012-7023.
(30) (a) Kagan, H. B.; Dang, T. P. *J. Chem. Soc. D.* **1971**, 481. (b) Kagan, H. B.; Dang Tuan, P. *J. Am. Chem. Soc.* **1972**, *94*, 6429-6433.
(31) (a) Vineyard, B. D.; Knowles, W. S.; Sabacky, M. J.; Bachman, G. L.; Weinkauff, D. J. *J. Am. Chem. Soc.* **1977**, *99*, 5946-5952. (b) Knowles, W. S. *Acc. Chem. Res.* **1983**, *16*, 106-112.
(32) Miyashita, A.; Yasuda, A.; Takaya, H.; Toriumi, K.; Ito, T.; Souchi, T.; Noyori, R. *J. Am. Chem. Soc.* **1980**, *102*, 7932-7934.
(33) (a) Burk, M. J. *J. Am. Chem. Soc.* **1991**, *113*, 8518-8519. (b) Burk, M. J.; Feaster, J. E.; Nugent, W. A.; Harlow, R. L. *J. Am. Chem. Soc.* **1993**, *115*, 10125-10138. (c) Burk, M. J.; Gross, M. F.; Martinez, J. P. *J. Am. Chem. Soc.* **1995**, *117*, 9375-9376. (d) Burk, M. J. *Acc. Chem. Res.* **2000**, *33*, 363-372.

enantiopure derivatives,[34] have been used in large-scale rhodium-catalyzed hydrogenations for the industrial production of valuable synthetic drugs such as L-DOPA, Sitagliptin and Imagabalin (Figure 10).[34]

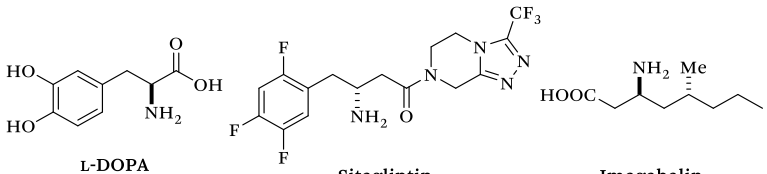

L-DOPA
(treatment of Parkinson's disease)

Sitagliptin
(antihyperglycemic agent)

Imagabalin
(anticonvulsant agent)

Figure 10. Biologically active compounds produced by Rh-mediated asymmetric hydrogenations.[34]

Among the structural features in chelating ligands that may have an influence in the catalytic activity of the derived metal complexes, the ligand-metal-ligand angle (a.k.a. bite angle[35], see Figure 11) deserves special mention. The magnitude of the bite angle (β) value strongly affects the geometry of the metal species involved in the catalytic cycle and consequently the outcome of the reaction. The influence of this parameter in catalysis has been extensively studied in various metal-catalyzed (stereoselective) transformations,[35] especially in Rh-mediated hydroformylations.[36] In this last reaction, wide bite angle ligands favor the formation of linear aldehydes.[35,37]

(34) (a) Blaser, H. U.; Spindler, F.; Studer, M. *Appl. Catal., A* **2001**, *221*, 119-143. (b) Blaser, H.-U., Pugin, B., Spindler, F., Topics in Organometallic Chemistry. In *Organometallics as Catalysts in the Fine Chemical Industry*; Beller, M., Blaser H. -U., Eds.; Springer-Verlag: Berlin, 2012; Vol. 42, pp 65-102.
(35) For relevant revision works within this topic, see: (a) Dierkes, P.; van Leeuwen, P. W. N. M. *J. Chem. Soc., Dalton Trans.* **1999**, 1519-1530. (b) van Leeuwen, P. W. N. M.; Kamer, P. C. J.; Reek, J. N. H.; Dierkes, P. *Chem. Rev.* **2000**, *100*, 2741-2769. (c) van der Veen, L. A.; Kamer, P. C. J.; van Leeuwen, P. W. N. M. *CATTECH* **2002**, *6*, 116-120. (d) Freixa, Z.; Van Leeuwen, P. W. N. M. *Dalton Trans.* **2003**, 1890-1901. (e) Birkholz, M.-N.; Freixa, Z.; van Leeuwen, P. W. N. M. *Chem. Soc. Rev.* **2009**, *38*, 1099-1118.
(36) For selected book chapters in hydroformylation reactions, see: (a) Whiteker, G. T., Cobley, C. J., Topics in Organometallic Chemistry. In *Organometallics as Catalysts in the Fine Chemical Industry*; Beller, M., Blaser H.-U., Eds.; Springer-Verlag: Berlin, 2012, Vol. 42, pp 35-46. (b) Börner, A.; Franke, R. *Hydroformylation: Fundamentals, Processes, and Applications in Organic Synthesis;* WILEY-VCH Verlag GmbH & Co. KGaA: Weinheim 2016; Vol. 2, pp 1-702. For a selected review, see: (c) Chikkali, S. H.; van der Vlugt, J. I.; Reek, J. N. H. *Coord. Chem. Rev.* **2014**, *262*, 1-15.
(37) (a) Freixa, Z.; van Leeuwen, P. W. N. M. *Coord. Chem. Rev.* **2008**, *252*, 1755-1786. (b) Li, Y.-Q.; Wang, P.; Zhang, H.; Zhao, X.-L.; Lu, Y.; Popovic, Z.; Liu, Y. *J. Mol. Catal. A: Chem.* **2015**, *402*, 37-45.

On the other hand, rhodium complexes derived from narrow bite angle ligands behave in the opposite way and favor the formation of branched aldehydes.[35,38]

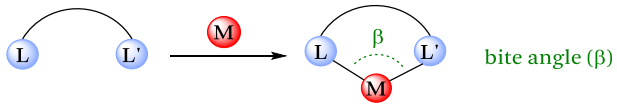

Figure 11. The bite angle (β) in metal complexes (M = catalytic metal, L, L' = ligands).

Representative examples of high performing wide and narrow bite angle phosphorus ligands in Rh-mediated hydroformylation reactions are listed in Figure 12.

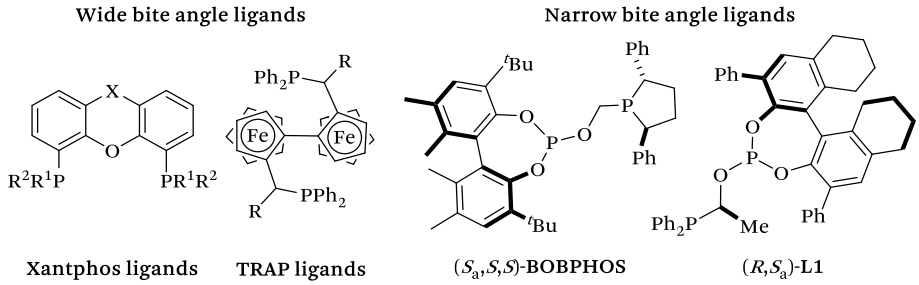

Figure 12. Relevant examples of high performing wide and narrow bite angle phosphorus ligands in Rh-mediated hydroformylations.[37,38]

The use of two inequivalent ligating groups in an enantiopure bidentate ligand introduces an additional handle to control the steric and electronic properties of the coordination sphere around the metal. This structural feature may be beneficial to control regioselectivity and may potentially lead to higher enantioselectivities due to specific binding of the substrate, as in the case of asymmetric hydroformylation reactions.[36]

Particularly, phosphine-phosphite (P–OP) ligands represent a relevant example of C_1-symmetric ligands that present electronic and steric dissimilarities in the coordination groups. Since the development of the first phosphine-phosphite ligands in 1993,[39] numerous phosphine-phosphite

(38) (a) Cobley, C. J.; Froese, R. D. J.; Klosin, J.; Qin, C.; Whiteker, G. T.; Abboud, K. A. *Organometallics* **2007**, *26*, 2986-2999. (b) Fernández-Pérez, H.; Benet-Buchholz, J.; Vidal-Ferran, A. *Org. Lett.* **2013**, *15*, 3634-3637. (c) Fernández-Pérez, H.; Benet-Buchholz, J.; Vidal-Ferran, A. *Chem. – Eur. J.* **2014**, *20*, 15375-15384. (d) Noonan, G. M.; Cobley, C. J.; Mahoney, T.; Clarke, M. L. *Chem. Commun.* **2014**, *50*, 1475-1477. (e) Pittaway, R.; Fuentes, J. A.; Clarke, M. L. *Org. Lett.* **2017**, *19*, 2845-2848.
(39) (a) Sakai, N.; Mano, S.; Nozaki, K.; Takaya, H. *J. Am. Chem. Soc.* **1993**, *115*, 7033-7034. (b) Baker, M. J.; Pringle, P. G. *J. Chem. Soc., Chem. Commun.* **1993**, 314-316.

ligands, which mediate a broad range of catalytic asymmetric transformations, have been reported.[40]

Over the past years our research group has developed a general synthetic strategy for the preparation of a structurally diverse library of highly modular phosphine-phosphite ligands bearing *privileged*[41] modules (or molecular fragments) in enantioselective catalysis (Scheme 2).

Scheme 2. General retrosynthetic strategy for the preparation of enantiopure phosphine-phosphite ligands developed by the group and selected optimal ligands for Rh-mediated asymmetric transformations[38b,c,42b–d]

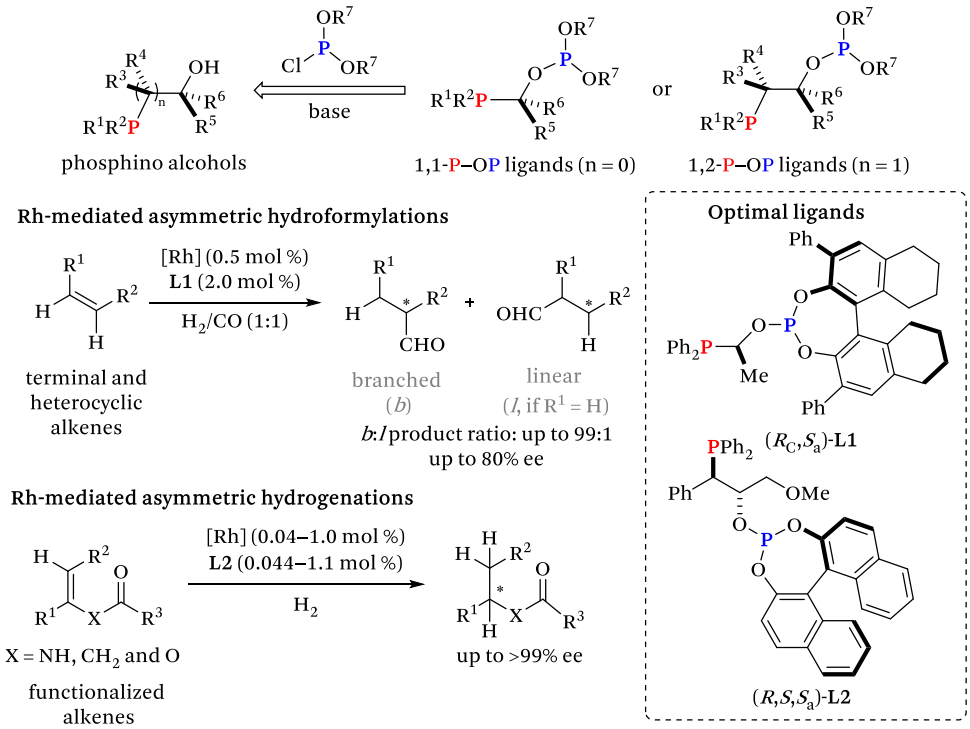

(40) For a general review on the preparation and application of phosphine-phosphite ligands in asymmetric catalysis, see: (a) Fernández-Pérez, H.; Etayo, P.; Panossian, A.; Vidal-Ferran, A. *Chem. Rev.* **2011**, *111*, 2119-2176. (b) Pizzano, A. *Chem. Rec.* **2016**, *16*, 2595-2618.

(41) For the definition of the concept *privileged ligand* in asymmetric catalysis, see: Yoon, T. P.; Jacobsen, E. N. *Science* **2003**, *299*, 1691-1693.

(42) (a) Donald, S. M. A.; Vidal-Ferran, A.; Maseras, F. *Can. J. Chem.* **2009**, *87*, 1273-1279. (b) Fernández-Pérez, H.; Donald, S. M. A.; Munslow, I. J.; Benet-Buchholz, J.; Maseras, F.; Vidal-Ferran, A. *Chem. – Eur. J.* **2010**, *16*, 6495-6508. (c) Etayo, P.; Núñez-Rico, J. L.; Fernández-Pérez, H.; Vidal-Ferran, A. *Chem. – Eur. J.* **2011**, *17*, 13978-13982. (d) Núñez-Rico, J. L.; Etayo, P.; Fernández-Pérez, H.; Vidal-Ferran, A. *Adv. Synth. Catal.* **2012**, *354*, 3025-3035.

The versatility of the synthetic strategy allowed for the preparation of an array of structurally diverse P–OP ligands incorporating variable carbon-chain lengths between the two ligating groups and different stereogenic elements in the structure (Scheme 2). This structurally diverse set of ligands was used to generate highly efficient and well-defined Rh- and Ir-based catalytic systems for the Rh-mediated asymmetric hydroformylations of terminal and heterocyclic alkenes,[38b,c] Rh-mediated asymmetric hydrogenations of functionalized alkenes[38b,c,42] and Ir-mediated asymmetric hydrogenations of C=N-containing heterocycles.[43] The highest performing ligands in Rh-mediated asymmetric transformations are listed in Scheme 2.

AIMS OF RESEARCH

It should be pointed out that during the course of the present PhD thesis, the library of phosphine-phosphite ligands developed by the group was broadened and new phosphite fragments were incorporated into the structures of the P–OP ligands (**L3**–**L6**, see Figure 13).

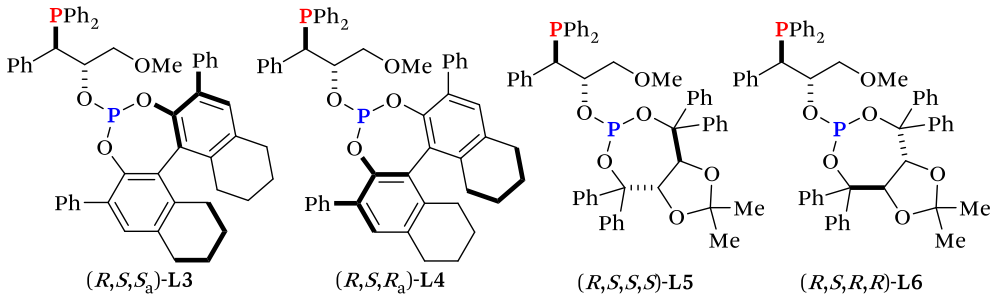

Figure 13. Phosphine-phosphite ligands incorporating 3,3'-diphenyl-substituted H_8-BINOL (**L3** and **L4**) and TADDOL (**L5** and **L6**) phosphite-derived fragments.

The synthetic methodology for the preparation of those enantiopure ligands (**L3**–**L6**, see Figure 13) and their corresponding Rh-complexes (with formula

(43) (a) Núñez-Rico, J. L.; Fernández-Pérez, H.; Benet-Buchholz, J.; Vidal-Ferran, A. *Organometallics* **2010**, *29*, 6627-6631. (b) Núñez-Rico, J. L.; Vidal-Ferran, A. *Org. Lett.* **2013**, *15*, 2066-2069. (c) Núñez-Rico, J. L.; Fernández-Pérez, H.; Vidal-Ferran, A. *Green Chem.* **2014**, *16*, 1153-1157. (d) Balakrishna, B.; Bauzá, A.; Frontera, A.; Vidal-Ferran, A. *Chem. – Eur. J.* **2016**, *22*, 10607-10613.

(44) Phosphine-phosphite ligands listed in Figure 13 (**L3**–**L6**) were found to be the optimal ligands for the transformations presented in Chapters II–IV. I would like thank to Dr. Héctor Fernández for supplying ligands **L3–L6** and **L4**, and Dr. Balakrishna Bugga for supplying ligands **L5**, **L6** and the Rh-complex [Rh(nbd)(**L3**)]BF_4.

[Rh(nbd)(**L3–L6**)]BF_4) was also optimized by Dr. Balakrishna Bugga during his PhD studies.[45,46]

With the aim of developing new ligands for high performing stereoselective catalytic systems, it should be noticed that narrow bite angle[35] ligands (with only one carbon spacer between the two ligating groups) bearing P-stereogenic phosphino groups[47] represent an interesting understudied class of chiral ligands. We envisaged that these ligands could provide a very constrained environment around the metal center with high enantioselectivities in the overall process.[48] Hence, we decided to direct our efforts toward developing a synthetic strategy for the preparation of these new type of ligands and evaluating their catalytic performance in Rh-mediated asymmetric hydrogenation and hydroformylation reactions (Figure 14).

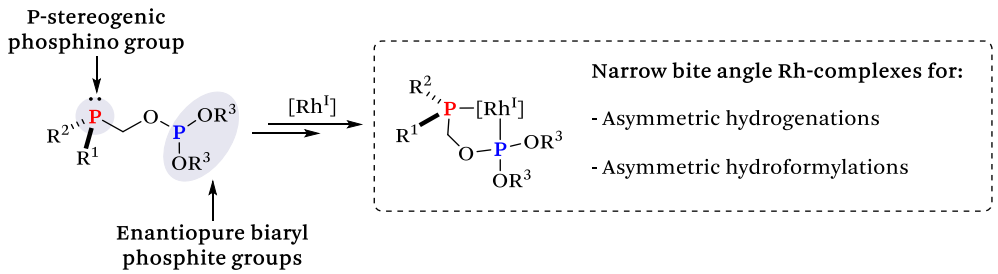

Figure 14. General structures of narrow bite angle phosphine-phosphite ligands containing P-stereogenic phosphino groups and the corresponding Rh^I-complexes.

Considering the excellent catalytic properties of the Rh-catalysts prepared by the group[38b,c,42,43] we also oriented further investigations to exploit the applicability of Rh-complexes derived from phosphine-phosphite ligands to the development of new hydrogenative transformations toward the preparation of synthetically valuable compounds (with industrial, biological or pharmaceutical interest). Based on this idea, we decided to turn our attention to developing new catalytic methodologies for the preparation of

(45) Balakrishna, B.; Development of P–OP Ligands with New Structural Motifs for Rhodium- and Iridium-Mediated Asymmetric Hydrogenations. PhD Thesis. Universitat Rovira i Virgili, Tarragona (Spain), 2016.
(46) Balakrishna, B.; Vidal-Ferran, A. *Synthesis* **2016**, *48*, 997-1001.
(47) P-stereogenic phosphino groups have proved to be highly efficient stereodirecting ligating groups in asymmetric catalysis. For a representative review on efficient ligands bearing P-stereogenic phosphino groups, see: Grabulosa, A.; Granell, J.; Muller, G. *Coord. Chem. Rev.* **2007**, *251*, 25-90.
(48) For highly efficient narrow bite angle phosphine-phosphite ligands, see: refs. 38b–d.

optically enriched sulfoxides by kinetically resolving α,β-unsaturated sulfoxides by hydrogenation (Scheme 3).

Scheme 3. Hydrogenative kinetic resolution of α,β-unsaturated sulfoxides

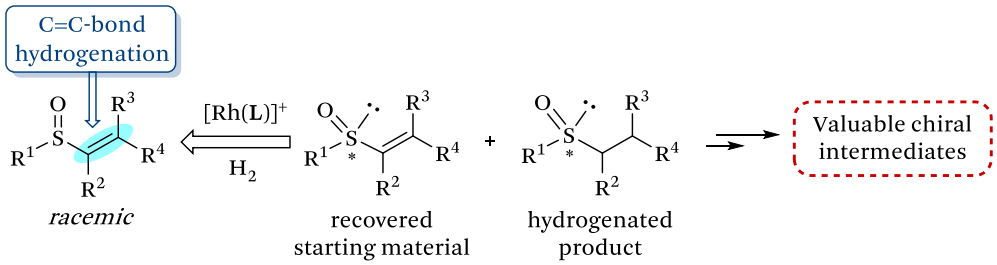

We considered that the resolved sulfoxides could find broad applicability in diverse research areas such as in asymmetric synthesis (e.g. as chiral ligands or auxiliaries)[49] or in the pharmaceutical industry (as enantiopure sulfoxide-containing drugs).[50] Regarding the literature precedents on the reported catalytic methodologies for the preparation of enantioenriched sulfoxides by asymmetric hydrogenation, we found that examples in the literature were scarce.[51]

We also decided to direct our investigations to the development of other catalytic asymmetric hydrogenative methodologies leading to valuable enantioenriched molecules from simple substrates. In this context, our group reviewed the most effective metal-catalyzed desymmetrization reactions of achiral and *meso* compounds involving reductive transformations.[26a] Through an extensive revision of all the reported methodologies concerning reductive transformations,[26a] several unsolved catalytic reactions (in terms of catalytic activity and reaction stereocontrol) were identified. Among those, the enantioselective desymmetrization of achiral 1,4-dienes by asymmetric hydrogenation (Scheme 4) deserve mention. Notably, the hydrogenative

(49) (a) Trost, B. M.; Rao, M. *Angew. Chem., Int. Ed.* **2015**, *54*, 5026-5043. (b) Sipos, G.; Drinkel, E. E.; Dorta, R. *Chem. Soc. Rev.* **2015**, *44*, 3834-3860. (c) Otocka, S.; Kwiatkowska, M.; Madalinska, L.; Kielbasinski, P. *Chem. Rev.* **2017**, *117*, 4147-4181.
(50) (a) Fernández, I.; Khiar, N. *Chem. Rev.* **2003**, *103*, 3651-3705. (b) Legros, J.; Dehli, J. R.; Bolm, C. *Adv. Synth. Catal.* **2005**, *347*, 19-31. (c) Bentley, R. *Chem. Soc. Rev.* **2005**, *34*, 609-624.
(51) For the most recent relevant examples on catalytic reductive methodologies, see: (a) Ando, D.; Bevan, C.; Brown, J. M.; Price, D. W. *J. Chem. Soc., Chem. Commun.* **1992**, 592-594. (b) Dornan, P. K.; Kou, K. G. M.; Houk, K. N.; Dong, V. M. *J. Am. Chem. Soc.* **2014**, *136*, 291-298.

desymmetrization of 1,4-dienes could lead to valuable chiral building blocks for the preparation of more complex molecules.[52]

Scheme 4. Hydrogenative desymmetrization of achiral 1,4-dienes

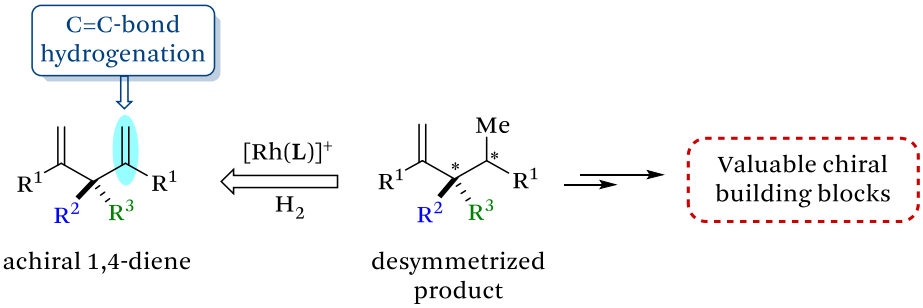

The main challenges associated to this transformation reside in the need of discovering a catalytic system capable of controlling both chemoselectivity (the selective monohydrogenation of the starting material) and stereoselectivity (the differentiation of two enantiotopic vinyl groups). Although pioneering work had been previously done through Rh(bisphosphine)-mediated asymmetric hydrogenations,[53] moderated stereoselectivities were achieved without a complete control on the reaction chemoselectivity. Taking this pioneering work into consideration, we also decided to address the challenge of developing an appropriate chemo- and stereo-selective catalytic system for the hydrogenative desymmetrization of achiral 1,4-dienes (Scheme 4).

Therefore, the aims of the present thesis are as follows:

1. To develop a synthetic methodology for the preparation of narrow bite angle phosphine-phosphite ligands with a single C-atom between the two phosphorus functionalities and P-stereogenic phosphino groups, to study the coordination of these ligands with the commonly used Rh-precursors for asymmetric hydrogenations and hydroformylations, and to assess the catalytic performance of the resulting Rh-complexes in asymmetric hydrogenations and hydroformylations of structurally diverse alkenes.

(52) (a) Stymiest, J. L.; Bagutski, V.; French, R. M.; Aggarwal, V. K. *Nature* **2008**, *456*, 778-782. (b) Scott, H. K.; Aggarwal, V. K. *Chem. – Eur. J.* **2011**, *17*, 13124-13132.
(53) Nguyen, B.; Brown, J. M. *Adv. Synth. Catal.* **2009**, *351*, 1333-1343.

2. To broaden the applicability of the library of phosphine-phosphite ligands developed by the group to other challenging stereoselective hydrogenative transformations, such as the hydrogenative kinetic resolution of α,β-unsaturated sulfoxides and the stereoselective hydrogenative desymmetrization of achiral 1,4-dienes, with the aim of developing efficient synthetic methodologies for the preparation of highly enantioenriched valuable products.

UNIVERSITAT ROVIRA I VIRGILI
RHODIUM CATALYSIS IN ENANTIOSELECTIVE HYDROGENATIVE TRANSFORMATIONS: FROM THE DESIGN OF NEW LIGANDS TO REACTIONS OF ATYPICAL SUBSTRATES
Joan Ramon Lao Mulinari

CHAPTER I

1,1-P–OP Ligands with P-Stereogenic Phosphino Groups in Asymmetric Hydrogenations and Hydroformylations

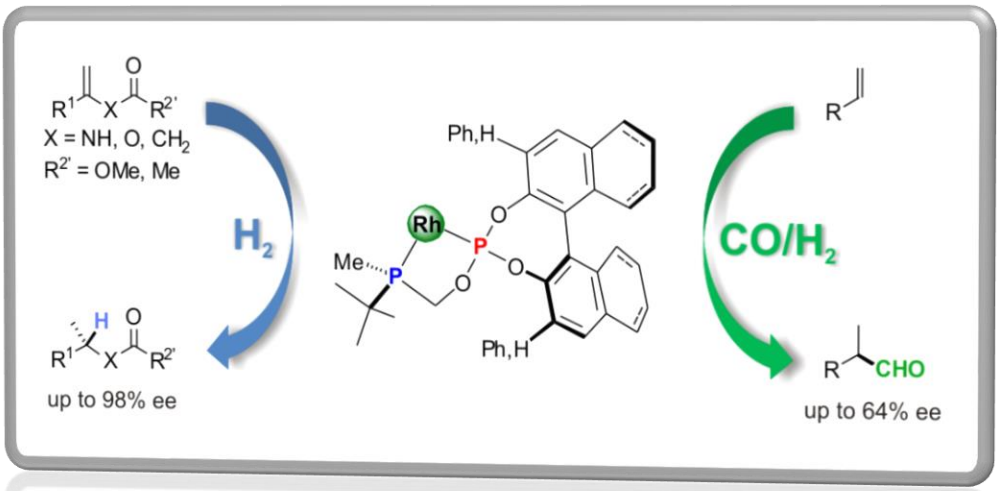

UNIVERSITAT ROVIRA I VIRGILI
RHODIUM CATALYSIS IN ENANTIOSELECTIVE HYDROGENATIVE TRANSFORMATIONS: FROM THE DESIGN OF NEW LIGANDS TO REACTIONS OF ATYPICAL SUBSTRATES
Joan Ramon Lao Mulinari

1,1-P–OP Ligands with P-Stereogenic Phosphino Groups in Asymmetric Hydrogenations and Hydroformylations

1.1. ABSTRACT

A new series of narrow bite angle phosphine–phosphite (1,1-P–OP) ligands have been efficiently prepared from the enantiopure (S_P)-*tert*-butyl-(hydroxymethyl)methylphosphino borane complex, a crucial intermediate. The catalytic performance of the ligands in Rh-mediated asymmetric hydrogenations and hydroformylations is described. The corresponding rhodium complexes provided excellent efficiencies (full conversion in all cases) and high enantioselectivities (up to 98% ee) for the asymmetric hydrogenation of structurally diverse functionalized alkenes. Furthermore, rhodium catalysts derived from these 1,1-P–OP ligands were highly active and gave excellent regioselectivities (branched/linear product ratios of up to 97/3) and moderate enantioselectivities in the hydroformylation of different terminal olefins.

1.2. INTRODUCTION

Hybrid bidentate enantiopure P-containing ligands have efficiently mediated a wide range of applications in transition-metal-catalyzed reactions that lead to a rich array of structurally diverse enantiopure (or enantioenriched) products.[54] Phosphine–phosphite (P–OP) ligands,[40] first developed by the groups of Takaya[39a] and Pringle,[39b] are an important example of non-symmetric ligands whose coordinated functional groups differ electronically and sterically. The P–OP ligand BINAPHOS has found applications in many mechanistically unrelated enantioselective transformations,[40] thus making it one of the few *privileged ligands*[41] in asymmetric catalysis.

Several related P–OP ligands, encompassing diverse carbon backbones, different stereogenic elements, and variable distances between the coordinated functional groups, have been reported for asymmetric catalysis.[40] Among these, narrow bite angle[35] P–OP ligands are an attractive,

(54) See Wassenaar, J.; Reek, J. N. H. *Org. Biomol. Chem.* **2011**, *9*, 1704-1713., and the references cited therein.

understudied class of compounds. Interestingly, narrow bite angle ligands provide a rigid asymmetric environment around the metal center, which translates into high catalytic efficiency in several asymmetric transformations.[38b–e] The short length of the spacer between the two phosphorus functionalities (only one carbon atom) is the primary factor responsible for the low bite angle values observed (e.g. P–Rh–PO angles of ca. 80° in rhodium complexes derived from 1,1-P–OP ligands[38b]). Interestingly, although P-stereogenic phosphines are highly efficient stereodirecting binding groups in asymmetric catalysis,[47] these groups have not been explored as molecular fragments in 1,1-P–OP ligands.

1.3. RESULTS AND DISCUSSION

Seeking to develop new and efficient ligands for asymmetric transformations of interest,[38b,c,42,43] we prepared the modular 1,1-P–OP ligands **L7**–**L10** (Scheme 5).

Scheme 5. Synthesis of 1,1-P–OP ligands L7–L10

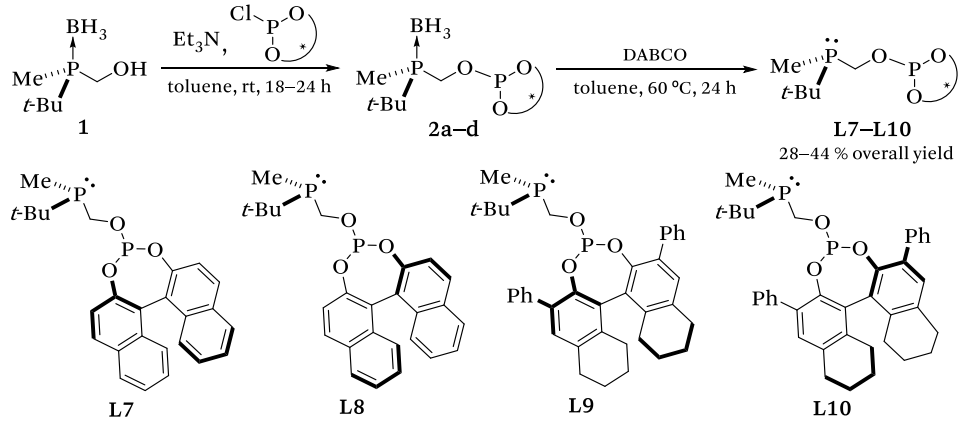

These ligands incorporate the attractive *tert*-butyl(methyl)-phosphino stereogenic group, which is well-known as a highly efficient stereodirecting moiety in asymmetric catalysis.[55] Herein are reported the synthesis of the

(55) For selected examples of highly efficient ligands containing the chiral *tert*-butyl(methyl)phosphino fragment, see: (a) Imamoto, T.; Watanabe, J.; Wada, Y.; Masuda, H.; Yamada, H.; Tsuruta, H.; Matsukawa, S.; Yamaguchi, K. *J. Am. Chem. Soc.* **1998**, *120*, 1635-1636. (b) Hoge, G.; Wu, H.-P.; Kissel, W. S.; Pflum, D. A.; Greene, D. J.; Bao, J. *J. Am. Chem. Soc.* **2004**, *126*, 5966-5967. (c) Imamoto, T.; Sugita, K.; Yoshida, K. *J. Am. Chem. Soc.* **2005**, *127*, 11934-11935. (d) Tamura, K.; Sugiya, M.; Yoshida, K.; Yanagisawa, A.; Imamoto, T. *Org. Lett.* **2010**, *12*, 4400-4403.

enantiomerically pure 1,1-P–OP ligands **L7**–**L10**, and their catalytic performance in Rh-mediated asymmetric hydrogenations and hydroformylations. The ligands **L7**–**L10** were readily prepared in a one-pot process (Scheme 5) from borane complex **1**, based on a geminal phosphino alcohol.[55c,56] The first step involved the *O*-phosphorylation of **1** with diverse chlorophosphite derivatives using triethylamine as the auxiliary base to yield the corresponding P–OP borane complexes **2a–d**. The (relatively clean) resulting crude mixtures containing **2a–d** were immediately cleaved with DABCO in toluene at 60 °C, leading to the corresponding P–OP ligands **L7**–**L10** in 28–44% yield after chromatography. Interestingly, the P–OP borane complexes **2c,d** were found to be highly crystalline, and their structures were confirmed by X-ray analysis.[57]

The ability of the new 1,1-P–OP ligands to form complexes with transition-metal precursors was also studied. Cationic Rh^{I}-complexes derived from the aforementioned P–OP ligands, which are suitable for asymmetric hydrogenation (i.e. [Rh(nbd)(**L7**–**L10**)]BF_4), were efficiently isolated upon reaction of stoichiometric amounts of the 1,1-P–OP ligand (**L7** or **L8**) with $[Rh(nbd)_2]BF_4$ in dichloromethane and subsequent precipitation. The NMR data for the resulting complexes confirmed a five-membered 1/1 chelate coordination mode of the P–OP ligand to the rhodium center.[57]

Interestingly, during attempts to obtain single crystals of [Rh(nbd)(**L7**)]BF_4 for X-ray diffraction from a solvent mixture containing toluene, the product **3** ([Rh(η^6-C_7H_8)(**L7**)]BF_4) was unexpectedly isolated. X-ray analysis revealed that this product has an η^6-arene coordination mode (Figure 15). In fact, the stability of Rh^{I}–η^6-arene complexes with chelating diphosphines is well known.[58] Interestingly, formation of the Rh-complex **3** ([Rh(η^6-C_7H_8)(**L7**)]BF_4) involved a rare displacement of the diene ligand (norbornadiene) by toluene in the absence of molecular hydrogen. In this structure, the P–OP ligand showed a bidentate coordination mode with a narrow bite angle of 81.32(12)°.

(56) Compound **1** was prepared using slightly modified procedures from the following publications: (a) Genet, C.; Canipa, S. J.; O'Brien, P.; Taylor, S. *J. Am. Chem. Soc.* **2006**, *128*, 9336-9337. (b) Carbone, G.; O'Brien, P.; Hilmersson, G. *J. Am. Chem. Soc.* **2010**, *132*, 15445-15450.

(57) See the Experimental Section for details.

(58) (a) Osborn, J. A.; Schrock, R. R. *J. Am. Chem. Soc.* **1971**, *93*, 3089-3091. (b) Fischer, C.; Thede, R.; Drexler, H.-J.; König, A.; Baumann, W.; Heller, D. *Chem. – Eur. J.* **2012**, *18*, 11920-11928.

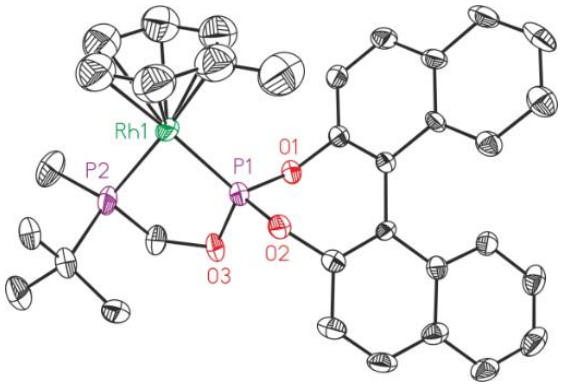

Figure 15. Crystal structure of **3** ([Rh(η^6-C_7H_8)(**L7**)]BF_4) (ORTEP drawing with thermal ellipsoids at the 50% probability level). The hydrogen atoms, solvent molecules, and BF_4 counterion have been omitted for clarity.

Coordination of the 1,1-P–OP ligands **L7**–**L10** to the rhodium precursor [Rh(κ^2O,O′-acac)$(CO)_2$], which is commonly used in hydroformylations, was also studied. For example, direct reaction of stoichiometric amounts of **L7** with the precursor in toluene gave the complex [Rh(κ^2O,O′-acac)(**L7**)].

The $^{31}P\{^1H\}$ NMR and MS data confirm the existence of a 1/1 chelate formed by bidentate coordination between the metal center and the two phosphorus ligand groups.[57] The ready formation of these complexes greatly facilitated subsequent studies on the corresponding hydroformylations, as the required precatalysts were cleanly generated in situ. In hydrogenation studies the Rh-precatalysts derived from the 1,1-P–OP ligands **L7**–**L10** were assessed for reactivity against a set of structurally diverse functionalized alkenes: an itaconic acid derivative (**4a**), an α-arylenamide (**4b**), an α-arylenol ester (**4c**), and an α-(acylamino)acrylate derivative (**4d**). The reaction conditions and hydrogenation results are summarized in Table 1.

In general, regardless of the substrate, compounds **4a–d** were efficiently hydrogenated with full conversions and with variable degrees of enantioselectivity (ee values up to 98%, see Table 1). Analysis of the results indicates the existence of matched and mismatched effects for the diastereomeric ligands **L7** and **L8**: the latter, which contains an (S_a)-configured phosphite fragment, provided higher enantioselectivities (entries 5–8 in Table 1) than did the former, which contains the (R_a)-derived phosphite fragment (compare entries 1–4 in Table 1).

Table 1. Asymmetric hydrogenation of the substrates 4a–d with the P–OP ligands L7–L10[a]

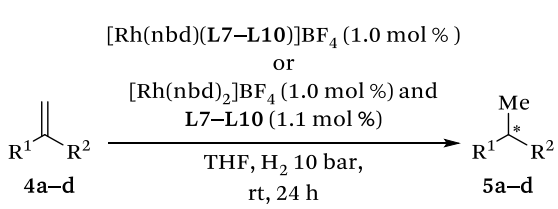

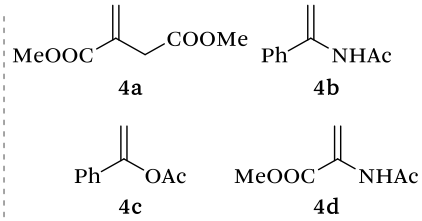

entry	ligand	substrate	ee, %;[b] (*config.*)[c]
1	L7	**4a**	65 (*R*)
2		**4b**	89 (*S*)
3		**4c**	23 (*S*)
4		**4d**	8 (*R*)
5	L8	**4a**	80 (*S*)
6		**4b**	89 (*R*)
7		**4c**	83 (*R*)
8		**4d**	94 (*R*)
9	L9	**4a**	84 (*R*)
10		**4b**	89 (*S*)
11		**4c**	93 (*S*)
12		**4d**	98 (*S*)
13	L10	**4a**	75 (*S*)
14		**4b**	93 (*R*)
15		**4c**	81 (*R*)
16		**4d**	79 (*R*)

[a] Reactions were run in a parallel reactor. All the catalytic reactions were run under the specified conditions. Complete conversion was achieved in all cases (as determined by ^{1}H NMR). [b] Determined by GC or HPLC analysis on chiral stationary phases. [c] The absolute configuration was assigned by comparison of the specific rotation with reported data.

Interestingly, the presence of a more sterically hindered 3,3′-diphenyloctahydro-1,1′-binaphthalene-2,2′-diol-derived phosphite group (ligands **L9** and **L10**) led to the opposite matched–mismatched effects (Table 1): in these cases, higher enantioselectivities were obtained for substrates **4a,c,d** by the combined effects of the (S_P)-phosphino and (R_a)-phosphite molecular fragments in ligand **L9**. In fact, among all of the

P–OP ligands tested, **L9** gave the best performance in the asymmetric hydrogenation of **4a,c,d**. Regarding the stereochemistry of the hydrogenation products, when ligand **L9** (which contains an (R_a)-phosphite group) was used, the final products had opposite configuration to those obtained when ligand **L8** or **L10** (each of which contains an (S_a)-phosphite group) was used.[59] This observation indicates that the direction of stereodiscrimination is controlled mainly by the phosphite fragment, as has previously been reported by the present authors for asymmetric hydrogenations mediated by rhodium complexes derived from 1,2-P–OP ligands.[42b]

The P–OP ligands **L7–L10** were also screened in the asymmetric hydroformylation of three structurally diverse terminal olefins: styrene (**6a**), vinyl acetate (**6b**), and (allyloxy)trimethylsilane (**6c**) (Table 2). For this purpose, the reactions were run under standard hydroformylation conditions, using 0.5 mol % of in situ preformed [Rh(κ^2O,O′-acac)(**L7–L10**)] complexes, in toluene at 40 °C under CO/H_2 (1/1, 10 bar) overnight. The results indicate that the outcome of the catalysis experiments depended on both the substrate and the ligand. For example, in the hydroformylation of styrene (**6a**), all of the catalysts derived from the P–OP ligands **L7–L10** were highly active and gave conversions higher than 90% (Table 2). In addition, excellent branched/linear product ratios (up to 97/3) were observed for the whole set of prepared ligands.

Regarding the stereochemistry of the hydroformylation product of styrene, ligands **L7** and **L9** (both of which have an (R_a)-phosphite group) favored the formation of the (*R*)-configured hydroformylation product, whereas ligands **L8** and **L10** (both of which have an (S_a)-phosphite group) gave the opposite result. The catalysts derived from ligands **L7–L10** mediated the hydroformylation of (allyloxy)trimethylsilane (**6c**) in good conversion, but the branched to linear product ratios obtained with this substrate were lower than those obtained with styrene. For both substrates (**6a**,**c**), the phosphite group was the principal steric director: reversing its axial chirality led to switching of the configuration in the products.

(59) Interestingly, the hydrogenation product from reaction of **4d** and ligand **L7** (which contains an (R_a)-phosphite fragment; entry 4 in Table 1) had the same configuration as those obtained from ligands **L8** and **L10** containing the (S_a)-phosphite fragment (entry 4 in Table 1). This observation suggests a substrate- and ligand-dependent mechanistic scenario in the hydrogenations involving ligand **L7**. However, any mechanistic rationalizations about processes with low enantioselectivity (e.g., 8% ee; entry 4 in Table 1) should be made judiciously.

Table 2. Asymmetric hydroformylation of the substrates 6a–c with the P–OP ligands L7–L10[a]

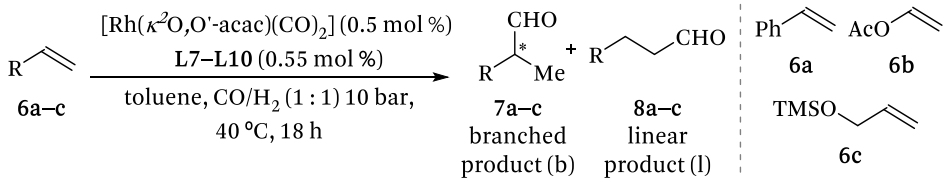

entry	ligand	substrate	conv., %[b]	b:l ratio[c]	ee, %;[c] (*config.*)[d]
1	**L7**	**6a**	90	95:5	64 (*R*)
2	**L8**		94	95:5	21 (*S*)
3	**L9**		97	97:3	49 (*R*)
4	**L10**		97	97:3	7 (*S*)
5	**L7**	**6b**	35	88:12	53 (*S*)
6	**L8**		52	93:7	38 (*S*)
7	**L9**		52	95:5	61 (*S*)
8	**L10**		67	97:3	18 (*S*)
9	**L7**	**6c**	88	49:51	6 (*R*)
10	**L8**		74	48:52	5 (*S*)
11	**L9**		>99	79:21	60 (*R*)
12	**L10**		96	73:27	9 (*S*)

[a]Reactions were run in a parallel reactor. All hydroformylations were run under the specified conditions. [b]Conversions were determined by ^{1}H NMR. [c]Branched/linear product ratios and enantiomeric excesses were determined by GC on chiral stationary phases. [d]The absolute configuration was assigned by comparison of the elution order in GC analysis with reported data.

Interestingly, the incorporation of a bulkier phosphite moiety was an important parameter: for styrene (**6a**) higher ee values were obtained using the 3,3′-unsubstituted ligand **L7**, whereas for the allylic substrate **6c**, higher ee values were obtained with the 3,3′-diphenyloctahydro-1,1′-binaphthalene-2,2′-diol-derived ligand **L9** (Δee = 54%; compare entries 9 and 11 in Table 2). Vinyl acetate (**6b**) was the most difficult hydroformylation substrate, as evidenced by the lower conversions obtained with the ligands **L7–L10** (Table 2). Nevertheless, regioselectivities toward the branched product remained remarkably high (branched/linear ratios up to 97/3). Interestingly, reaction of this particular substrate with each of the tested ligands gave the (*S*)-configured product exclusively; in this case, the configuration of the

phosphite moiety did not influence the stereochemical outcome of the reaction. These results clearly indicate that the P-stereogenic group is the principal steric director of the hydroformylation and that it overrides the stereodirecting effects of the phosphite moiety in ligands **L7–L10**.[60]

1.4. CONCLUSIONS

In summary, a convenient synthesis of a new series of 1,1-P–OP ligands (**L7–L10**) containing the stereogenic (S_P)-*tert*-butyl(hydroxymethyl)methylphosphine fragment and a one carbon spacer between the two phosphorus functionalities has been developed. The efficiency of these ligands has been demonstrated in asymmetric hydrogenations and hydroformylations of diverse substrates. The results indicate that, although the optimal ligand for a given combination of transformation and substrate is not easy to predict, for a given ligand the direction of stereoinduction can easily be predicted (Figure 16).

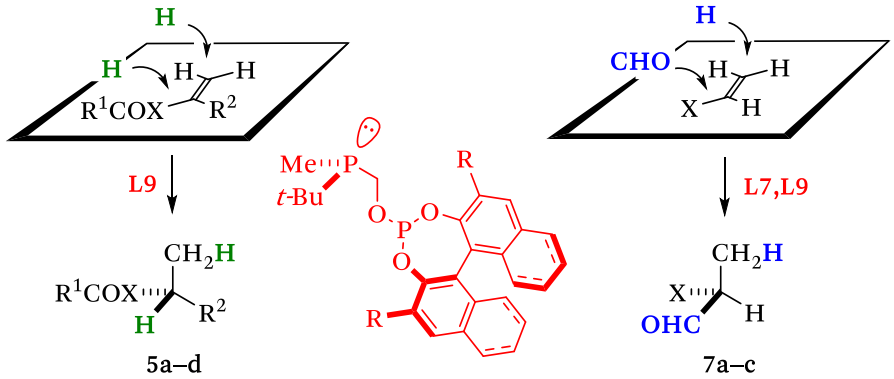

Figure 16. Stereochemical outcome for the hydrogenations and hydroformylations mediated by the 1,1-P–OP ligands **L7** and **L9**.

Considering their simple preparation, these new narrow bite angle ligands should prove valuable for asymmetric catalysis. The authors are currently performing mechanistic studies to elucidate the role of each ligand fragment in stereoinduction and catalytic studies to develop further applications.

(60) The ligands with an (R_a)-phosphite fragment (**L7** and **L9**) led to the (*R*)-, (*S*)- and (*R*)-configured products of **7a**, **7b** and **7c**, respectively. This stereochemistry implies incorporation of the CHO and H groups into the *Si*-alkene face (differences in the CIP (*R*)- or (*S*)- prefixes arise from changes in the CIP priority rules, and not from attack at the other enantiotopic face of the alkene).

1.5. EXPERIMENTAL SECTION

1.5.1 General considerations

All starting materials were purchased from commercial sources unless otherwise stated. Air- and moisture-sensitive manipulations or reactions were done under inert atmosphere using anhydrous solvents, either in a glove box or with standard Schlenk techniques. Glassware was dried under vacuum and was heated with a hot air gun before use. All solvents were dried in a Solvent Purification System (SPS). Silica gel 60 (230–400 mesh) was used for column chromatography. NMR spectra were recorded in $CDCl_3$, unless otherwise cited. ^1H NMR and $^{13}C\{^1H\}$ NMR chemical shifts are quoted in ppm relative to the residual solvent peaks, whereas $^{31}P\{^1H\}$ NMR chemical shifts are quoted in ppm relative to 85% phosphoric acid in water. High-resolution mass spectra (HRMS) were recorded using either MALDI or ESI ionization (each in positive mode). IR spectra were recorded using Attenuated Total Reflection (ATR) technique, unless otherwise stated. Enantiomeric excesses were determined by GC or HPLC analyses, using chiral stationary phases. Melting points were measured in open capillaries and are uncorrected. GC analyses were performed on a chromatograph equipped with a FID detector. HPLC analyses were performed on a chromatograph equipped with a diode array UV detector (DAD).

1.5.2. General synthetic procedure for the P–OP ligands L7–L10

The following procedure was performed in a glove box: to a stirring solution of the azeotropically-dried (2 x 5 mL of anhydrous toluene) phosphino alcohol borane complex **1**[61] (128 mg, 0.87 mmol) and Et_3N (241 μL, 1.73 mmol) in anhydrous toluene (12 mL) was slowly added a solution of the required chlorophosphite (487 mg, 0.95 mmol) in anhydrous toluene (4.6 mL), and the resulting mixture was stirred overnight at room temperature. The reaction mixture was filtered through a short pad of dried and deoxygenated silica gel under N_2 atmosphere eluting with anhydrous toluene (2 x 20 mL). The solvent was removed in vacuo to afford the desired corresponding P–OP borane complexes **2a–d**, which were used in the next step without further purification. To a solution of the previously prepared P–OP borane complex

(61) The enantiopure phosphino-alcohol borane complex **1** was prepared using slightly modified procedures from refs. 55c and 56a,b.

(591 mg, theoretical 0.95 mmol) in anhydrous toluene (12 mL) was added dropwise a solution of DABCO (239 mg, 2.09 mmol) in anhydrous toluene (4.7 mL) under N_2 atmosphere. Finally, the reaction mixture was heated to 60 °C for 24 h under Ar atmosphere. The crude reaction mixture was brought to room temperature, rapidly filtered through a short pad of dried, deoxygenated silica gel eluting with anhydrous toluene (2 x 20 mL). The solvent was removed in vacuo to afford the desired corresponding P–OP ligands **L7–L10** as foamy white solids.

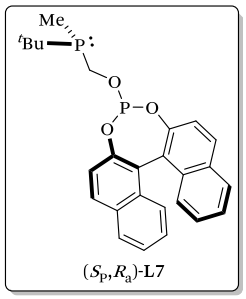

(S_P,R_a)-L7

The general procedure was followed starting from **1** and the chlorophosphite derived from (R_a)-BINOL to yield the P–OP borane complex **2a** as a white solid. DABCO-mediated borane cleavage of the P–OP borane complex afforded the desired P–OP ligand **L7** as a foamy white solid (193 mg, 28% yield), mp = 102–105 °C. ^{1}H NMR (400 MHz, $CDCl_3$) δ 8.01–7.94 (m, 4H), 7.54–7.30 (m, 8H), 4.23 (ddd, J = 12.4 Hz, J = 6.5 Hz, J = 3.2 Hz, 1H), 4.00 (dt, J = 14.0 Hz, J = 7.1 Hz, 1H), 1.04–1.01 (m, 12H). ^{13}C {^{1}H} NMR (126 MHz, $CDCl_3$) δ 148.9 (d, J = 5.4 Hz, C), 147.4 (d, J = 2.4 Hz, C), 132.8 (C), 132.5 (C), 131.5 (C), 130.9 (C), 130.4 (CH), 130.0 (CH), 128.3 (CH), 128.2 (CH), 126.9 (CH), 126.2 (CH), 126.2 (CH), 125.0 (CH), 124.8 (CH), 124.0 (d, J = 5.1 Hz, C), 122.5 (d, J = 2.2 Hz, C), 121.8 (CH), 121.6 (CH), 63.3 (dd, J = 21.0 Hz, J = 2.4 Hz, CH_2), 27.3 (d, J = 13.1 Hz, CH_3), 3.7 (d, J = 17.4 Hz, CH_3). ^{31}P{^{1}H} NMR (162 MHz, $CDCl_3$) δ 142.74 (s), −11.44 (s). $[\alpha]^{27}_D$ = −326.6 (*c* 0.05, THF). HRMS (ESI$^+$) *m/z* calcd for $C_{26}H_{27}O_3P_2$ $[M+H]^+$ 449.1430, found 449.1428.

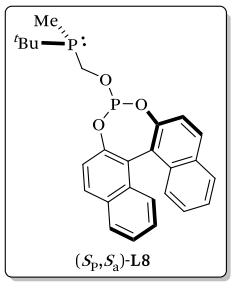

(S_P,S_a)-L8

The general procedure was followed starting from **1** and the chlorophosphite derived from (S_a)-BINOL to yield the P–OP borane complex **2b** as a white solid. DABCO-mediated borane cleavage of the P–OP borane complex afforded the desired P–OP ligand **L8** as a foamy white solid (167 mg, 30% yield), mp = 106–107 °C. ^{1}H NMR (500 MHz, $CDCl_3$) δ 7.99–7.94 (m, 4H), 7.53–7.35 (m, 8H), 4.28 (dt, J = 14.1 Hz, J = 7.1 Hz, 1H), 4.00 (ddd, J = 12.5 Hz, J = 6.4 Hz, J = 3.9 Hz, 1H), 1.04 (d, J = 11.9 Hz, 9H), 0.98 (d, J = 3.2 Hz, 3H). ^{13}C {^{1}H} NMR (126 MHz, $CDCl_3$) δ 148.9 (d, J = 5.1 Hz, C), 147.4 (C), 132.8 (C), 132.5 (C), 131.5 (C),

130.9 (C), 130.4 (CH), 130.0 (CH), 128.3 (CH), 128.2 (CH), 126.9 (CH), 126.2 (CH), 126.2 (CH), 125.0 (CH), 124.8 (CH), 124.0 (d, J = 5.2 Hz, C), 122.5 (C), 121.8 (CH), 121.6 (CH), 63.2 (d, J= 21.4 Hz, CH_2), 27.3 (d, J=13.0 Hz, C), 3.6 (d, J= 17.3 Hz, CH_3). $^{31}P\{^1H\}$ NMR (162 MHz, $CDCl_3$) δ 141.59 (s), –11.28 (s). $[\alpha]^{25}_D$ = +50.1 (*c* 0.27, THF). HRMS (ESI$^+$) *m/z* calcd for $C_{26}H_{27}O_3P_2$ $[M+H]^+$ 449.1430, found 449.1427.

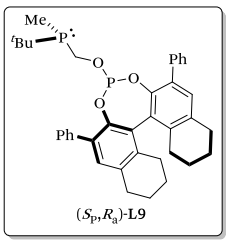

(S_P,R_a)-**L9**

The general procedure was followed starting from **1** and the chlorophosphite derived from (R_a)-3,3'-diphenyl-5,5',6,6',7,7',8,8'-octahydro-[1,1'-binaphtalene]-2,2'-diol[62] to yield the P–OP borane complex **2c** as a crystalline white solid. DABCO-mediated borane cleavage of the P–OP borane complex afforded the desired P–OP ligand **L9** as a foamy white solid (158 mg, 32% yield), mp = 85–89 °C. ^1H NMR (500 MHz, $CDCl_3$) δ 7.63–7.57 (m, 4H), 7.40–7.18 (m, 8H), 3.52–3.45 (m, 1H), 3.14–3.10 (m, 1H), 2.91–2.88 (m, 4H), 2.74–2.72 (m, 2H), 2.43–2.41 (m, 4H), 1.87–1.69 (m, 8H), 0.85 (d, J = 11.8 Hz, 9H), 0.66 (d, J = 3.0 Hz, 3H). $^{13}C\{^1H\}$ NMR (126 MHz, $CDCl_3$) δ 143.4 (C), 143.0 (C), 138.2 (C), 137.5 (C), 137.0 (C) 134.4 (C), 133.8 (C), 132.0 (C), 131.1 (C), 130.4 (C), 130.4 (C), 130.2 (CH), 130.1 (CH), 129.7 (CH), 129.6 (CH), 129.1 (C), 128.0 (CH), 127.9 (CH), 126.9 (CH), 126.8 (CH), 61.2 (dd, J= 23.1 Hz, J= 8.4 Hz, CH_2), 29.3 (CH_2), 27.8 (CH_2), 27.8 (CH_2), 27.3 (d, J =12.9 Hz, C), 27,2 (C), 22.8 (CH_2), 22.8 (CH_2), 22.7 (CH_2), 22.6 (CH_2), 3.3 (d, J = 17.5 Hz, CH_3). $^{31}P\{^1H\}$ NMR (202 MHz, $CDCl_3$) δ 139.86 (d, J= 10.4 Hz), –12.10 (d, J= 10.0 Hz). $[\alpha]^{27}_D$ = –270.5 (*c* 0.19, THF). HRMS (ESI$^+$) *m/z* calcd for $C_{38}H_{43}O_3P_2$ $[M+H]^+$ 609.2682, found 609.2673.

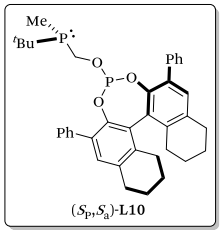

(S_P,S_a)-**L10**

The general procedure was followed starting from **1** and the chlorophosphite derived from (S_a)-3,3'-diphenyl-5,5',6,6',7,7',8,8'-octahydro-[1,1'-binaphtalene]-2,2'-diol[62] to yield the P–OP borane complex **2d** as a white crystalline solid. DABCO-mediated borane cleavage of the P–OP borane complex afforded the desired P–OP ligand **L10** as a foamy white solid (231 mg, 44% yield), mp = 63–65 °C. ^1H NMR (500 MHz,

(62) Erre, G.; Junge, K.; Enthaler, S.; Addis, D.; Michalik, D.; Spannenberg, A.; Beller, M. *Chem.–Asian J.* **2008**, *3*, 887.

$CDCl_3$) δ 7.64–7.57 (m, 4H), 7.40–7.20 (m, 8H), 3.47–3.42 (m, 1H), 3.34–3.28 (m, 1H), 2.92–2.89 (m, 4H), 2.75–2.72 (m, 2H), 2.45–2.42 (m, 4H), 1.88–1.69 (m, 8H), 0.83 (d, J = 11.9 Hz, 9H), 0.73 (d, J = 2.9 Hz, 3H). $^{13}C\{^1H\}$ NMR (126 MHz, $CDCl_3$) δ 143.5 (d, J = 3.0 Hz, C), 143.0 (C), 138.35 (C), 137.5 (C), 137.0 (C) 134.4 (C), 133.8 (C), 132.0 (C), 131.2 (C), 130.5 (C), 130.2 (CH), 130.2 (CH), 130.0 (CH), 129.8 (CH), 129.6 (CH), 129.1 (C), 128.0 (CH), 127.9 (CH), 126.9 (CH), 126.7 (CH), 61.3 (dd, J = 19.8 Hz, J = 10.7 Hz, CH_2), 29.2 (CH_2), 27.8 (CH_2), 27.8 (CH_2), 27.2 (d, J = 12.9 Hz, C), 22.8 (CH_2), 22.7 (CH_2), 22.6 (CH_2), 3.3 (d, J = 17.1 Hz, CH_3). $^{31}P\{^1H\}$ NMR (162 MHz, $CDCl_3$) δ 137.08 (d, J = 11.0 Hz), −11.65 (d, J = 10.6 Hz). $[\alpha]^{27}_D$ = +400.5 (c 0.26, THF). HRMS (ESI$^+$) m/z calcd for $C_{38}H_{43}O_3P_2$ $[M+H]^+$ 609.2682, found 609.2683.

1.5.3. General synthetic procedure for the Rh-complexes [Rh(nbd)(L7,L8)]BF_4

To a stirring solution of $[Rh(nbd)_2]BF_4$ (179 mg, 0.47 mmol) in anhydrous CH_2Cl_2 (5 mL) was slowly added by cannula a solution of the P–OP ligand **L7** or **L8** (178 mg, 0.47 mmol) in anhydrous CH_2Cl_2 (5 mL), and the reaction was stirred for 2 h at room temperature under Ar atmosphere. The solvent was concentrated in vacuo to reach a final volume of ca. 2.5 mL. Anhydrous Et_2O (30 mL) was slowly added by syringe and the resulting solution was slowly stirred to yield an orange suspension. The solvent was filtered off over Celite® under Ar by using a cannula filter, and the resulting solid was washed with anhydrous Et_2O (2 x 20 mL) and dried in vacuo to afford the pure Rh-complex [Rh(nbd)(**L7**,**L8**)]BF_4 as an orange solid.

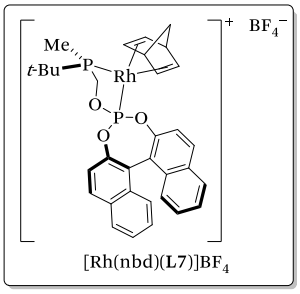

The general procedure was followed starting from $[Rh(nbd)_2]BF_4$ and the P–OP ligand **L7** to yield the pure rhodium (I) complex [Rh(nbd)(**L7**)]BF_4 as an orange solid (331.4 mg, 96% yield), mp = 225 °C (decomp.). ^1H NMR (400 MHz, CD_2Cl_2) δ 8.20–8.01 (m, 4H), 7.77–7.26 (m, 8H), 4.33 (dd, J = 18.7 Hz, J = 12.2 Hz, 1H), 4.06 (ddd, J = 21.6 Hz, J = 12.2 Hz, J = 2.9 Hz, 1H), 1.69 (d, J = 8.7 Hz, 3H), 1.33 (d, J = 15.6 Hz, 9H). $^{13}C\{^1H\}$ NMR (126 MHz, CD_2Cl_2) δ 146.6 (d, J = 12.8 Hz, C), 146.2 (C), 132.4 (C), 132.2 (C), 131.8 (C), 131.4 (CH), 131.1 (CH), 128.6 (CH), 128.5 (CH), 127.0 (CH), 127.0 (CH), 126.9 (CH), 126.6 (CH), 126.1 (CH), 125.9 (CH), 122.6 (C), 121.8 (C), 120.5 (CH), 120.3 (CH), 101.8 (CH), 73.7 (CH_2), 63.9 (dd, J = 22.9 Hz,

J = 17.9 Hz, CH_2), 56.7 (CH), 46.2 (CH), 44.2 (d, *J* = 8.9 Hz, CH), 32.5 (d, *J* = 23.5 Hz, C), 26.5 (CH_3), 6.4 (d, *J* = 21.5 Hz, CH_3). $^{31}P\{^1H\}$ NMR (162 MHz, CD_2Cl_2) δ 171.2 (dd, *J* = 278.1 Hz, *J* = 45.3 Hz), 77.1 (dd, *J* = 150.1 Hz, *J* = 45.1 Hz). $[\alpha]^{26}_D$ = −125.2 (*c* 0.14, CH_2Cl_2). HRMS (MALDI$^+$) *m/z* calcd for $C_{33}H_{34}O_3P_2Rh$ $[M–BF_4]^+$ 643.1033, found 643.0957.

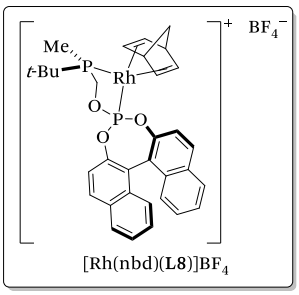

[Rh(nbd)(**L8**)]BF_4

The general procedure was followed starting from [Rh(nbd)$_2$]BF_4 and the P–OP ligand **L8** to yield the pure rhodium (I) complex [Rh(nbd)(**L8**)]BF_4 as an orange solid (136.2 mg, 67% yield), mp = 245 °C (decomp.). ^1H NMR (400 MHz, CD_2Cl_2) δ 8.22–8.01 (m, 4H), 7.67–7.33 (m, 8H), 6.03 (bs, 1H), 4.46 (ddd, *J* = 33.9 Hz, *J* = 12.4 Hz, *J* = 5.0 Hz, 1H), 4.24 (bs, 2H), 4.07 (ddd, *J* = 12.4 Hz, *J* = 6.8 Hz, *J* = 1.5 Hz, 1H), 3.73–3.69 (m, 2H), 1.86–1.83 (m, 3H), 1.67 (dd, *J* = 9.2 Hz, *J* = 1.1 Hz, 3H), 1.30 (d, *J* = 15.7 Hz, 9H). $^{13}C\{^1H\}$ NMR (126 MHz, CD_2Cl_2) δ 146.8 (d, *J* = 13.1 Hz, C), 145.9 (d, *J* = 6.0 Hz, C), 132.4 (C), 132.1 (C), 131.9 (C), 131.8 (C), 131.3 (C), 131.1 (CH), 131.1 (CH), 128.7 (CH), 128.6 (CH), 127.1 (CH), 127.0 (CH), 126.9 (CH), 126.6 (CH), 126.1 (CH), 125.9 (CH), 123.3 (C), 121.7 (C), 120.6 (CH), 120.6 (CH), 73.3 (CH_2), 67.7 (CH), 63.7 (dd, *J* = 24.7 Hz, *J* = 18.0 Hz, CH_2), 56.9 (CH), 46.3 (CH), 33.6 (d, *J* = 22.9 Hz, C), 27.3 (d, *J* = 5.4 Hz, CH_3), 25.5 (CH), 4.6 (d, *J* = 23.1 Hz, CH_3). $^{31}P\{^1H\}$ NMR (162 MHz, CD_2Cl_2) δ 172.0 (dd, *J* = 277.6 Hz, *J* = 46.8 Hz), 79.6 (dd, *J* = 150.0 Hz, *J* = 47.4 Hz). $[\alpha]^{26}_D$ = +108.9 (*c* 0.25, CH_2Cl_2). HRMS (MALDI$^+$) *m/z* calcd for $C_{33}H_{34}O_3P_2Rh$ $[M–BF_4]^+$ 643.1033, found 643.0865.

1.5.4. In situ coordination studies of the complex [Rh(κ^{2}O,O'-acac)(L7)]

The ability of the P–OP ligands **L7–L10** to coordinate to the neutral rhodium precursor suitable for asymmetric hydroformylation [Rh(κ^{2}O,O'-acac)(CO)$_2$] was studied by NMR and HRMS. Stoichiometric amounts of [Rh(κ^{2}O,O'-acac)(CO)$_2$] were added to the selected P–OP ligand **L7**, and the resulting corresponding pre-catalyst [Rh(κ^{2}O,O'-acac)(P–OP)] was studied by NMR. The NMR and HRMS data corroborate a bidentate coordination of the ligands to the metal center.

[Rh(κ^2O,O'-acac)(**L7**)]. $^{31}P\{^1H\}$ NMR (162 MHz, d_8-toluene) δ 176.7 (dd, J = 323.6 Hz, J = 75.5 Hz), 94.3 (dd, J = 178.6 Hz, J = 74.8 Hz). HRMS (MALDI$^+$) *m/z* calcd for $C_{31}H_{33}O_5P_2Rh$ $[M]^+$ 650.0853, found 650.0814.

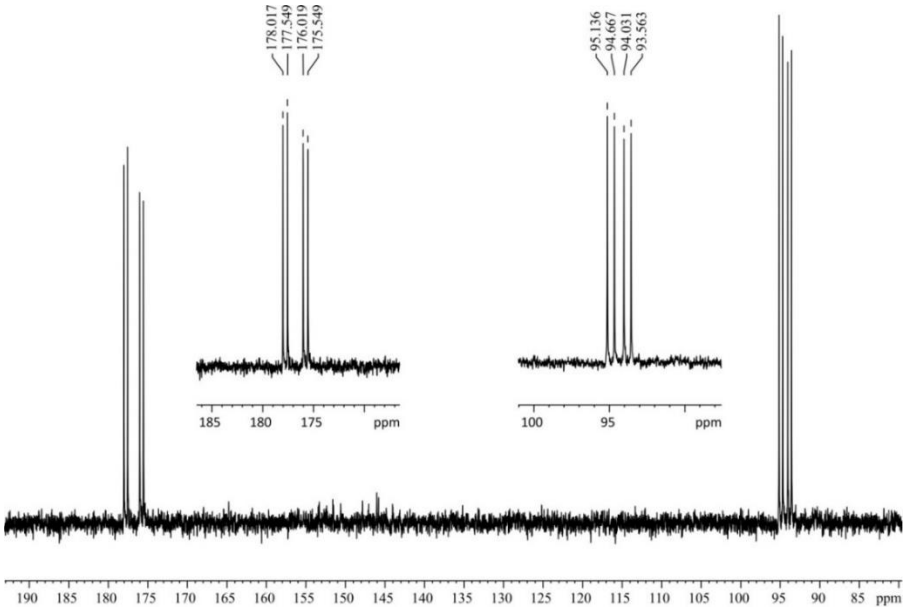

Figure 17. $^{31}P\{^1H\}$ NMR (162 MHz, d_8-toluene) spectrum of the Rh-complex [Rh(κ^2O,O'-acac)(**L7**)].

1.5.5. General procedure for the Rh-mediated asymmetric hydrogenations

The following procedure was performed in a glove box: A solution of the required amount of the rhodium precursor $[Rh(nbd)_2]BF_4$ and the P–OP ligand (10% molar excess relative to the rhodium precursor), or of the $[Rh(nbd)(P–OP)]BF_4$ complex (in the case of the use of preformed precatalysts), and the corresponding alkene (0.1 mmol) in anhydrous and degassed THF were placed in a glass vessel. In all cases the molar concentration of a given substrate was adjusted to 0.2 M. The reaction mixtures were loaded into an autoclave reactor (HEL Cat-24 parallel pressure multi-reactor) under N_2. The autoclave reactor was purged three times with H_2 and finally, pressurized with H_2 at 20 bar. The reaction mixtures were stirred for 24 h at rt. The autoclave reactor was then slowly depressurized. The general work-up for the hydrogenation crudes was: rapid filtration on silica gel (2 cm of silica in a Pasteur pipette) eluting with EtOAc (1.5 mL) and evaporation of the solvent in vacuo. Conversions were determined by ^1H NMR,

and the enantioselectivities of the hydrogenation products were determined by GC or HPLC analysis on chiral stationary phases.

1.5.6. Characterization of the hydrogenation products and determination of the enantiomeric excesses

Hydrogenation product of 4a (5a):[33b] GC conditions: Supelco Beta Dex™ 225 column (30 m x 0.25 mm x 0.25 μm), isothermal 70 °C, 15 psi He. Retention times for the enantiomers: 51.7 min (*S*) and 54.9 min (*R*).

Hydrogenation product of 4b (5b):[63] HPLC conditions: Daicel Chiralpak® AD-H (25 cm x 0.46 cm), 95:5 *n*-hexane/2-propanol, 1.0 mL/min, 216 nm. Retention times for the enantiomers: 13.0 min (*R*) and 16.5 min (*S*).

Hydrogenation product of 4c (5c):[64] HPLC conditions: Daicel Chiralcel® OD-H (25 cm x 0.46 cm), 99:1 *n*-hexane/2-propanol, 0.3 mL/min, 216 nm. Retention times for the enantiomers: 20.0 min (*R*) and 21.8 min (*S*).

Hydrogenation product of 4d (5d):[33b] GC conditions: Supelco Beta Dex™ 120 column (30 m x 0.25 mm x 0.25 μm), isothermal 90 °C, 15 psi He. Retention times for the enantiomers: 54.7 min (*S*) and 55.3 min (*R*).

1.5.7. General procedure for the Rh-mediated asymmetric hydroformylations

The following procedure was performed in a glove box: A solution of the required amount of rhodium precursor [Rh(κ^2O,O'-acac)(CO)$_2$], the P–OP ligand (10% molar excess relative to the rhodium precursor) and the corresponding alkene (0.1 mmol) in anhydrous and degassed toluene was placed in a glass vessel. In all cases the molar concentration of a given substrate was adjusted to 0.5 M. The reaction mixtures were loaded into an autoclave reactor (HEL Cat-24 parallel pressure multi-reactor) under N_2. The autoclave reactor was purged three times with 1:1 H_2/CO and finally, pressurized with 1:1 H_2/CO at 10 bar. The reaction mixtures were stirred for 18 h at 40 °C. The autoclave reactor was then slowly depressurized.

(63) Yu, L.; Wang, Z.; Wu, J.; Tu, S.; Ding, K. *Angew. Chem., Int. Ed.* **2010**, *49*, 3627-3630.
(64) Paeivioe, M.; Mavrynsky, D.; Leino, R.; Kanerva, L. T. *Eur. J. Org. Chem.* **2011**, 1452-1457.

Conversions were determined by ^{1}H NMR, and the enantioselectivities and regioselectivities of the hydroformylation products were determined by GC analysis on chiral stationary phases without treating the samples.

1.5.8. Characterization of the hydroformylation products and determination of the enantiomeric excesses

Hydroformylation product of 6a (7a and 8a):[65] GC conditions: Supelco Beta Dex™ 225 column (30 m x 0.25 mm x 0.25 μm). Temperature program: 100 °C for 5 min, then 4 °C/min to 160 °C. Retention times: 12.3 min (*R*) and 12.6 min (*S*) for the enantiomers of **7a** (branched regioisomer), and 16.3 min for **8a** (linear regioisomer).

Hydroformylation product of 6b (7b and 8b):[65] GC conditions: Supelco Beta Dex™ 225 column (30 m x 0.25 mm x 0.25 μm). Temperature program: 100 °C for 5 min, then 4 °C/min to 160 °C. Retention times: 6.9 min (*R*) and 8.6 min (*S*) for the enantiomers of **7b** (branched regioisomer), and 11.7 min for **8b** (linear regioisomer).

Hydroformylation product of 6c (7c and 8c):[66] GC conditions: Supelco Beta Dex™ 225 column (30 m x 0.25 mm x 0.25 μm). Temperature program: isothermal 65 °C. Retention times: 19.3 min (*R*) and 20.3 min (*S*) for the enantiomers of **7c** (branched regioisomer), and 35.4 min for **8c** (linear regioisomer).

1.5.9. Single-crystal X-ray structure determinations

The ORTEP-Plot of **3** ([Rh(η^6-C_7H_8)(**L7**)]BF_4) is presented in Figure 15.

Crystal preparation: Crystals of the P–OP borane complexes **2c–d** were grown via slow evaporation of the solvent (toluene) and crystals of the rhodium complex **3** ([Rh(η^6-C_7H_8)(**L7**)]BF_4) were obtained from a solution of the rhodium complex [Rh(nbd)(**L7**)]BF_4 in a mixture of toluene and

(65) (a) Cobley, C. J.; Klosin, J.; Qin, C.; Whiteker, G. T. *Org. Lett.* **2004**, *6*, 3277-3280. (b) Cobley, C. J.; Klosin, J.; Qin, C.; Whiteker, G. T. *Org. Lett.* **2005**, *7*, 1197. (c) Zhao, B.; Peng, X.; Wang, Z.; Xia, C.; Ding, K. *Chem. – Eur. J.* **2008**, *14*, 7847-7857.
(66) McDonald, R. I.; Wong, G. W.; Neupane, R. P.; Stahl, S. S.; Landis, C. R. *J. Am. Chem. Soc.* **2010**, *132*, 14027-14029.

dichloromethane. The measured crystals were prepared under inert conditions immersed in perfluoropolyether as protecting oil for manipulation.

Data collection: Crystal structure of compounds **2c–d** and **3** ([Rh(η^6-C_7H_8)(**L7**)]BF_4) were determined using a Bruker-Nonius diffractometer equipped with an APPEX 2 4K CCD area detector, a FR591 rotating anode with MoKα radiation, Montel mirrors as monochromator and a Kryoflex low temperature device (T = −173 °C). Full-sphere data collection was used with ω and φ scans. *Programs used:* Data collection APEX-2,[67] data reduction Bruker Saint[68] V/.60A and absorption correction SADABS.[69]

Structure Solution and Refinement: Crystal structure solutions were achieved using direct methods as implemented in SHELXTL.[70] The crystal data and structure parameters are listed in Table 3.

Comments to the 3 ([Rh(η^6-C_7H_8)(L7)]BF_4) structure: The asymmetric unit contains one molecule of the cationic metal complex, one BF_4 anion and a half molecule of dichloromethane. The metal complex molecule is partially disordered in two orientations (ratio: 68:32). The BF_4 anion is disordered in two orientations (ratio 54:46). The dichloromethane molecules are also disordered in diffuse positions with occupancy of 0.25 and 0.25. The compound crystallizes in the chiral space group $P2_1$ and the absolute structure was determined correctly (Flack: 0.046(53), Parson's: 0.043(23)).[71]

Comments to the structure of 2c: The asymmetric unit contains two independent molecules of the analyzed compound and three molecules of toluene. One of the main molecules is partially disordered (ratio 60:40). One of the toluene molecules is also disordered in two positions (ratio 55:45). The

(67) Data collection with APEX II v2009.1-02. Bruker (2007). Bruker AXS Inc., Madison, Wisconsin, USA.
(68) Data reduction with Bruker SAINT V7.60A. Bruker (2007). Bruker AXS Inc., Madison, Wisconsin, USA.
(69) SADABS: V2008/1 Bruker (2001). Bruker AXS Inc., Madison, Wisconsin, USA. Blessing, *Acta Cryst.* (1995) A51 33-38.
(70) Sheldrick, G.M. *Acta Cryst.* **2008** A64, 112-122. SHELXTL versions V6.12 and 6.14.
(71) Parsons, S.; Flack ,H. *Acta Cryst.* A39 (2004) S61.

compound crystallizes in the chiral space group P_1 and the absolute structure was determined correctly (Flack: 0.014(51), Parson's: 0.056(27)).71

Comments to the structure of 2d: This compound crystallizes in the chiral space group $P2_12_12_1$ and the absolute structure was determined correctly (Flack: 0.013((49), Parson's: 0.010(9)).71 The atoms C5, C6, C7 and C8 are disordered in two conformations (ratio 60:40).

Complete crystallographic data have been deposited at the Cambridge Crystallographic Data Center (reference numbers CCDC 995568–995570 for compounds **3** ([Rh(η^6-C_7H_8)(**L7**)]BF_4), **2c** and **2d**, respectively) and may be obtained free of charge from the CCDC, 12 Union Road, Cambridge, CB2 1EZ, U.K. (fax, +44-1223-336033; web: http://www.ccdc.cam.ac.uk/conts/retrieving.html).

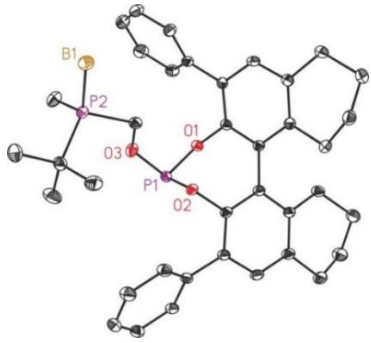

Figure 18. ORTEP-Plot (thermal ellipsoids shown at 50 % probability level) showing one of the independent molecules in the crystal structure of compound **2c** with toluene molecules and all hydrogen atoms omitted for clarity.

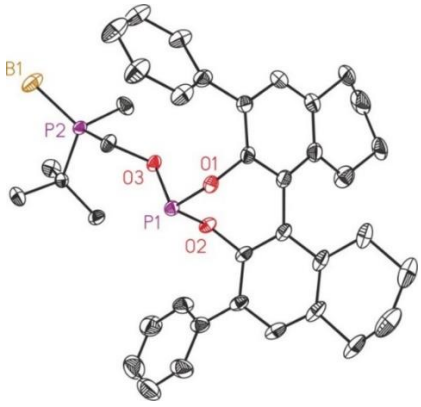

Figure 19. ORTEP-Plot (thermal ellipsoids shown at 50 % probability level) of compound **2d** with and all hydrogen atoms omitted for clarity.

Table 3. Crystal data and structural parameters for 3 ([Rh(η^6-C_7H_8)(L7)]BF_4)

compound	3 ([Rh(η^6-C_7H_8)(L7)]BF_4)
Formula	$C_{33}H_{34}BF_4O_3P_2Rh + 0.5\ (CH_2Cl_2)$
Solvent	CH_2Cl_2
Formula weight	772.72
Temperature (K)	100(2)
Wavelength (Å)	0.71073
Crystal system	Monoclinic
Space group	$P2_1$
a (Å)	10.2792(8)
b (Å)	9.3315(7)
c (Å)	18.8328(13)
α (°)	90
β (°)	100.810(2)
γ (°)	90
Volume (Å^3)	1774.4(2)
Z	2
ρ (Mg/m^3)	1.466
μ (mm^{-1})	0.699
Crystal size (mm^3)	0.20 x 0.10 x 0.04
θ_{max} (°)	31.832
Reflect. collected	17149
Independent reflection	7358 [R(int) = 0.0242]
Absorpt. correction	SADABS
Goodnes-of-fit (F^2)	1.067
R1/wR2 [I>2σ(I)]	0.0768/0.2223
R1/wR2 (all data)	0.0807/0.2277
Flack param. (std)	0.04(2)
Peak/hole (e/Å^{-3})	2.190/–0.717

Table 4. Bond lengths [Å] and angles [°] for 3 ([Rh(η^6-C_7H_8)(L7)]BF_4)

Bond lengths [Å]			
Rh1-P1	2.200(3)	C7-C8	1.382(8)
Rh1-P2	2.230(4)	C8-C9	1.437(8)
Rh1-C31	2.277(12)	C9-C10	1.440(7)
Rh1-C30	2.278(11)	C10-C11	1.487(7)
Rh1-C32	2.308(11)	C11-C20	1.378(7)
Rh1-C29	2.314(12)	C11-C12	1.435(7)
Rh1-C27	2.345(10)	C12-C13	1.413(8)
Rh1-C28	2.366(12)	C12-C17	1.433(8)
Rh1'-P1	2.031(6)	C13-C14	1.396(9)
Rh1'-P2'	2.224(10)	C14-C15	1.380(11)
Rh1'-C30'	2.35(3)	C15-C16	1.395(11)
Rh1'-C32'	2.39(3)	C16-C17	1.424(9)
Rh1'-C27'	2.394(18)	C17-C18	1.413(10)
Rh1'-C29'	2.42(3)	C18-C19	1.327(10)
Rh1'-C31'	2.43(3)	C19-C20	1.421(8)
Rh1'-C28'	2.47(3)	P2-C26	1.797(12)
P1-O3	1.586(17)	P2-C21	1.822(14)
P1-O2	1.603(5)	P2-C22	1.855(11)
P1-O1	1.616(5)	O3-C21	1.442(10)
P1-O3'	1.67(4)	C22-C25	1.476(19)
O1-C1	1.412(7)	C22-C23	1.506(14)
O2-C20	1.388(8)	C22-C24	1.536(16)
C1-C10	1.371(8)	P2'-C26'	1.797(13)
C1-C2	1.396(8)	P2'-C21'	1.823(15)
C2-C3	1.383(10)	P2'-C22'	1.857(12)
C3-C4	1.422(10)	O3'-C21'	1.442(11)
C4-C5	1.391(7)	C22'-C25'	1.475(19)
C4-C9	1.407(7)	C22'-C23'	1.506(15)
C5-C6	1.408(11)	C22'-C24'	1.537(17)
C6-C7	1.416(10)	C27-C28	1.382(8)

C27-C32	1.400(8)	B1-F3	1.371(10)
C27-C33	1.495(7)	B1-F1	1.385(11)
C28-C29	1.417(11)	B1-F2	1.386(10)
C29-C30	1.416(11)	B1-F4	1.398(10)
C30-C31	1.385(9)	B1'-F3'	1.366(11)
C31-C32	1.439(9)	B1'-F1'	1.382(12)
C27'-C28'	1.385(8)	B1'-F2'	1.387(12)
C27'-C32'	1.403(8)	B1'-F4'	1.398(12)
C27'-C33'	1.510(9)	C1S-Cl1S	1.774(11)
C28'-C29'	1.415(11)	C1S-Cl2S	1.776(12)
C29'-C30'	1.415(11)	C1S'-Cl1'	1.773(13)
C30'-C31'	1.384(9)	C1S'-Cl2'	1.775(13)
C31'-C32'	1.439(9)		

Bond angles [°]

P1-Rh1-P2	81.32(12)	C29-Rh1-C27	62.2(3)
P1-Rh1-C31	129.2(3)	P1-Rh1-C28	126.4(3)
P2-Rh1-C31	126.5(3)	P2-Rh1-C28	125.6(3)
P1-Rh1-C30	162.9(4)	C31-Rh1-C28	75.2(3)
P2-Rh1-C30	103.6(3)	C30-Rh1-C28	64.1(4)
C31-Rh1-C30	35.4(3)	C32-Rh1-C28	62.7(3)
P1-Rh1-C32	106.6(3)	C29-Rh1-C28	35.2(3)
P2-Rh1-C32	162.3(3)	C27-Rh1-C28	34.1(2)
C31-Rh1-C32	36.6(3)	P1-Rh1'-P2'	85.8(3)
C30-Rh1-C32	64.3(3)	P1-Rh1'-C30'	166.1(6)
P1-Rh1-C29	159.5(4)	P2'-Rh1'-C30'	103.3(7)
P2-Rh1-C29	103.6(3)	P1-Rh1'-C32'	105.8(6)
C31-Rh1-C29	63.7(3)	P2'-Rh1'-C32'	155.7(7)
C30-Rh1-C29	35.9(3)	C30'-Rh1'-C32'	61.9(6)
C32-Rh1-C29	74.6(3)	P1-Rh1'-C27'	101.3(5)
P1-Rh1-C27	106.6(3)	P2'-Rh1'-C27'	165.2(6)
P2-Rh1-C27	158.6(3)	C30'-Rh1'-C27'	72.4(6)
C31-Rh1-C27	63.9(3)	C32'-Rh1'-C27'	34.1(3)
C30-Rh1-C27	74.7(3)	P1-Rh1'-C29'	151.9(7)
C32-Rh1-C27	35.0(2)	P2'-Rh1'-C29'	108.2(7)

C32'-Rh1'-C29'	71.4(7)	C2-C1-O1	116.0(6)
C27'-Rh1'-C29'	60.1(5)	C3-C2-C1	118.4(6)
P1-Rh1'-C31'	132.5(6)	C2-C3-C4	119.9(6)
P2'-Rh1'-C31'	122.9(7)	C5-C4-C9	120.9(5)
C30'-Rh1'-C31'	33.6(4)	C5-C4-C3	118.7(5)
C32'-Rh1'-C31'	34.8(4)	C9-C4-C3	120.5(5)
C27'-Rh1'-C31'	61.1(5)	C4-C5-C6	119.2(6)
C29'-Rh1'-C31'	60.0(6)	C5-C6-C7	120.8(5)
P1-Rh1'-C28'	119.8(6)	C8-C7-C6	119.9(7)
P2'-Rh1'-C28'	132.3(6)	C7-C8-C9	119.7(6)
C30'-Rh1'-C28'	61.3(6)	C4-C9-C8	119.3(4)
C32'-Rh1'-C28'	60.1(6)	C4-C9-C10	119.3(5)
C27'-Rh1'-C28'	33.1(4)	C8-C9-C10	121.4(5)
C29'-Rh1'-C28'	33.7(4)	C1-C10-C9	117.0(5)
C31'-Rh1'-C28'	70.6(7)	C1-C10-C11	120.0(5)
O3-P1-O2	104.9(7)	C9-C10-C11	123.0(5)
O3-P1-O1	98.3(6)	C20-C11-C12	117.9(5)
O2-P1-O1	101.0(2)	C20-C11-C10	120.1(5)
O2-P1-O3'	102.4(15)	C12-C11-C10	121.9(5)
O1-P1-O3'	90.6(14)	C13-C12-C17	118.1(5)
O2-P1-Rh1'	122.3(3)	C13-C12-C11	123.5(5)
O1-P1-Rh1'	120.3(3)	C17-C12-C11	118.4(5)
O3'-P1-Rh1'	114.5(5)	C14-C13-C12	121.3(6)
O3-P1-Rh1	116.1(3)	C15-C14-C13	120.6(7)
O2-P1-Rh1	111.1(2)	C14-C15-C16	120.1(6)
O1-P1-Rh1	122.9(2)	C15-C16-C17	120.8(6)
C1-O1-P1	117.9(4)	C18-C17-C16	121.1(6)
C20-O2-P1	123.1(4)	C18-C17-C12	119.9(6)
C10-C1-C2	124.7(5)	C16-C17-C12	119.0(6)

C18-C19-C20	119.7(6)	C23'-C22'-P2'	107.5(8)
C11-C20-O2	120.3(5)	C24'-C22'-P2'	108.4(12)
C11-C20-C19	122.5(6)	C28-C27-C32	122.0(6)
O2-C20-C19	117.1(5)	C28-C27-C33	119.4(8)
C26-P2-C21	105.3(8)	C32-C27-C33	118.6(8)
C26-P2-C22	104.9(6)	C28-C27-Rh1	73.8(5)
C21-P2-C22	105.2(5)	C32-C27-Rh1	71.1(5)
C26-P2-Rh1	114.1(6)	C33-C27-Rh1	128.3(3)
C21-P2-Rh1	106.8(4)	C27-C28-C29	118.6(7)
C22-P2-Rh1	119.4(5)	C27-C28-Rh1	72.1(4)
C21-O3-P1	114.8(10)	C29-C28-Rh1	70.4(4)
O3-C21-P2	109.9(7)	C30-C29-C28	120.9(7)
C25-C22-C23	112.5(13)	C30-C29-Rh1	70.7(5)
C25-C22-C24	109.8(10)	C28-C29-Rh1	74.4(4)
C23-C22-C24	110.2(10)	C31-C30-C29	119.8(8)
C25-C22-P2	108.1(8)	C31-C30-Rh1	72.3(5)
C23-C22-P2	107.5(6)	C29-C30-Rh1	73.4(5)
C24-C22-P2	108.6(10)	C30-C31-C32	119.7(7)
C26'-P2'-C21'	105.5(10)	C30-C31-Rh1	72.3(5)
C26'-P2'-C22'	104.6(8)	C32-C31-Rh1	72.9(4)
C21'-P2'-C22'	105.0(7)	C27-C32-C31	119.1(6)
C26'-P2'-Rh1'	117.7(11)	C27-C32-Rh1	73.9(5)
C21'-P2'-Rh1'	105.1(8)	C31-C32-Rh1	70.5(4)
C22'-P2'-Rh1'	117.7(8)	C28'-C27'-C32'	121.5(7)
C21'-O3'-P1	117.2(15)	C28'-C27'-C33'	120.1(9)
O3'-C21'-P2'	109.8(9)	C32'-C27'-C33'	118.4(8)
C25'-C22'-C23'	112.7(14)	C28'-C27'-Rh1'	76.3(10)
C25'-C22'-C24'	110.0(12)	C32'-C27'-Rh1'	72.6(11)
C23'-C22'-C24'	110.1(12)	C33'-C27'-Rh1'	123.1(13)

C27'-C28'-C29'	118.7(8)	F3-B1-F1	113.2(10)
C27'-C28'-Rh1'	70.6(9)	F3-B1-F2	111.2(10)
C29'-C28'-Rh1'	71.2(15)	F1-B1-F2	106.3(9)
C28'-C29'-C30'	120.8(7)	F3-B1-F4	108.1(9)
C28'-C29'-Rh1'	75.2(15)	F1-B1-F4	107.2(9)
C30'-C29'-Rh1'	70.4(17)	F2-B1-F4	110.7(10)
C31'-C30'-C29'	119.7(9)	F3'-B1'-F1'	113.8(13)
C31'-C30'-Rh1'	76.1(16)	F3'-B1'-F2'	111.8(12)
C29'-C30'-Rh1'	75.1(18)	F1'-B1'-F2'	105.0(12)
C30'-C31'-C32'	119.4(8)	F3'-B1'-F4'	108.1(12)
C30'-C31'-Rh1'	70.3(15)	F1'-B1'-F4'	106.4(12)
C32'-C31'-Rh1'	71.0(15)	F2'-B1'-F4'	111.7(13)
C27'-C32'-C31'	119.1(7)	Cl1S-C1S-Cl2S	110.6(10)
C27'-C32'-Rh1'	73.3(10)	Cl1'-C1S'-Cl2'	110.2(11)
C31'-C32'-Rh1'	74.2(15)		

Table 5. Torsion angles [°] for 3 ([Rh(η^6-C_7H_8)(L7)]BF_4)

Torsion angles [°]			
O3-P1-O1-C1	−160.1(7)	O3-P1-O2-C20	64.3(7)
O2-P1-O1-C1	−53.0(5)	O1-P1-O2-C20	−37.5(5)
O3'-P1-O1-C1	−155.8(13)	O3'-P1-O2-C20	55.6(13)
Rh1'-P1-O1-C1	85.1(5)	Rh1'-P1-O2-C20	−174.5(4)
Rh1-P1-O1-C1	71.3(5)	Rh1-P1-O2-C20	−169.4(4)
P1-O1-C1-C10	75.3(7)	C20-C11-C12-C13	173.3(6)
P1-O1-C1-C2	−107.0(6)	C10-C11-C12-C13	−3.5(8)
C10-C1-C2-C3	−1.1(11)	C20-C11-C12-C17	−5.7(8)
O1-C1-C2-C3	−178.8(6)	C10-C11-C12-C17	177.5(5)
C1-C2-C3-C4	−2.0(11)	C17-C12-C13-C14	−3.2(9)

C2-C3-C4-C5	–178.2(7)	C11-C12-C13-C14	177.8(6)
C2-C3-C4-C9	1.3(11)	C12-C13-C14-C15	2.1(10)
C9-C4-C5-C6	1.1(10)	C13-C14-C15-C16	0.7(11)
C3-C4-C5-C6	–179.4(7)	C14-C15-C16-C17	–2.4(11)
C4-C5-C6-C7	–4.4(11)	C15-C16-C17-C18	–179.6(7)
C5-C6-C7-C8	3.0(11)	C15-C16-C17-C12	1.2(10)
C6-C7-C8-C9	1.6(10)	C13-C12-C17-C18	–177.7(6)
C5-C4-C9-C8	3.5(9)	C11-C12-C17-C18	1.4(8)
C3-C4-C9-C8	–176.0(6)	C13-C12-C17-C16	1.5(8)
C5-C4-C9-C10	–178.1(6)	C11-C12-C17-C16	–179.5(5)
C3-C4-C9-C10	2.4(9)	C16-C17-C18-C19	–176.8(6)
C7-C8-C9-C4	–4.8(9)	C12-C17-C18-C19	2.4(10)
C7-C8-C9-C10	176.8(6)	C17-C18-C19-C20	–1.7(10)
C2-C1-C10-C9	4.7(9)	C12-C11-C20-O2	–177.1(5)
O1-C1-C10-C9	–177.7(5)	C10-C11-C20-O2	–0.2(8)
C2-C1-C10-C11	–174.4(6)	C12-C11-C20-C19	6.6(9)
O1-C1-C10-C11	3.2(9)	C10-C11-C20-C19	–176.5(6)
C4-C9-C10-C1	–5.2(8)	P1-O2-C20-C11	70.3(7)
C8-C9-C10-C1	173.2(6)	P1-O2-C20-C19	–113.2(6)
C4-C9-C10-C11	173.9(5)	C18-C19-C20-C11	–3.0(10)
C8-C9-C10-C11	–7.7(8)	C18-C19-C20-O2	–179.4(6)
C1-C10-C11-C20	–51.0(8)	O2-P1-O3-C21	139.9(12)
C9-C10-C11-C20	129.9(6)	O1-P1-O3-C21	–116.3(13)
C1-C10-C11-C12	125.7(6)	O3'-P1-O3-C21	–146(17)
C9-C10-C11-C12	–53.4(8)	Rh1'-P1-O3-C21	8.9(15)
Rh1-P1-O3-C21	16.8(17)	C21'-P2'-C22'-C24'	–62.3(16)
P1-O3-C21-P2	–33.4(17)	Rh1'-P2'-C22'-C24'	–178.7(15)
C26-P2-C21-O3	157.1(12)	C32-C27-C28-C29	–0.07(17)
C22-P2-C21-O3	–92.4(12)	C33-C27-C28-C29	–179.96(15)
Rh1-P2-C21-O3	35.4(12)	Rh1-C27-C28-C29	–54.7(3)
C26-P2-C22-C25	–81.6(11)	C32-C27-C28-Rh1	54.6(4)
C21-P2-C22-C25	167.6(9)	C33-C27-C28-Rh1	–125.3(4)
Rh1-P2-C22-C25	47.8(9)	C27-C28-C29-C30	0.11(16)

C26-P2-C22-C23	156.7(11)	Rh1-C28-C29-C30	−55.4(4)
C21-P2-C22-C23	46.0(11)	C27-C28-C29-Rh1	55.5(4)
Rh1-P2-C22-C23	−73.8(10)	C28-C29-C30-C31	−0.4(4)
C26-P2-C22-C24	37.5(12)	Rh1-C29-C30-C31	−57.5(4)
C21-P2-C22-C24	−73.2(9)	C28-C29-C30-Rh1	57.2(3)
Rh1-P2-C22-C24	167.0(8)	C29-C30-C31-C32	0.5(5)
O3-P1-O3'-C21'	32(13)	Rh1-C30-C31-C32	−57.6(4)
O2-P1-O3'-C21'	139(3)	C29-C30-C31-Rh1	58.1(4)
O1-P1-O3'-C21'	−119(3)	C28-C27-C32-C31	0.3(4)
Rh1'-P1-O3'-C21'	5(4)	C33-C27-C32-C31	−179.8(3)
Rh1-P1-O3'-C21'	13(4)	Rh1-C27-C32-C31	56.1(4)
P1-O3'-C21'-P2'	−23(4)	C28-C27-C32-Rh1	−55.8(4)
C26'-P2'-C21'-O3'	154(3)	C33-C27-C32-Rh1	124.1(4)
C22'-P2'-C21'-O3'	−96(3)	C30-C31-C32-C27	−0.5(5)
Rh1'-P2'-C21'-O3'	29(3)	Rh1-C31-C32-C27	−57.8(4)
C26'-P2'-C22'-C25'	−70.6(19)	C30-C31-C32-Rh1	57.3(5)
C21'-P2'-C22'-C25'	178.6(17)	C32'-C27'-C28'-C29'	5(3)
Rh1'-P2'-C22'-C25'	62.2(16)	C33'-C27'-C28'-C29'	−175(3)
C26'-P2'-C22'-C23'	167.5(17)	Rh1'-C27'-C28'-C29'	−54(2)
C21'-P2'-C22'-C23'	56.7(16)	C32'-C27'-C28'-Rh1'	59.4(13)
Rh1'-P2'-C22'-C23'	−59.7(15)	C33'-C27'-C28'-Rh1'	−120.6(13)
C26'-P2'-C22'-C24'	48.5(19)	C27'-C28'-C29'-C30'	−2(5)
Rh1'-C28'-C29'-C30'	−56(3)	C28'-C27'-C32'-C31'	−1(3)
C27'-C28'-C29'-Rh1'	54(2)	C33'-C27'-C32'-C31'	179(3)
C28'-C29'-C30'-C31'	−6(5)	Rh1'-C27'-C32'-C31'	60(2)
Rh1'-C29'-C30'-C31'	−64(3)	C28'-C27'-C32'-Rh1'	−61.2(13)
C28'-C29'-C30'-Rh1'	58(3)	C33'-C27'-C32'-Rh1'	118.8(13)
C29'-C30'-C31'-C32'	10(5)	C30'-C31'-C32'-C27'	−7(4)
Rh1'-C30'-C31'-C32'	−53(3)	Rh1'-C31'-C32'-C27'	−60(2)
C29'-C30'-C31'-Rh1'	64(3)	C30'-C31'-C32'-Rh1'	53(3)

Table 6. Crystal data and structural parameters for and 2c,d

compound	2c	2d
Formula	$C_{38}H_{45}BO_3P_2$ + 1.5 (C_7H_8)	0.5 ($C_{38}H_{45}BO_3P_2$)
Solvent	C_7H_8	
Formula weight	760.69	331.24
Temperature (K)	100(2)	100(2)
Wavelength (Å)	0.71073	0.71073
Crystal system	Triclinic	Orthorhombic
Space group	P_1	$P2_12_12_1$
a (Å)	10.9989(12)	8.7598(19)
b (Å)	11.2875(12)	14.617(3)
c (Å)	18.3289(19)	26.903(6)
α (°)	103.662(3)	90
β (°)	90.306(4)	90
γ (°)	105.477(3)	90
Volume (Å^3)	2125.3(4)	3444.8(13)
Z	2	8
ρ (Mg/m^3)	1.189	1.200
μ (mm^{-1})	0.143	0.161
Crystal size (mm^3)	0.18 x 0.08 x 0.04	0.30 x 0.15 x 0.15
θ_{max} (°)	31.882	35.322
Reflect. collected	36290	146108
Independent reflection	17554 [R(int) = 0.0302]	14826 [R(int) = 0.0338]
Absorpt. correction	SADABS	SADABS
Goodnes-of-fit (F^2)	1.080	1.085
R1/wR2 [I>2σ(I)]	0.0398/ 0.0980	0.0358/ 0.0963
R1/wR2 (all data)	0.0482/0.1085	0.0378/0.0983
Flack param. (std)	0.06(3)	0.010(9)
Peak/hole (e/Å^{-3})	0.505/−0.383	0.609/−0.268

Table 7. Bond lengths [Å] and angles [°] for 2c

Bond lengths [Å]			
P1A-O3A	1.6000(18)	C19A-C27A	1.481(3)
P1A-O2A	1.638(2)	C21A-C22A	1.400(3)
P1A-O1A	1.6525(18)	C21A-C26A	1.401(3)
O1A-C1A	1.405(3)	C22A-C23A	1.384(4)
O2A-C20A	1.404(3)	C23A-C24A	1.392(4)
O3A-C33A	1.454(3)	C24A-C25A	1.383(4)
C1A-C10A	1.387(4)	C25A-C26A	1.390(4)
C1A-C2A	1.408(3)	C27A-C32A	1.394(4)
C2A-C3A	1.394(3)	C27A-C28A	1.404(3)
C2A-C21A	1.483(3)	C28A-C29A	1.392(4)
C3A-C4A	1.392(4)	C29A-C30A	1.375(5)
C4A-C9A	1.409(3)	C30A-C31A	1.392(4)
C4A-C5A	1.523(3)	C31A-C32A	1.389(4)
C5A-C6A	1.524(4)	C33A-P2A	1.824(3)
C6A-C7A	1.519(4)	P2A-C38A	1.804(6)
C7A-C8A	1.529(3)	P2A-C34A	1.873(6)
C8A-C9A	1.516(4)	P2A-B1A	1.918(7)
C9A-C10A	1.411(3)	C34A-C36A	1.538(5)
C10A-C11A	1.494(3)	C34A-C37A	1.539(5)
C11A-C20A	1.400(3)	C34A-C35A	1.549(5)
C11A-C12A	1.418(3)	C34'-C36'	1.536(4)
C12A-C17A	1.404(3)	C34'-C37'	1.540(3)
C12A-C13A	1.516(3)	C34'-C35'	1.542(3)
C13A-C14A	1.527(3)	P1B-O3B	1.6062(16)
C14A-C15A	1.521(5)	P1B-O1B	1.6435(19)
C15A-C16A	1.513(4)	P1B-O2B	1.6530(17)
C16A-C17A	1.520(3)	P2B-C38B	1.811(2)
C17A-C18A	1.390(4)	P2B-C33B	1.824(2)
C18A-C19A	1.392(4)	P2B-C34B	1.844(3)
C19A-C20A	1.403(3)	P2B-B1B	1.924(3)

O1B-C1B	1.394(3)	C22B-C23B	1.395(3)
O2B-C20B	1.409(2)	C23B-C24B	1.391(4)
O3B-C33B	1.450(3)	C24B-C25B	1.388(4)
C1B-C10B	1.402(3)	C25B-C26B	1.392(3)
C1B-C2B	1.403(3)	C27B-C28B	1.396(3)
C2B-C3B	1.395(3)	C27B-C32B	1.410(3)
C2B-C21B	1.491(3)	C28B-C29B	1.393(4)
C3B-C4B	1.395(3)	C29B-C30B	1.391(3)
C4B-C9B	1.405(3)	C30B-C31B	1.387(4)
C4B-C5B	1.511(3)	C31B-C32B	1.381(4)
C5B-C6B	1.528(3)	C34B-C36B	1.536(3)
C6B-C7B	1.521(4)	C34B-C37B	1.540(3)
C7B-C8B	1.531(4)	C34B-C35B	1.542(3)
C8B-C9B	1.521(3)	C1S-C2S	1.389(4)
C9B-C10B	1.418(3)	C1S-C6S	1.396(4)
C10B-C11B	1.495(3)	C1S-C7S	1.506(5)
C11B-C20B	1.395(3)	C2S-C3S	1.377(5)
C11B-C12B	1.419(3)	C3S-C4S	1.379(5)
C12B-C17B	1.400(3)	C4S-C5S	1.384(5)
C12B-C13B	1.517(3)	C5S-C6S	1.388(5)
C13B-C14B	1.532(3)	C1T-C2T	1.376(11)
C14B-C15B	1.516(4)	C1T-C6T	1.393(9)
C15B-C16B	1.525(4)	C1T-C7T	1.515(10)
C16B-C17B	1.523(3)	C2T-C3T	1.385(11)
C17B-C18B	1.393(4)	C3T-C4T	1.416(10)
C18B-C19B	1.400(3)	C4T-C5T	1.411(13)
C19B-C20B	1.399(3)	C5T-C6T	1.361(11)
C19B-C27B	1.478(3)	C1T'-C2T'	1.392(7)
C21B-C22B	1.397(3)	C1T'-C6T'	1.402(6)
C21B-C26B	1.405(3)	C1T'-C7T'	1.503(7)

C2T'-C3T'	1.379(7)	C1U-C7U	1.506(5)
C3T'-C4T'	1.377(7)	C2U-C3U	1.392(5)
C4T'-C5T'	1.377(7)	C3U-C4U	1.393(5)
C5T'-C6T'	1.383(7)	C4U-C5U	1.384(5)
C1U-C2U	1.394(4)	C5U-C6U	1.381(5)
C1U-C6U	1.396(4)		

Bond angles [°]

O3A-P1A-O2A	106.96(10)	C1A-C10A-C9A	119.5(2)
O3A-P1A-O1A	97.77(9)	C1A-C10A-C11A	117.1(2)
O2A-P1A-O1A	98.91(9)	C9A-C10A-C11A	123.4(2)
C1A-O1A-P1A	110.29(15)	C20A-C11A-C12A	118.9(2)
C20A-O2A-P1A	123.29(16)	C20A-C11A-C10A	119.2(2)
C33A-O3A-P1A	128.31(15)	C12A-C11A-C10A	121.6(2)
C10A-C1A-O1A	118.2(2)	C17A-C12A-C11A	119.4(2)
C10A-C1A-C2A	123.1(2)	C17A-C12A-C13A	120.2(2)
O1A-C1A-C2A	118.6(2)	C11A-C12A-C13A	120.3(2)
C3A-C2A-C1A	115.9(2)	C12A-C13A-C14A	112.8(2)
C3A-C2A-C21A	122.1(2)	C15A-C14A-C13A	109.7(3)
C1A-C2A-C21A	122.0(2)	C16A-C15A-C14A	110.6(2)
C4A-C3A-C2A	122.9(2)	C15A-C16A-C17A	114.2(2)
C3A-C4A-C9A	119.8(2)	C18A-C17A-C12A	119.4(2)
C3A-C4A-C5A	118.0(2)	C18A-C17A-C16A	118.5(2)
C9A-C4A-C5A	122.0(2)	C12A-C17A-C16A	122.1(2)
C4A-C5A-C6A	113.9(2)	C17A-C18A-C19A	123.2(2)
C7A-C6A-C5A	110.0(2)	C18A-C19A-C20A	116.6(2)
C6A-C7A-C8A	108.9(2)	C18A-C19A-C27A	120.9(2)
C9A-C8A-C7A	111.9(2)	C20A-C19A-C27A	122.5(2)
C4A-C9A-C10A	118.5(2)	C11A-C20A-C19A	122.5(2)
C4A-C9A-C8A	120.1(2)	C11A-C20A-O2A	118.46(19)
C10A-C9A-C8A	121.2(2)	C19A-C20A-O2A	119.1(2)

C22A-C21A-C26A	1187.6(2)	C36'-C34'-C35'	109.9(3)
C22A-C21A-C2A	120.7(2)	C37'-C34'-C35'	109.4(3)
C26A-C21A-C2A	120.6(2)	O3B-P1B-O1B	106.72(10)
C23A-C22A-C21A	120.4(2)	O3B-P1B-O2B	97.36(8)
C22A-C23A-C24A	120.6(3)	O1B-P1B-O2B	98.63(9)
C25A-C24A-C23A	119.4(3)	C38B-P2B-C33B	103.51(11)
C24A-C25A-C26A	120.6(2)	C38B-P2B-C34B	108.47(13)
C25A-C26A-C21A	120.4(2)	C33B-P2B-C34B	108.11(11)
C32A-C27A-C28A	118.7(2)	C38B-P2B-B1B	112.88(13)
C32A-C27A-C19A	121.7(2)	C33B-P2B-B1B	107.68(13)
C28A-C27A-C19A	119.6(2)	C34B-P2B-B1B	115.42(13)
C29A-C28A-C27A	120.5(3)	C1B-O1B-P1B	123.85(14)
C30A-C29A-C28A	120.0(3)	C20B-O2B-P1B	110.12(13)
C29A-C30A-C31A	120.1(3)	C33B-O3B-P1B	127.41(15)
C32A-C31A-C30A	120.2(3)	O1B-C1B-C10B	118.8(2)
C31A-C32A-C27A	120.4(3)	O1B-C1B-C2B	118.62(19)
O3A-C33A-P2A	109.62(17)	C10B-C1B-C2B	122.6(2)
C38A-P2A-C33A	100.3(3)	C3B-C2B-C1B	117.08(19)
C38A-P2A-C34A	118.2(3)	C3B-C2B-C21B	119.3(2)
C33A-P2A-C34A	105.5(2)	C1B-C2B-C21B	123.6(2)
C38A-P2A-B1A	108.6(8)	C2B-C3B-C4B	122.4(2)
C33A-P2A-B1A	106.7(7)	C3B-C4B-C9B	119.7(2)
C34A-P2A-B1A	115.8(6)	C3B-C4B-C5B	117.3(2)
C36A-C34A-C37A	109.1(4)	C9B-C4B-C5B	123.0(2)
C36A-C34A-C35A	109.6(4)	C4B-C5B-C6B	113.5(2)
C37A-C34A-C35A	108.3(4)	C7B-C6B-C5B	109.1(2)
C36A-C34A-P2A	107.2(4)	C6B-C7B-C8B	109.7(2)
C37A-C34A-P2A	108.6(4)	C9B-C8B-C7B	111.99(19)
C35A-C34A-P2A	113.9(4)	C4B-C9B-C10B	119.4(2)
C36'-C34'-C37'	109.1(3)	C4B-C9B-C8B	119.8(2)

C10B-C9B-C8B	120.7(2)	C24B-C25B-C26B	120.6(2)
C1B-C10B-C9B	118.7(2)	C25B-C26B-C21B	120.4(2)
C1B-C10B-C11B	119.4(2)	C28B-C27B-C32B	118.1(2)
C9B-C10B-C11B	121.61(19)	C28B-C27B-C19B	120.6(2)
C20B-C11B-C12B	118.2(2)	C32B-C27B-C19B	121.3(2)
C20B-C11B-C10B	117.77(19)	C29B-C28B-C27B	121.0(2)
C12B-C11B-C10B	124.0(2)	C30B-C29B-C28B	120.0(2)
C17B-C12B-C11B	118.8(2)	C31B-C30B-C29B	119.6(2)
C17B-C12B-C13B	120.31(19)	C32B-C31B-C30B	120.6(2)
C11B-C12B-C13B	120.5(2)	C31B-C32B-C27B	120.7(2)
C12B-C13B-C14B	113.3(2)	O3B-C33B-P2B	109.74(16)
C15B-C14B-C13B	110.1(2)	C36B-C34B-C37B	109.0(2)
C14B-C15B-C16B	110.0(2)	C36B-C34B-C35B	109.9(2)
C17B-C16B-C15B	112.6(2)	C37B-C34B-C35B	109.3(2)
C18B-C17B-C12B	120.6(2)	C36B-C34B-P2B	113.62(18)
C18B-C17B-C16B	117.7(2)	C37B-C34B-P2B	107.32(18)
C12B-C17B-C16B	121.7(2)	C35B-C34B-P2B	107.63(18)
C17B-C18B-C19B	122.0(2)	C2S-C1S-C6S	118.2(3)
C20B-C19B-C18B	116.0(2)	C2S-C1S-C7S	121.7(3)
C20B-C19B-C27B	122.93(19)	C6S-C1S-C7S	120.1(3)
C18B-C19B-C27B	121.0(2)	C3S-C2S-C1S	121.2(3)
C11B-C20B-C19B	124.0(2)	C2S-C3S-C4S	120.2(3)
C11B-C20B-O2B	117.5(2)	C3S-C4S-C5S	119.8(3)
C19B-C20B-O2B	118.4(2)	C4S-C5S-C6S	120.0(3)
C22B-C21B-C26B	118.8(2)	C5S-C6S-C1S	120.6(3)
C22B-C21B-C2B	122.4(2)	C2T-C1T-C6T	117.9(7)
C26B-C21B-C2B	118.7(2)	C2T-C1T-C7T	121.1(7)
C23B-C22B-C21B	120.0(2)	C6T-C1T-C7T	120.9(7)
C24B-C23B-C22B	121.0(2)	C1T-C2T-C3T	122.7(7)
C25B-C24B-C23B	119.1(2)	C2T-C3T-C4T	118.8(8)

C5T-C4T-C3T	118.2(8)	C5T'-C6T'-C1T'	119.8(6)
C6T-C5T-C4T	120.8(7)	C2U-C1U-C6U	117.8(3)
C5T-C6T-C1T	121.5(8)	C2U-C1U-C7U	121.5(3)
C2T'-C1T'-C6T'	118.0(6)	C6U-C1U-C7U	120.8(3)
C2T'-C1T'-C7T'	122.7(7)	C3U-C2U-C1U	121.2(3)
C6T'-C1T'-C7T'	119.3(7)	C2U-C3U-C4U	120.0(3)
C3T'-C2T'-C1T'	121.4(6)	C5U-C4U-C3U	119.2(3)
C4T'-C3T'-C2T'	120.2(6)	C6U-C5U-C4U	120.5(3)
C3T'-C4T'-C5T'	119.2(7)	C5U-C6U-C1U	121.3(3)
C4T'-C5T'-C6T'	121.4(7)		

Table 8. Torsion angles [°] for 2c

Torsion angles [°]			
O3A-P1A-O1A-C1A	–176.23(16)	C2A-C3A-C4A-C5A	–172.8(2)
O2A-P1A-O1A-C1A	–67.61(16)	C3A-C4A-C5A-C6A	–174.9(2)
O3A-P1A-O2A-C20A	75.96(18)	C9A-C4A-C5A-C6A	8.2(3)
O1A-P1A-O2A-C20A	–25.05(17)	C4A-C5A-C6A-C7A	–41.7(3)
O2A-P1A-O3A-C33A	-69.0(2)	C5A-C6A-C7A-C8A	65.7(3)
O1A-P1A-O3A-C33A	32.8(2)	C6A-C7A-C8A-C9A	–54.9(3)
P1A-O1A-C1A-C10A	79.5(2)	C3A-C4A-C9A-C10A	–0.7(3)
P1A-O1A-C1A-C2A	–96.3(2)	C5A-C4A-C9A-C10A	176.1(2)
C10A-C1A-C2A-C3A	–3.4(3)	C3A-C4A-C9A-C8A	–174.7(2)
O1A-C1A-C2A-C3A	172.2(2)	C5A-C4A-C9A-C8A	2.1(3)
C10A-C1A-C2A-C21A	177.4(2)	C7A-C8A-C9A-C4A	21.5(3)
O1A-C1A-C2A-C21A	–7.0(3)	C7A-C8A-C9A-C10A	–152.3(2)
C1A-C2A-C3A-C4A	–2.1(3)	O1A-C1A-C10A-C9A	–168.9(2)
C21A-C2A-C3A-C4A	177.1(2)	C2A-C1A-C10A-C9A	6.7(3)
C2A-C3A-C4A-C9A	4.1(4)	O1A-C1A-C10A-C11A	10.2(3)

C2A-C1A-C10A-C11A	−174.2(2)	C12A-C11A-C20A-O2A	−176.9(2)
C4A-C9A-C10A-C1A	−4.5(3)	C10A-C11A-C20A-O2A	−3.5(3)
C8A-C9A-C10A-C1A	169.4(2)	C18A-C19A-C20A-C11A	−2.5(4)
C4A-C9A-C10A-C11A	176.5(2)	C27A-C19A-C20A-C11A	179.1(2)
C8A-C9A-C10A-C11A	−9.6(3)	C18A-C19A-C20A-O2A	178.0(2)
C1A-C10A-C11A-C20A	−56.7(3)	C27A-C19A-C20A-O2A	−0.4(4)
C9A-C10A-C11A-C20A	122.3(3)	P1A-O2A-C20A-C11A	68.7(3)
C1A-C10A-C11A-C12A	116.5(3)	P1A-O2A-C20A-C19A	−111.8(2)
C9A-C10A-C11A-C12A	−64.4(3)	C3A-C2A-C21A-C22A	135.1(2)
C20A-C11A-C12A-C17A	−2.3(4)	C1A-C2A-C21A-C22A	−45.7(3)
C10A-C11A-C12A-C17A	−175.6(2)	C3A-C2A-C21A-C26A	−43.2(3)
C20A-C11A-C12A-C13A	173.2(2)	C1A-C2A-C21A-C26A	135.9(2)
C10A-C11A-C12A-C13A	−0.1(4)	C26A-C21A-C22A-C23A	−0.4(4)
C17A-C12A-C13A-C14A	19.5(4)	C2A-C21A-C22A-C23A	−178.7(3)
C11A-C12A-C13A-C14A	−156.0(3)	C21A-C22A-C23A-C24A	−0.1(5)
C12A-C13A-C14A-C15A	−51.6(3)	C22A-C23A-C24A-C25A	0.7(5)
C13A-C14A-C15A-C16A	63.5(3)	C23A-C24A-C25A-C26A	−0.7(4)
C14A-C15A-C16A-C17A	−42.0(4)	C24A-C25A-C26A-C21A	0.1(4)
C11A-C12A-C17A-C18A	0.1(4)	C22A-C21A-C26A-C25A	0.4(4)
C13A-C12A-C17A-C18A	−175.4(3)	C2A-C21A-C26A-C25A	178.7(2)
C11A-C12A-C17A-C16A	177.4(3)	C18A-C19A-C27A-C32A	131.0(3)
C13A-C12A-C17A-C16A	1.8(4)	C20A-C19A-C27A-C32A	−50.6(4)
C15A-C16A-C17A-C18A	−173.0(3)	C18A-C19A-C27A-C28A	−47.4(4)
C15A-C16A-C17A-C12A	9.7(4)	C20A-C19A-C27A-C28A	130.9(3)
C12A-C17A-C18A-C19A	1.0(4)	C32A-C27A-C28A-C29A	1.4(4)
C16A-C17A-C18A-C19A	−176.4(3)	C19A-C27A-C28A-C29A	179.9(3)
C17A-C18A-C19A-C20A	0.2(4)	C27A-C28A-C29A-C30A	−2.1(5)
C17A-C18A-C19A-C27A	178.6(3)	C28A-C29A-C30A-C31A	0.8(5)
C12A-C11A-C20A-C19A	3.6(4)	C29A-C30A-C31A-C32A	1.2(5)
C10A-C11A-C20A-C19A	177.1(2)	C30A-C31A-C32A-C27A	−1.9(5)

C28A-C27A-C32A-C31A	0.6(4)	C2B-C3B-C4B-C5B	−179.4(2)
C19A-C27A-C32A-C31A	−177.8(3)	C3B-C4B-C5B-C6B	−174.5(2)
P1A-O3A-C33A-P2A	−159.05(15)	C9B-C4B-C5B-C6B	6.9(3)
O3A-C33A-P2A-C38A	−50.4(3)	C4B-C5B-C6B-C7B	−42.8(3)
O3A-C33A-P2A-C34A	72.9(3)	C5B-C6B-C7B-C8B	66.4(2)
O3A-C33A-P2A-B1A	−163.5(8)	C6B-C7B-C8B-C9B	−52.4(3)
C38A-P2A-C34A-C36A	−76.5(5)	C3B-C4B-C9B-C10B	4.2(3)
C33A-P2A-C34A-C36A	172.5(4)	C5B-C4B-C9B-C10B	−177.2(2)
B1A-P2A-C34A-C36A	54.7(10)	C3B-C4B-C9B-C8B	−171.4(2)
C38A-P2A-C34A-C37A	165.7(5)	C5B-C4B-C9B-C8B	7.1(3)
C33A-P2A-C34A-C37A	54.7(4)	C7B-C8B-C9B-C4B	15.9(3)
B1A-P2A-C34A-C37A	−63.1(9)	C7B-C8B-C9B-C10B	−159.7(2)
C38A-P2A-C34A-C35A	44.9(6)	O1B-C1B-C10B-C9B	−177.65(19)
C33A-P2A-C34A-C35A	−66.2(4)	C2B-C1B-C10B-C9B	1.9(3)
B1A-P2A-C34A-C35A	176.1(9)	O1B-C1B-C10B-C11B	−4.4(3)
O3B-P1B-O1B-C1B	76.48(17)	C2B-C1B-C10B-C11B	175.2(2)
O2B-P1B-O1B-C1B	−23.94(17)	C4B-C9B-C10B-C1B	−4.8(3)
O3B-P1B-O2B-C20B	−177.06(16)	C8B-C9B-C10B-C1B	170.9(2)
O1B-P1B-O2B-C20B	−68.82(16)	C4B-C9B-C10B-C11B	−177.9(2)
O1B-P1B-O3B-C33B	−67.2(2)	C8B-C9B-C10B-C11B	−2.3(3)
O2B-P1B-O3B-C33B	34.1(2)	C1B-C10B-C11B-C20B	−55.1(3)
P1B-O1B-C1B-C10B	68.3(2)	C9B-C10B-C11B-C20B	117.9(2)
P1B-O1B-C1B-C2B	−111.3(2)	C1B-C10B-C11B-C12B	124.5(2)
O1B-C1B-C2B-C3B	−178.93(19)	C9B-C10B-C11B-C12B	−62.4(3)
C10B-C1B-C2B-C3B	1.5(3)	C20B-C11B-C12B-C17B	−6.9(3)
O1B-C1B-C2B-C21B	4.2(3)	C10B-C11B-C12B-C17B	173.5(2)
C10B-C1B-C2B-C21B	−175.3(2)	C20B-C11B-C12B-C13B	166.1(2)
C1B-C2B-C3B-C4B	−2.1(3)	C10B-C11B-C12B-C13B	−13.6(3)
C21B-C2B-C3B-C4B	174.9(2)	C17B-C12B-C13B-C14B	−22.9(3)
C2B-C3B-C4B-C9B	−0.7(3)	C11B-C12B-C13B-C14B	164.2(2)

C12B-C13B-C14B-C15B	49.2(3)	C22B-C23B-C24B-C25B	0.5(5)
C13B-C14B-C15B-C16B	−63.3(3)	C23B-C24B-C25B-C26B	−0.2(5)
C14B-C15B-C16B-C17B	49.4(3)	C24B-C25B-C26B-C21B	−0.8(4)
C11B-C12B-C17B-C18B	3.7(3)	C22B-C21B-C26B-C25B	1.4(4)
C13B-C12B-C17B-C18B	−169.3(2)	C2B-C21B-C26B-C25B	−177.9(2)
C11B-C12B-C17B-C16B	−176.9(2)	C20B-C19B-C27B-C28B	133.7(2)
C13B-C12B-C17B-C16B	10.2(4)	C18B-C19B-C27B-C28B	−42.9(3)
C15B-C16B-C17B-C18B	156.0(2)	C20B-C19B-C27B-C32B	−47.2(3)
C15B-C16B-C17B-C12B	−23.4(4)	C18B-C19B-C27B-C32B	136.2(2)
C12B-C17B-C18B-C19B	2.2(4)	C32B-C27B-C28B-C29B	−0.2(3)
C16B-C17B-C18B-C19B	−177.2(2)	C19B-C27B-C28B-C29B	178.9(2)
C17B-C18B-C19B-C20B	−4.6(3)	C27B-C28B-C29B-C30B	0.1(3)
C17B-C18B-C19B-C27B	172.2(2)	C28B-C29B-C30B-C31B	−0.3(4)
C12B-C11B-C20B-C19B	4.6(3)	C29B-C30B-C31B-C32B	0.6(4)
C10B-C11B-C20B-C19B	−175.8(2)	C30B-C31B-C32B-C27B	−0.7(4)
C12B-C11B-C20B-O2B	−170.62(19)	C28B-C27B-C32B-C31B	0.5(3)
C10B-C11B-C20B-O2B	9.0(3)	C19B-C27B-C32B-C31B	−178.7(2)
C18B-C19B-C20B-C11B	1.1(3)	P1B-O3B-C33B-P2B	−160.07(14)
C27B-C19B-C20B-C11B	−175.6(2)	C38B-P2B-C33B-O3B	−48.5(2)
C18B-C19B-C20B-O2B	176.26(19)	C34B-P2B-C33B-O3B	66.38(18)
C27B-C19B-C20B-O2B	−0.5(3)	B1B-P2B-C33B-O3B	−168.29(17)
P1B-O2B-C20B-C11B	80.4(2)	C38B-P2B-C34B-C36B	43.2(2)
P1B-O2B-C20B-C19B	−95.1(2)	C33B-P2B-C34B-C36B	−68.4(2)
C3B-C2B-C21B-C22B	137.7(3)	B1B-P2B-C34B-C36B	171.01(18)
C1B-C2B-C21B-C22B	−45.5(3)	C38B-P2B-C34B-C37B	−77.38(19)
C3B-C2B-C21B-C26B	−43.1(3)	C33B-P2B-C34B-C37B	171.01(17)
C1B-C2B-C21B-C26B	133.7(2)	B1B-P2B-C34B-C37B	50.4(2)
C26B-C21B-C22B-C23B	−1.0(4)	C38B-P2B-C34B-C35B	165.11(16)
C2B-C21B-C22B-C23B	178.2(2)	C33B-P2B-C34B-C35B	53.50(18)
C21B-C22B-C23B-C24B	0.1(4)	B1B-P2B-C34B-C35B	−67.12(19)

C6S-C1S-C2S-C3S	–0.6(5)	C6T'-C1T'-C2T'-C3T'	1(2)
C7S-C1S-C2S-C3S	177.9(3)	C7T'-C1T'-C2T'-C3T'	178.5(13)
C1S-C2S-C3S-C4S	–0.2(5)	C1T'-C2T'-C3T'-C4T'	–0.8(17)
C2S-C3S-C4S-C5S	0.9(5)	C2T'-C3T'-C4T'-C5T'	1.4(16)
C3S-C4S-C5S-C6S	–0.9(5)	C3T'-C4T'-C5T'-C6T'	–2.4(19)
C4S-C5S-C6S-C1S	0.1(5)	C4T'-C5T'-C6T'-C1T'	3(2)
C2S-C1S-C6S-C5S	0.6(5)	C2T'-C1T'-C6T'-C5T'	–2.0(19)
C7S-C1S-C6S-C5S	–177.9(3)	C7T'-C1T'-C6T'-C5T'	–179.5(14)
C6T-C1T-C2T-C3T	–0.6(15)	C6U-C1U-C2U-C3U	0.5(4)
C7T-C1T-C2T-C3T	178.9(11)	C7U-C1U-C2U-C3U	–179.0(3)
C1T-C2T-C3T-C4T	3.0(15)	C1U-C2U-C3U-C4U	0.0(5)
C2T-C3T-C4T-C5T	–3.1(15)	C2U-C3U-C4U-C5U	–0.1(5)
C3T-C4T-C5T-C6T	0.9(17)	C3U-C4U-C5U-C6U	–0.3(5)
C4T-C5T-C6T-C1T	1.6(17)	C4U-C5U-C6U-C1U	0.8(4)
C2T-C1T-C6T-C5T	–1.8(15)	C2U-C1U-C6U-C5U	–0.9(4)
C7T-C1T-C6T-C5T	178.7(12)	C7U-C1U-C6U-C5U	178.6(3)

Table 9. Bond lengths [Å] and angles [°] for 2d

Bond lengths [Å]			
P1-O3	1.6197(10)	C1-C10	1.3963(18)
P1-O1	1.6383(10)	C1-C2	1.3997(19)
P1-O2	1.6425(10)	C2-C3	1.395(2)
P2-C34	1.8045(15)	C2-C21	1.482(2)
P2-C33	1.8295(13)	C3-C4	1.398(2)
P2-C35	1.8482(13)	C4-C9	1.407(2)
P2-B1	1.9164(17)	C4-C5	1.503(6)
O1-C1	1.4005(16)	C4-C5'	1.559(9)
O2-C20	1.4008(15)	C5-C6	1.534(8)
O3-C33	1.4411(15)	C6-C7	1.544(6)

C7-C8	1.469(3)	C19-C20	1.4058(19)
C5'-C6'	1.524(10)	C19-C27	1.483(2)
C6'-C7'	1.507(9)	C21-C22	1.399(2)
C7'-C8	1.556(5)	C21-C26	1.403(2)
C8-C9	1.520(2)	C22-C23	1.389(2)
C9-C10	1.4044(19)	C23-C24	1.390(3)
C10-C11	1.494(2)	C24-C25	1.380(3)
C11-C20	1.391(2)	C25-C26	1.398(2)
C11-C12	1.4114(18)	C27-C32	1.398(2)
C12-C17	1.406(2)	C27-C28	1.405(2)
C12-C13	1.508(2)	C28-C29	1.395(4)
C13-C14	1.536(2)	C29-C30	1.388(5)
C14-C15	1.513(4)	C30-C31	1.386(4)
C15-C16	1.497(3)	C31-C32	1.399(3)
C16-C17	1.517(2)	C35-C36	1.5328(18)
C17-C18	1.393(3)	C35-C38	1.5343(18)
C18-C19	1.400(2)	C35-C37	1.5355(18)

Bond angles [°]

O3-P1-O1	103.47(5)	C2-C1-O1	119.48(11)
O3-P1-O2	93.28(5)	C3-C2-C1	116.10(13)
O1-P1-O2	100.53(5)	C3-C2-C21	122.35(13)
C34-P2-C33	103.02(7)	C1-C2-C21	121.42(13)
C34-P2-C35	107.98(7)	C2-C3-C4	122.49(14)
C33-P2-C35	107.55(6)	C3-C4-C9	120.01(14)
C34-P2-B1	112.36(9)	C3-C4-C5	119.9(3)
C33-P2-B1	109.31(8)	C9-C4-C5	119.9(3)
C35-P2-B1	115.76(7)	C3-C4-C5'	116.4(4)
C1-O1-P1	118.47(8)	C9-C4-C5'	122.7(5)
C20-O2-P1	112.22(8)	C4-C5-C6	110.7(5)
C33-O3-P1	116.58(8)	C5-C6-C7	109.1(4)
C10-C1-C2	123.19(12)	C8-C7-C6	110.2(3)
C10-C1-O1	117.20(11)	C6'-C5'-C4	114.5(8)

C7'-C6'-C5'	111.7(6)	C11-C20-O2	116.86(11)
C6'-C7'-C8	117.4(5)	C11-C20-C19	123.05(12)
C7-C8-C9	114.5(2)	O2-C20-C19	119.99(12)
C9-C8-C7'	112.8(3)	C22-C21-C26	118.03(14)
C10-C9-C4	118.59(14)	C22-C21-C2	121.70(13)
C10-C9-C8	119.55(14)	C26-C21-C2	120.16(15)
C4-C9-C8	121.57(14)	C23-C22-C21	120.84(15)
C1-C10-C9	119.26(13)	C22-C23-C24	120.41(17)
C1-C10-C11	117.16(11)	C25-C24-C23	119.74(16)
C9-C10-C11	123.45(12)	C24-C25-C26	120.10(16)
C20-C11-C12	119.56(13)	C25-C26-C21	120.87(17)
C20-C11-C10	117.39(11)	C32-C27-C28	117.89(18)
C12-C11-C10	122.68(13)	C32-C27-C19	121.38(14)
C17-C12-C11	118.49(14)	C28-C27-C19	120.60(16)
C17-C12-C13	121.62(13)	C29-C28-C27	120.4(2)
C11-C12-C13	119.69(14)	C30-C29-C28	120.9(2)
C12-C13-C14	112.76(16)	C31-C30-C29	119.5(2)
C15-C14-C13	112.35(16)	C30-C31-C32	119.9(2)
C16-C15-C14	109.86(16)	C27-C32-C31	121.46(18)
C15-C16-C17	112.64(16)	O3-C33-P2	110.26(8)
C18-C17-C12	120.01(12)	C36-C35-C38	109.82(11)
C18-C17-C16	118.46(15)	C36-C35-C37	109.08(11)
C12-C17-C16	121.52(17)	C38-C35-C37	109.24(11)
C17-C18-C19	122.84(13)	C36-C35-P2	113.74(9)
C18-C19-C20	115.81(14)	C38-C35-P2	107.16(9)
C18-C19-C27	120.99(13)	C37-C35-P2	107.71(9)
C20-C19-C27	123.20(12)		

Table 10. Torsion angles [°] for 2d

Torsion angles [°]			
O3-P1-O1-C1	–52.61(9)	C6'-C7'-C8-C9	38.8(6)
O2-P1-O1-C1	43.38(9)	C3-C4-C9-C10	–1.2(3)
O3-P1-O2-C20	157.94(9)	C5-C4-C9-C10	173.9(3)
O1-P1-O2-C20	53.58(10)	C5'-C4-C9-C10	–170.3(5)
O1-P1-O3-C33	–100.03(9)	C3-C4-C9-C8	172.64(18)
O2-P1-O3-C33	158.32(9)	C5-C4-C9-C8	–12.3(4)
P1-O1-C1-C10	–73.14(13)	C5'-C4-C9-C8	3.5(5)
P1-O1-C1-C2	102.87(12)	C7-C8-C9-C10	–166.9(2)
C10-C1-C2-C3	1.8(2)	C7'-C8-C9-C10	160.3(3)
O1-C1-C2-C3	–173.96(13)	C7-C8-C9-C4	19.4(3)
C10-C1-C2-C21	177.66(13)	C7'-C8-C9-C4	–13.5(3)
O1-C1-C2-C21	1.91(19)	C2-C1-C10-C9	–6.3(2)
C1-C2-C3-C4	3.1(3)	O1-C1-C10-C9	169.55(12)
C21-C2-C3-C4	–172.71(16)	C2-C1-C10-C11	177.68(12)
C2-C3-C4-C9	–3.4(3)	O1-C1-C10-C11	–6.47(17)
C2-C3-C4-C5	–178.5(3)	C4-C9-C10-C1	5.8(2)
C2-C3-C4-C5'	166.4(5)	C8-C9-C10-C1	–168.13(14)
C3-C4-C5-C6	–154.0(4)	C4-C9-C10-C11	–178.44(14)
C9-C4-C5-C6	30.9(6)	C8-C9-C10-C11	7.6(2)
C5'-C4-C5-C6	–75(3)	C1-C10-C11-C20	61.12(17)
C4-C5-C6-C7	–55.9(5)	C9-C10-C11-C20	–114.72(15)
C5-C6-C7-C8	64.3(5)	C1-C10-C11-C12	–111.89(14)
C3-C4-C5'-C6'	174.0(6)	C9-C10-C11-C12	72.27(19)
C9-C4-C5'-C6'	–16.5(10)	C20-C11-C12-C17	2.20(19)
C5-C4-C5'-C6'	66(3)	C10-C11-C12-C17	175.07(12)
C4-C5'-C6'-C7'	39.0(10)	C20-C11-C12-C13	–172.88(12)
C5'-C6'-C7'-C8	–52.2(8)	C10-C11-C12-C13	–0.01(19)
C6-C7-C8-C9	–44.6(4)	C17-C12-C13-C14	12.4(2)
C6-C7-C8-C7'	49.0(6)	C11-C12-C13-C14	–172.71(14)
C6'-C7'-C8-C7	–61.1(6)	C12-C13-C14-C15	–42.2(2)

C13-C14-C15-C16	62.5(2)	C23-C24-C25-C26	0.6(3)
C14-C15-C16-C17	−50.6(2)	C24-C25-C26-C21	0.0(3)
C11-C12-C17-C18	2.1(2)	C22-C21-C26-C25	−1.0(2)
C13-C12-C17-C18	177.05(13)	C2-C21-C26-C25	175.32(16)
C11-C12-C17-C16	−177.20(13)	C18-C19-C27-C32	−141.48(15)
C13-C12-C17-C16	−2.2(2)	C20-C19-C27-C32	37.9(2)
C15-C16-C17-C18	−157.57(16)	C18-C19-C27-C28	34.3(2)
C15-C16-C17-C12	21.7(2)	C20-C19-C27-C28	−146.32(15)
C12-C17-C18-C19	−3.4(2)	C32-C27-C28-C29	1.2(3)
C16-C17-C18-C19	175.90(13)	C19-C27-C28-C29	−174.66(17)
C17-C18-C19-C20	0.32(19)	C27-C28-C29-C30	−1.9(3)
C17-C18-C19-C27	179.77(13)	C28-C29-C30-C31	0.9(4)
C12-C11-C20-O2	170.81(11)	C29-C30-C31-C32	0.6(4)
C10-C11-C20-O2	−2.43(17)	C28-C27-C32-C31	0.3(2)
C12-C11-C20-C19	−5.51(19)	C19-C27-C32-C31	176.19(16)
C10-C11-C20-C19	−178.75(12)	C30-C31-C32-C27	−1.3(3)
P1-O2-C20-C11	−81.26(12)	P1-O3-C33-P2	−141.82(7)
P1-O2-C20-C19	95.18(12)	C34-P2-C33-O3	−39.54(11)
C18-C19-C20-C11	4.18(18)	C35-P2-C33-O3	74.38(10)
C27-C19-C20-C11	−175.25(12)	B1-P2-C33-O3	−159.20(11)
C18-C19-C20-O2	−172.03(11)	C34-P2-C35-C36	66.03(11)
C27-C19-C20-O2	8.54(18)	C33-P2-C35-C36	−44.52(11)
C3-C2-C21-C22	−144.84(16)	B1-P2-C35-C36	−167.04(11)
C1-C2-C21-C22	39.5(2)	C34-P2-C35-C38	−172.41(10)
C3-C2-C21-C26	39.0(2)	C33-P2-C35-C38	77.04(10)
C1-C2-C21-C26	−136.65(15)	B1-P2-C35-C38	−45.48(13)
C26-C21-C22-C23	1.4(2)	C34-P2-C35-C37	−54.98(11)
C2-C21-C22-C23	−174.84(15)	C33-P2-C35-C37	−165.53(9)
C21-C22-C23-C24	−0.8(3)	B1-P2-C35-C37	71.95(13)
C22-C23-C24-C25	−0.2(3)		

1.5.10. NMR spectra of new compounds

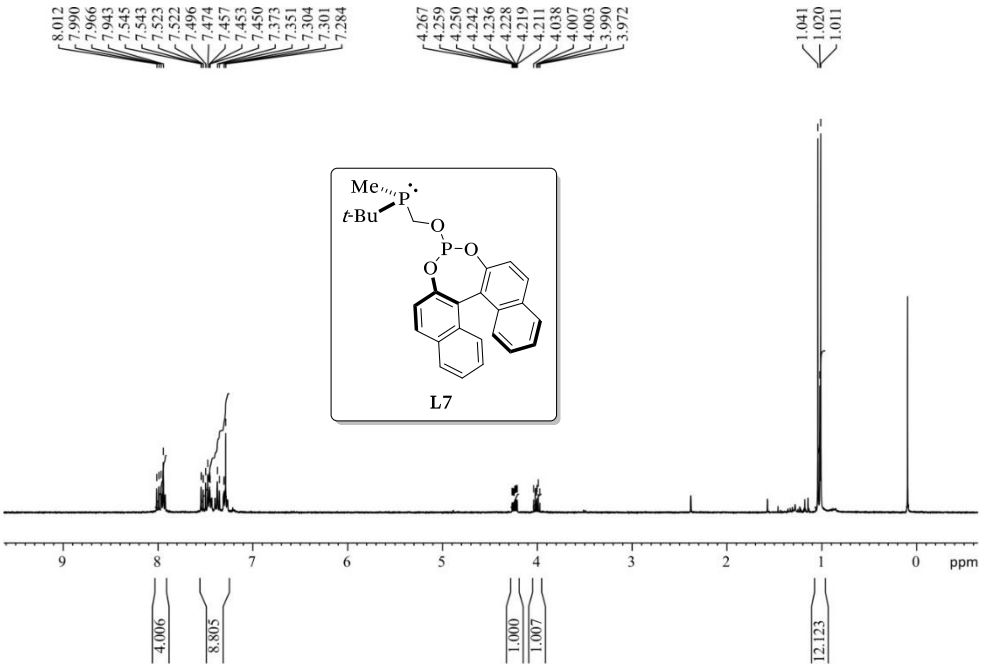

Figure 20. ^{1}H NMR (400 MHz, $CDCl_3$) of the P–OP ligand **L7**.

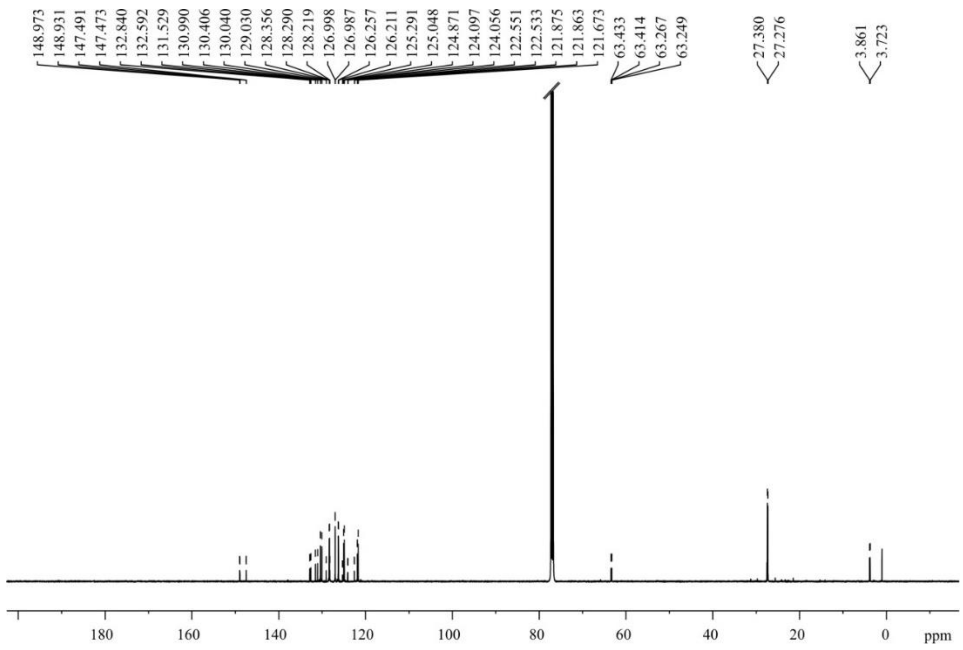

Figure 21. $^{13}C\{^{1}H\}$ NMR (126 MHz, $CDCl_3$) of the P–OP ligand **L7**.

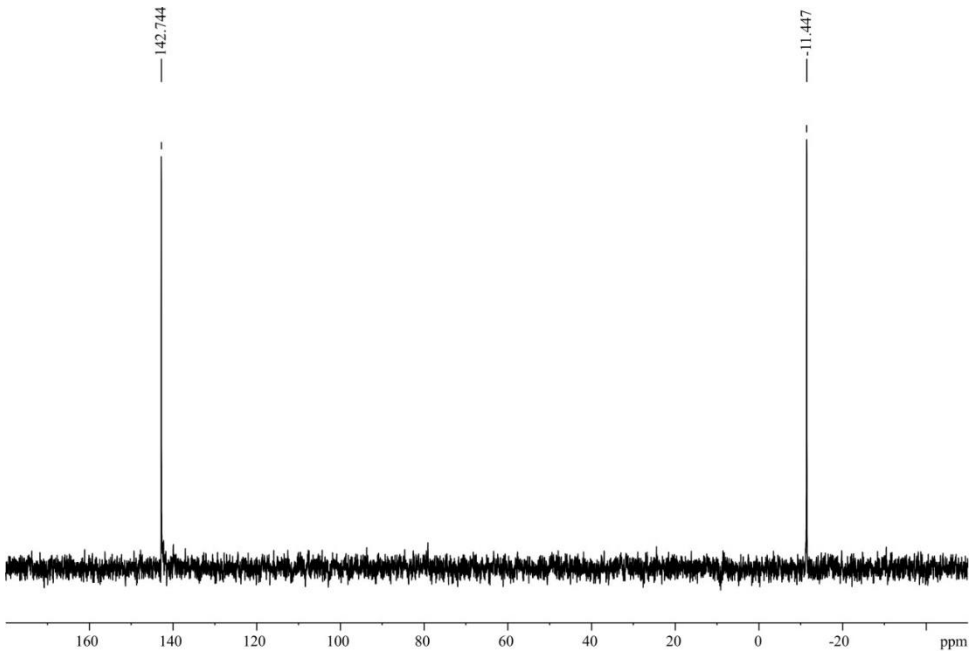

Figure 22. $^{31}P\{^{1}H\}$ NMR (162 MHz, $CDCl_3$) of P–OP ligand **L7**.

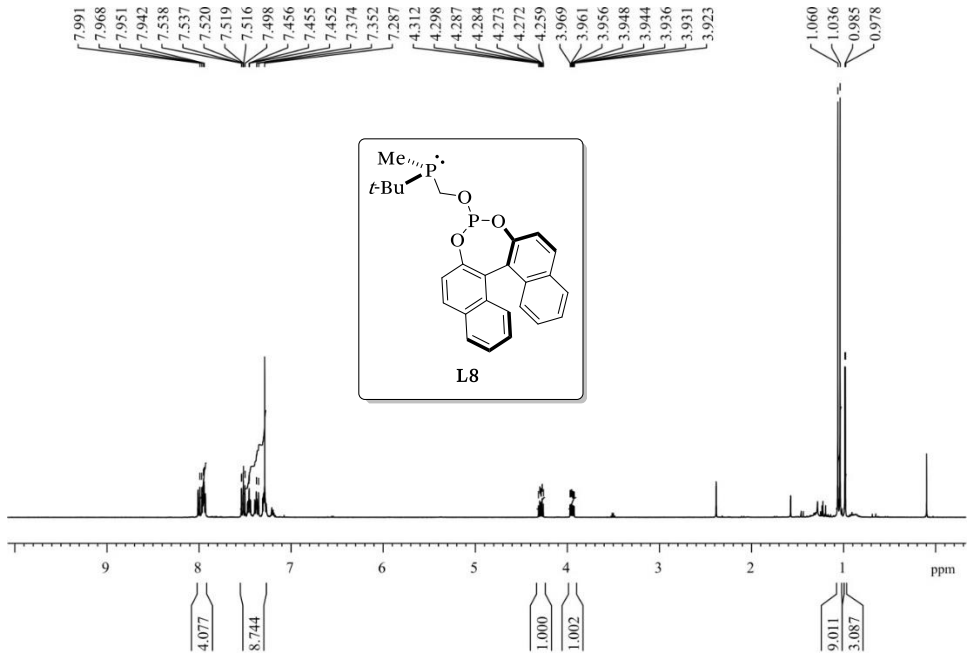

Figure 23. ^{1}H NMR (500 MHz, $CDCl_3$) of the P–OP ligand **L8**.

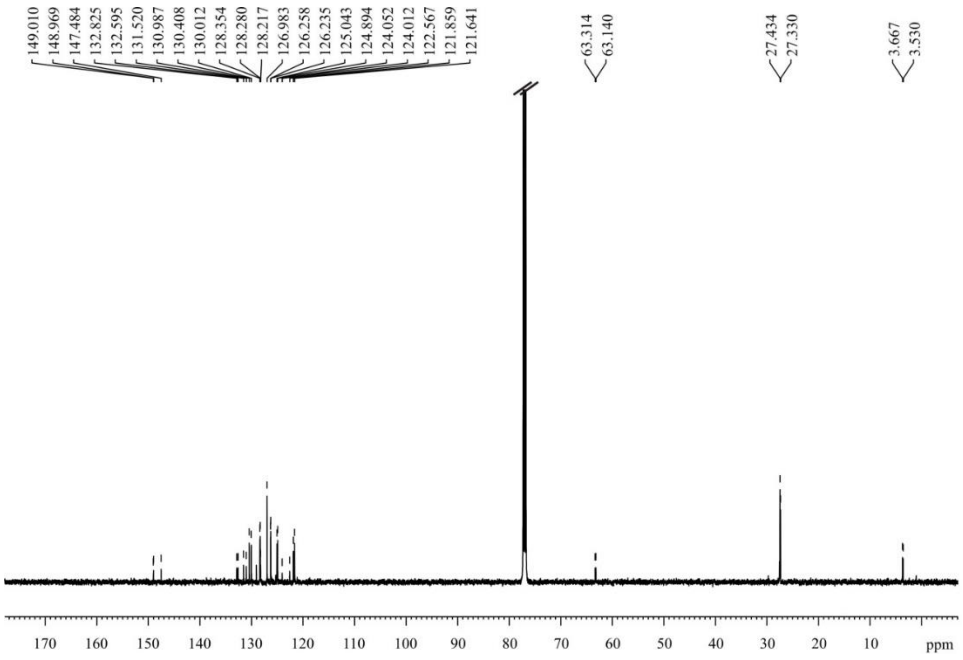

Figure 24. $^{13}C\{^{1}H\}$ NMR (126 MHz, $CDCl_3$) of the P–OP ligand **L8**.

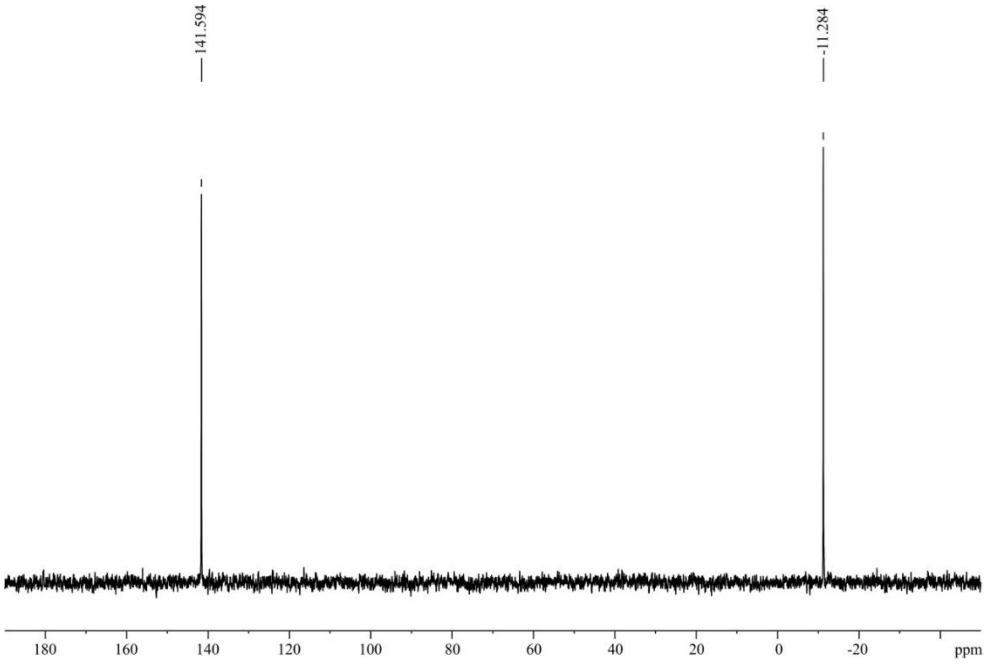

Figure 25. $^{31}P\{^{1}H\}$ NMR (162 MHz, $CDCl_3$) of the P–OP ligand **L8**.

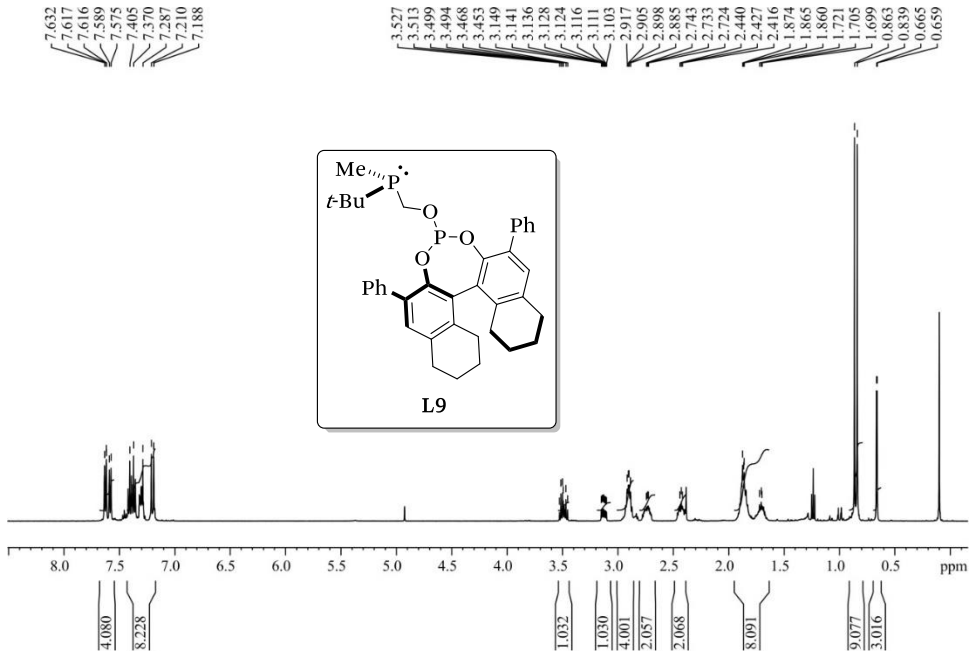

Figure 26. ^{1}H NMR (500 MHz, $CDCl_3$) of the P–OP ligand **L9**.

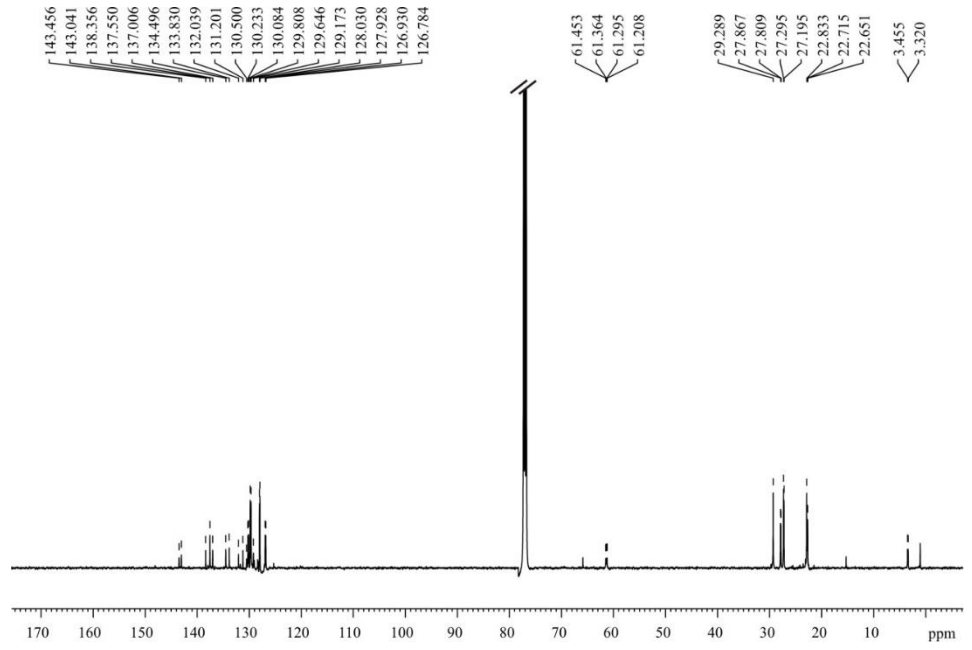

Figure 27. $^{13}C\{^{1}H\}$ NMR (126 MHz, $CDCl_3$) of the P–OP ligand **L9**.

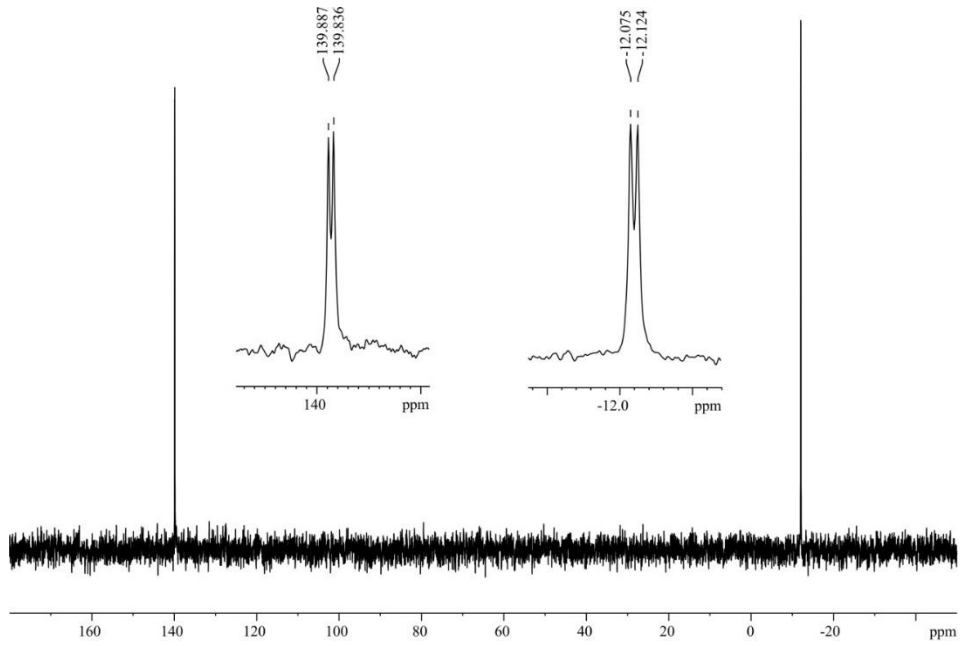

Figure 28. $^{31}P\{^{1}H\}$ NMR (202 MHz, $CDCl_3$) of the P–OP ligand **L9**.

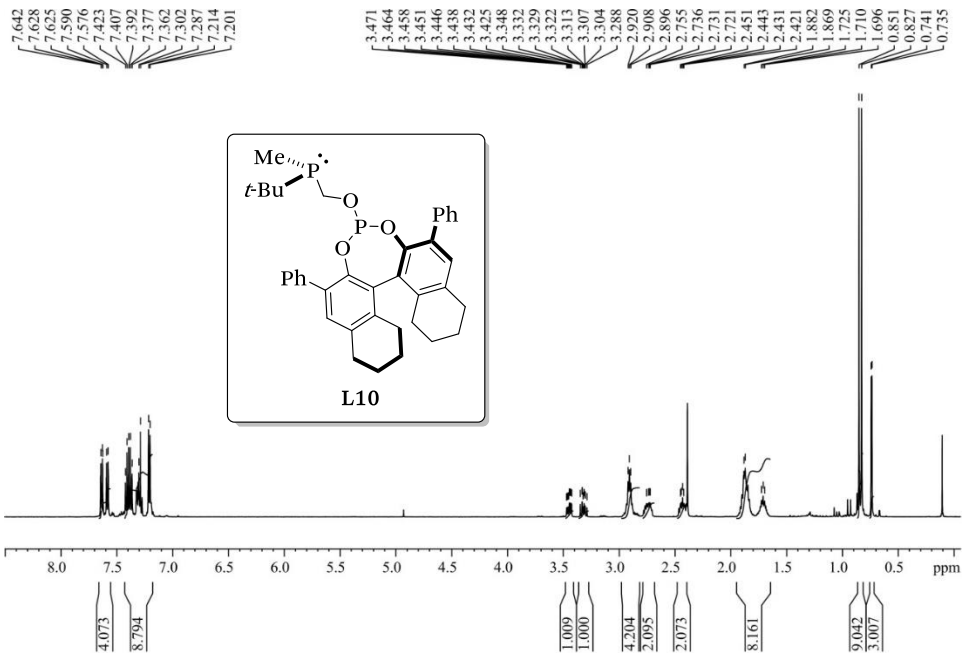

Figure 29. ^{1}H NMR (500 MHz, $CDCl_3$) of the P–OP ligand **L10**.

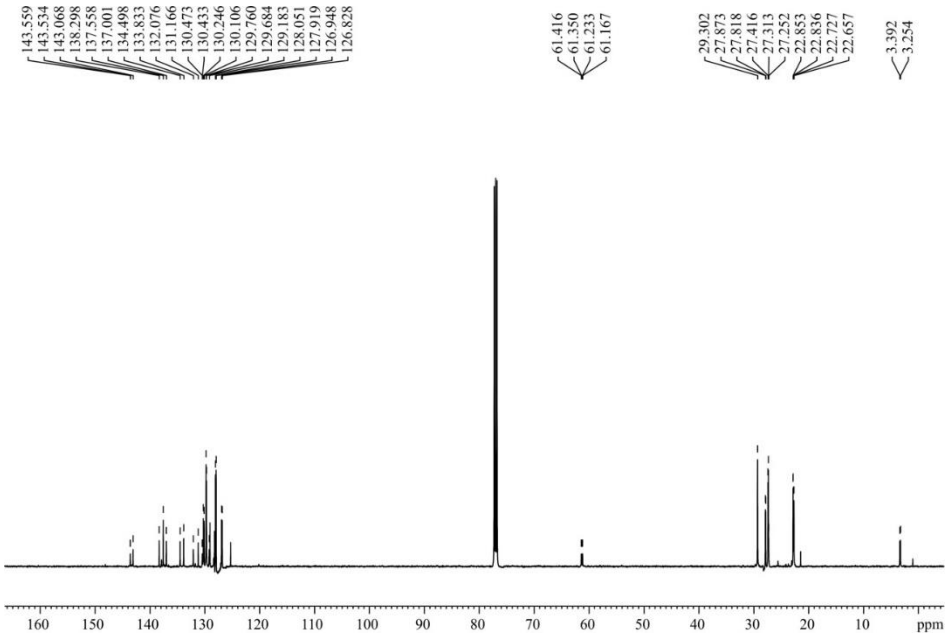

Figure 30. $^{13}C\{^{1}H\}$ NMR (126 MHz, $CDCl_3$) of the P–OP ligand **L10**.

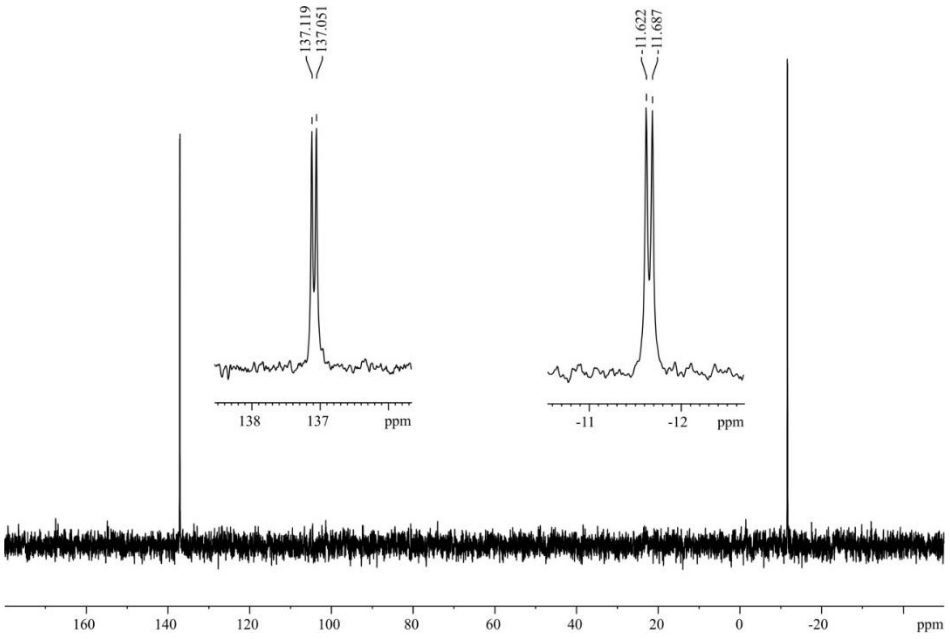

Figure 31. $^{31}P\{^{1}H\}$ NMR (162 MHz, $CDCl_3$) of the P–OP ligand **L10**.

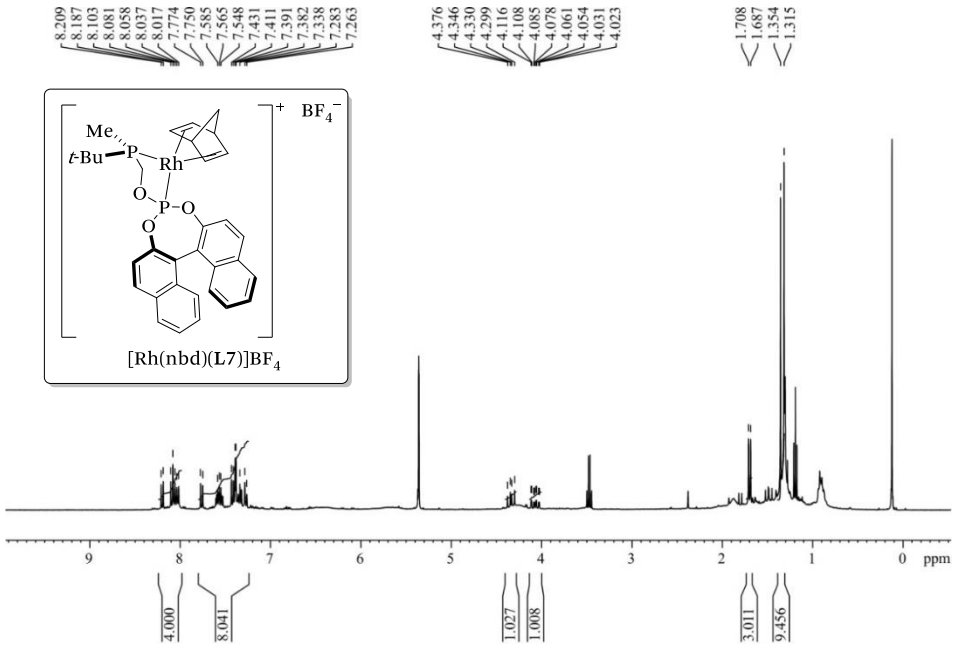

Figure 32. ^{1}H NMR (400 MHz, CD_2Cl_2) of the rhodium complex [Rh(nbd)(**L7**)]BF_4.

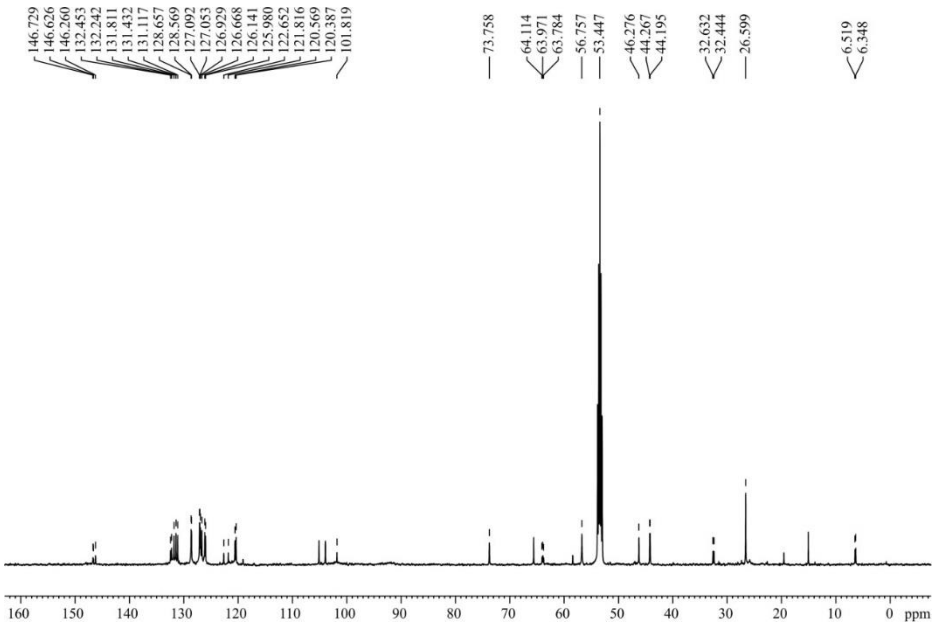

Figure 33. $^{13}C\{^{1}H\}$ NMR (126 MHz, CD_2Cl_2) of the rhodium complex [Rh(nbd)(**L7**)]BF_4.

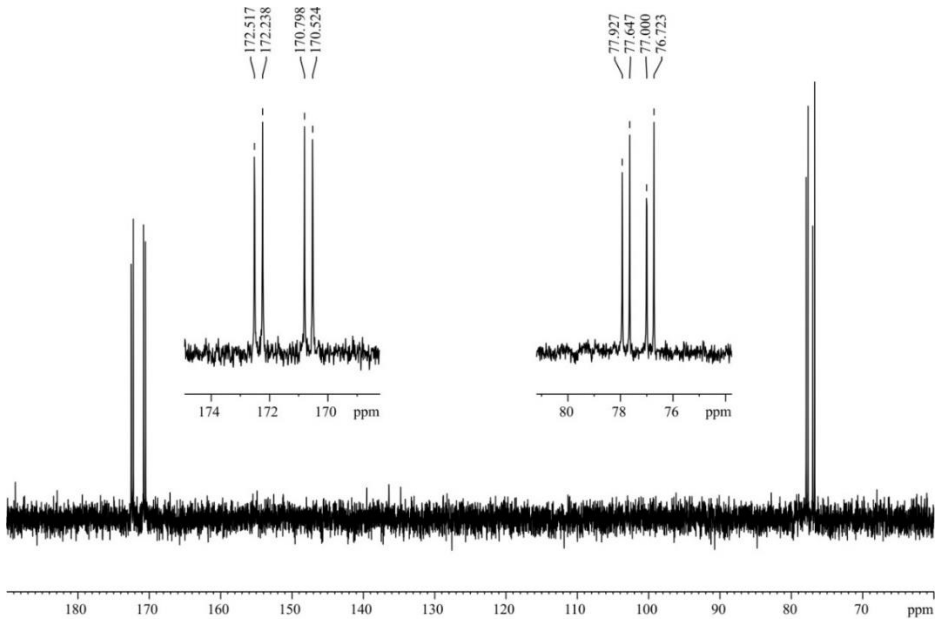

Figure 34. $^{31}P\{^{1}H\}$ NMR (162 MHz, CD_2Cl_2) of the rhodium complex [Rh(nbd)(**L7**)]BF_4.

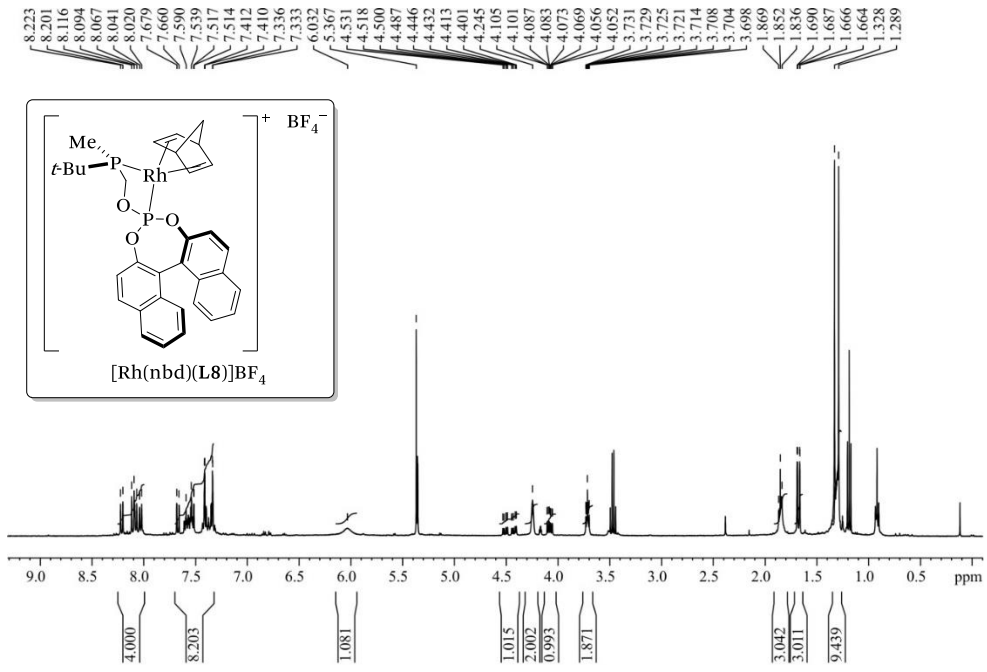

Figure 35. ^{1}H NMR (400 MHz, CD_2Cl_2) of the rhodium complex [Rh(nbd)(**L8**)]BF_4.

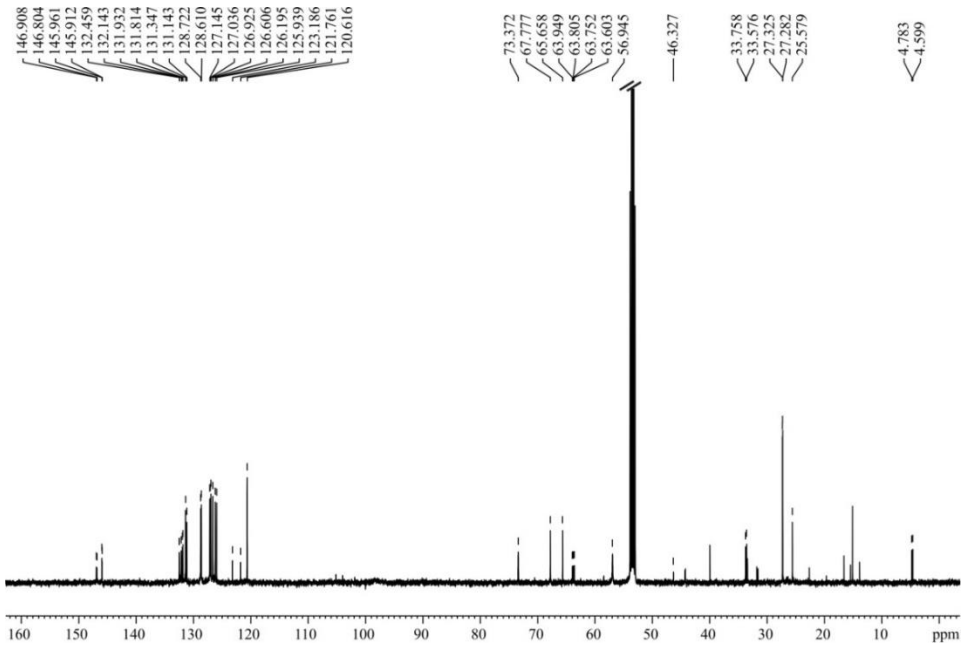

Figure 36. $^{13}C\{^{1}H\}$ NMR (126 MHz, CD_2Cl_2) of the rhodium complex [Rh(nbd)(**L8**)]BF_4.

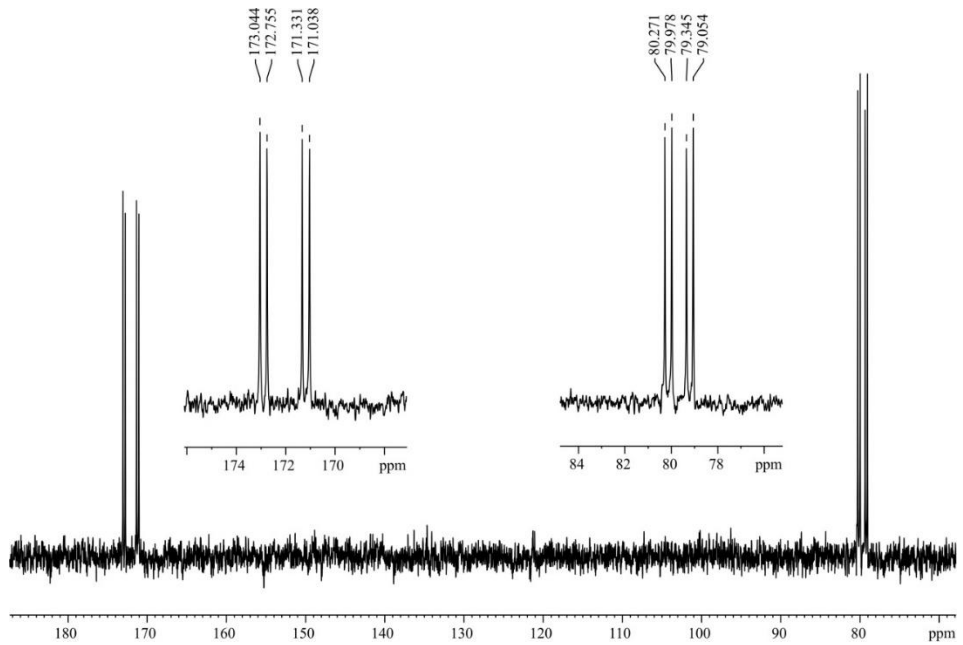

Figure 37. $^{31}P\{^{1}H\}$ NMR (162 MHz, CD_2Cl_2) of the rhodium complex [Rh(nbd)(**L8**)]BF_4.

1.5.11. Selected GC/HPLC data from catalytic experiments

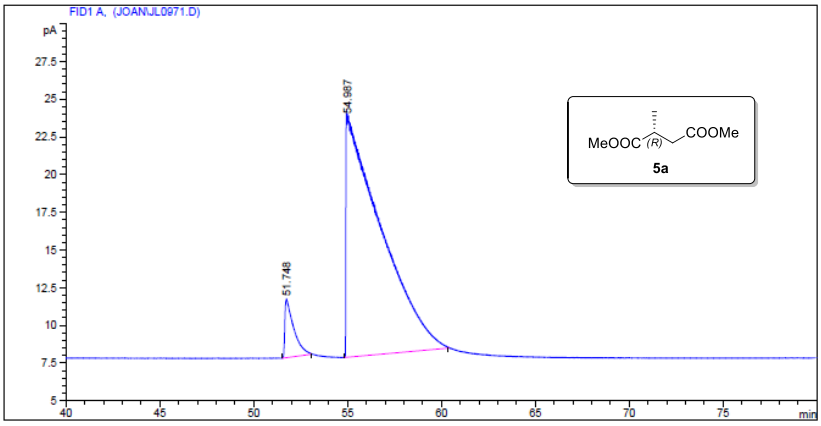

Peak #	RetTime [min]	Type	Width [min]	Area [pA*s]	Height [pA]	Area %
1	51.748	PB	0.4147	126.59939	3.90054	5.78189
2	54.987	PB	1.5174	2062.98608	15.94596	94.21811

Figure 38. Chiral GC trace for the asymmetric hydrogenation of the substrate **4a** using a rhodium complex of the P–OP ligand **L9** (Table 1, entry 9).

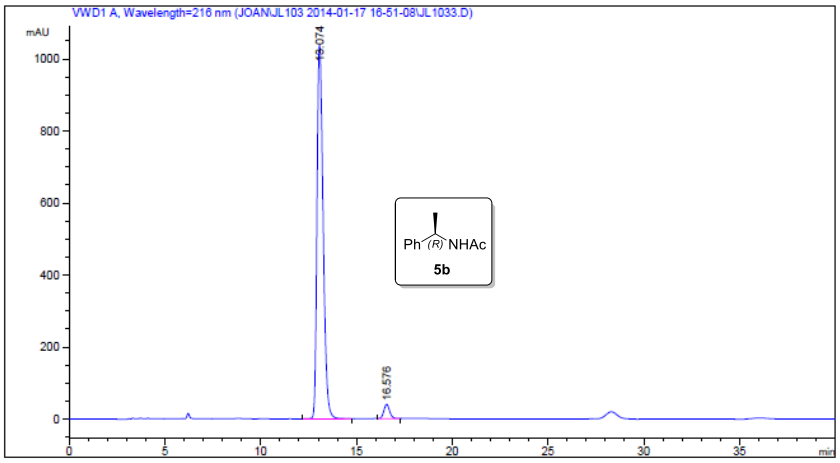

Peak #	RetTime [min]	Type	Width [min]	Area mAU *s	Height [mAU]	Area %
1	13.074	BB	0.3466	2.30947e4	1039.31140	96.5099
2	16.576	VB	0.3253	835.16736	39.74018	3.4901

Figure 39. Chiral HPLC trace for the asymmetric hydrogenation of the substrate **4b** using a rhodium complex of the P–OP ligand **L10** (Table 1, entry 14).

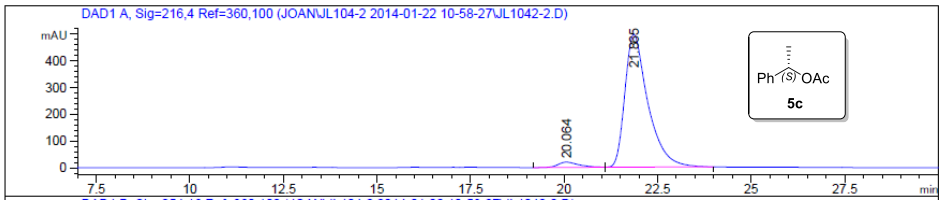

Peak #	RetTime [min]	Type	Width [min]	Area [mAU*s]	Height [mAU]	Area %
1	20.064	BV	0.5653	758.94098	19.88310	3.4498
2	21.865	VBA	0.6321	2.12404e4	495.48294	96.5502

Figure 40. Chiral HPLC trace for the asymmetric hydrogenation of the substrate **4c** using a rhodium complex of the P–OP ligand **L9** (Table 1, entry 11).

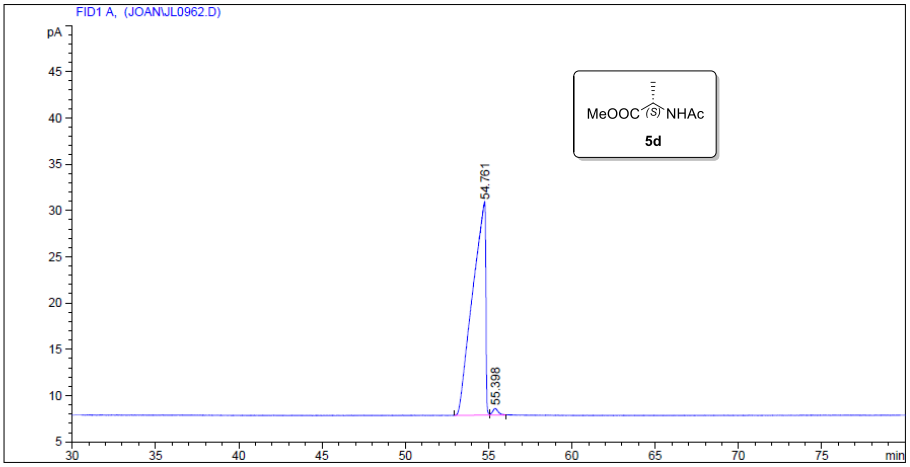

Peak #	RetTime [min]	Type	Width [min]	Area [pA*s]	Height [pA]	Area %
1	54.761	PV	0.6700	1253.83301	22.92766	98.71575
2	55.398	VB	0.3389	16.31184	7.02559e-1	1.28425

Figure 41. Chiral GC trace for the asymmetric hydrogenation of the substrate **4d** using a rhodium complex of the P–OP ligand **L9** (Table 1, entry 12).

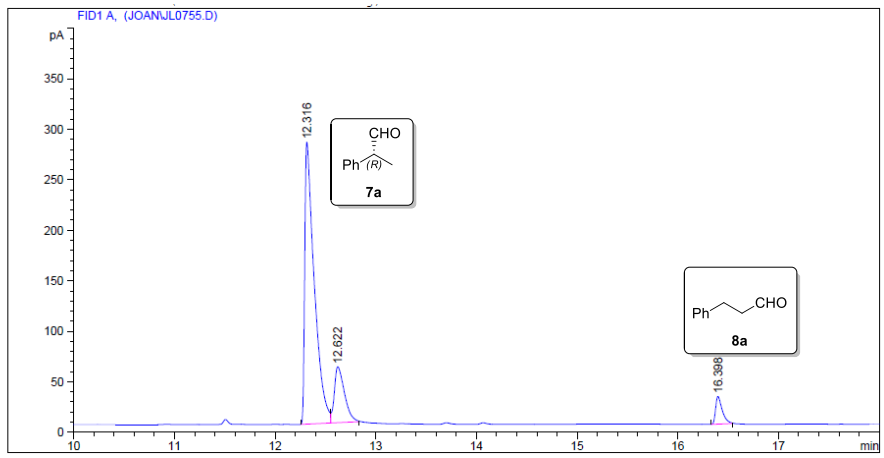

Peak #	RetTime [min]	Type	Width [min]	Area [pA*s]	Height [pA]	Area %
1	12.316	PV	0.0888	1836.79163	279.03909	78.18432
2	12.622	VB	0.0957	387.42645	55.34950	16.49108
3	16.398	PB	0.0673	125.09145	27.39982	5.32461

Figure 42. Chiral GC trace for the asymmetric hydroformylation of the substrate **6a** using a rhodium complex of the P–OP ligand **L7** (Table 2, entry 1).

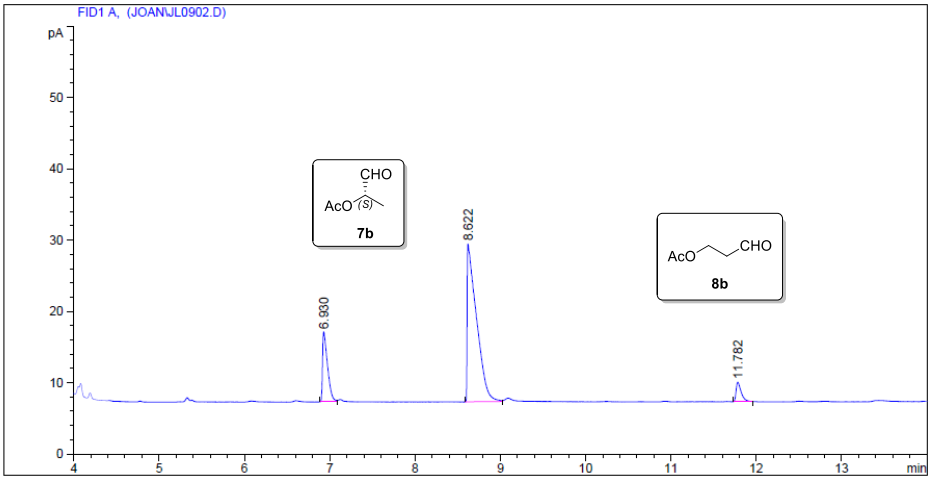

Peak #	RetTime [min]	Type	Width [min]	Area [pA*s]	Height [pA]	Area %
1	6.930	BV	0.0559	39.91382	9.81654	18.08497
2	8.622	PB	0.0953	169.45572	22.14535	76.78046
3	11.782	PB	0.0598	11.33207	2.73869	5.13457

Figure 43. Chiral GC trace for the asymmetric hydroformylation of the substrate **6b** using a rhodium complex of the P–OP ligand **L9** (Table 2, entry 7).

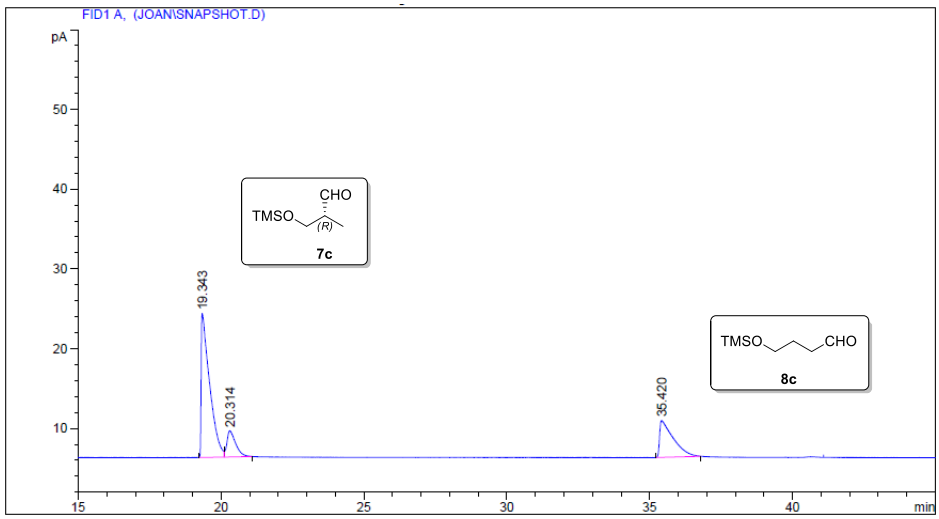

Peak #	RetTime [min]	Type	Width [min]	Area [pA*s]	Height [pA]	Area %
1	19.343	BV	0.2535	370.15320	18.02958	62.45171
2	20.314	VB	0.2786	69.90077	3.28104	11.79356
3	35.420	BB	0.4102	152.64909	4.61084	25.75473

Figure 44. Chiral GC trace for the asymmetric hydroformylation of the substrate **6c** using a rhodium complex of the P–OP ligand **L9** (Table 2, entry 11).

CHAPTER II

Hydrogenative Kinetic Resolution of Vinyl Sulfoxides

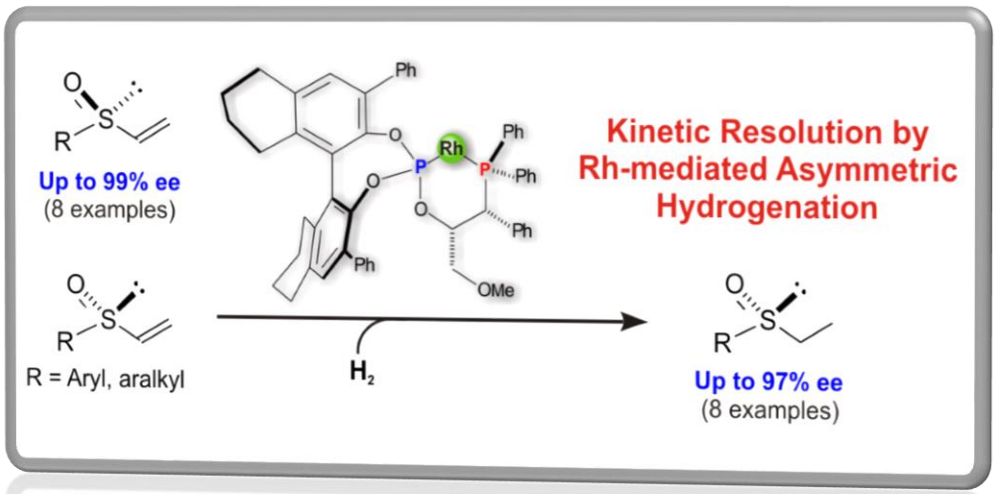

UNIVERSITAT ROVIRA I VIRGILI
RHODIUM CATALYSIS IN ENANTIOSELECTIVE HYDROGENATIVE TRANSFORMATIONS: FROM THE DESIGN OF NEW LIGANDS TO REACTIONS OF ATYPICAL SUBSTRATES
Joan Ramon Lao Mulinari

Hydrogenative Kinetic Resolution of Vinyl Sulfoxides

2.1. ABSTRACT

Enantiopure sulfoxides are valuable precursors of organosulfur compounds with broad application in organic and pharmaceutical chemistry. An unprecedented strategy for obtaining highly enantioenriched sulfoxides based on a hydrogenative kinetic resolution using Rh-complexes of phosphine-phosphite ligands as catalysts is reported. After optimization, highly efficient conditions for the kinetic resolution of racemic sulfoxides have been identified. This methodology has been applied to a set of racemic aralkyl or aryl vinyl sulfoxides and allowed for the isolation of both recovered and reduced products in excellent yields and enantioselectivities (up to 99% and 97% ee, respectively; 16 examples).

2.2. INTRODUCTION

Optically pure sulfoxides are a valuable family of chiral compounds which have proven to be highly efficient chiral ligands [49a,b,50a,72] as well as useful intermediates in the synthesis of relevant biologically active compounds.[50a,b] Among the approaches that asymmetric catalysis offers, kinetic resolution (KR) of racemic sulfoxides[73] should be considered an appealing method for the preparation of two optically pure sulfoxides in only one synthetic step, provided that some requisites are fulfilled. First and foremost, it is necessary that efficient enantioselective catalysts working at low catalyst loadings are available and, second, that starting materials and products can be isolated in good yields and enantiomerically enriched forms.[74]

(72) For selected recent reviews, see: Fernández, I.; Khiar, N. In *Organosulfur Chemistry in Asymmetric Synthesis*; Toru, T., Bolm, C., Eds.; WILEY-VCH Verlag GmbH & Co. KGaA: Weinheim, 2008; p 265.
(73) For example, see: Kagan, H. B. In *Organosulfur Chemistry in Asymmetric Synthesis*; Toru, T., Bolm, C., Eds.; WILEY-VCH Verlag GmbH & Co. KGaA: Weinheim, 2008; p 1.
(74) Keith, J. M.; Larrow, J. F.; Jacobsen, E. N. *Adv. Synth. Catal.* **2001**, *343*, 5-26.

While the reported non-enzymatic KRs on racemic sulfoxides are mainly based on oxidative transformations (Scheme 6(a)),[73,75] non-oxidative KRs, including reductive transformations (Scheme 6(b)), have received much less attention. Moreover, non-oxidative KRs have normally offered unsatisfactory stereoselectivities, with the exception of enzymatic[76] transformations and hydrogenative dynamic kinetic resolutions (DKR) of allyl sulfoxides.[77]

Scheme 6. Kinetic resolution strategies for racemic sulfoxides

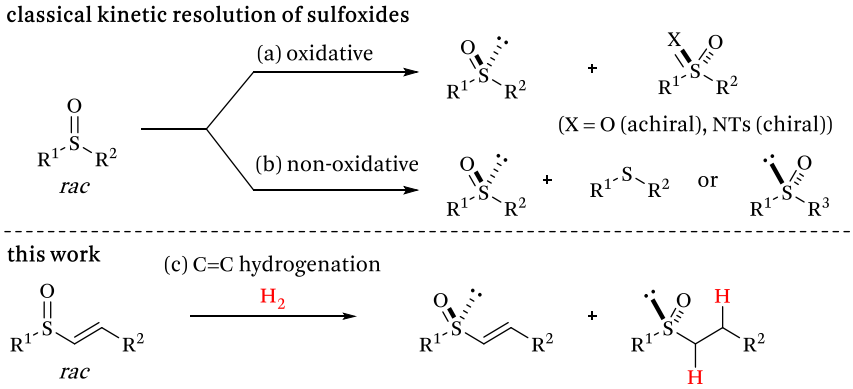

There are a few studies reporting reductive KRs of vinyl sulfoxides with optically active reagents;[78] however, to the best of our knowledge, there are no previous reports on the KR of vinyl sulfoxides via asymmetric hydrogenation.[79]

(75) The following article has been selected as an oxidative method considering oxidative as all transformations in which the formal oxidation state of the sulfur-atom increases: Wang, J.; Frings, M.; Bolm, C. *Chem. – Eur. J.* **2014**, *20*, 966-969.
(76) For selected examples on enzymatically catalyzed KRs, see for example: (a) Boyd, D. R.; Sharma, N. D.; King, A. W. T.; Shepherd, S. D.; Allen, C. C. R.; Holt, R. A.; Luckarift, H. R.; Dalton, H. *Org. Biomol. Chem.* **2004**, *2*, 554-561. (b) Boyd, D. R.; Sharma, N. D.; Byrne, B. E.; Haughey, S. A.; Kennedy, M. A.; Allen, C. C. R. *Org. Biomol. Chem.* **2004**, *2*, 2530-2537.
(77) Though DKRs are not the same as the aimed transformations in this manuscript (KRs), the following reference on the DKR of allyl sulfoxides has been included due to the high enantioselectivities achieved (up to 90% ee). See ref. 51b.
(78) (a) Mikolajczyk, M.; Para, M. *J. Chem. Soc. D* **1969**, 1192-1193. (b) Mikolajczyk, M.; Drabowicz, J. *Phosphorus Sulfur Relat. Elem.* **1976**, *1*, 301-303. (c) Drabowicz, J.; Pacholczyk, M. *Phosphorus Sulfur Relat. Elem.* **1981**, *10*, 233-235. (d) Annunziata, R.; Borgogno, G.; Montanari, F.; Quici, S.; Cucinella, S. *J. Chem. Soc., Perkin Trans. 1* **1981**, 113-118.
(79) To the best of our knowledge, the only reported transformation, which is close to the chemistry herein described (see ref. 51a) and involves asymmetric hydrogenation of vinyl sulfoxides and kinetic resolution of one vinyl sulfone.

Our group recently reported the highly enantioselective hydrogenation of a structurally diverse set of substrates mediated by phosphine–phosphite (P–OP)[42,43,80] ligands. The high catalytic activities achieved with our ligands prompted us to address the challenge of hydrogenatively resolving racemic vinyl sulfoxides (Scheme 6(c)), whose resolved products have found broad applicability in catalytic asymmetric synthesis.[49a,b,50a,b,72] Herein we describe our results, which include the catalyst optimization studies and the application of the lead catalyst to the highly efficient hydrogenative KR of an array of racemic aralkyl or aryl vinyl sulfoxides.

2.3. RESULTS AND DISCUSSION

At the onset of our study, we chose phenyl vinyl sulfoxide *rac*-**8a** as a model substrate. The reaction conditions and the results of this initial screening are summarized in Table 11.

Table 11. Ligand screening for the KR of *rac*-8a[a]

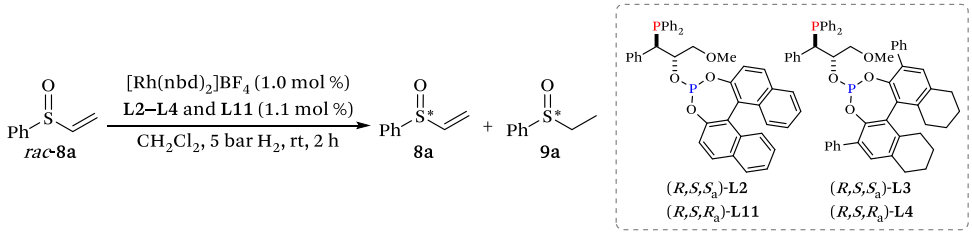

entry	ligand	conv., %[b]	ee of 8a, %;[c] (*config.*)[d]	ee of 9a, %;[c] (*config.*)[d]
1	**L2**	25	22 (*S*)	73 (*R*)
2	**L11**	16	7 (*R*)	37 (*S*)
3	**L3**	79	99 (*S*)	28 (*R*)
4	**L4**	81	85 (*R*)	20 (*S*)

[a][Substrate] = 0.2 M. [b]Determined by ^{1}H NMR. [c]Determined by HPLC on chiral stationary phases. [d]The absolute configuration was assigned by comparison with reported data.

As indicated in Table 11, both activity and selectivity were highly dependent on the P–OP ligand used. Rhodium complexes derived from ligands **L2** and **L11** afforded the hydrogenated product **9a** with 37–73% ee, though

(80) Lao, J. R.; Benet-Buchholz, J.; Vidal-Ferran, A. *Organometallics* **2014**, *33*, 2960-2963.

conversions were very low and ee values for the recovered starting material **8a** poor (see entries 1 and 2 in Table 11). In contrast, rhodium complexes of the new ligands **L3** and **L4** displayed an opposite trend with high conversions and excellent enantioselectivities for **8a** (up to 99% ee) (see entries 3 and 4 in Table 11). Therefore, these results clearly identified **L3** and **L4** as the optimal ligands for this chemistry with the stereogenic phosphite group being the principal stereochemical director (opposite absolute configurations for sulfoxides **8a** and **9a** are obtained depending on the configuration of the phosphite group: compare entries 1 with 2 for **L2** and **L11**, or entries 3 with 4 for **L3** and **L4** in Table 11, respectively).

Next, we proceeded to optimize the reaction conditions with P–OP ligands **L2** and **L3** in a range of different solvent mixtures.[81] The assayed reaction conditions and results are shown in Table 12.

Table 12. Solvent optimization using ligands L2 or L3[a]

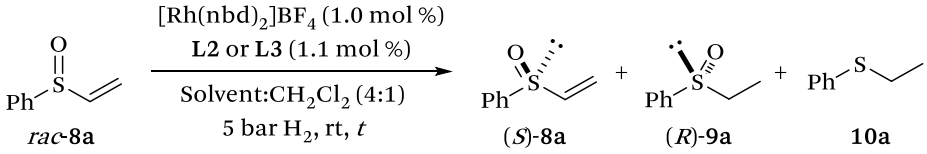

entry	L	solvent	*t*, h	conv., %[b]	8a:9a:10a[b]	ee of 8a, %;[c] (*S*)[d]	ee of 9a, %;[c] (*R*)[d]
1	**L2**	Cy	2	56	44:34:12	99	80
2	**L2**	MeOH	2	10	90:6:4	9	73
3	**L2**	MeTHF[e]	2	44	56:42:2	65	83
4	**L2**	Toluene	2	56	44:52:4	92	76
5	**L2**	CH_2Cl_2	2	25	75:25:0	22	73
6	**L3**	Cy	1	54	46:54:0	99	72
7	**L3**	MeOH	1	79	21:79:0	99	28
8	**L3**	MeTHF[e]	1	60	40:60:0	99	64
9	**L3**	Toluene	1	58	42:58:0	99	64
10	**L3**	CH_2Cl_2	1	68	32:68:0	99	45

[a, b, c, d] See notes *a*, *b*, *c* and *d* in Table 11. [e] MeTHF ≡ 2-methyl tetrahydrofuran.

(81) A certain amount of CH_2Cl_2 was kept in order to ensure the complete solubility of both the rhodium precursor and ligand.

According to these results, a mixture of cyclohexane and CH_2Cl_2 was identified as the optimal solvent for *rac*-**8a**, as it provided the highest ee values for sulfoxides **8a** and **9a** (see entries 1 and 6 in Table 12). Unfortunately, the rhodium complex derived from ligand **L2** led to the formation of significant amounts of ethyl phenyl sulfide **10a** as the byproduct arising from the overreduction of the starting material (entry 1 in Table 12).[82] This phenomenon was also observed for **L2** in all the mixtures of solvents tested (see entries 1 to 4 in Table 12). However, we were pleased to find that this side reaction was completely eliminated by using the rhodium complex derived from the P–OP ligand **L3**. Moreover, this catalyst provided at 54% conversion the recovered vinyl sulfoxide **8a** with perfect enantioselectivity (up to 99% ee in favor of the (*S*)-enantiomer) and the corresponding hydrogenated product **8a** (entry 6 in Table 12). With the optimal catalyst in hand, we then attempted to broaden the substrate scope to a set of structurally diverse vinyl sulfoxides (*rac*-**8a–h**). In order to maximize the yield for both the recovered and hydrogenated products (**8a–h** and **9a–h**, respectively), specific reaction conditions for **8a–h** and for **9a–h** were investigated.[83] The results and optimized reaction conditions are listed in Table 13.

As illustrated in Table 13, different substitution patterns on the aryl groups of vinyl sulfoxides *rac*-**8c–e** (*o*-F, *m*-F, and *p*-F substitution, respectively) were well tolerated to furnish sulfoxides **9c–e** in 56–80% isolated yield[84] with 90–97% ee, and the recovered vinyl sulfoxides **8c–e** in 54–80% isolated yield[84] with very high enantioselectivities (98–99% ee; see entries 5–10 in Table 13). The results obtained for the *ortho*-substituted substrate *rac*-**8c** were the best among all the substrates assessed (see entries 5 and 6 in Table 13). Plots of ee values of resolved products against conversion displayed that the highest enantioselectivities for such compounds were achieved in the range 40–60% conversion (see Figure 45, which corresponds to the KR of substrate *rac*-**8c**), demonstrating the high efficiency of this KR to provide unreacted starting material and hydrogenated product in high yields and ee's.

Electronic effects were also studied by the examination of *para*-substituted substrates *rac*-**8b**,**e**,**f**,**g** (*p*-Me, *p*-F, *p*-MeO, *p*-NO_2, respectively). Regardless of the electronic nature of the substituent on the aromatic ring, the substrates

(82) See the Experimental Section for details.
(83) The reaction conditions were optimized by modifying the reaction times (controlling in this way the value of conversion) in an optimal compromise amongst enantiopurity and amounts of unreacted starting material and product.
(84) Yields are calculated with respect to the 50 mol % amount of starting material that was subjected to KR.

were hydrogenated leading to both unreacted and reduced sulfoxides with high enantioselectivities (from 82 to 99% ee) in 56–76% isolated yields[84] (see entries 3, 4, and 9–14 in Table 13).

Table 13. Substrate scope of the hydrogenative KR of racemic vinyl sulfoxides *rac*-8a–h[a]

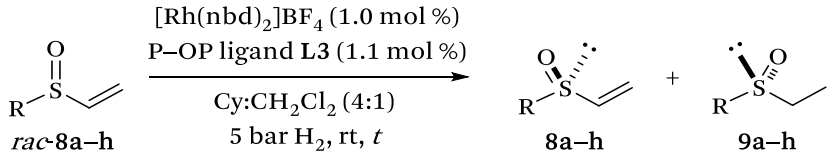

entry	R	*t*, min	conv.,%[b]	product, isol. yield, %;[84] ee, %;[c] (*config.*)[d]	*s*[e]
1[f]	Ph	60	54	**8a**, 74, 99 (*S*)	30
2	(*rac*-**8a**)	30	44	**9a**, 62, 86 (*R*)	35
3	*p*-Me-Ph	80	55	**8b**, 74, 98 (*S*)	25
4	(*rac*-**8b**)	10	35	**9b**, 58, 95 (*R*)	55
5	*o*-F-Ph	15	55	**8c**, 80, 99 (*S*)	56
6	(*rac*-**8c**)	8	42	**9c**, 80, 97 (*R*)	148
7	*m*-F-Ph	30	61	**8d**, 54, 98 (*S*)	25
8	(*rac*-**8d**)	10	39	**9d**, 76, 92 (*R*)	44
9	*p*-F-Ph	30	54	**8e**, 70, 98 (*S*)	33
10	(*rac*-**8e**)	15	44	**9e**, 56, 90 (*R*)	40
11	*p*-MeO-Ph	120	64	**8f**, 64, 99 (*S*)	26
12	(*rac*-**8f**)	30	39	**9f**, 76, 88 (*R*)	29
13	*p*-NO_2-Ph	25	66	**8g**, 64, 99 (*S*)	13
14	(*rac*-**8g**)	10	40	**9g**, 72, 82 (*R*)	18
15[g]	Bn	240	67	**8h**, 62, 99 (*R*)[h]	11
16[g]	(*rac*-**8h**)	25	33	**9h**, 56, 80 (*S*)[h]	13

[a, b, c] See notes *a, b* and *c* in Table 11. [d] The absolute configuration of **8a,b** and **9a,b,f–h** were established by comparison with reported optical rotations. The absolute configuration of **8c–h** and **9c–e** were tentatively assigned by analogy with the stereochemical outcome of the reactions leading to **8a,b** and **9a,b,f–h**.[82] [e] The selectivity factor (*s*)[74] was determined by the equation $s = \ln[1-C(1+ee_9)]/\ln[1-C(1-ee_9)]$ where $C = ee_8/(ee_8+ee_9)$.[18] [f] This result has been already shown in Table 12. [g] Solvent ratio used was Cy:CH_2Cl_2 (2.6:1). [h] The opposite *R* or *S* prefixes in **8h** and **9h** arise from different priorities in the CIP rules.

However, an electron-withdrawing group at the *para*-position increased the reaction rate (compare entries 9, 10 and 13, 14 with entries 3, 4 and 11, 12 in Table 13). The lead catalytic system was also capable of efficiently resolving benzyl vinyl sulfoxide (*rac*-**8h**): hydrogenation of *rac*-**8h** for 4 h provided (*R*)-**8h** in 62% isolated yield[84] with perfect enantioselectivity (99% ee, entry 15 in Table 13). The optimal reaction conditions for the hydrogenated product (*S*)-**9h** led to its isolation in 56% isolated yield[84] and 80% ee (entry 16 in Table 13). In order to demonstrate the practicality of this KR method, experiments at the mmol scale were performed for racemic substrates *rac*-**8a**,**g** to afford products **8a**,**g** and **9a**,**g** with the same efficiency as catalytic experiments.[82]

To shed light on the favored stereodifferentiating routes, we studied the coordination of (*R*)-**8g** and (*S*)-**8g** to the [Rh(P–OP)]$^+$ complex of the lead ligand (**L3**). We pursued the in situ preparation of [Rh(**8g**)(**L3**)]BF_4 by hydrogenation of [Rh-(nbd)(**L3**)]BF_4 in 1,2-dimethoxyethane followed by the addition of 1.1 equiv of (*R*)-**8g** or (*S*)-**8g**.

Based on related literature precedents,[77,79] we hypothesized that the KR proceeds via hydrogenation of the C=C bond with chelating assistance of the oxygen atom of the sulfoxide group. Examination of the NMR data in solution indicated that both (*R*)-**8g** and (*S*)-**8g** coordinate to the [Rh(P–OP)]$^+$ motif.

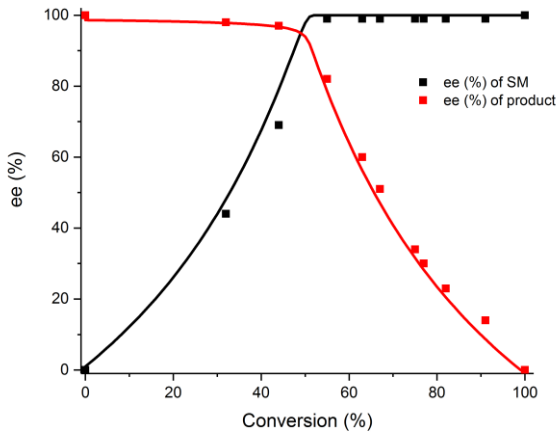

Figure 45. Ee values (%) of **8c** (SM) and **9c** (product) vs conversion (%).

The coordination of (*S*)-**8g** led to the formation of a stable complex at rt, as evidenced by the sharpness of the vinylic signals in the ^{1}H NMR spectrum.[82] The formation of the substrate–catalyst adduct [Rh((*R*)-**8g**)(**L3**)]$^+$ was evidenced by the appearance of broad vinylic signals in the ^{1}H NMR spectrum,

which sharpened up upon recording the spectra at a lower temperature (253 K). With regard to the geometry of the complexes between (*R*)-**8g** or (*S*)-**8g** and the [Rh(P–OP)]$^+$ motif, cross-peaks only between the olefinic protons and the phosphino group in heteronuclear ^{1}H–^{31}P correlation experiments were observed.[82] These observations strongly suggest that the C=C bonds of (*R*)-**8g** and (*S*)-**8g** are coordinated to the phosphino group in a *cis* fashion, as these data are practically coincident with that reported in the literature for *cis*-coordinated C=C and phosphorus groups in related rhodium complexes.[85] Furthermore, intense cross-peaks between the olefinic H–C$_\beta$ proton *trans* to H–C$_\alpha$ and aromatic protons of the diphenylphosphino group in NOESY correlation experiments were observed for bound (*S*)-**8g**, thus confirming the previous structural assignment.[82] This coordination mode of the C=C double bond places the R group of the sulfoxide in close proximity to the phosphite group, which accounts for this group being the principal stereochemical director in the KR comparing the results of these coordination studies and the configuration of the resolved products, a tentative reaction pathway for the stereochemical outcome of the KR is proposed in Figure 46.

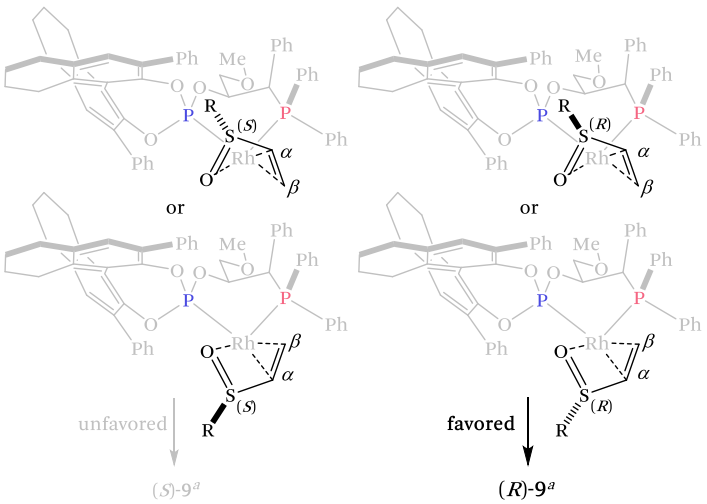

Figure 46. Tentative reaction pathways for the hydrogenative KR of racemic vinyl sulfoxides in the Rh-**L3** complexes with the C=C and P (red) groups coordinated in a *cis* fashion ([a]*R* or *S* configurations of the product have been established assuming the highest CIP's priority for the R group).

(85) (a) Bircher, H.; Bender, B. R.; von Philipsborn, W. v. *Magn. Reson. Chem.* **1993**, *31*, 293-298. (b) Gridnev, I. D.; Higashi, N.; Asakura, K.; Imamoto, T. *J. Am. Chem. Soc.* **2000**, *122*, 7183-7194. (c) Suárez, A.; Méndez-Rojas, M. A.; Pizzano, A. *Organometallics* **2002**, *21*, 4611-4621.

2.4. CONCLUSIONS

In summary, we have developed a highly efficient hydrogenative KR of vinyl sulfoxides mediated by rhodium complexes of P–OP ligand **L3**, which are responsible for the differentiation of the reaction rates of the two enantiomers of the starting material toward hydrogenation. This KR method is an unprecedented approach for preparing optically active vinyl sulfoxides and their hydrogenated products in notable yields and high enantioselectivities (up to 99% ee). The easy availability of racemic vinyl sulfoxides, together with the excellent catalytic profile of the catalyst derived from **L3**, makes the herein described synthetic methodology a valuable synthetic entry for chiral sulfoxides. Further studies on the application of this synthetic methodology, together with mechanistic investigations, are underway in our laboratory and will be reported in due course.

2.5. EXPERIMENTAL SECTION

2.5.1. General Considerations

Air- and moisture-sensitive manipulations or reactions were done under inert atmosphere using anhydrous solvents, either in a glove box or with standard Schlenk techniques. Glassware was dried under vacuum and was heated with a hot air gun before use. All solvents were dried in a Solvent Purification System (SPS). Silica gel 60 (230–400 mesh) was used for column chromatography. NMR spectra were recorded on a Bruker Avance 400 MHz or 500 MHz Ultrashield spectrometers in $CDCl_3$, unless otherwise cited. ^{1}H NMR and $^{13}C\{^{1}H\}$ NMR chemical shifts are quoted in ppm relative to the residual solvent peaks. $^{31}P\{^{1}H\}$ NMR chemical shifts are quoted in ppm relative to 85% phosphoric acid in water. $^{19}F\{^{1}H\}$ chemical shifts are quoted in ppm relative to $CFCl_3$ in $CDCl_3$. High-resolution mass spectra (HRMS) were recorded using ESI ionization method in positive mode. GC-MS analyses were performed on an Agilent 6890N using EI as ionization method. Enantiomeric excesses were determined by HPLC analyses, using chiral stationary phases. HPLC analyses were performed on an Agilent 1200 Series chromatograph equipped with a diode array UV detector (DAD). Optical rotations were measured on a Jasco P-1030 polarimeter.

2.5.2. General synthetic procedure for the P–OP ligands L3 and L4

The preparation of the P–OP ligands **L2** and **L11** has been previously described in the literature.[86]

The borane complex of the corresponding phosphino alcohol (1*R*,2*S*)-1-(diphenylphosphino)-3-methoxy-1-phenylpropan-2-ol[86]; 1.0 mmol) and 1,4-diazabyciclo[2.2.2]octane DABCO (2.2 mmol) in dry toluene (5.0 mL) were placed in a flame-dried Schlenk flask. The reaction mixture was heated at 60 °C for 2 h. After cooling to room temperature the solution was run through a short SiO_2 pad (3.0 g), and then further eluted with toluene (6.0 mL). The corresponding phosphino alcohol solution was immediately used in the following step. This solution was added drop wise via cannula to a solution of the appropriate chlorophosphite (1.10 mmol) and Et_3N (2.50 mmol) in dry toluene (15.0 mL). The mixture was stirred for 16 h at room temperature. The reaction mixture was filtered through Celite® and the filtrate was evaporated in vacuo. The resulting residue was dissolved in diethyl ether (20.0 mL) and passed through a short Al_2O_3 pad (3.0 g). Solvent evaporation yielded the corresponding phosphine-phosphite ligands.

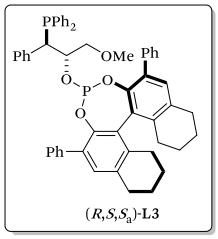

(*R*,*S*,*S*$_a$)-**L3**

Phosphine-phosphite ligand **L3** was synthesized following the general procedure starting from the corresponding phosphine-borane complex (0.740 g, 2.03 mmol), DABCO (0.51 g, 4.47 mmol), Et_3N (0.71 mL, 5.08 mmol), and the chlorophosphite derived from (*S*)-3,3'-diphenyl-5,5',6,6',7,7',8,8'-octahydro-[1,1'-binaphthaene]--2,2'-diol[87] (1.140 g, 2.23 mmol). It was obtained as a white solid (1.187 g, 71% yield). mp = 102–107 °C; $[\alpha]^{28}_{D}$ = –288.0 (*c* 0.51, THF); ^{1}H NMR (400 MHz, $CDCl_3$) δ 7.75–7.73 (m, 2H), 7.48–7.45 (m, 2H), 7.37–7.02 (m, 23H), 3.87–3.84 (m, 1H), 3.57 (d, *J* = 4.7 Hz, 1H), 2.97–2.70 (m, 9H), 2.58–2.36 (m, 2H), 2.03–1.66 (m, 10H); ^{13}C{^{1}H} NMR as DEPTQ135 (100 MHz, $CDCl_3$) δ 143.4 (C), 142.8 (C), 138.4 (C), 138.3 (C), 137.3 (C), 137.1 (C), 137.0 (C),

(86) For the preparation of the P–OP ligands (**L2** and **L11**) and their intermediates see: Fernández-Pérez, H.; Pericàs, M. A.; Vidal-Ferran, A. *Adv. Synth. Catal.* **2008**, *350*, 1984-1990.
(87) (*S*)- and (*R*)-3,3'-diphenyl-5,5',6,6',7,7',8,8'-octahydro-[1,1'-binaphthalene]-2,2'-diol were efficiently prepared using the reported method from the following listed in ref 62.

136.9 (C), 136.8 (C), 136.5 (C), 136.4 (C), 136.2 (C), 134.5 (CH), 134.3 (CH), 134.2 (C), 133.4 (CH), 133.2 (C), 133.1 (CH), 132.4 (C), 131.8 (CH), 131.7 (CH), 131.0 (C), 130.9 (C), 130.8 (C), 130.7 (CH), 130.4 (CH), 129.9 (CH), 129.6 (CH), 129.4 (C), 129.0 (CH), 128.5 (CH), 128.4 (CH), 128.3 (CH), 127.9 (CH), 127.8 (CH), 127.7 (CH), 127.6 (CH), 127.0 (CH), 126.5 (CH), 126.3 (CH), 72.1 (dd, J = 19.6 Hz, J = 12.5 Hz, CH), 71.0 (dd, J = 4.3 Hz, CH_2), 58.2 (CH_3), 46.5 (dd, J = 13.3 Hz, J = 4.7 Hz, CH), 29.4 (CH_2), 29.3 (CH_2), 27.9 (CH_2), 27.7 (CH_2), 23.0 (CH_2), 22.92 (CH_2), 22.89 (CH_2), 22.7 (CH_2); $^{31}P\{^1H\}$ NMR (162 MHz, $CDCl_3$) δ 148.3 (d, J = 23.8 Hz, P–O), –9.6 (d, J = 23.8 Hz, P–C); HRMS (ESI$^+$) *m/z* calcd for $C_{54}H_{51}O_4P_2$ $[M+H]^+$ 825.3257, found 825.3248.

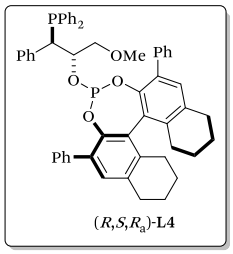

(R,S,R_a)-L4

Phosphine-phosphite ligand **L4** was synthesized following the general procedure starting from the corresponding phosphine-borane complex (0.300 g, 0.82 mmol), DABCO (0.21 g, 1.8 mmol), Et_3N (0.29 mL, 2.06 mmol), and the chlorophosphite derived from (*R*)-3,3'-diphenyl-5,5',6,6',7,7',8,8'-octahydro-[1,1'-binaphthalene]-2,2'-diol[87] (0.465 g, 0.91 mmol). It was obtained as a white solid (0.400 g, 59% yield). mp = 107–110 °C; $[\alpha]^{29}_D$ = –376.9 (*c* 0.62, THF); ^1H NMR (400 MHz, $CDCl_3$) δ 7.66–7.63 (m, 2H), 7.57–7.54 (m, 2H), 7.39–7.24 (m, 12H), 7.14–6.98 (m, 12H), 3.93–3.86 (m, 1H), 3.64–3.63 (m, 1H), 2.97–2.86 (m, 7H), 2.76–2.67 (m, 3H), 2.55–2.34 (m, 3H), 1.96–1.65 (m, 3H); $^{13}C\{^1H\}$ NMR as DEPTQ135 (100 MHz, $CDCl_3$) δ 143.22 (C), 143.16 (C), 143.1 (C), 138.2 (C), 138.1 (C), 137.7 (C), 137.5 (C), 137.4 (C), 137.3 (C), 137.2 (C), 136.9 (C), 136.8 (C), 136.5 (C), 134.5 (CH), 134.3 (CH), 134.2 (C), 133.3 (CH), 133.1 (CH), 132.1 (C), 132.0 (C), 131.4 (C), 131.1 (CH), 131.0 (CH), 130.6 (CH), 130.4 (CH), 129.8 (CH), 129.72 (CH), 129.70 (CH), 129.3 (C), 129.2 (C), 128.9 (CH), 128.33 (CH), 128.30 (CH), 128.2 (CH), 128.0 (CH), 127.8 (CH), 127.70 (CH), 127.66 (CH), 127.6 (CH), 126.9 (CH), 126.8 (CH), 126.27 (CH), 126.26 (CH), 73.6 (dd, J = 12.6 Hz, J = 9.9 Hz, CH), 71.6 (dd, J = 8.4 Hz, J = 4.4 Hz, CH_2), 58.2 (CH_3), 46.7 (dd, J = 15.4 Hz, J = 5.9 Hz, CH), 29.4 (CH_2), 29.3 (CH_2), 27.9 (CH_2), 27.7 (CH_2), 23.0 (CH_2), 22.88 (CH_2), 22.86 (CH_2), 22.7 (CH_2); $^{31}P\{^1H\}$ NMR (162 MHz, $CDCl_3$) δ 143.9 (d, J = 3.2 Hz, P–O), –8.2 (d, J = 3.2 Hz, P–C); HRMS (ESI$^+$) *m/z* calcd for $C_{54}H_{51}O_4P_2$ $[M+H]^+$ 825.3257, found 825.3238.

2.5.3. General synthetic procedure for vinyl sulfoxides *rac*-8a–g

Racemic phenyl vinyl sulfoxide (**8a**) was purchased from Sigma-Aldrich. Racemic vinyl sulfoxides *rac*-**8b–g** were prepared following an already reported synthetic methodology with slight modifications.[88]

The corresponding thiol (0.176 mol) was added under an Ar atmosphere to a stirred solution of sodium ethoxide (12.7 g, 95%, 0.178 mol) in ethanol (80.0 mL) and the resulting solution was stirred for 30 min at room temperature. After that time, the solution of the corresponding thiolate was slowly added to a pre-cooled (0 °C) stirring solution of 1,2-dibromoethane (23.3 mL, 0.264 mol) in ethanol (20.0 mL) within 1 h under Ar. Stirring was continued for an additional 1 h at room temperature and then a solution of sodium ethoxide (0.443 mol) in ethanol (150 mL) was added, under the same reaction conditions. The reaction mixture was stirred under reflux overnight under Ar. After that, the reaction crude was cooled and treated with 300.0 mL of water, extracted with CH_2Cl_2 (3 x 200 mL), washed with water (2 x 100 mL), brine (1 x 100 mL), and dried over anhydrous $MgSO_4$. After filtration, solvent was removed in vacuo and the resulting residue was distilled under reduced pressure to afford the corresponding vinyl sulfide. To a stirring solution of the freshly distilled sulfide (0.086 mol) in CH_2Cl_2 (50.0 mL) was carefully added a solution of *m*-CPBA (21.2 g, ≥77%, ca. 0.094 mol) in CH_2Cl_2 (150 mL) at −78 °C under Ar atmosphere. Stirring was continued for 1 h and then, the reaction mixture was allowed to reach room temperature. Stirring was continued for an additional 1 h and after that time, 300.0 mL of sat. $NaHCO_3$ were added. The resulting suspension was extracted with CH_2Cl_2 (2 x 200 mL), washed with water (1 x 200 mL), brine (1 x 200 mL) and dried over anhydrous $MgSO_4$. After filtration, solvent was removed in vacuo to yield the crude product. Purification by distillation under reduced pressure or by silica gel column chromatography (using a solvent mixture of Hexanes:EtOAc) yielded the desired pure vinyl sulfoxide.

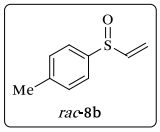

rac-8b

(*p*-Me)-phenyl vinyl sulfoxide (*rac*-**8b**): The general procedure was followed starting from *p*-methylbenzenethiol to yield the

(88) Racemic sulfoxides **8b–g** were prepared using a slightly modified procedures from the following publications: (a) Paquette, L. A.; Carr, R. V. C. *Org. Synth.* **1986**, *64*, 157-163. (b) Zhao, Y.; Higashihara, T.; Sugiyama, K.; Hirao, A. *J. Am. Chem. Soc.* **2005**, *127*, 14158-14159.

desired vinyl sulfoxide *rac*-**8b** as colorless oil (3.62 g, 11% overall yield). Spectral data were in agreement with those reported.[88b]

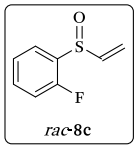

rac-**8c**

(*o*-F)-phenyl vinyl sulfoxide (*rac*-**8c**): The general procedure was followed starting from *o*-fluorobenzenethiol to yield the desired vinyl sulfoxide *rac*-**8c** as colorless oil (5.40 g, 42% overall yield). bp = 126 °C (0.36 mbar); ^{1}H NMR (500 MHz, $CDCl_3$) δ 7.77–7.74 (m, 1H), 7.50–7.45 (m, 1H), 7.37–7.34 (m, 1H), 7.14–7.10 (m, 1H), 6.78 (ddd, J = 16.5 Hz, J = 9.6 Hz, J = 1.6 Hz, CH), 6.20 (d, J = 16.5 Hz, 1H, CHH), 5.91 (dd, J = 9.6 Hz, 1H, CHH); ^{13}C{^{1}H} NMR (125 MHz, $CDCl_3$) δ 158.0 (d, J = 247.4 Hz, C–F), 141.0 (d, J = 1.5 Hz, CH), 132.7 (d, J = 7.6 Hz, CH), 130.9 (d, J = 16.6 Hz, C–S), 125.5 (d, J = 3.5 Hz, CH), 125.2 (d, J = 2.4 Hz, CH), 120.8 (CH_2); ^{19}F{^{1}H} NMR (471 MHz, $CDCl_3$) δ –114.9 (s); HRMS (ESI$^+$) *m/z* calcd for C_8H_8FOS $[M+H]^+$ 171.0274, found 171.0275.

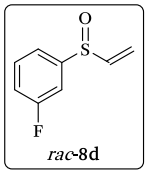

rac-**8d**

(*m*-F)-phenyl vinyl sulfoxide (*rac*-**8d**): The general procedure was followed starting from *m*-fluorobenzenethiol to yield the desired vinyl sulfoxide *rac*-**8d** as colorless oil (3.62 g, 15% overall yield). bp = 113 °C (0.5 mbar); ^{1}H NMR (400 MHz, $CDCl_3$) δ 7.52–7.47 (m, 1H), 7.40–7.35 (m, 2H), 7.20–7.15 (m, 1H), 6.60 (dd, J = 16.5 Hz, J = 9.6 Hz, CH), 6.21 (dd, J = 16.5 Hz, J = 0.5 Hz, 1H, CHH), 5.92 (dd, J = 9.6 Hz, J = 0.5 Hz, 1H, CHH); ^{13}C{^{1}H} NMR (100 MHz, $CDCl_3$) δ 163.1 (d, J = 251.3 Hz, C–F), 145.9 (d, J = 5.5 Hz, C–S), 142.6 (CH), 131.1 (d, J = 7.6 Hz, CH), 121.3 (CH_2), 120.1 (d, J = 3.3 Hz, CH), 118.3 (d, J = 21.7 Hz, CH), 111.6 (d, J = 23.9 Hz, CH); ^{19}F{^{1}H} NMR (376 MHz, $CDCl_3$) δ –109.5 (s); HRMS (ESI$^+$) *m/z* calcd for C_8H_7NaFOS $[M+Na]^+$ 193.0094, found 193.0087.

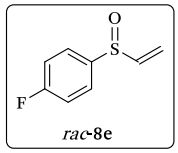

rac-**8e**

(*p*-F)-phenyl vinyl sulfoxide (*rac*-**8e**): The general procedure was followed starting from *p*-fluorobenzenethiol to yield the desired vinyl sulfoxide *rac*-**8e** as colorless oil (5.32 g, 34% overall yield). Spectral data were in agreement with those reported.[89]

(89) Bader, A.; Wuensch, J. R. *Macromolecules* **1995**, *28*, 3794-3800.

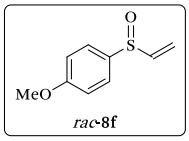

rac-**8f**

(*p*-MeO)-phenyl vinyl sulfoxide (*rac*-**8f**): The general procedure was followed starting from *p*-methoxy-benzenethiol to yield the desired vinyl sulfoxide *rac*-**8f** as yellowish oil (6.9 g, 22% overall yield). Spectral data were in agreement with those reported.[90]

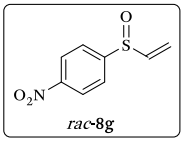

rac-**8g**

(*p*-NO_2)-phenyl vinyl sulfoxide (*rac*-**8g**): The general procedure was followed starting from *p*-nitrobenzenethiol to yield the desired vinyl sulfoxide *rac*-**8g** as a yellow solid (3.00 g, 25% overall yield). Spectral data were in agreement with those reported.[90]

2.5.4. Synthesis of vinyl sulfoxide *rac*-8h

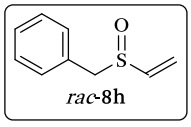

rac-**8h**

Benzyl vinyl sulfoxide (*rac*-**8h**):[91] A 35% (w/w) solution of H_2O_2 in water (1.67 mL, 19.1 mmol) was carefully added to a stirred solution of dibenzyl disulfide[92] (0.72 g, 4.78 mmol) in glacial acetic acid (4.8 mL). The reaction mixture was stirred for 1.5 h at room temperature. After that time, the excess of acid was neutralized by the addition of 4 M solution of NaOH (20.0 mL) in water. The resulting mixture was extracted with CH_2Cl_2 (3 x 20.0 mL), dried over anhydrous $MgSO_4$, filtered and concentrated under reduced pressure to yield the crude product. Purification by silica gel column chromatography using a solvent gradient (from 1:0 to 95:5 of Hexanes:EtOAc) yielded the desired vinyl sulfoxide *rac*-**8h** as colorless oil (0.69 g, 87% yield). Spectral data were in agreement with those reported.[93]

(90) Chen, M. S.; Prabagaran, N.; Labenz, N. A.; White, M. C. *J. Am. Chem. Soc.* **2005**, *127*, 6970-6971.
(91) Racemic sulfoxide **8h** was prepared using a slightly modified procedure from the following publication: Golchoubian, H.; Hosseinpoor, F. *Molecules* **2007**, *12*, 304-310.
(92) Dibenzyl disulfide was efficiently prepared using the reported method from the following publication: Lin, Y. A.; Chalker, J. M.; Floyd, N.; Bernardes, G. J. L.; Davis, B. G. *J. Am. Chem. Soc.* **2008**, *130*, 9642-9643. The spectral data and yield were in agreement with the reported data.
(93) Abe, H.; Fujii, H.; Masunari, C.; Itani, J.; Kashino, S.; Shibaike, K.; Harayama, T. *Chem. Pharm. Bull.* **1997**, *45*, 778-785.

2.5.5. General procedure for the KR by Rh-mediated asymmetric hydrogenations

The following procedure was performed in a glove box: A solution of the required amount of the rhodium precursor $[Rh(nbd)_2]BF_4$ (0.001 mmol), the P–OP ligand (0.0011 mmol) and the corresponding vinyl sulfoxide (0.1 mmol) in anhydrous and degassed CH_2Cl_2 was placed in a glass vessel. In all cases the molar concentration of a given substrate was adjusted to 0.2 M by adding the required amount of solvent. When a solvent mixture was required, solvent ratio was adjusted to solvent:CH_2Cl_2 (4:1). The reaction mixtures were loaded into an autoclave reactor (HEL Cat-24 parallel pressure multi-reactor) under N_2. The autoclave reactor was purged three times with H_2 gas (3 bar) and finally, pressurized with H_2 gas at 5 bar. The reaction mixtures were stirred at room temperature for the required time. The autoclave reactor was then depressurized. The general work-up for the reaction crudes was: rapid filtration on silica gel (2 cm of silica in a Pasteur pipette) eluting with EtOAc (1.5 mL) and evaporation of the solvent in vacuo. Further purification by silica gel column chromatography using a mixture of solvent (Hexanes:EtOAc) afforded the desired products. Conversions were determined by ^1H NMR, and the enantioselectivities of the reaction products were determined by HPLC analysis on chiral stationary phases.

2.5.6. Scale-up experiments

Preparative experiments using 1 mmol of substrate were performed following the general procedure for the KR by Rh-mediated asymmetric hydrogenations. The results are listed in the following table (Table 14).

Table 14. Scale-up experiments of the KR by Rh-mediated asymmetric hydrogenation of racemic vinyl sulfoxides *rac*-8a,g[a]

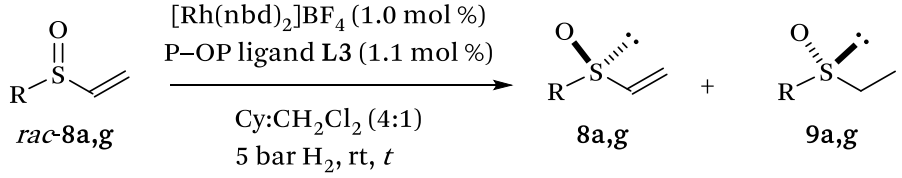

entry	R	mmol	*t*, min	conv., %[b]	8a–h, isol. yield,[84] %[c]	9a–h, isol. yield,[84] %[c]	ee of 8a–h, %;[c] (*config.*)[d]	ee of 9a–h, %;[c] (*config.*)[d]
1	Ph (*rac*-**8a**)	0.1	30	44	**8a**, 63	**9a**, 70	84 (*S*)	86 (*R*)
2		1.0	23	48	**8a**, 95	**9a**, 97	95 (*S*)	85 (*R*)
3	*p*-NO_2-Ph (*rac*-**8g**)	0.1	25	66	**8g**, 95	**9g**, 98	99 (*S*)	47 (*R*)
4		1.0	25	61	**8g**, 99	**9g**, 99	99 (*S*)	62 (*R*)

[a,b,c,d]See notes *a*, *b* and *c* in Table 11, and *d* in Table 13.

2.5.7. Complete data for Table 13

Table 15. Substrate scope of the KR by Rh-mediated asymmetric hydrogenation of racemic vinyl sulfoxides *rac*-8a–h with P–OP ligand L3[a]

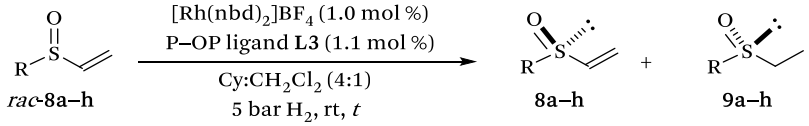

entry	R	*t*, min	conv., %[b]	8a–h, Isol. Yield,[84] %[c]	9a–h, Isol. Yield,[84] %[c]	ee of 8a–h, %;[c] (*config.*)[d]	ee of 9a–h, %;[c] (*config.*)[d]	*s*[e]
1	Ph	60	54	**8a**, 80	**9a**, 74	99 (*S*)	71 (*R*)	30
2	(*rac*-**8a**)	30	44	**8a**, 63	**9a**, 70	84 (*S*)	86 (*R*)	35
3	*p*-Me-Ph	75	55	**8b**, 83	**9b**, 82	98 (*S*)	70 (*R*)	25
4	(*rac*-**8b**)	10	35	**8b**, 97	**9b**, 82	44 (*S*)	95 (*R*)	55
5	*o*-F-Ph	15	55	**8c**, 88	**9c**, 73	99 (*S*)	82 (*R*)	56
6	(*rac*-**8c**)	8	42	**8c**, 88	**9c**, 94	69 (*S*)	97 (*R*)	14
7	*m*-F-Ph	30	61	**8d**, 62	**9d**, 67	98 (*S*)	72 (*R*)	25
8	(*rac*-**8d**)	10	39	**8d**, 84	**9d**, 98	58 (*S*)	92 (*R*)	44
9	*p*-F-Ph	30	54	**8e**, 75	**9e**, 79	98 (*S*)	77 (*R*)	33
10	(*rac*-**8e**)	15	44	**8e**, 68	**9e**, 64	74 (*S*)	90 (*R*)	40
11	*p*-MeO-Ph	120	64	**8f**, 76	**9f**, 83	99 (*S*)	69 (*R*)	26
12	(*rac*-**8f**)	35	39	**8f**, 87	**9f**, 97	59 (*S*)	88 (*R*)	29
13	*p*-NO_2-Ph	25	66	**8g**, 95	**9g**, 98	99 (*S*)	47 (*R*)	13
14	(*rac*-**8g**)	10	40	**8g**, 88	**9g**, 89	56 (*S*)	82 (*R*)	18
15[f,g]	Bn	240	67	**8h**, 95	**9h**, 84	99 (*R*)	42 (*S*)	11
16[f,g]	(*rac*-**8h**)	25	33	**8h**, 99	**9h**, 86	45 (*R*)	80 (*S*)	13

[a,b,c,d,e]See notes *a*, *b* and *c* in Table 11, and *d* and *e* in Table 13. [f]Solvent ratio used was Cy:CH_2Cl_2 (2.6:1). [g]The opposite *R* or *S* prefixes in products **8h** and **9h** arise from different priorities in the CIP rules.

2.5.8. In situ NMR coordination studies of the substrate-catalyst adducts [Rh(*rac*-8g)(L3)]BF_4, (*R*)-8g and (*S*)-8g

A glass vessel was filled with a solution of [Rh(nbd)(**L3**)]BF_4 (22.8 mg, 0.0206 mmol) in 1,2-dimethoxyethane (DME, 2.0 mL) and was introduced in an autoclave. The autoclave reactor was purged three times with H_2 (3 bar) and finally, pressurized with H_2 at 4 bar. The mixture was stirred for 1 h, and then depressurized. To the resulting solution, *rac*-**8g** (4.47 mg, 0.022 mmol) was added and stirred for one additional hour. The solution was then evaporated to dryness, dissolved in CD_2Cl_2 (0.6 mL) and the in situ formed substrate-catalyst adducts [Rh(*rac*-**8g**)(**L3**)]BF_4 were characterized by NMR spectroscopy and ESI-HRMS (Figure 47 to Figure 53): ^{1}H NMR (500 MHz, CD_2Cl_2) δ 8.34–8.28 (m, 4H), 7.84–7.12 (m, 24H), 6.88–6.87 (m, 1H), 6.67–6.63 (m, 1H), 4.65–4.59 (m, 2H, vinylic CH_bH_c of coordinated (*S*)-**8g**), 4.01 (d, J = 16.7 Hz, 1H), 3.67 (bs, 1H), 3.61–3.56 (m, 1H, vinylic CH_a of coordinated (*S*)-**8g**), 3.21–2.33 (m, 13H), 1.97–1.67 (m, 8H); $^{13}C\{^1H\}$ NMR as DEPTQ135 (125 MHz, CD_2Cl_2) δ 150.0 (C), 148.0 (C), 139.1 (C), 138.5 (C), 137.9 (C), 137.3 (C), 136.6 (C), 135.8 (CH), 135.5 (CH), 131.8 (C), 131.7 (CH), 131.4 (CH), 131.0 (CH), 130.8 (CH), 130.7 (C), 130.2 (CH), 129.8 (C), 129.44 (CH), 129.36 (CH), 129.3 (CH), 129.1 (CH), 128.5 (CH), 128.4 (CH), 128.3 (CH), 128.1 (CH), 127.9 (CH), 127.7 (CH), 126.6 (C), 126.2 (C), 124.7 (CH), 124.6 (CH), 74.9 (CH), 69.7 (dd, J = 10.8 Hz, J = 6.9 Hz, CH_2), 69.0 (d, J = 14.5 Hz, vinylic CH_bH_c of coordinated (*S*)-**8g**), 58.4 (CH_3), 56.6 (d, J = 22.8 Hz, vinylic CH_a of coordinated (*S*)-**8g**), 38.0 (d, J= 32.0 Hz, CH), 29.2 (CH_2), 29.0 (CH_2), 27.9 (CH_2), 27.7 (CH_2), 22.5 (CH_2), 22.4 (CH_2), 22.33 (CH_2), 22.32 (CH_2); $^{31}P\{^1H\}$ NMR (162 MHz, $CDCl_3$) δ 133.4 (dd, J = 256.1 Hz, J = 79.5 Hz, P–O), 22.8 (d, J = 152.8 Hz, J = 79.5 Hz, P–C); HRMS (ESI^+) *m/z* calcd for $C_{54}H_{50}O_4P_2Rh$ $[M–(S)\text{-}8g–BF_4]^+$ 927.2234, found 927.2203.[94]

(94) Very broad signals were observed for coordinated (*R*)-**8g** (see Figure 57).

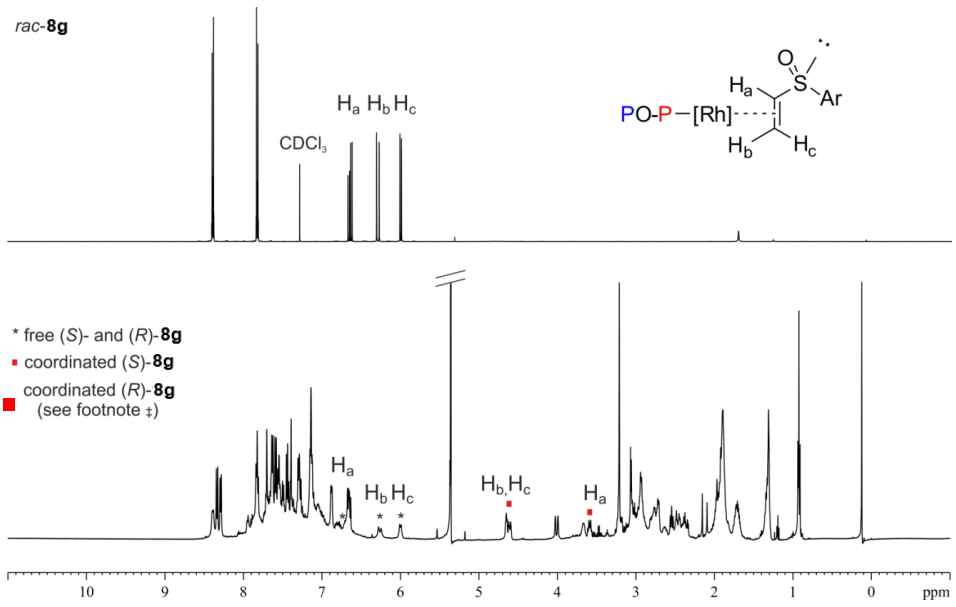

Figure 47. ^{1}H NMR spectrum (500 MHz, CD_2Cl_2) of the in situ generated substrate-catalyst adducts from [Rh(**L3**)]$^{+}$ and *rac*-**8g** (bottom); ^{1}H NMR spectrum (500 MHz, $CDCl_3$) of *rac*-**8g** (top).

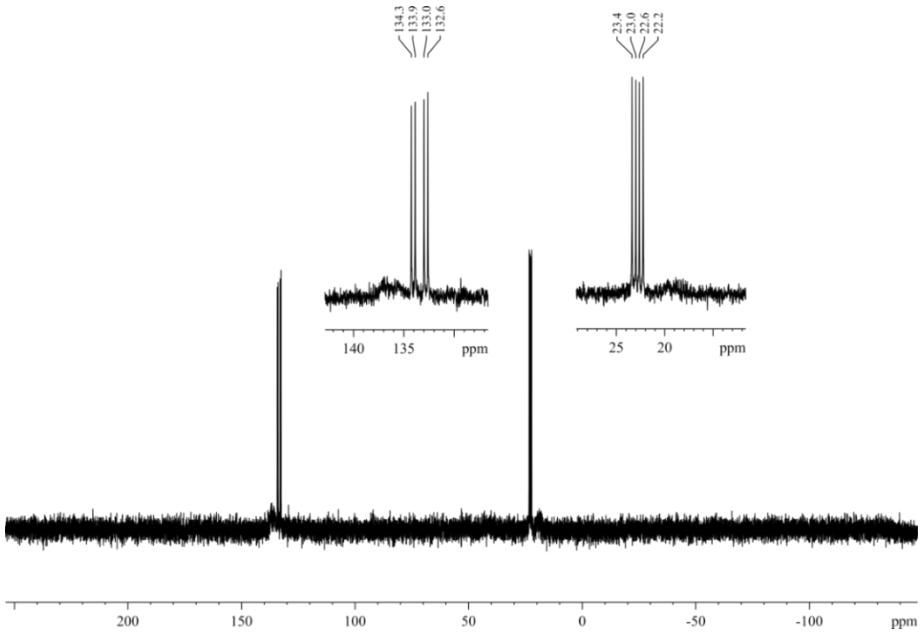

Figure 48. ^{31}P{^{1}H} NMR spectrum (202 MHz, CD_2Cl_2) of the in situ generated substrate-catalyst adducts from [Rh(**L3**)]$^{+}$ and *rac*-**8g**.

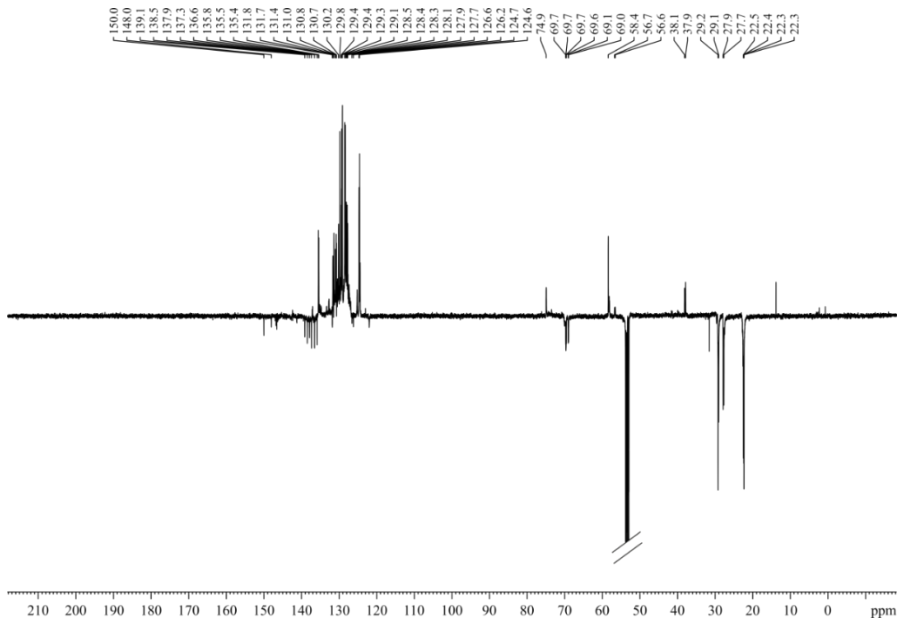

Figure 49. $^{13}C\{^{1}H\}$ NMR spectrum as DEPTQ135 (125 MHz, CD_2Cl_2) of the in situ generated substrate-catalyst adducts from [Rh(**L3**)]$^+$ and *rac*-**8g**.

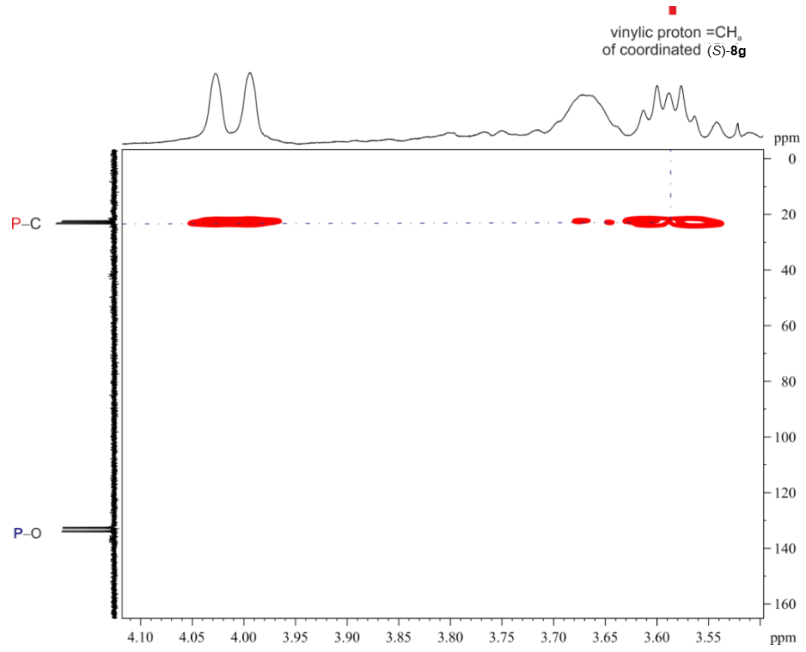

Figure 50. 2D ^{1}H-^{31}P NMR spectrum (CD_2Cl_2) of the in situ generated substrate-catalyst adducts from [Rh(**L3**)]$^+$ and *rac*-**8g**, expanded view of the olefinic proton-phosphine cross peak.

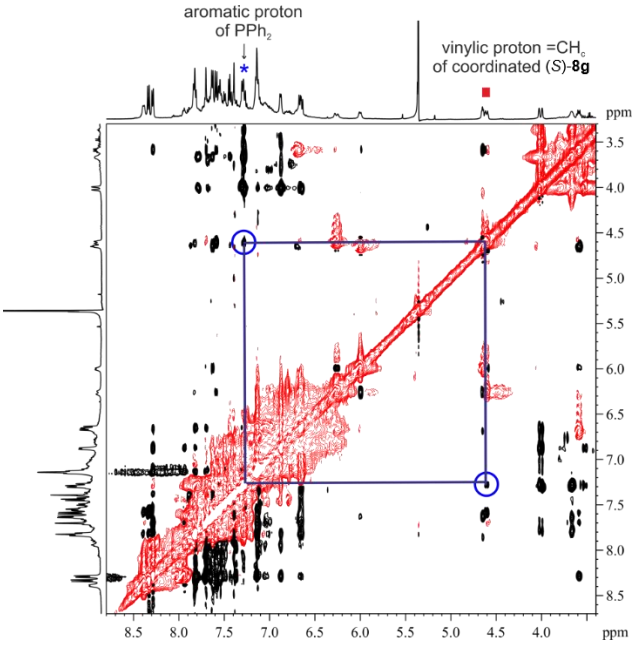

Figure 51. NOESY spectrum (CD_2Cl_2) of the of the in situ generated substrate-catalyst adducts from [Rh(**L3**)]$^+$ and *rac*-**8g**, expanded view of the olefinic proton-aromatic proton of phosphine cross peak.

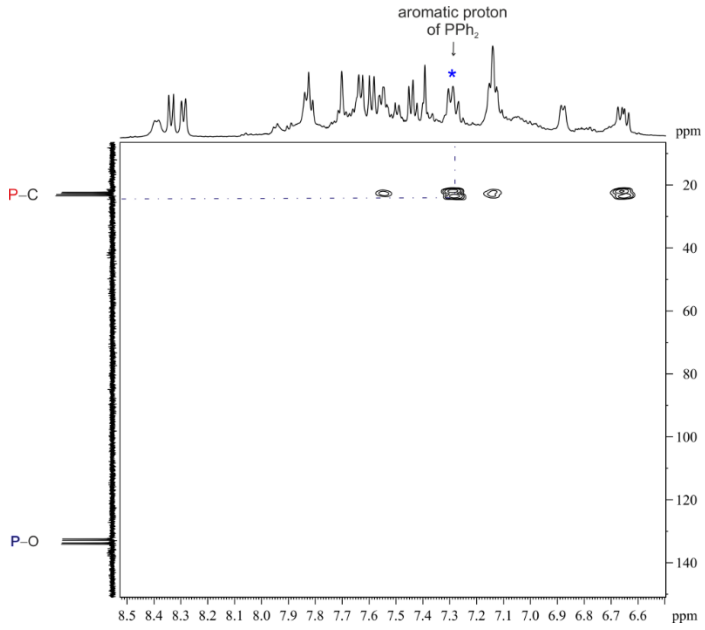

Figure 52. 2D ^{1}H-^{31}P NMR spectrum (CD_2Cl_2) of the in situ generated substrate-catalyst adducts from [Rh(**L3**)]$^+$ and *rac*-**8g**, expanded view of the aromatic proton-phosphine cross peak.

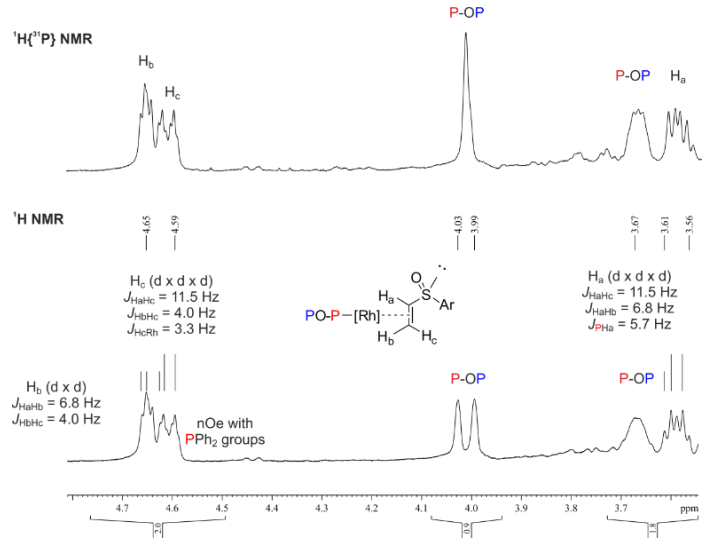

Figure 53. Expanded view of the ^1H NMR spectrum (500 MHz, CD_2Cl_2) of the in situ generated substrate-catalyst adducts from [Rh(**L3**)]$^+$ and *rac*-**8g** (bottom); expanded view of the $^1H\{^{31}P\}$ NMR spectrum (500 MHz, CD_2Cl_2) of the in situ generated substrate-catalyst adducts from [Rh(**L3**)]$^+$ and *rac*-**8g** (top).

A coordination experiment using the enantiopure vinyl sulfoxide (*S*)-**8g** was then carried out following the aforementioned general procedure. NMR spectral data was in agreement with those previously reported for the complex obtained from *rac*-**8g**. NMR spectra for the in situ generated substrate-catalyst adducts [Rh((*S*)-**8g**)(**L3**)]BF_4 are shown in Figure 54 and Figure 55.

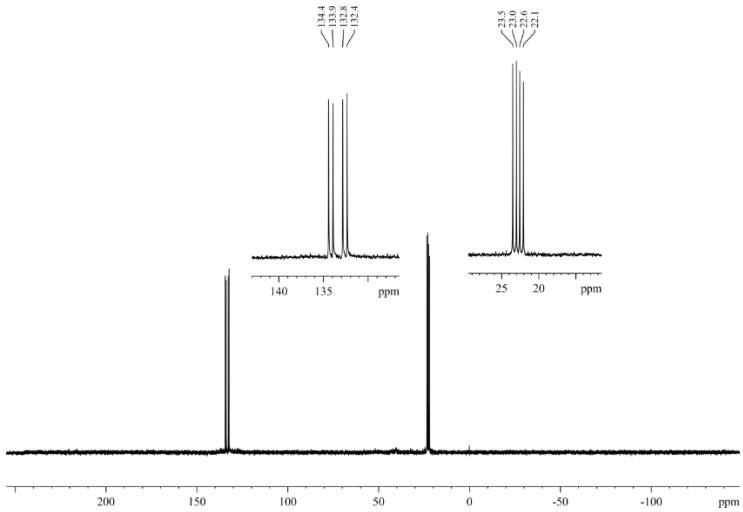

Figure 54. $^{31}P\{^1H\}$ NMR spectrum (162 MHz, CD_2Cl_2) of the in situ generated substrate-catalyst adduct [Rh((*S*)-**8g**)(**L3**)]BF_4.

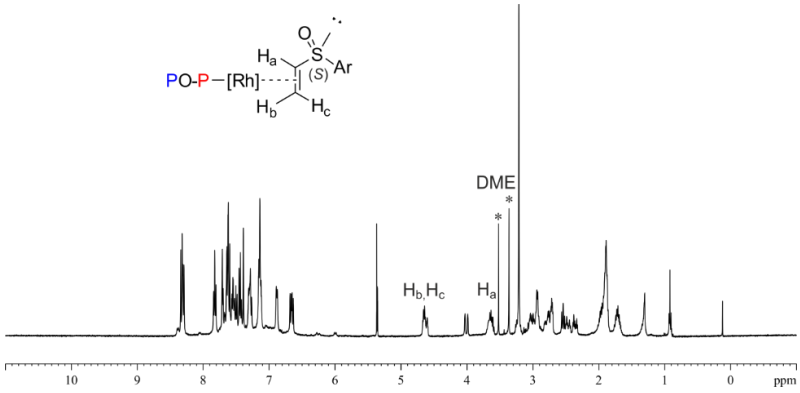

Figure 55. ^{1}H NMR spectrum (400 MHz, CD_2Cl_2) of the in situ generated substrate-catalyst adduct [Rh((*S*)-**8g**)(**L3**)]BF_4.

Finally, the coordination behavior of enantiopure vinyl sulfoxide (*R*)-**8g** with respect to the metal-ligand fragment was performed following the aforementioned general procedure. Due to the broadness of the resulting signals (Figure 56 and Figure 57), NMR spectra were acquired at low temperature (253 K). Upon cooling, the signals sharpened and the signals for the substrate-catalyst adduct [Rh((*R*)-**8g**)(**L3**)]BF_4 could be assigned (Figure 56 to Figure 59).

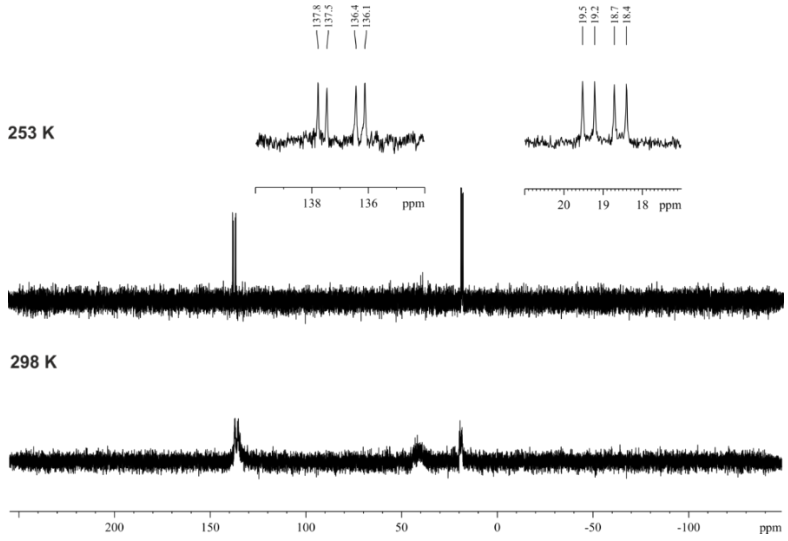

Figure 56. $^{31}P\{^{1}H\}$ NMR spectrum (162 MHz, CD_2Cl_2, 298 K) of the in situ generated substrate-catalyst adduct [Rh((*R*)-**8g**)(**L3**)]BF_4 (bottom); $^{31}P\{^{1}H\}$ NMR spectrum (162 MHz, CD_2Cl_2, 253 K) of the in situ generated substrate-catalyst adduct [Rh((*R*)-**8g**)(**L3**)]BF_4 (top).

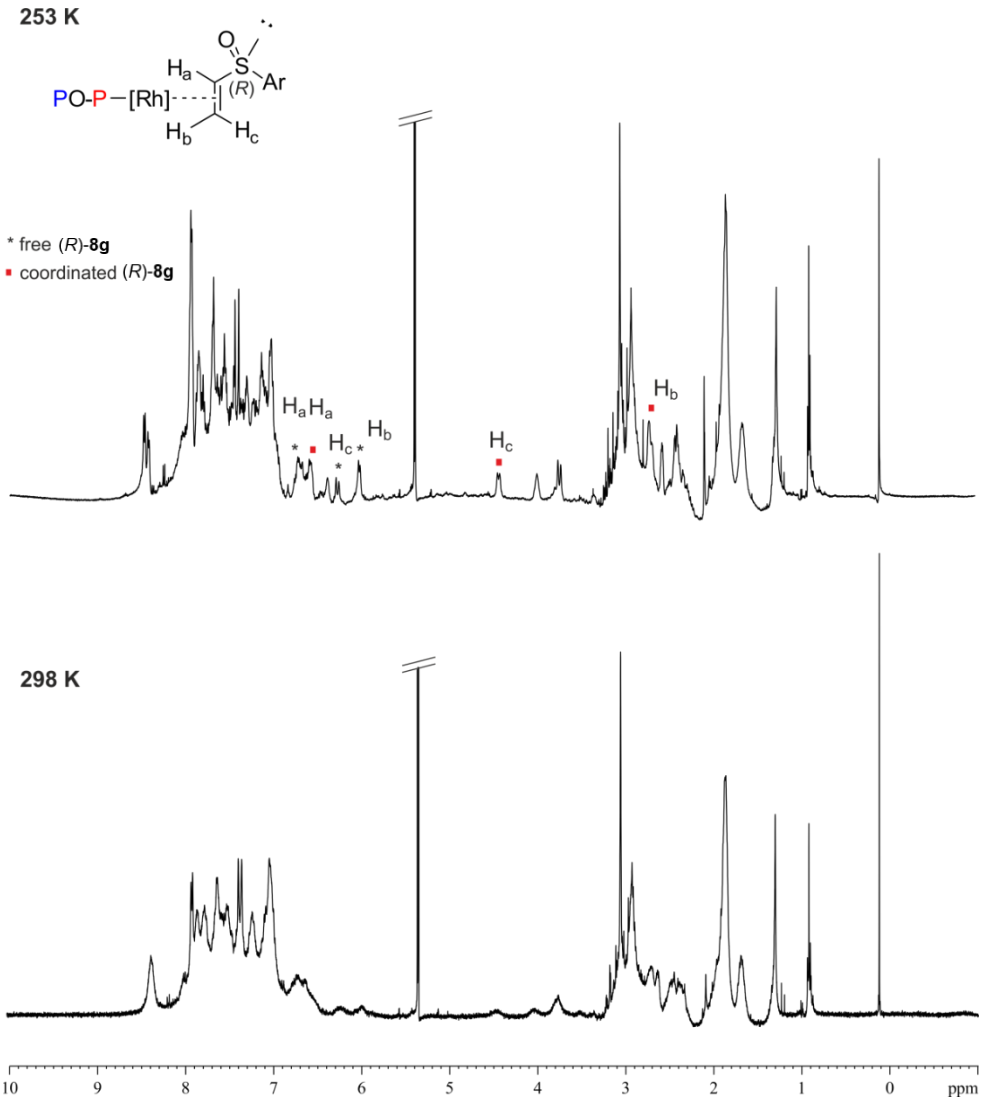

Figure 57. ^{1}H NMR spectrum (500 MHz, CD_2Cl_2, 298 K) of the in situ generated substrate-catalyst adduct [Rh((*R*)-**8g**)(**L3**)]BF_4 (bottom); ^{1}H NMR spectrum (500 MHz, CD_2Cl_2, 253 K) of the in situ generated substrate-catalyst adduct [Rh((*R*)-**8g**)(**L3**)]BF_4 (top).

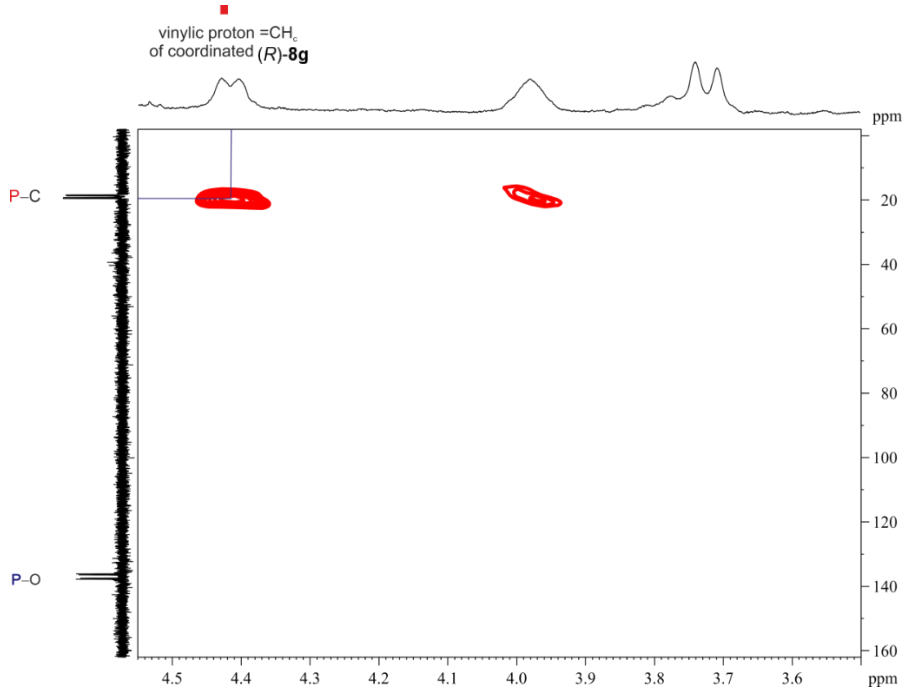

Figure 58. 2D ^{1}H-^{31}P NMR spectrum (CD_2Cl_2, 253 K) of the in situ generated substrate-catalyst adduct [Rh((*R*)-**8g**)(**L3**)]BF_4, expanded view of the olefinic proton-phosphine cross peak.

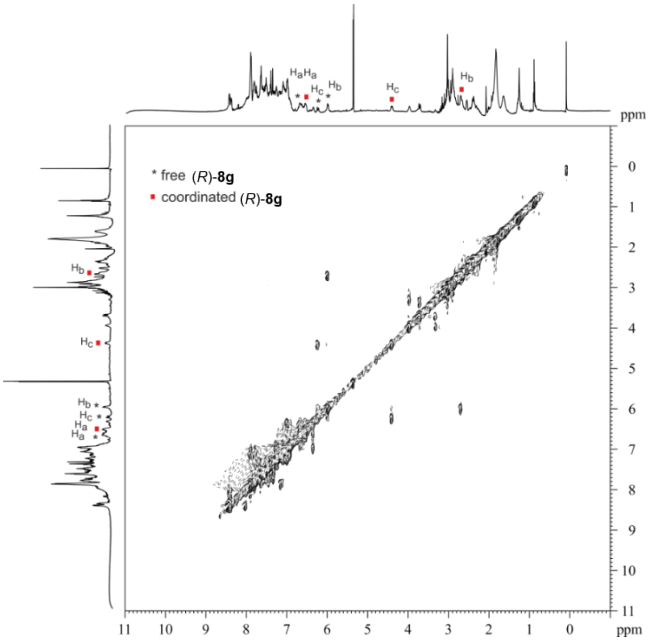

Figure 59. NOESY spectrum (CD_2Cl_2, 253K) of the in situ generated substrate-catalyst adduct [Rh((*R*)-**8g**)(**L3**)]BF_4.

2.5.9. Determination of the enantiomeric excess and the absolute configuration of reaction products 8a–h and 9a–h

The absolute configuration of compounds **8a,b** and **9a,b,f–h** were established by comparison with reported optical rotations. The absolute configuration of products of **8c–h** and **9c–e** were tentatively assigned by analogy with the stereochemical outcome of the reactions leading to **8a,b** and **9a,b,f–h**.

HPLC conditions for products **8a** and **9a**: Daicel Chiralcel® (25 cm x 0.46 cm) OB-H, 85:15 *n*-hexane/2-propanol, 0.5 mL/min, 254 nm. Retention times for the enantiomers: 24.4 min (*S*)-**9a**, 30.6 min (*S*)-**8a**, 50.4 min (*R*)-**8a**, 60.2 min (*R*)-**9a**.

HPLC conditions for products **8b** and **9b**: Daicel Chiralcel® (25 cm x 0.46 cm) OB-H, 85:15 *n*-hexane/2-propanol, 1.0 mL/min, 254 nm. Retention times for the enantiomers: 8.4 min (*S*)-**9b**, 10.5 min (*S*)-**8b**, 19.6 min (*R*)-**8b**, 28.7 min (*R*)-**9b**.

HPLC conditions for products **8c** and **9c**: Daicel Chiralcel® (25 cm x 0.46 cm) OB-H, 85:15 *n*-hexane/2-propanol, 1.0 mL/min, 254 nm. Retention times for the enantiomers: 7.2 min (*S*)-**9c**, 8.6 min (*S*)-**8c**, 16.9 min (*R*)-**8c**, 18.3 min (*R*)-**9c**.

HPLC conditions for products **8d** and **9d**: Daicel Chiralcel® (25 cm x 0.46 cm) OB-H, 85:15 *n*-hexane/2-propanol, 1.0 mL/min, 254 nm. Retention times for the enantiomers: 9.6 min (*S*)-**9d**, 10.5 min (*S*)-**8d**, 16.2 min (*R*)-**8d**, 18.8 min (*R*)-**9d**.

HPLC conditions for products **8e** and **9e**: Daicel Chiralpak® (25 cm x 0.46 cm) ID, 98:2 *n*-hexane/2-propanol, 1.0 mL/min, 254 nm. Retention times for the enantiomers: 44.7 min (*R*)-**8e**, 45.7 min (*S*)-**8e**, 62.2 min (*S*)-**9e**, 64.2 min (*R*)-**9e**.

HPLC conditions for products **8f** and **9f**: Daicel Chiralcel® (25 cm x 0.46 cm) OB-H, 85:15 *n*-hexane/2-propanol, 1.0 mL/min, 254 nm. Retention times for the enantiomers: 14.2 min (*S*)-**9f**, 22.0 min (*S*)-**8f**, 33.0 min (*R*)-**8f**, 56.1 min (*R*)-**9f**.

HPLC conditions for products **8g** and **9g**: Daicel Chiralpak® (25 cm x 0.46 cm) ID, 85:15 *n*-hexane/2-propanol, 1.0 mL/min, 254 nm. Retention times for the enantiomers: 20.4 min (*S*)-**8g**, 21.5 min (*S*)-**9g**, 22.2 min (*R*)-**8g**, 23.6 min (*R*)-**9g**.

HPLC conditions for products **8h** and **9h**: Daicel Chiralcel® (25 cm x 0.46 cm) OB-H, 95:5 *n*-hexane/2-propanol, 1.0 mL/min, 210 nm. Retention times for the enantiomers: 31.4 min (*R*)-**9h**, 34.2 min (*R*)-**8h**, 38.6 min (*S*)-**9h**, 47.6 min (*S*)-**8h**.

(*S*)-phenyl vinyl sulfoxide (*S*)-**8a** (Table 13, entry 1): Spectral data were in agreement with those reported;[95] 99% ee, $[\alpha]^{28}_{D}$ = −267.1 (*c* 0.4, $CHCl_3$) [Lit:[95] $[\alpha]^{20}_{D}$ = +271.6 (*c* 0.5, $CHCl_3$) for 95% ee (*R*)].

(*R*)-ethyl phenyl sulfoxide (*R*)-**9a** (Table 13, entry 2): Spectral data were in agreement with those reported;[95] 86% ee, $[\alpha]^{27}_{D}$ = +151.5 (*c* 0.3, EtOH) [Lit:[95] $[\alpha]^{25}_{D}$ = +184.7 (*c* 1.2, EtOH) for 90% ee (*R*)].

(*S*)-(*p*-Me)-phenyl vinyl sulfoxide (*S*)-**8b** (Table 13, entry 3): Spectral data were in agreement with those reported;[88b] 98% ee, $[\alpha]^{27}_{D}$ = −389.7 (*c* 0.3, acetone) [Lit:[96] $[\alpha]^{25}_{D}$ = +446 (*c* 1.65, acetone) for 99% ee (*R*)].

(*R*)-ethyl (*p*-Me)-phenyl sulfoxide (*R*)-**9b** (Table 13, entry 4): Spectral data were in agreement with those reported;[97] 95% ee, $[\alpha]^{28}_{D}$ = +84.8 (*c* 0.4, $CHCl_3$) [Lit:[98] $[\alpha]^{23}_{D}$ = −247 (*c* 2.60, $CHCl_3$) for 99% ee (*S*)].

(*S*)-(*o*-F)-phenyl vinyl sulfoxide (*S*)-**8c** (Table 13, entry 5): New compound; spectroscopic date of vinyl sulfoxide **8c** was in agreement with that obtained for *rac*-**8c**; 99% ee, $[\alpha]^{28}_{D}$ = −384.9 (*c* 0.7, $CHCl_3$).

(*R*)-ethyl (*o*-F)-phenyl sulfoxide (*R*)-**9c** (Table 13, entry 6): New compound; 97% ee, $[\alpha]^{28}_{D}$ = +88.6 (*c* 0.6, $CHCl_3$); ^{1}H NMR (500 MHz, $CDCl_3$) δ 7.83–7.79 (m, 1H), 7.51–7.46 (m, 2H), 7.40–7.36 (m, 1H), 7.13–7.09 (m, 1H), 3.12–3.03 (m,

(95) Liao, S.; Čorić, I.; Wang, Q.; List, B. *J. Am. Chem. Soc.* **2012**, *134*, 10765-10768.
(96) de Castries, A.; Escande, A.; Fensterbank, H.; Magnier, E.; Marrot, J.; Larpent, C. *Tetrahedron* **2007**, *63*, 10330-10336.
(97) Yoshino, T.; Imori, S.; Togo, H. *Tetrahedron* **2006**, *62*, 1309-1317.
(98) Blakemore, P. R.; Burge, M. S. *J. Am. Chem. Soc.* **2007**, *129*, 3068-3069.

1H), 2.90–2.81 (m, 1H), 1.23 (t, J= 7.2 Hz, 3H); $^{13}C\{^1H\}$ NMR (125 MHz, $CDCl_3$) δ 157.7 (d, J= 246.7 Hz, C–F), 132.6 (d, J= 7.7 Hz, CH), 130.3 (d, J= 16.8 Hz, C–S), 126.4 (d, J= 2.1 Hz, CH), 125.1 (d, J= 3.0 Hz, CH), 115.6 (d, J= 20.2 Hz, CH), 48.0 (d, J = 1.2 Hz, CH_2), 5.6 (CH_3); $^{19}F\{^1H\}$ NMR (471 MHz, $CDCl_3$) δ −114.6 (s); HRMS (ESI^+) *m/z* calcd for $C_8H_{10}FOS$ $[M+H]^+$ 170.0431, found 173.0435.

(*S*)-(*m*-F)-phenyl vinyl sulfoxide (*S*)-**8d** (Table 13, entry 7): New compound; spectroscopic data of vinyl sulfoxide **8d** were in agreement with those obtained for *rac*-**8d**; 98% ee, $[\alpha]^{29}_D$ = −166.7 (*c* 0.3, $CHCl_3$).

(*R*)-ethyl (*m*-F)-phenyl sulfoxide (*R*)-**9d** (Table 13, entry 8): New compound; 92% ee, $[\alpha]^{29}_D$ = +95.0 (*c* 0.5, $CHCl_3$); ^1H NMR (400 MHz, $CDCl_3$) δ 7.54–7.49 (m, 1H), 7.41–7.36 (m, 2H), 7.22–7.17 (m, 1H), 2.99–2.90 (m, 1H), 2.82–2.73 (m, 1H), 1.23 (t, J = 7.3 Hz, 3H); $^{13}C\{^1H\}$ NMR (100 MHz, $CDCl_3$) δ 163.1 (d, J= 251.8 Hz, C–F), 146.0 (d, J= 5.5 Hz, C–S), 130.8 (d, J= 7.6 Hz, CH), 119.8 (d, J= 3.2 Hz, CH), 118.0 (d, J= 21.6, CH), 111.5 (d, J= 23.9 Hz, CH), 50.3 (CH_2), 5.7 (CH_3); $^{19}F\{^1H\}$ NMR (376 MHz, $CDCl_3$) δ −109.9 (s); HRMS (ESI^+) *m/z* calcd for $C_8H_{10}FOS$ $[M+H]^+$ 170.0431, found 170.0433.

(*S*)-(*p*-F)-phenyl vinyl sulfoxide (*S*)-**8e** (Table 13, entry 9): Spectral data were in agreement with those reported;[89] 98% ee, $[\alpha]^{29}_D$ = −292.1 (*c* 0.2, $CHCl_3$).

(*R*)-ethyl (*p*-F)-phenyl sulfoxide (*R*)-**8e** (Table 13, entry 10): Spectral data were in agreement with those reported;[99] 90% ee, $[\alpha]^{29}_D$ = +135.3 (*c* 0.2, $CHCl_3$).

(*S*)-(*p*-MeO)-phenyl vinyl sulfoxide (*S*)-**8f** (Table 13, entry 11): Spectral data were in agreement with those reported;[90] 99% ee, $[\alpha]^{29}_D$ = −197.8 (*c* 0.6, $CHCl_3$).

(*R*)-ethyl-(*p*-MeO)-phenyl sulfoxide (*R*)-**9f** (Table 13, entry 12): Spectral data were in agreement with those reported;[100] 88% ee, $[\alpha]^{29}_D$ = +81.4 (*c* 0.6, $CHCl_3$) [Lit:[100] $[\alpha]^{25}_D$ = +166 (*c* 1.2, $CHCl_3$) for 93% ee (*R*)].

(99) Carrea, G.; Redigolo, B.; Riva, S.; Colonna, S.; Gaggero, N.; Battistel, E.; Bianchi, D. *Tetrahedron: Asymmetry* **1992**, *3*, 1063-1068.
(100) García Ruano, J. L.; Alemparte, C.; Teresa Aranda, M.; Zarzuelo, M. M. *Org. Lett.* **2003**, *5*, 75-78.

(*S*)-(*p*-NO_2)-phenyl vinyl sulfoxide (*S*)-**8g** (Table 13, entry 13): Spectral data were in agreement with those reported;[90] 99% ee, $[\alpha]^{29}_D = -245.1$ (*c* 0.3, $CHCl_3$).

(*R*)-ethyl (*p*-NO_2)-phenyl sulfoxide (*R*)-**9g** (Table 13, entry 14): Spectral data were in agreement with those reported;[101] 82% ee, $[\alpha]^{29}_D = +134.0$ (*c* 0.3, $CHCl_3$) [Lit:[102] $[\alpha]^{25}_D = -107.5$ (*c* 1.65, $CHCl_3$) for 57% ee (*S*)].

(*R*)-benzyl vinyl sulfoxide (*R*)-**8h** (Table 13, entry 15): Spectral data were in agreement with those reported;[93] 99% ee, $[\alpha]^{29}_D = -213.0$ (*c* 0.2, $CHCl_3$).

(*S*)-benzyl ethyl sulfoxide (*S*)-**9h** (Table 13, entry 16): 80% ee, $[\alpha]^{26}_D = -33.0$ (*c* 0.1, EtOH) [Lit:[103] $[\alpha]^{24}_D = +17$ (*c* 1.0, EtOH) for 32% ee (*R*)]; ^{1}H NMR (400 MHz, $CDCl_3$) δ 7.38–7.29 (m, 5H), 3.98 (dd, *J* = 34.2 Hz, *J* = 12.7 Hz, 2H), 2.69–2.51 (m, 2H), 1.33 (t, *J* = 7.4 Hz, 3H); $^{13}C\{^1H\}$ NMR (100 MHz, $CDCl_3$) δ 129.9 (CH), 128.9 (CH), 128.3 (CH), 57.5 (CH_2), 44.0 (CH_2), 6.58 (CH_3); HRMS (ESI^+) *m/z* calcd for $C_9H_{12}NaOS$ $[M+Na]^+$ 191.0501, found 191.0499.

2.5.10. Complete data from Figure 45

The catalytic experiments were performed following the general procedure for the KR by Rh-mediated asymmetric hydrogenations. The complete data from Figure 45 is shown in Table 16.

(101) Liao, S.; List, B. *Adv. Synth. Catal.* **2012**, *354*, 2363-2367.
(102) Tohma, H.; Takizawa, S.; Watanabe, H.; Fukuoka, Y.; Maegawa, T.; Kita, Y. *J. Org. Chem.* **1999**, *64*, 3519-3523.
(103) Glahsl, G.; Herrmann, R. *J. Chem. Soc., Perkin Trans. 1* **1988**, 1753-1757.

Table 16. KR by Rh-mediated asymmetric hydrogenation of racemic vinyl sulfoxide *rac*-8c at different reaction times[a]

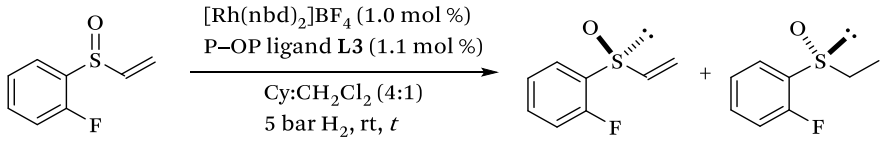

rac-8c (*S*)-8c (*R*)-9c

entry	*t*, min	conv., %[b]	ee of 8c, %;[c] (*S*)[d]	ee of 9c, %;[c] (*R*)[d]
1	6	32	44	98
2	8	44	69	97
3	15	55	99	82
4	30	63	99	60
5	45	67	99	51
6	60	75	99	34
7	80	77	99	30
8	100	82	99	23
9	120	91	99	14

[a,b,c,d]See notes *a*, *b* and *c* in Table 11, and *d* in Table 13.

2.5.11. NMR spectra of new compounds

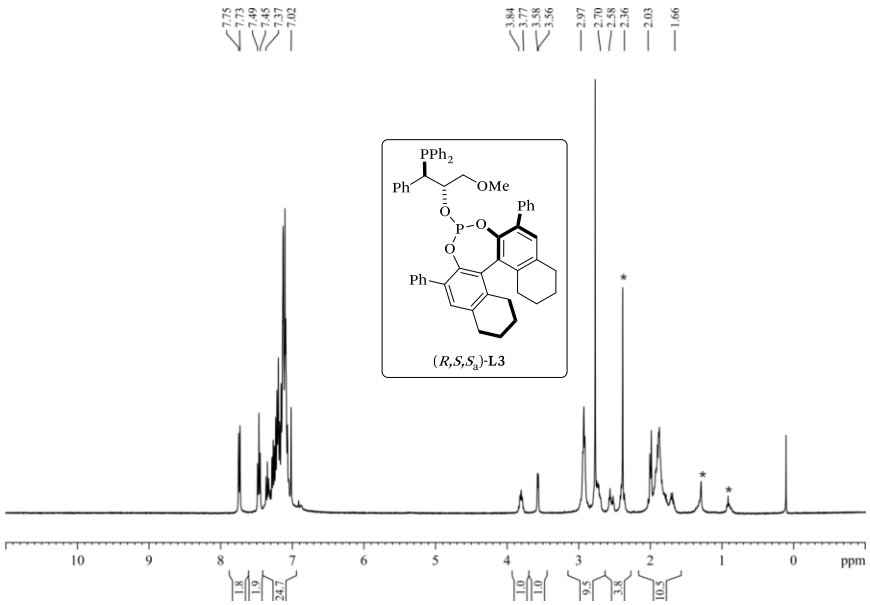

Figure 60. ^{1}H NMR (400 MHz, $CDCl_3$) of P–OP ligand **L3**.

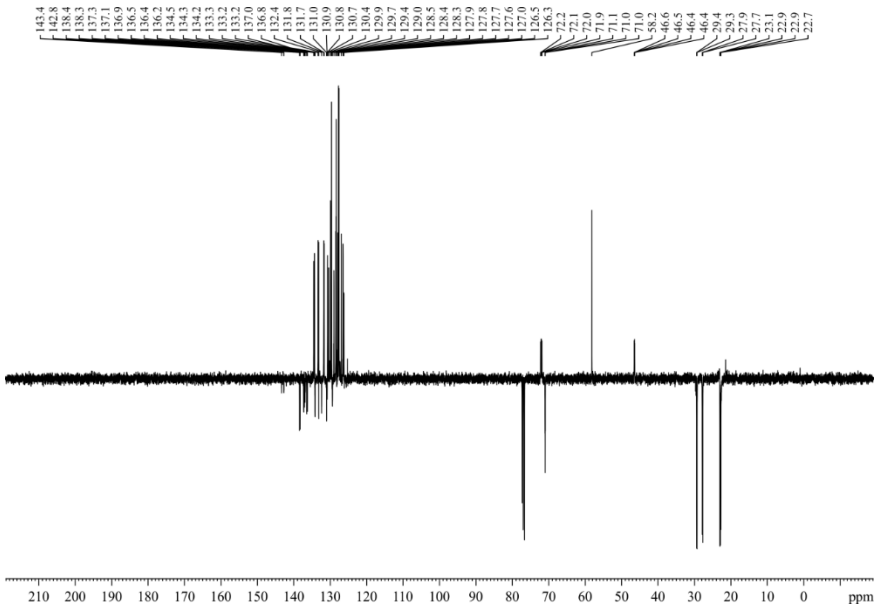

Figure 61. $^{13}C\{^{1}H\}$ NMR as DEPTQ135 (100 MHz, $CDCl_3$) of P–OP ligand **L3**.

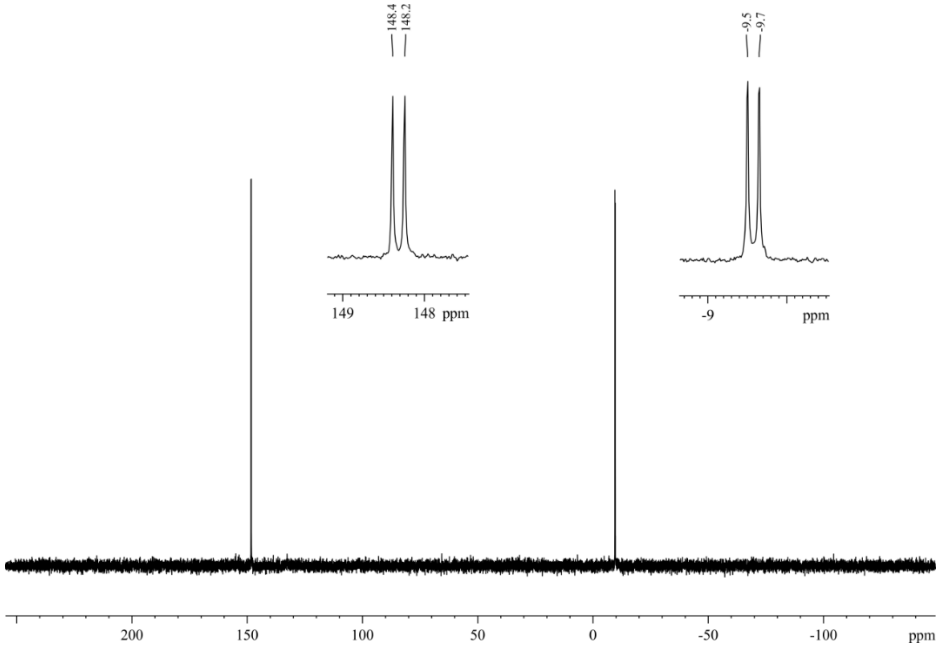

Figure 62. $^{31}P\{^{1}H\}$ NMR (162 MHz, $CDCl_3$) of P–OP ligand **L3**.

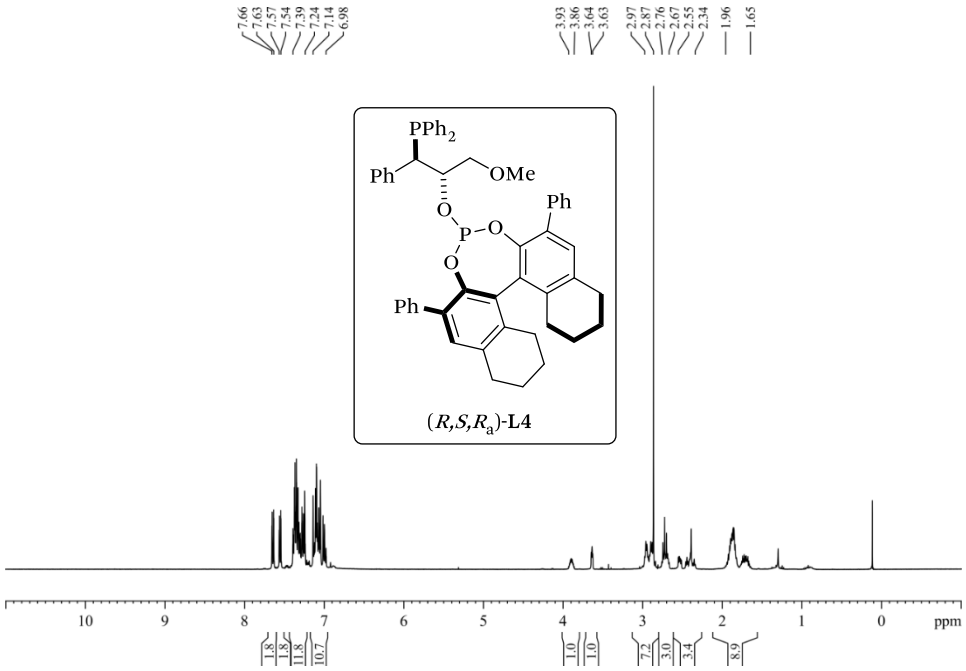

Figure 63. ^{1}H NMR (400 MHz, $CDCl_3$) of P–OP ligand **L4**.

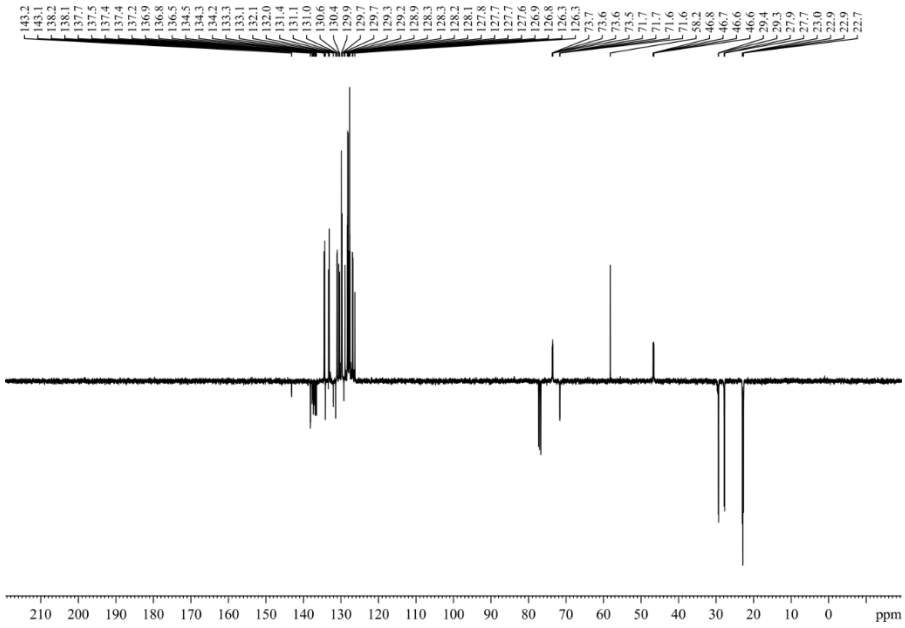

Figure 64. $^{13}C\{^{1}H\}$ NMR as DEPTQ135 (100 MHz, $CDCl_3$) of P–OP ligand **L4**.

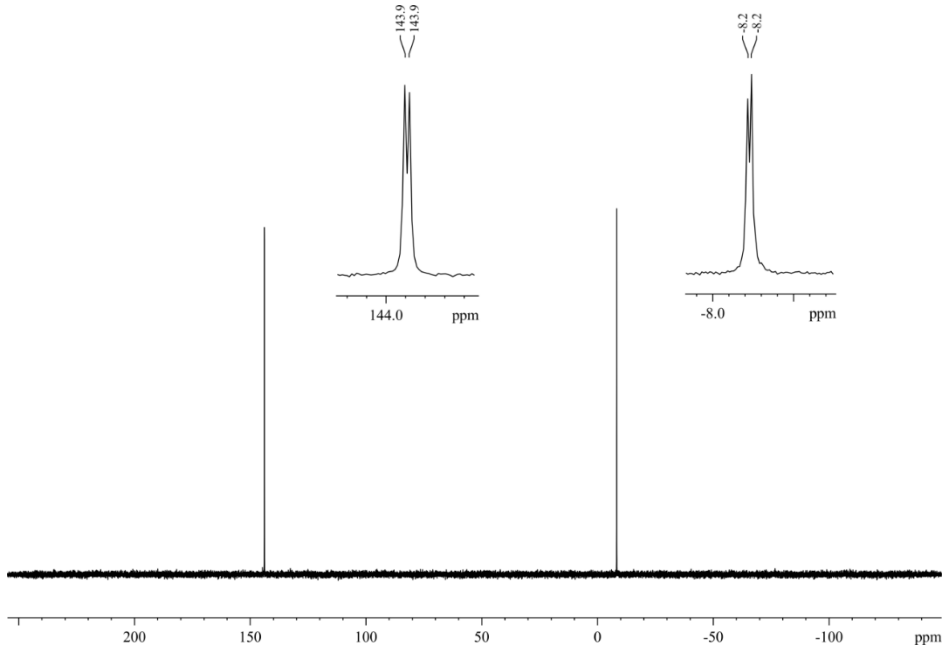

Figure 65. $^{31}P\{^{1}H\}$ NMR (162 MHz, $CDCl_3$) of P–OP ligand **L4**.

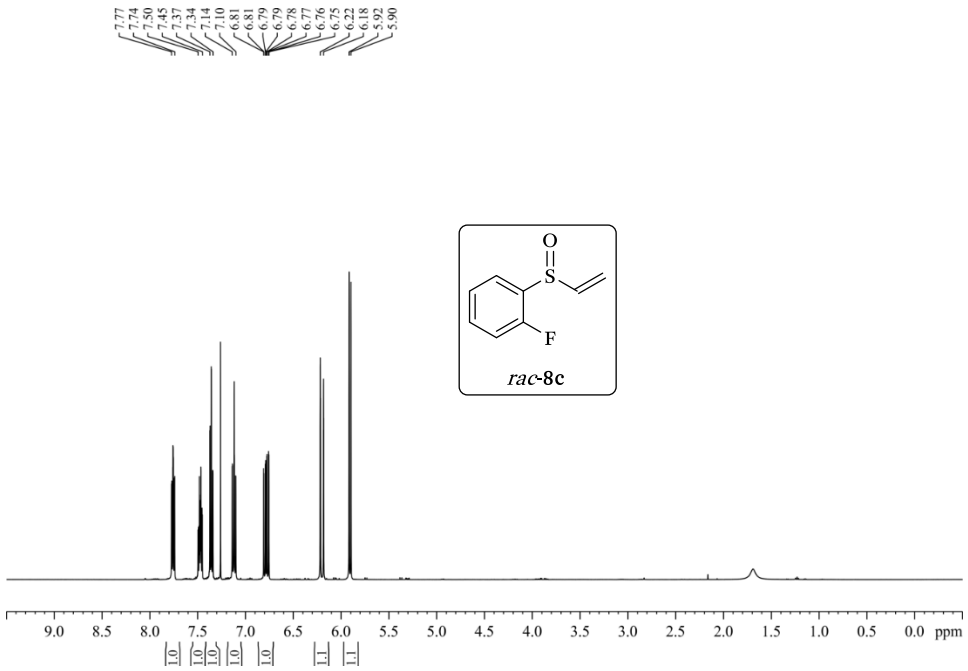

Figure 66. ^{1}H NMR (500 MHz, $CDCl_3$) of *rac*-**8c**.

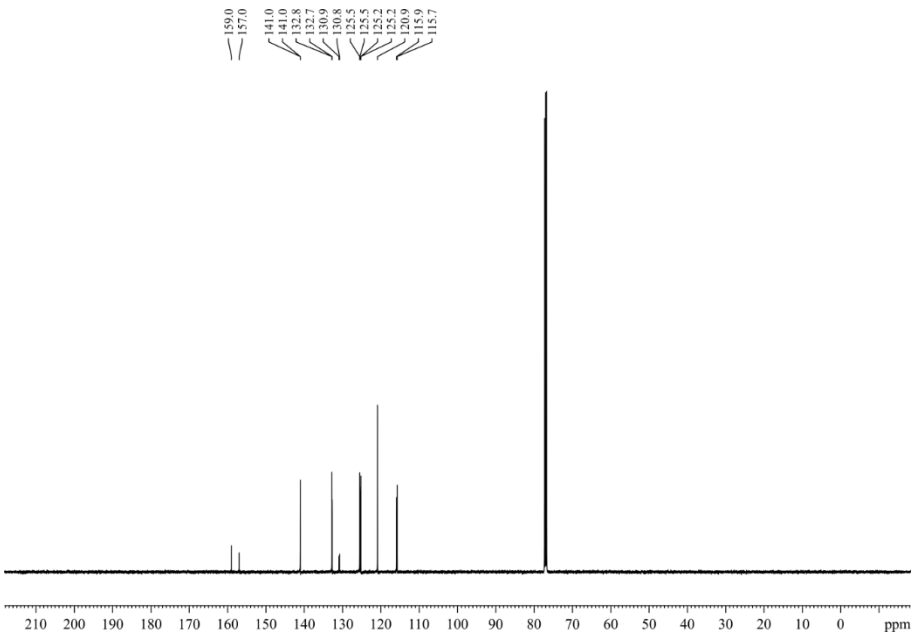

Figure 67. $^{13}C\{^{1}H\}$ NMR (125 MHz, $CDCl_3$) of *rac*-**8c**.

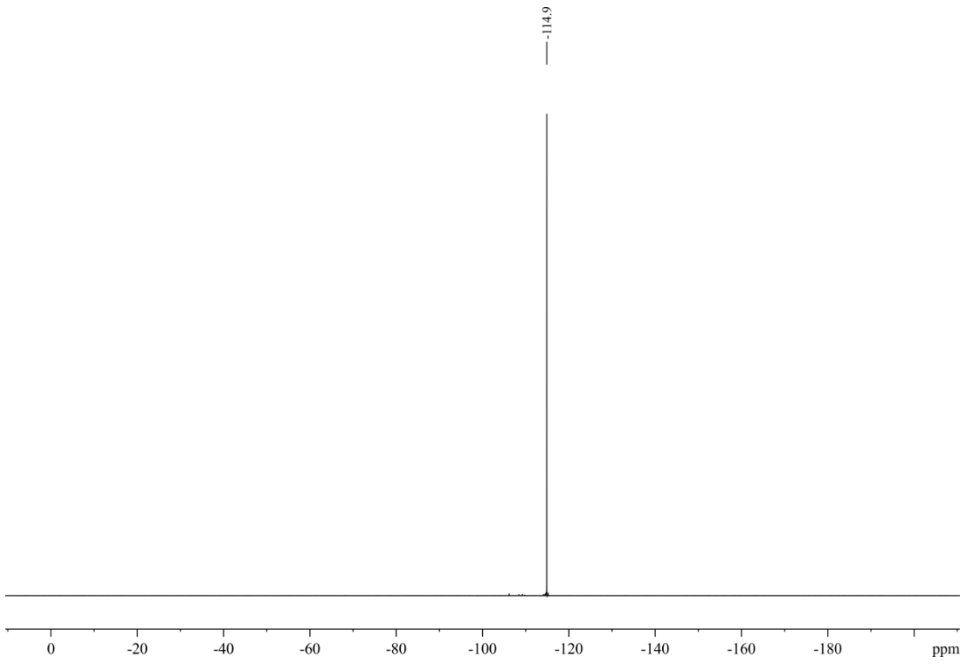

Figure 68. $^{19}F\{^{1}H\}$ NMR (471 MHz, $CDCl_3$) of *rac*-**8c**.

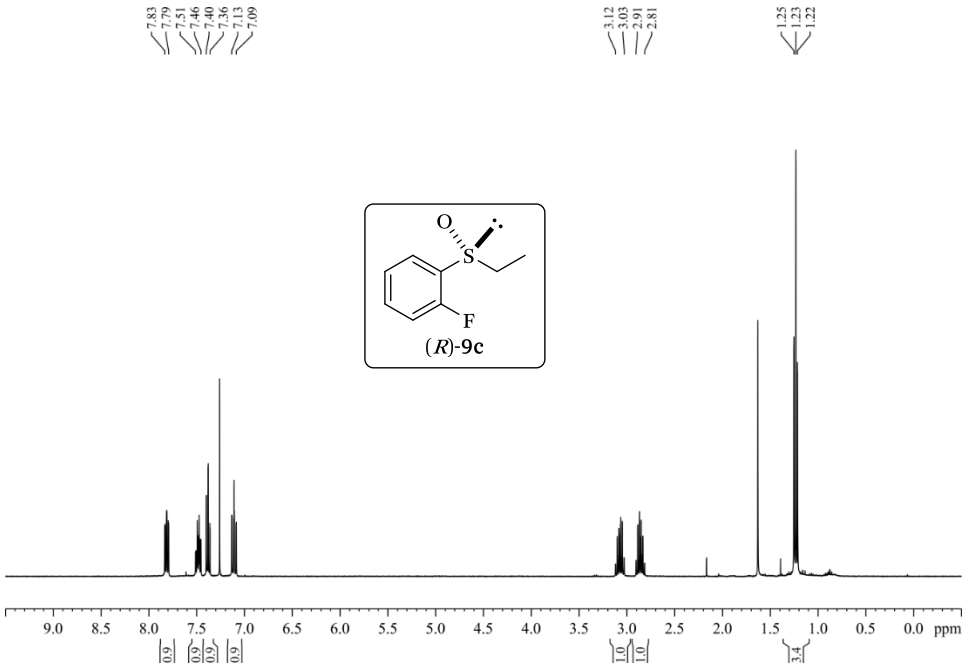

Figure 69. ^{1}H NMR (400 MHz, $CDCl_3$) of (*R*)-**9c**.

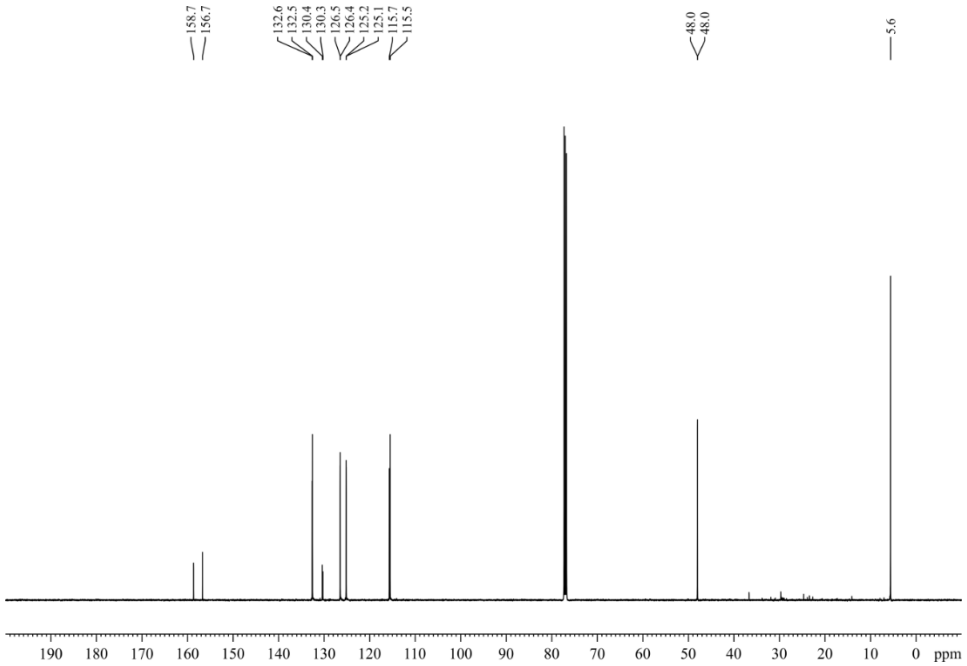

Figure 70. $^{13}C\{^{1}H\}$ NMR (125 MHz, $CDCl_3$) of (*R*)-**9c**.

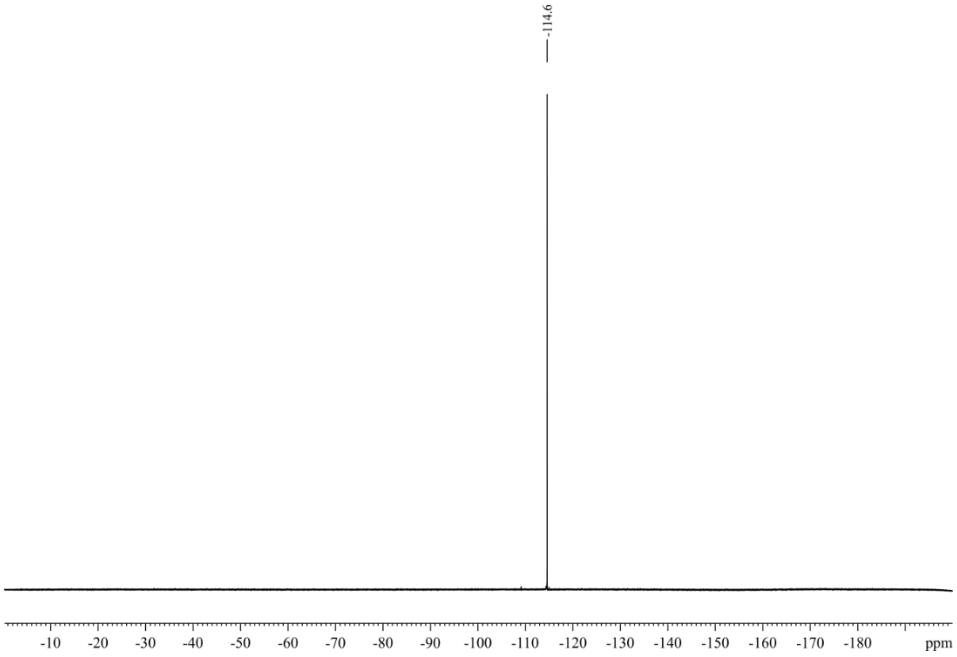

Figure 71. $^{19}F\{^{1}H\}$ NMR (376 MHz, $CDCl_3$) of (*R*)-**9c**.

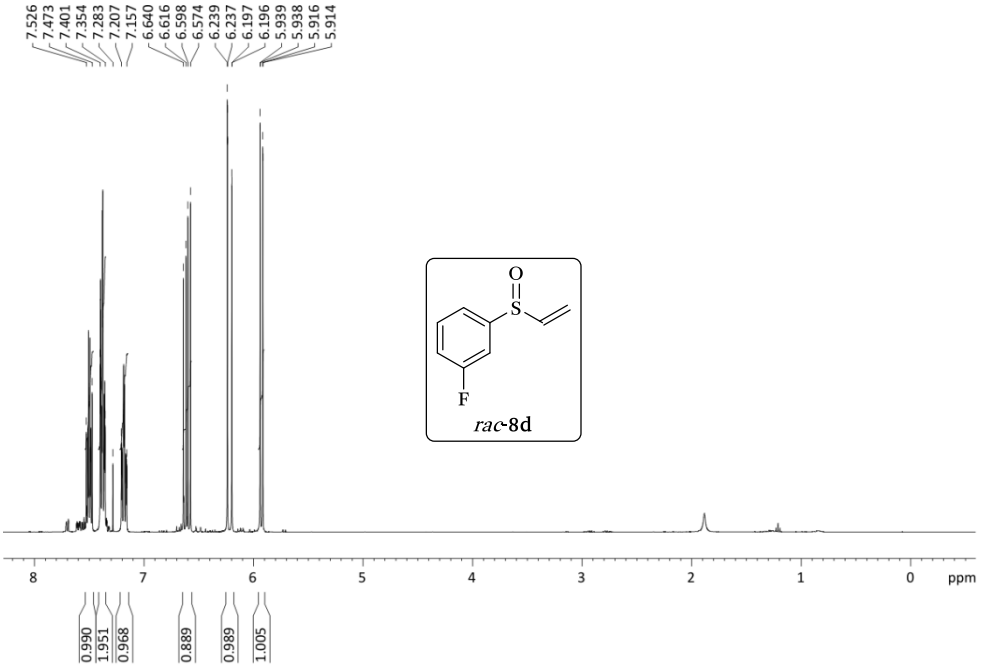

Figure 72. ^{1}H NMR (400 MHz, $CDCl_3$) of *rac*-**8d**.

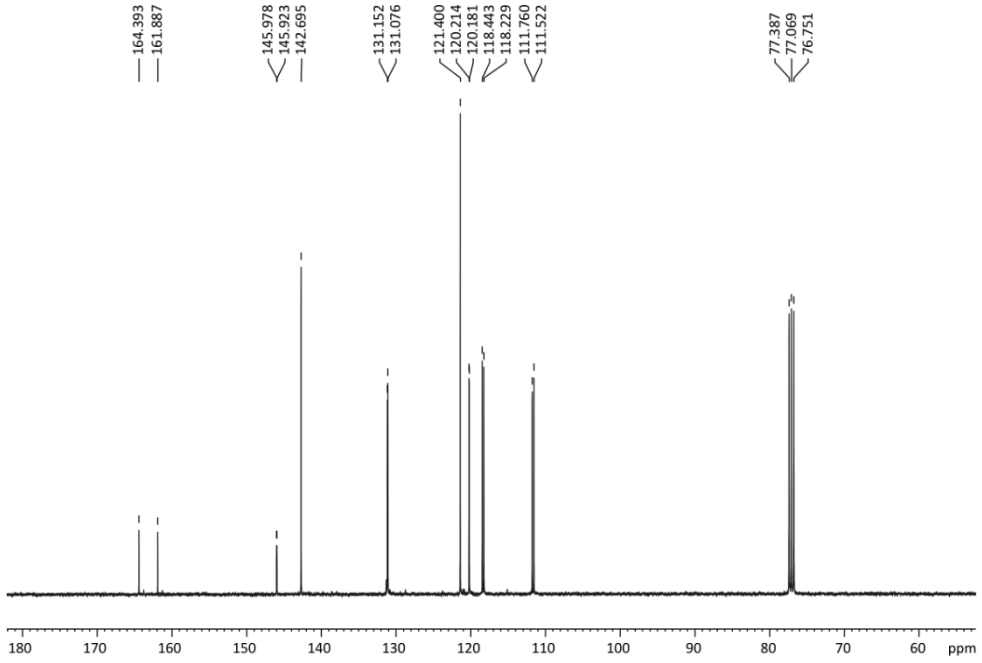

Figure 73. $^{13}C\{^{1}H\}$ NMR (100 MHz, $CDCl_3$) of *rac*-**8d**.

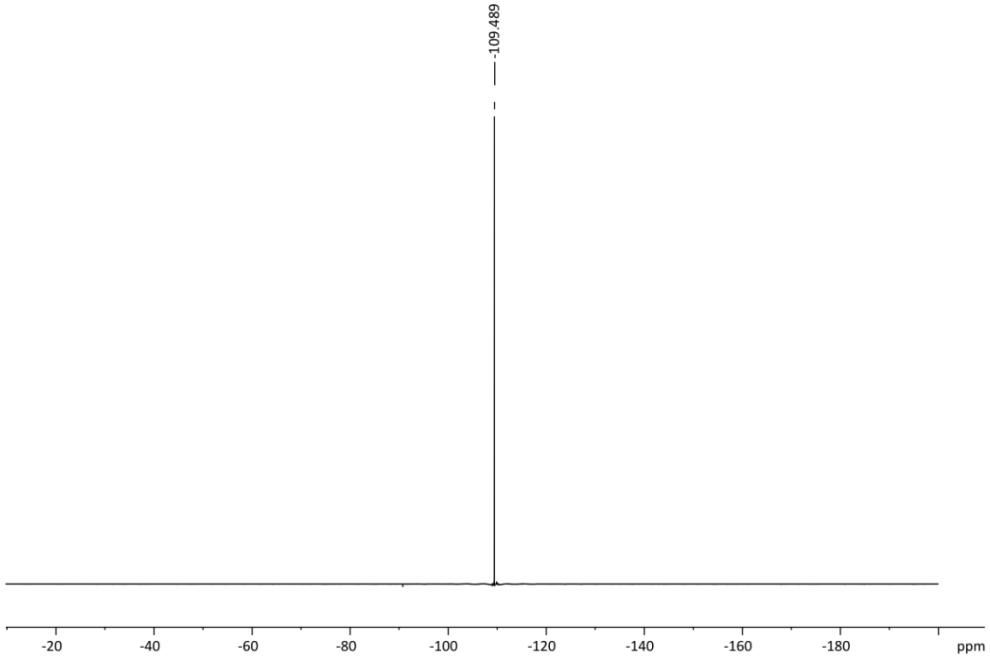

Figure 74. $^{19}F\{^{1}H\}$ NMR (376 MHz, $CDCl_3$) of *rac*-**8d**.

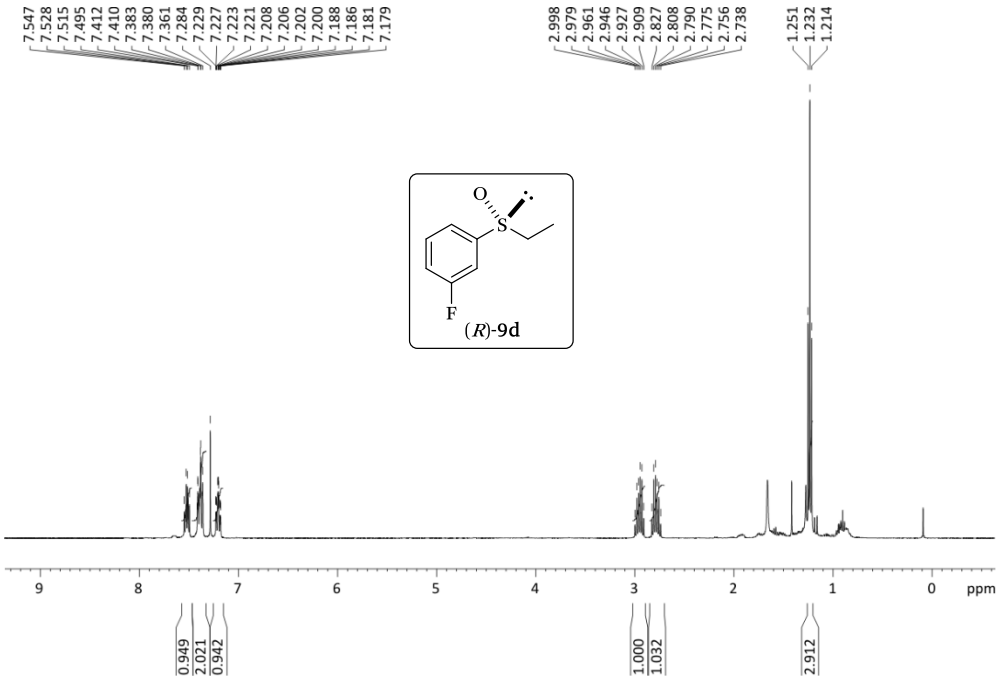

Figure 75. ^{1}H NMR (400 MHz, $CDCl_3$) of (*R*)-**9d**.

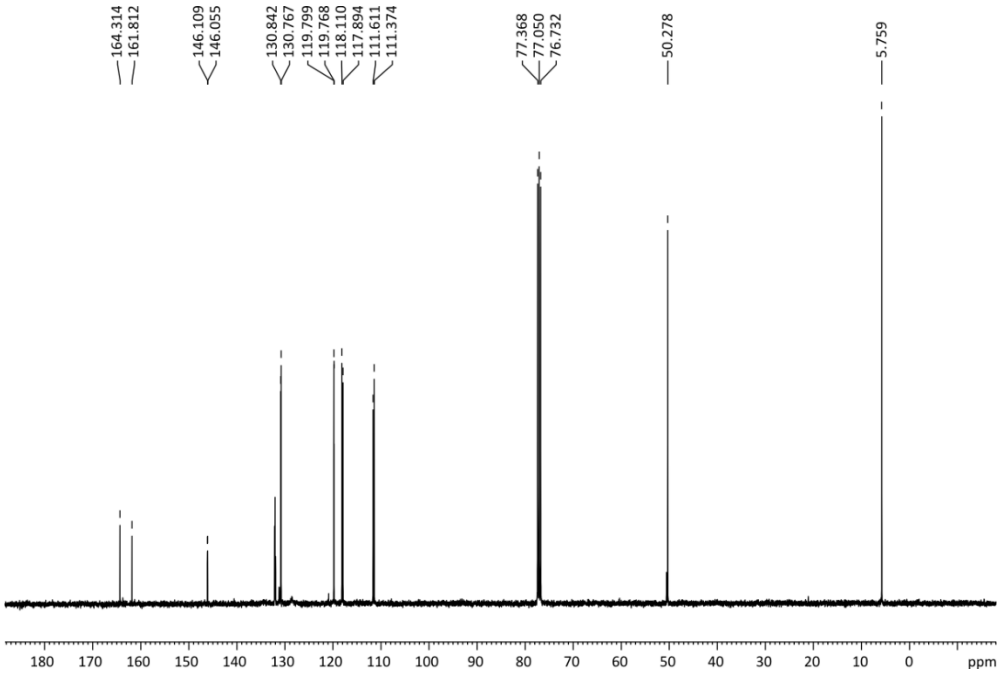

Figure 76. $^{13}C\{^{1}H\}$ NMR (100 MHz, $CDCl_3$) of (*R*)-**9d**.

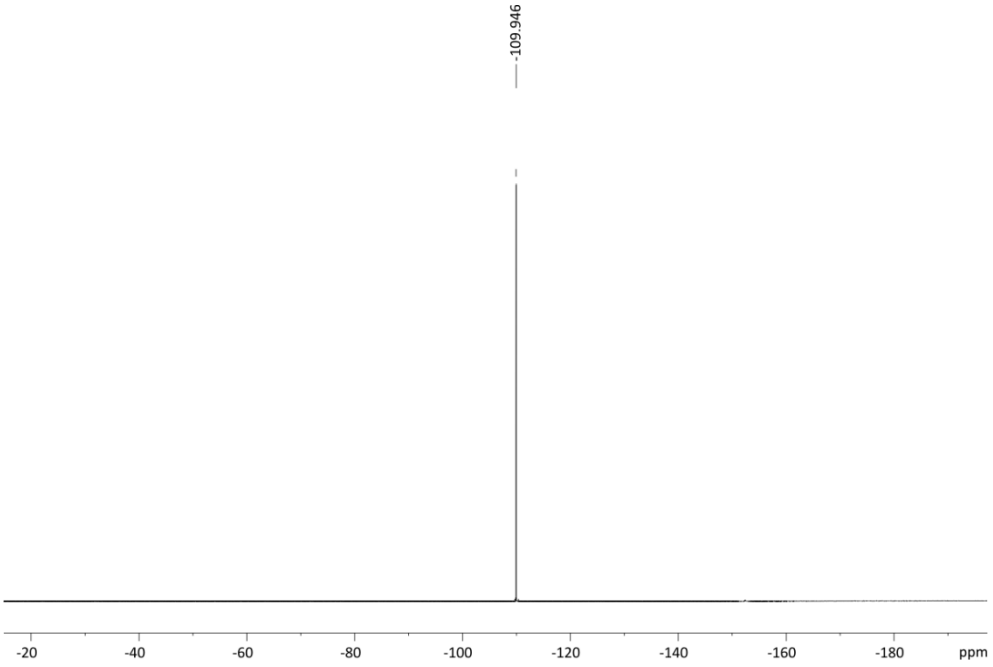

Figure 77. $^{19}F\{^{1}H\}$ NMR (376 MHz, $CDCl_3$) of (*R*)-**9d**.

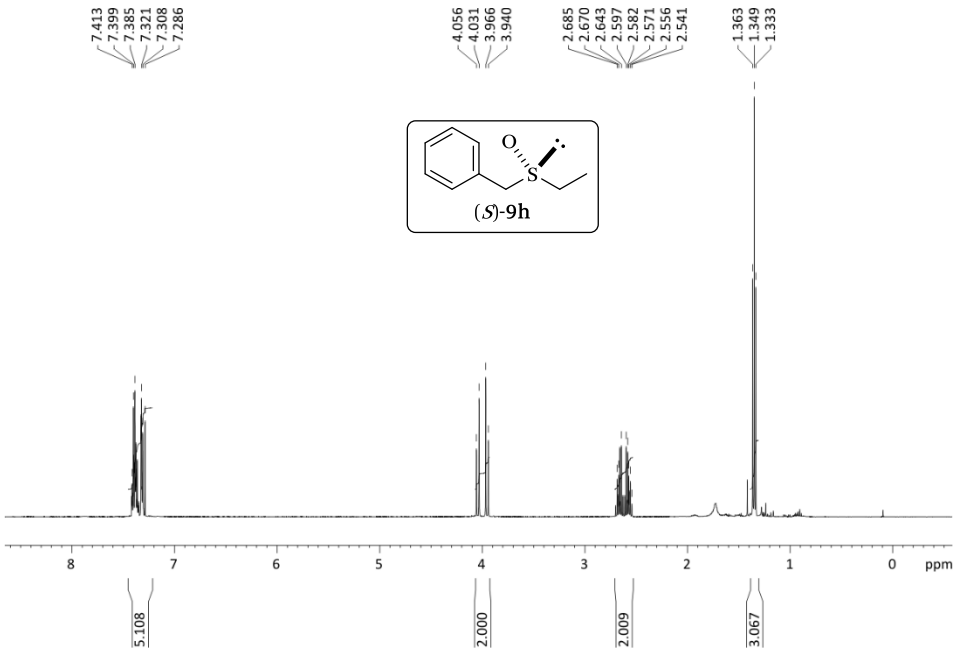

Figure 78. ^{1}H NMR (400 MHz, $CDCl_3$) of (*S*)-**9h**.

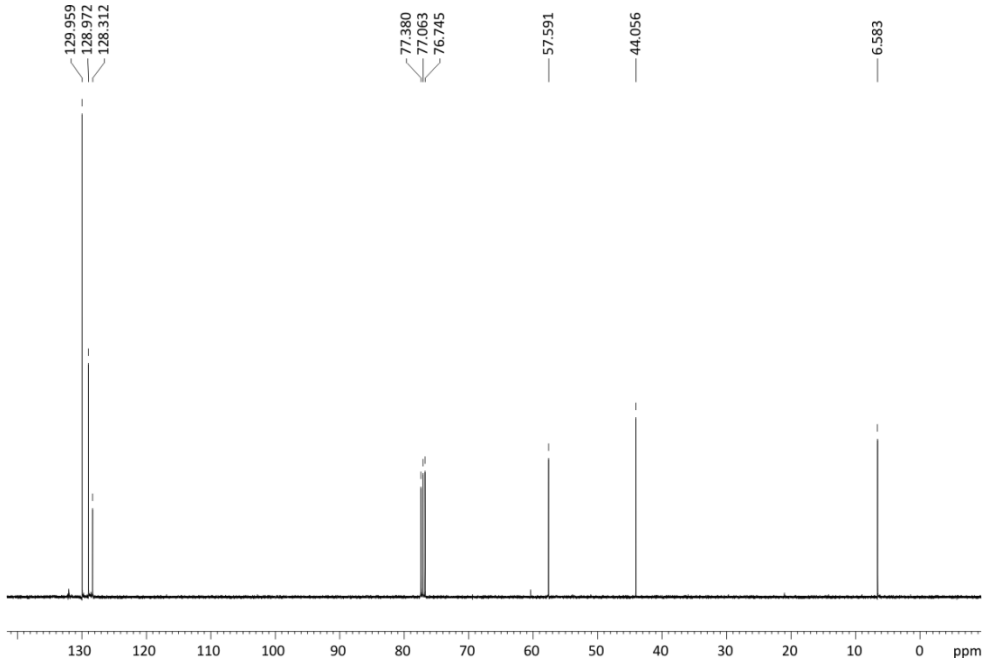

Figure 79. $^{13}C\{^{1}H\}$ NMR (100 MHz, $CDCl_3$) of (*S*)-**9h**.

2.5.12. Selected NMR and HPLC data from catalytic experiments

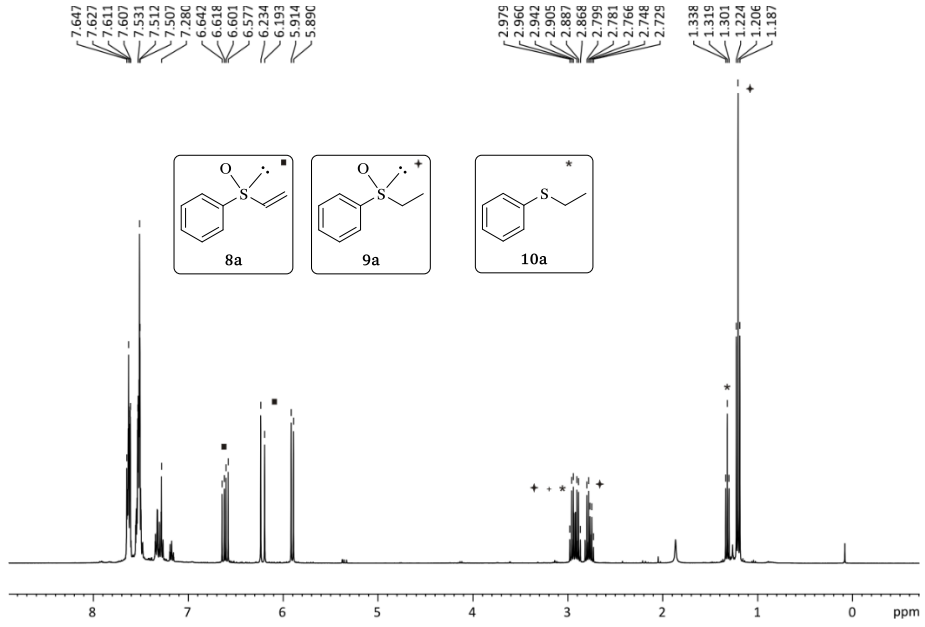

Figure 80. ^{1}H NMR spectrum of the mixture reaction for the KR by Rh-mediated asymmetric hydrogenation of *rac*-**8a** with P–OP ligand **L2** (Table 12, entry 1).

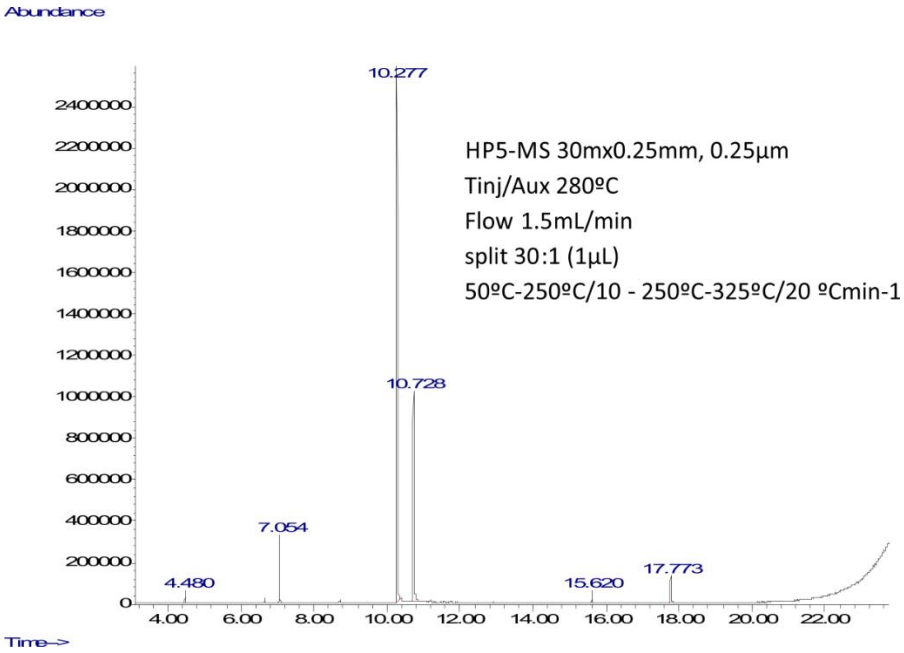

Figure 81. GC-MS analysis of the mixture reaction for the KR by Rh-mediated asymmetric hydrogenation of *rac*-**8a** with P–OP ligand **L2** (Table 11, entry 1).

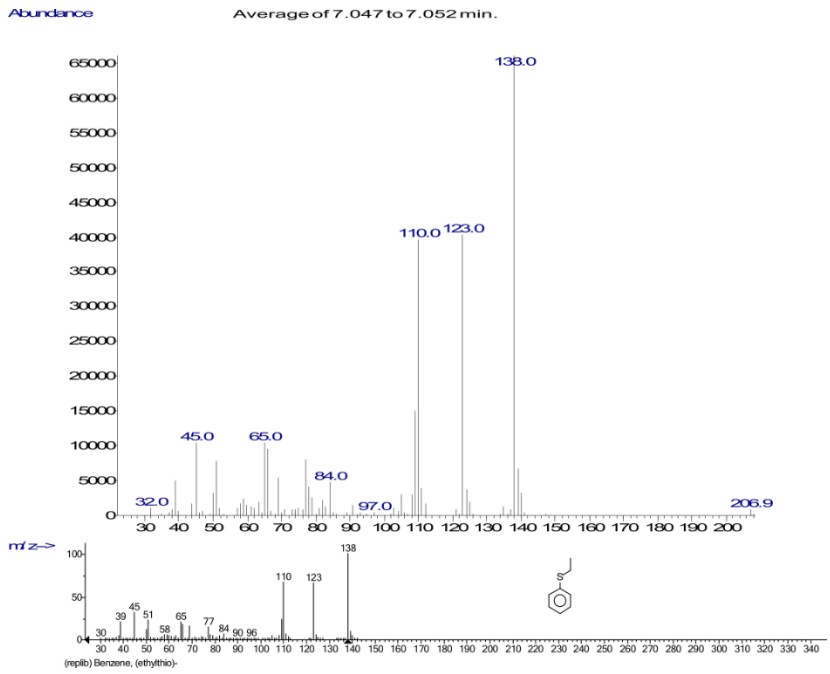

Figure 82. GC-MS analysis of the mixture reaction for the KR by Rh-mediated asymmetric hydrogenation of *rac*-**8a** with P–OP ligand **L2** (Table 12, entry 1).

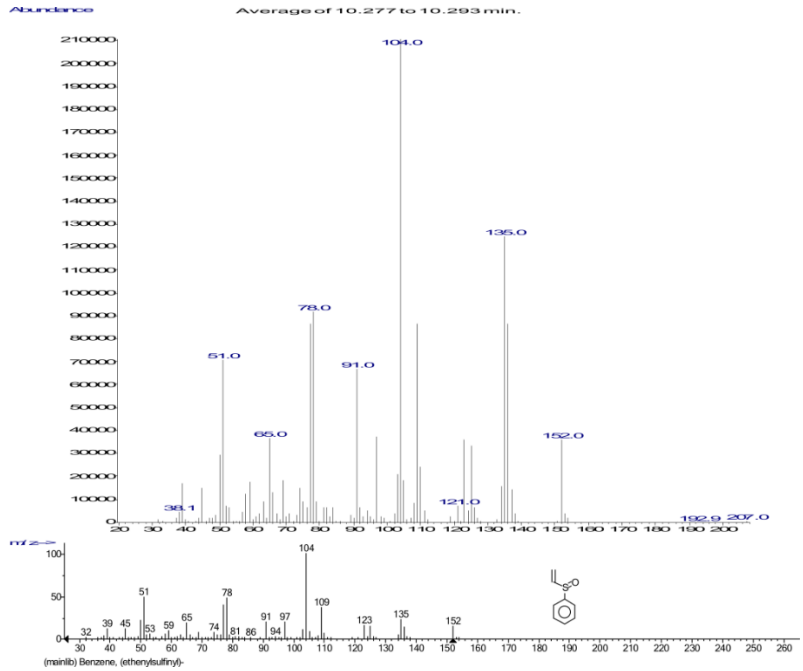

Figure 83. GC-MS analysis of the mixture reaction for the KR by Rh-mediated asymmetric hydrogenation of *rac*-**8a** with P–OP ligand **L2** (Table 12, entry 1).

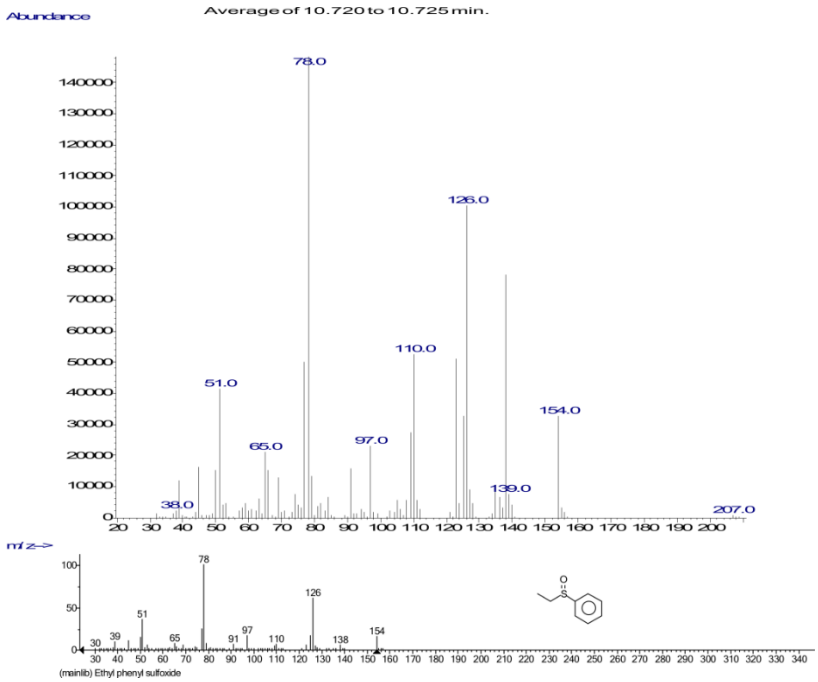

Figure 84. GC-MS analysis of the mixture reaction for the KR by Rh-mediated asymmetric hydrogenation of *rac*-**8a** with P–OP ligand **L2** (Table 12, entry 1).

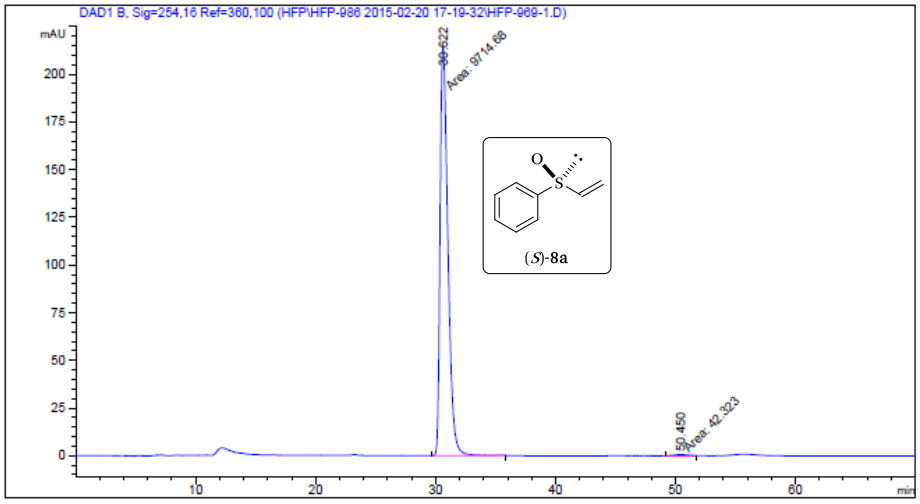

Peak #	RetTime [min]	Type	Width [min]	Area [mAU*s]	Height [mAU]	Area %
1	30.622	MM	0.7554	9714.68359	214.34058	99.5662
2	50.450	MM	1.2406	42.32296	5.68572e-1	0.4338

Figure 85. Chiral HPLC trace for the KR by asymmetric hydrogenation of *rac*-**8a**, product (*S*)-**8a** (Table 13, entry 1).

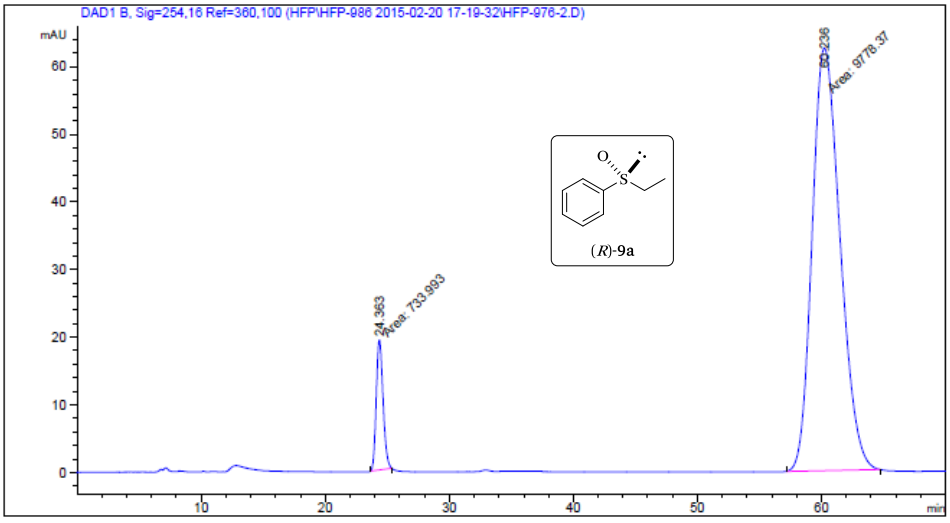

Peak #	RetTime [min]	Type	Width [min]	Area [mAU*s]	Height [mAU]	Area %
1	24.363	MM	0.6361	733.99341	19.23108	6.9822
2	60.236	MM	2.6073	9778.37207	62.50653	93.0178

Figure 86. Chiral HPLC trace for the KR by asymmetric hydrogenation of *rac*-**8a**, product (*R*)-**9a** (Table 13, entry 2).

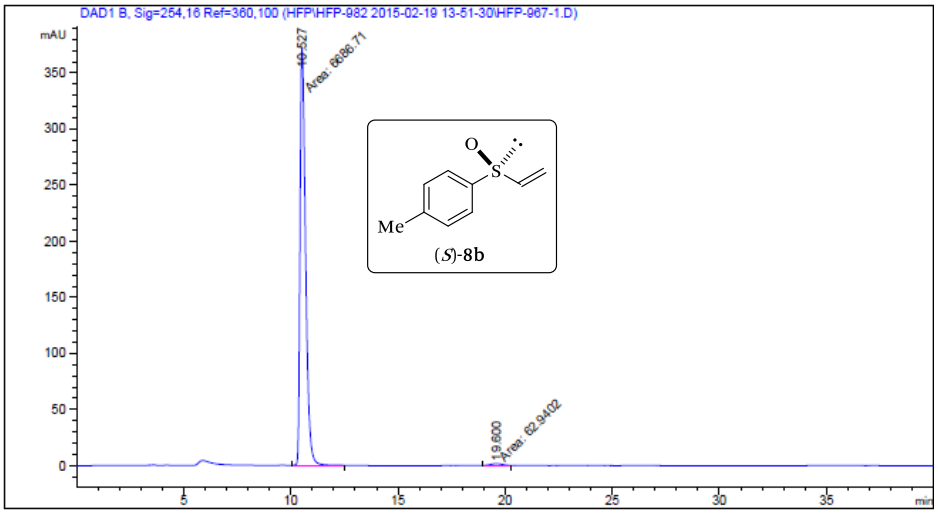

Peak #	RetTime [min]	Type	Width [min]	Area [mAU*s]	Height [mAU]	Area %
1	10.527	MM	0.2992	6686.70508	372.44263	99.0675
2	19.600	MM	0.6222	62.94017	1.68585	0.9325

Figure 87. Chiral HPLC trace for the KR by asymmetric hydrogenation of *rac*-**8b**, product (*S*)-**8b** (Table 13, entry 3).

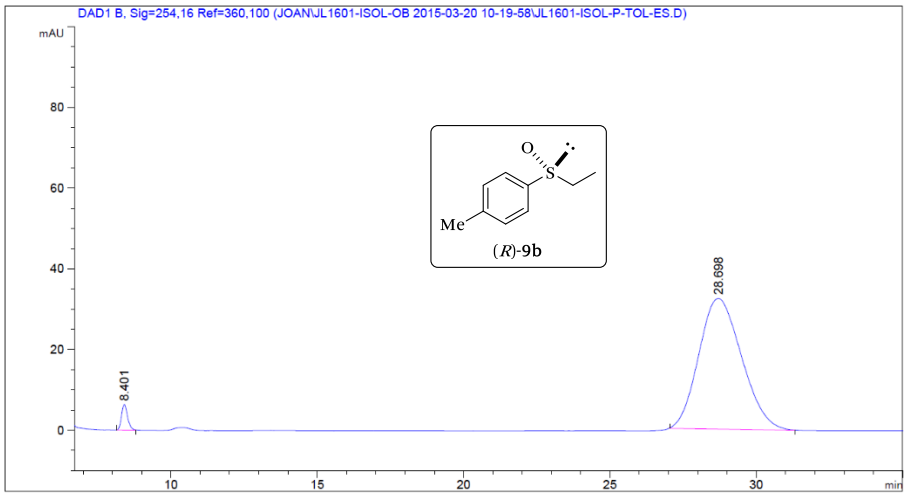

Peak #	RetTime [min]	Type	Width [min]	Area [mAU*s]	Height [mAU]	Area %
1	8.401	BB	0.2195	91.78746	6.39203	2.7095
2	28.698	BB	1.4889	3295.88721	32.39750	97.2905

Figure 88. Chiral HPLC trace for the KR by asymmetric hydrogenation of *rac*-**8b**, product (*R*)-**9b** (Table 13, entry 4).

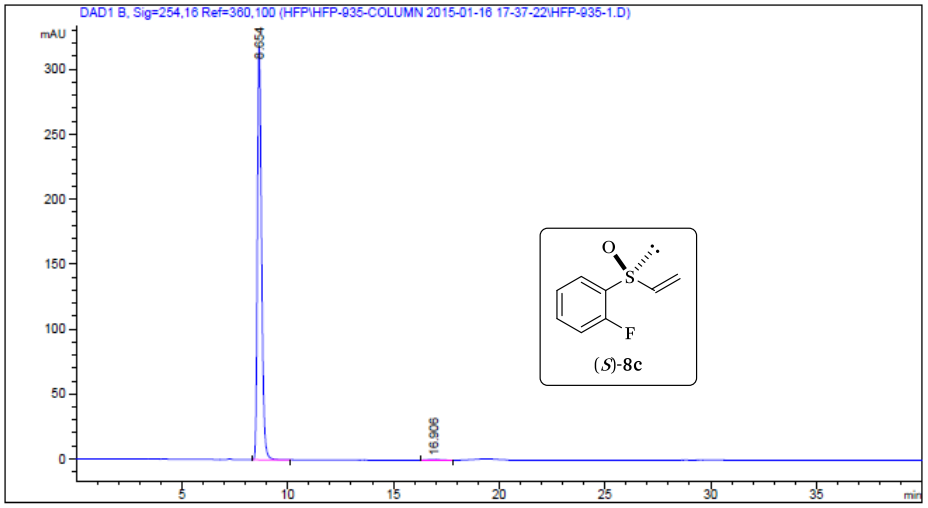

Peak #	RetTime [min]	Type	Width [min]	Area [mAU*s]	Height [mAU]	Area %
1	8.654	BB	0.2138	4401.23536	317.35577	99.7431
2	16.906	BB	0.5357	11.33543	3.24372e-1	0.2569

Figure 89. Chiral HPLC trace for the KR by asymmetric hydrogenation of *rac*-**8c**, product (*S*)-**8c** (Table 13, entry 5).

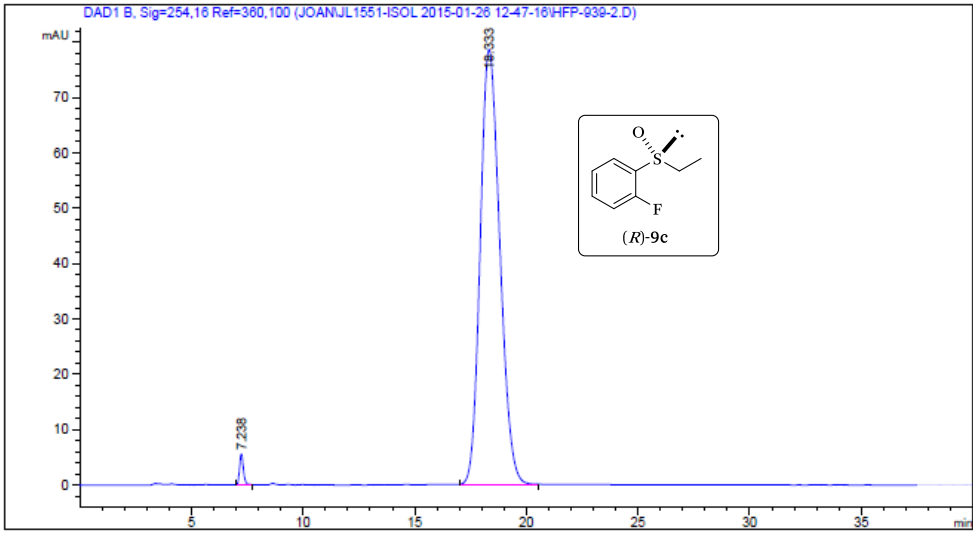

Peak #	RetTime [min]	Type	Width [min]	Area [mAU*s]	Height [mAU]	Area %
1	7.238	BB	0.1849	67.38874	5.57801	1.3863
2	18.333	BB	0.9520	4793.74707	78.54888	98.6137

Figure 90. Chiral HPLC trace for the KR by asymmetric hydrogenation of *rac*-**8c**, product (*R*)-**9c** (Table 13, entry 6).

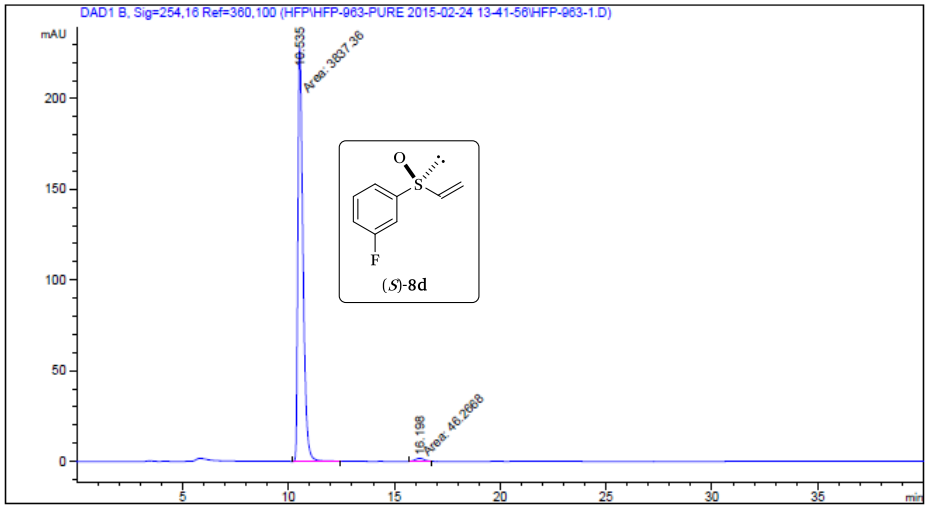

Peak #	RetTime [min]	Type	Width [min]	Area [mAU*s]	Height [mAU]	Area %
1	10.535	MM	0.2802	3837.35571	228.28548	98.8087
2	16.198	MM	0.4635	46.26677	1.66366	1.1913

Figure 91. Chiral HPLC trace for the KR by asymmetric hydrogenation of *rac*-**8d**, product (*S*)-**8d** (Table 13, entry 7).

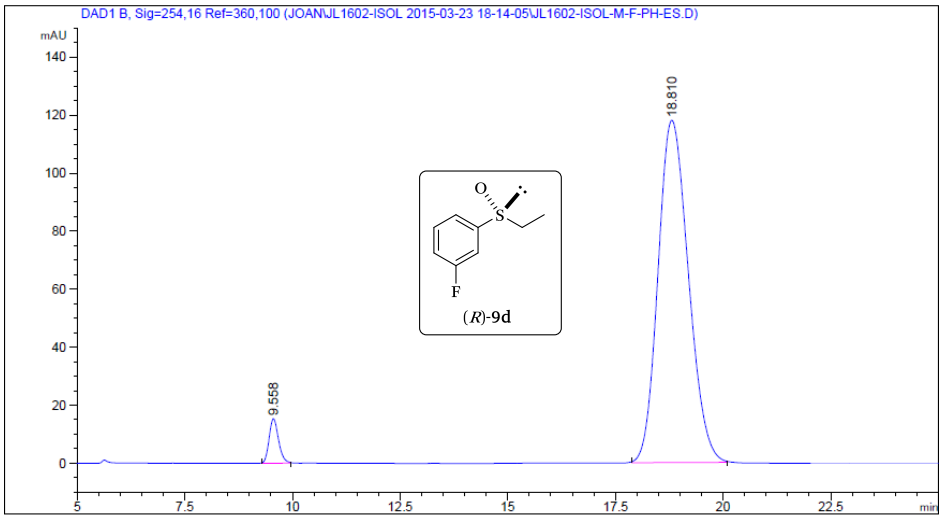

Peak #	RetTime [min]	Type	Width [min]	Area [mAU*s]	Height [mAU]	Area %
1	9.558	BB	0.2341	234.24553	15.34178	3.8963
2	18.810	BB	0.7656	5777.68848	117.93549	96.1037

Figure 92. Chiral HPLC trace for the KR by asymmetric hydrogenation of *rac*-**8d**, product (*R*)-**9d** (Table 13, entry 8).

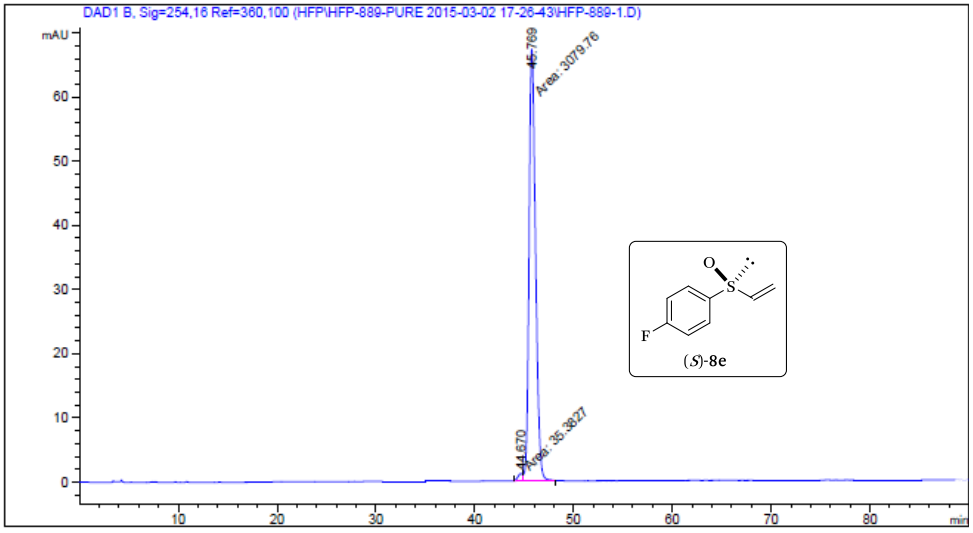

Peak #	RetTime [min]	Type	Width [min]	Area [mAU*s]	Height [mAU]	Area %
1	44.670	MF	0.5364	35.38271	1.09931	1.1358
2	45.769	FM	0.7632	3079.76025	67.25636	98.8642

Figure 93. Chiral HPLC trace for the KR by asymmetric hydrogenation of *rac*-**8e**, product (*S*)-**8e** (Table 13, entry 9).

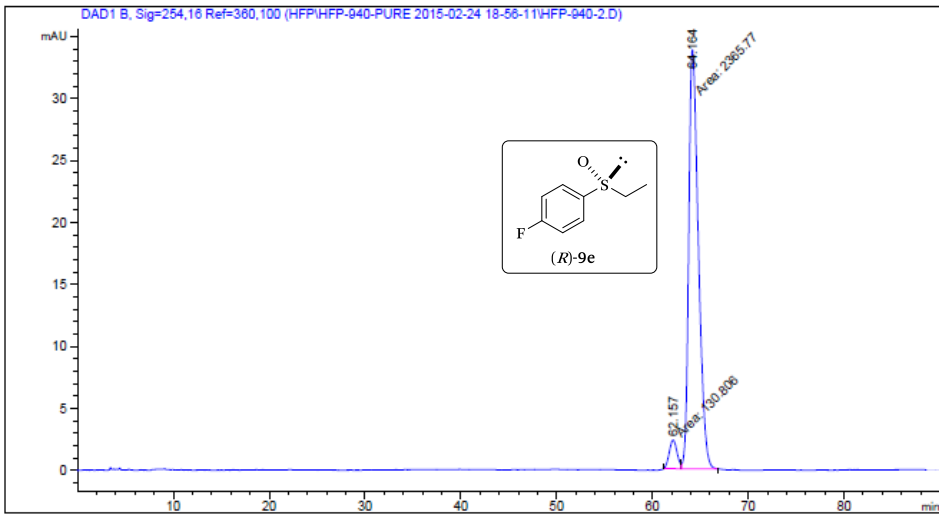

Peak #	RetTime [min]	Type	Width [min]	Area [mAU*s]	Height [mAU]	Area %
1	62.157	MF	0.9462	130.80611	2.30401	5.2394
2	64.164	FM	1.1663	2365.77368	33.80746	94.7606

Figure 94. Chiral HPLC trace for the KR by asymmetric hydrogenation of *rac*-**8e**, product (*R*)-**9e** (Table 13, entry 10).

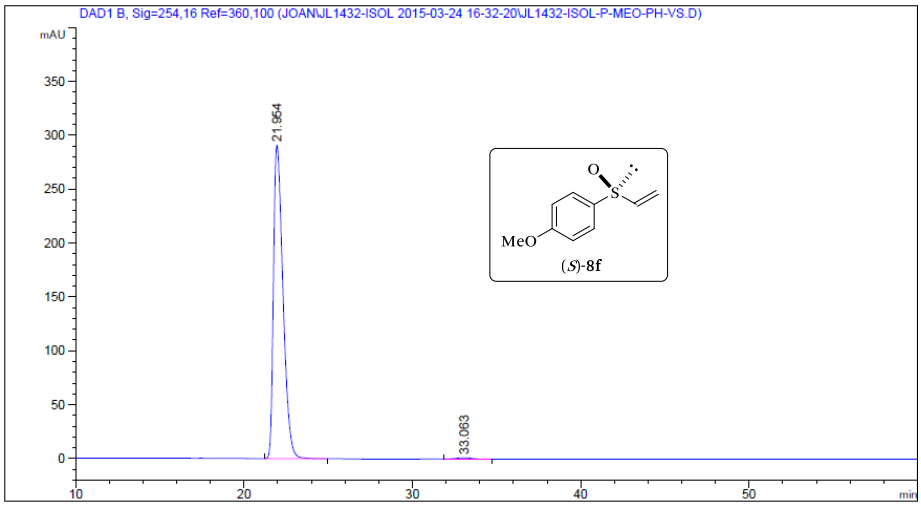

Peak #	RetTime [min]	Type	Width [min]	Area [mAU*s]	Height [mAU]	Area %
1	21.954	BB	0.6059	1.14126e4	290.77945	99.3763
2	33.063	BB	0.8831	71.62148	1.16854	0.6237

Figure 95. Chiral HPLC trace for the KR by asymmetric hydrogenation of *rac*-**8f**, product (*S*)-**8f** (Table 13, entry 11).

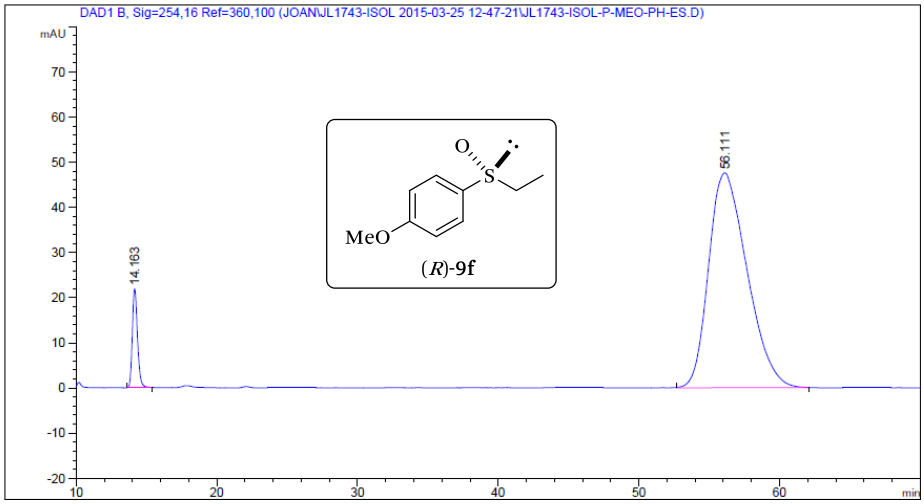

Peak #	RetTime [min]	Type	Width [min]	Area [mAU*s]	Height [mAU]	Area %
1	14.163	BB	0.3938	558.23401	21.87165	5.8261
2	56.111	BB	2.7929	9023.45117	47.57251	94.1739

Figure 96. Chiral HPLC trace for the KR by asymmetric hydrogenation of *rac*-**8f**, product (*R*)-**9f** (Table 13, entry 12).

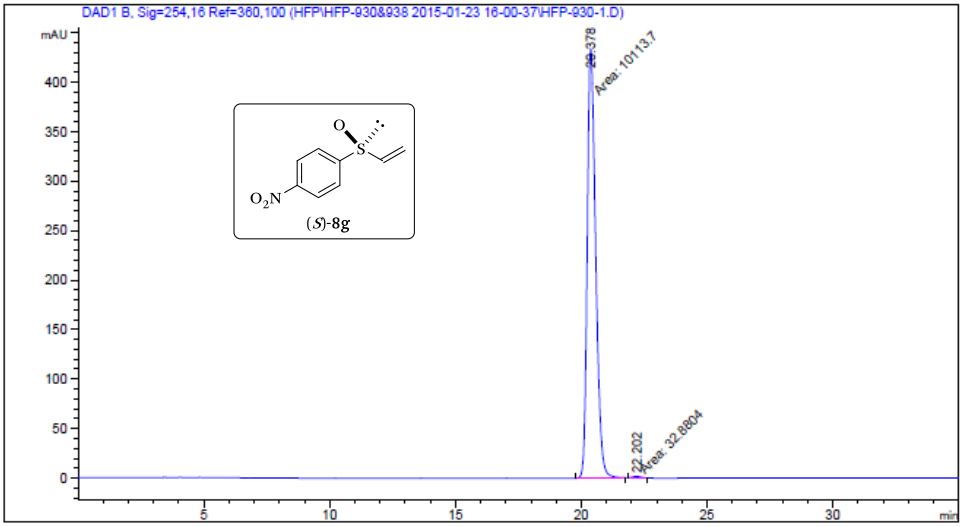

Peak #	RetTime [min]	Type	Width [min]	Area [mAU*s]	Height [mAU]	Area %
1	20.378	MM	0.3884	1.01137e4	433.95914	99.6759
2	22.202	MM	0.3575	32.88037	1.53291	0.3241

Figure 97. Chiral HPLC trace for the KR by asymmetric hydrogenation of *rac*-**8g**, product (*S*)-**8g** (Table 13, entry 13).

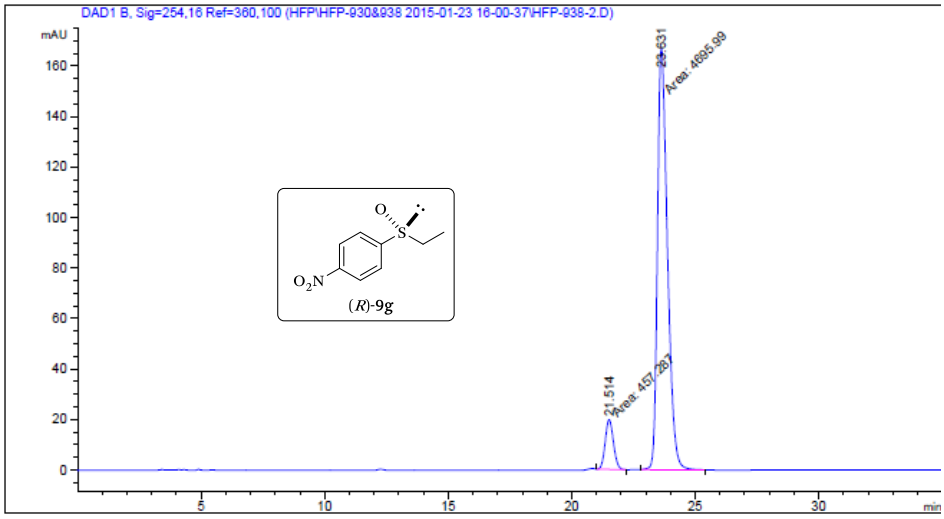

Peak #	RetTime [min]	Type	Width [min]	Area [mAU*s]	Height [mAU]	Area %
1	21.514	MM	0.3867	457.28745	19.70822	8.8737
2	23.631	MM	0.4689	4695.99316	166.92313	91.1263

Figure 98. Chiral HPLC trace for the KR by asymmetric hydrogenation of *rac*-**8g**, product (*R*)-**9g** (Table 13, entry 14).

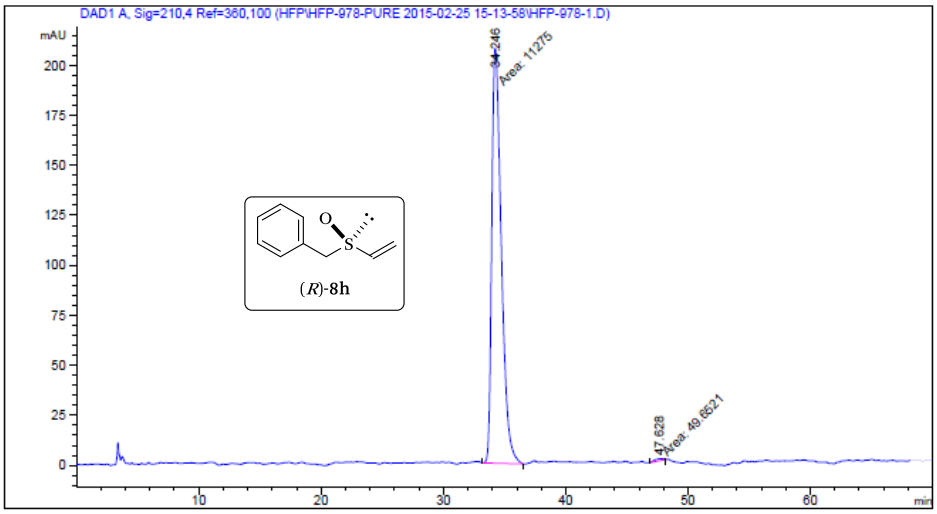

Peak #	RetTime [min]	Type	Width [min]	Area [mAU*s]	Height [mAU]	Area %
1	34.246	MM	0.9055	1.12750e4	207.53459	99.5616
2	47.628	MM T	0.8189	49.65206	1.01049	0.4384

Figure 99. Chiral HPLC trace for the KR by asymmetric hydrogenation of *rac*-**8h**, product (*R*)-**8h** (Table 13, entry 15).

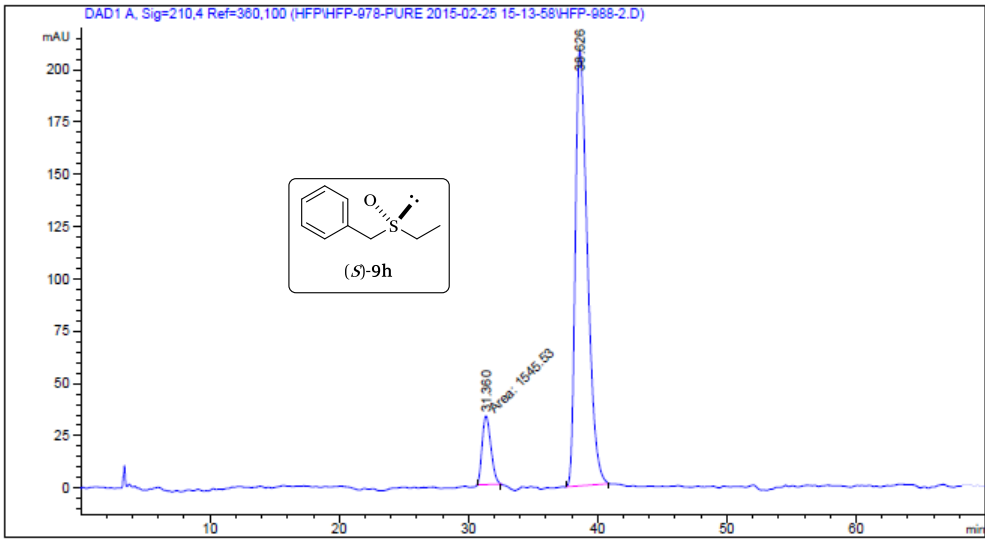

Peak #	RetTime [min]	Type	Width [min]	Area [mAU*s]	Height [mAU]	Area %
1	31.360	MM	0.7868	1545.63479	32.78763	10.2375
2	38.626	BB	1.0058	1.35513e4	208.09079	89.7625

Figure 100. Chiral HPLC trace for the KR by asymmetric hydrogenation of *rac*-**8h**, product (*S*)-**9h** (Table 13, entry 16).

CHAPTER III

Exploiting Substrate's Diversity for Preparing Synthetically Valuable Sulfoxides via Asymmetric Hydrogenative Kinetic Resolution

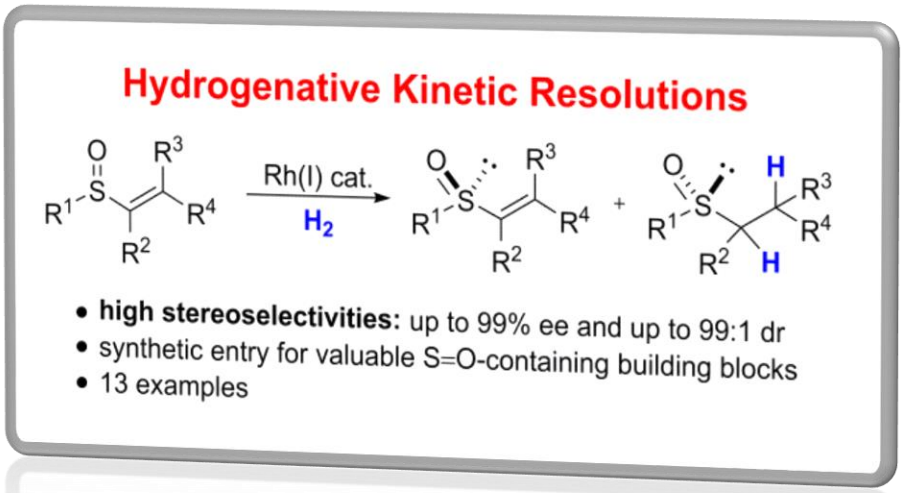

UNIVERSITAT ROVIRA I VIRGILI
RHODIUM CATALYSIS IN ENANTIOSELECTIVE HYDROGENATIVE TRANSFORMATIONS: FROM THE DESIGN OF NEW LIGANDS TO REACTIONS OF ATYPICAL SUBSTRATES
Joan Ramon Lao Mulinari

Exploiting Substrate's Diversity for Preparing Synthetically Valuable Sulfoxides via Asymmetric Hydrogenative Kinetic Resolution

3.1. ABSTRACT

A detailed study is disclosed on the Rh-mediated hydrogenative kinetic resolution of α,β-unsaturated sulfoxides with alkyl and aryl substituents at the α-, *E*- and *Z*-positions of the double bond. This stereoselective catalytic methodology has allowed for the preparation of highly enantioenriched (or even enantiopure) alkyl and aryl substituted (un)saturated sulfoxides via a simple and efficient synthetic operation. Moreover, the application of the hydrogenative KR to the preparation of valuable optically active sulfoxide-containing building blocks or biologically active intermediates is also described.

3.2. INTRODUCTION

The catalytic stereoselective synthesis of enantiopure sulfoxides has attracted the interest of the synthetic community due to the broad applicability of enantiopure sulfoxides in asymmetric synthesis (as chiral auxiliaries or ligands).[49a,b,104] Apart from their usefulness in asymmetric synthesis and due to the crucial role of sulfur in living systems,[105] sulfoxide groups can be found in a myriad of bioactive compounds that naturally participate in the metabolism (e.g., mustard oils[105] or L-methionine *S*-oxides[106]; see Figure 101) or in a broad array of enantiopure synthetic drugs (e.g., hydroxyamic acids[107] or sulfinyl propanamines[108] indicated in Figure 101). In recent decades, different (catalytic) stereoselective preparation methods of optically active sulfoxides have been developed by forming C–S or

(104) For other applications of optically active sulfoxides as chiral auxiliaries or catalysts, see ref. 49c.
(105) For the role of the sulfur atom in biological processes, see ref. 50c.
(106) Matsui, T.; Dekishima, Y.; Ueda, M. *Appl. Microbiol. Biotechnol.* **2014**, *98*, 7699-7706.
(107) Marson, C. M. *Anti-Cancer Agents Med. Chem.* **2009**, *9*, 661-692.
(108) Foster, B. J.; Hunden, D. C.; Lavagnino, E. R., US4902710A, 1990.

S–O bonds from prochiral sulfides.[109] More recently, efficient strategies based on kinetic resolutions (KR)[18] have been developed and were extremely useful from a synthetic point of view, as the two reaction products can be obtained in a highly enantioenriched (or even enantiopure) form.[75,110]

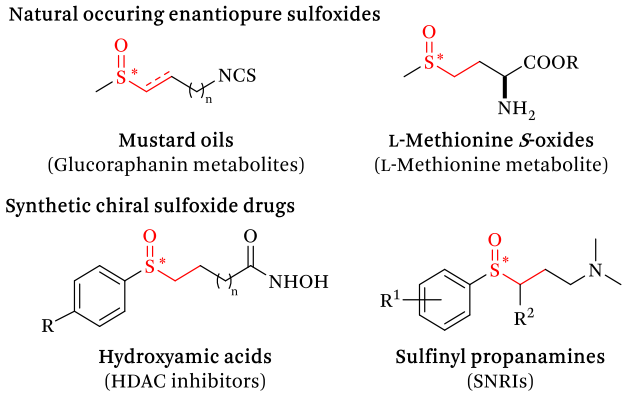

Figure 101. Selected examples of naturally occurring or synthetically produced biologically active sulfoxides.[105–108]

We recently reported efficient catalytic tools for the preparation of highly enantioenriched unsubstituted vinyl and ethyl sulfoxides through an unprecedented hydrogenative kinetic resolution mediated by a Rh-complex derived from a phosphine-phosphite[40] ligand (Scheme 7).[110]

Scheme 7. Kinetic resolution of α,β-unsaturated sulfoxides

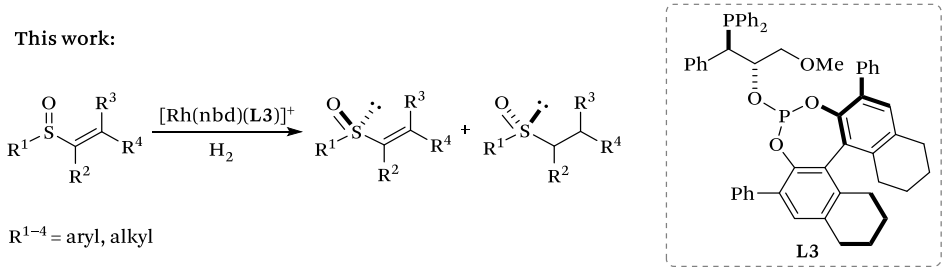

Given our ongoing interest in developing highly stereoselective catalytic tools,[43,44] and encouraged by the precise stereocontrol exhibited in the hydrogenative kinetic resolution of unsubstituted vinyl sulfoxides,[110] we

(109) For representative enantioselective sulfoxide syntheses, see: Wojaczynska, E.; Wojaczynski, J. *Chem. Rev.* **2010**, *110*, 4303-4356. and ref. 73.
(110) Lao, J. R.; Fernández-Pérez, H.; Vidal-Ferran, A. *Org. Lett.* **2015**, *17*, 4114-4117.

studied the effects of precisely positioning alkyl or aryl substituents at the α-, *E*- and *Z*-positions of the double bond in the (stereo)chemical outcome of the reactions (Scheme 7). The selective synthesis of some of the racemic starting α,β-unsaturated sulfoxides constituted a challenge. In the manuscript, we also detail interesting synthetic protocols for their preparation that can be useful for the synthetic community. Lastly, to demonstrate the synthetic utility of hydrogenative kinetic resolutions, we report herein the catalytic enantioselective synthesis of intermediates of selected biologically active relevant enantiopure sulfoxides.

3.3. RESULTS AND DISCUSSION

As previously mentioned, the initial set of substrates in our studies to explore the effects of structural complexity on the stereochemical outcome of the reaction encompassed racemic alkyl and aryl substituted α,β-unsaturated sulfoxides at the α-, *E*- and *Z*-positions (sulfoxides *rac*-**11a–f** in Figure 102). *trans*-Substituted α,β-unsaturated sulfoxides *rac*-**11a,b** were prepared straightforwardly following a Horner-Wittig protocol.[111] While *cis*-phenyl derivative *rac*-**11d** was easily prepared following a reported procedure,[112] we developed an efficient synthesis for the methyl substituted analog (*rac*-**11c**) by the chemoselective hydrogenation of allenylsulfoxide *rac*-**12** (Figure 102). After some experimentation, we identified selective hydrogenation conditions toward *rac*-**11c** (2.5 mol % of [Rh(nbd)(**L3**)]BF_4, 5 bar of H_2 and −10 °C). Experiments led to full conversions and under the developed reaction conditions, we observed that the addition of hydrogen occurred exclusively at the allene C_β–Cγ-position with complete (*Z*)-selectivity.[113] It is worth mentioning that the preparation of sufficient amounts of *rac*-**11c** following other synthetic protocols[114] remained elusive in our hands. However, we efficiently performed the hydrogenation of allenyl sulfoxide *rac*-**12** at the

(111) For details, see the Experimental Section and the following reference: Grayson, J. I.; Warren, S. *J. Chem. Soc., Perkin Trans. 1* **1977**, 2263-2272.
(112) Trostyanskaya, I. G.; Beletskaya, I. P. *Synlett* **2012**, *23*, 535-540.
(113) To the best of our knowledge, there is only one report on the Rh-mediated (*Z*)-selective hydrogenation of linear and cyclic unfunctionalized allenes towards the mono-alkene intermediates: Bhagwat, M. M.; Devaprabhakara, D. *Tetrahedron Lett.* **1972**, 1391-1392.
(114) (a) Craig, D.; Daniels, K.; MacKenzie, A. R. *Tetrahedron* **1993**, *49*, 11263-11304. (b) Van Steenis, J. H.; Van Es, J. J. G. S.; Van der Gen, A. *Eur. J. Org. Chem.* **2000**, 2787-2793.

mmol scale and we were able to include sulfoxide *rac*-**11c** as a substrate in our studies (Table 17). Lastly, α-substituted α,β-unsaturated sulfoxides *rac*-**11e,f** were conveniently prepared by reaction of the required organomagnesium reagent with methyl benzenesulfinate after adapting a previously reported synthetic procedure for analogous chemistry.[115]

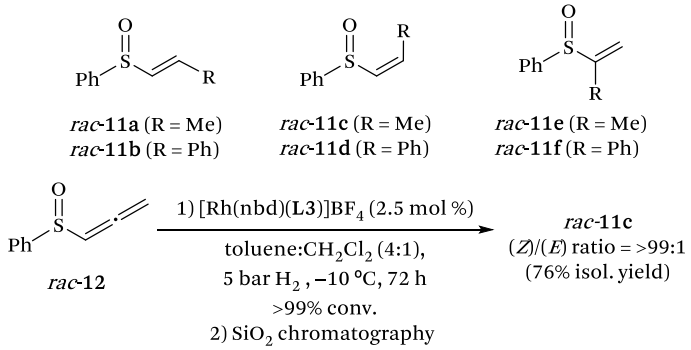

Figure 102. Initial set of substrates (*rac*-**11a–f**) and preparation of *rac*-**11c** by selective hydrogenation of racemic allenyl-substituted sulfoxide *rac*-**12**.

With the array of structurally diverse α,β-unsaturated sulfoxides at hand (*rac*-**11a–f**), we then turned our attention to the assessment of the catalytic activity of the highest performing Rh–catalysts (i.e., those incorporating the phosphine-phosphite ligand **L3**;[110] see Scheme 7) in hydrogenative kinetic resolutions of the new sulfoxides *rac*-**11a–f**. The presence of substituents at the vinyl moiety of these substrates translated into lower hydrogenation rates than those observed for sulfoxides containing the unsubstituted vinyl group.[110] After some experimentation, efficient kinetic resolution conditions [5 mol % of [Rh(nbd)(**L3**)]BF_4 as precatalyst and toluene and CH_2Cl_2 (4:1 v/v) as solvents] were identified and the hydrogen pressure and reaction temperature and time were specifically optimized for both recovered and hydrogenated products (Table 17).

In general terms, efficient and selective catalytic conditions were identified for all substrates, with the exception of compound *rac*-**11b** (efficient kinetic resolution conditions remained elusive for this substrate, as low enantioselectivities were observed under all reaction conditions assayed (entry 2 in Table 17).

(115) (a) Buezo, N. D.; De la Rosa, J. C.; Priego, J.; Alonso, I.; Carretero, J. C. *Chem. – Eur. J.* **2001**, *7*, 3890-3900. (b) Breit, B.; Breuninger, D. *J. Am. Chem. Soc.* **2004**, *126*, 10244-10245.

Table 17. Kinetic resolution of sulfoxides 11a–f[a]

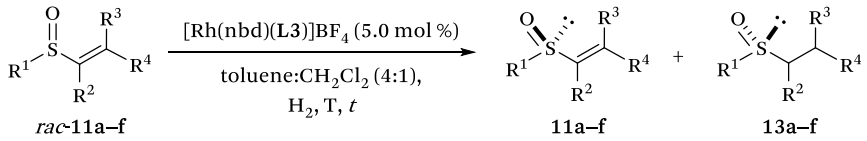

rac-11a–f 11a–f 13a–f

entry	R^1, R^2, R^3, R^4	P, bar	T, °C	*t*, h	conv.,[b] %	product, yield,[116] %; ee, %,[c] (*config.*)[d]	*s*[e]
1	Ph, H, H, Me (*rac*-**11a**)	10	0	66	61	**11a**, 78[f], 99 (*S*)	51
		10	–10	20[g]	25	**13a**, 50[f], 90 (*R*)	23
2	Ph, H, H, Ph (*rac*-**11b**)	5	rt	48	53	**11b**, 94[f], *rac*	-
		The hydrogenated product is the same as that of entry 4					
3[h]	Ph, H, Me, H (*rac*-**11c**)	8	rt	70	92	**11c**, 16[f], 99 (*S*)	8
		The hydrogenated product is the same as that of entry 1					
4	Ph, H, Ph, H (*rac*-**11d**)	20	rt	90	75	**11d**, 50[f], 62 (*S*)	3
		40	0	48	24	**13d**, 48[f], 56 (*R*)	4
5	Ph, Me, H, H (*rac*-**11e**)	5	rt	48	90	**11e**, 20[i], 99 (*S*)	10
		10	–10	72	21	**13e**, 32[i], 85 (*R*)	20
6	Ph, Ph, H, H (*rac*-**11f**)	5	rt	24	54	**11f**, 76[i], 99 (*R*)	91
		5	rt	3.5	42	**13f**, 49[i], 93 (R_S,R_C)	60

[a][Substrate] = 0.2 M. [b]Determined by ^{1}H NMR. [c]Determined by chiral HPLC. [d]The absolute configurations of products **11e,f** and **13e,f** were determined by comparison with reported optical rotations for **13e,f**.[117] The absolute configuration of products **11a–d** and **13a–d** were tentatively assigned by analogy with the results for **13e,f**. [e]The selectivity factor (*s*) was determined by the following equation: $s = \ln[1-C(1+ee_2)]/\ln[1-C(1-ee_2)]$ where $C = (ee_{11}/(ee_{11}+ee_{13}))$.[18] [f]Reaction products could not be separated by standard column chromatography. [g]Solvent mixture = Cy:CH_2Cl_2 (4:1 v/v). [h]5% of isomerized product **11a** was detected in the reaction crude as determined by NMR.[117] [i]dr ratio of *anti*-**13f**:*syn*-**13f** ≥ 99:1, as determined by ^{1}H NMR.[117]

(116) Yields are calculated with respect to the 50% mol amount of starting material and product.
(117) See the Experimental Section for further details.

Having mentioned this exception, it should be noted that the presence of methyl or phenyl substituents at the vinyl moiety (substrates *rac*-**11a** and *rac*-**11c–f**) was well tolerated and that enantioselectivities ranging from 62 to 99% ee and from 56 to 93% ee for recovered and hydrogenated products were observed, respectively (Table 17).[118]

As evidenced by the results, high selectivity factors (s = 51 and s = 23, entry 1 in Table 17) were observed in the kinetic resolution of (*E*)-Me-substituted substrate *rac*-**11a**. These selectivity factors translated into high enantioselectivities for the recovered and hydrogenated products (99% and 90% ee for **11a** and **13a**, respectively; entry 1 in Table 17). A lower selectivity factor was observed for the analogous α,β-unsaturated sulfoxide with the methyl group in the (*Z*)-position (*rac*-**11c**; s = 8, entry 3 in Table 17). Despite the low selectivity factor in the kinetic resolution of *rac*-**11c**, optically pure starting material **11c** could be obtained at 92% of conversion (99% ee for **11c**, entry 3 in Table 17). Although the enantioselectivity of the hydrogenated product from *rac*-**11c** could not be further improved, this result was no drawback for obtaining this product in high enantioselectivity with our method, as it can also be obtained by hydrogenatively resolving substrate *rac*-**11a** (entry 1 in Table 17) instead of *rac*-**11c**. Regarding the kinetic resolutions of (*Z*)- and (*E*)-2-phenylethenyl substituted sulfoxides *rac*-**11b** and *rac*-**11d**, those transformations proceeded with lower selectivity factors than those observed for the methyl substituted analogs *rac*-**11a** and *rac*-**11c** (compare entries 1 with 3 and 2 with 4 in Table 17).

The hydrogenative kinetic resolution of α,β-unsaturated sulfoxides bearing substituents at the α-position (*rac*-**11e,f**) proceeded with higher selectivity and under milder reaction conditions than those of the substrates with substituents at the β-position (*rac*-**11a–d**; compare entries 1–4 with 5–6 in Table 17). Substrates *rac*-**11e,f** provided the best results of the whole series (entries 5 and 6 in Table 17), with high to excellent ee values for the recovered starting material (99% ee both for **11e** and **11f**; entries 5 and 6 in Table 17) and for the hydrogenated products (85 and 93% ee for **13e** and **13f**, respectively; entries 5 and 6 in Table 17). Slightly beneficial effects on the enantioselectivity were observed for the phenyl substituted substrate (*rac*-**11f**) with selectivity values as high as s = 91 and s = 60 for **11f** and **13f**, respectively. Most remarkably, the hydrogenation of *rac*-**11f** took place with perfect diastereoselectivity, leading to the exclusive formation of the

(118) A complete list of experiments performed can be found in Table 18.

anti-diastereoisomer *anti*-**13f** (dr of *anti*-**13f**:*syn*-**13f** ≥ 99:1; entry 6 in Table 17).[119] The practicality of the hydrogenative kinetic resolution methodology was further demonstrated by preparing a number of advanced synthetic intermediates of biologically active molecules containing sulfoxide groups: (*R*)-sulforaphene,[120] (*S*)-sulforaphane,[121] and a histone deacetylase (HDAC) inhibitor[122] (Scheme 8 and Scheme 9).

Scheme 8. Preparation of advanced synthetic intermediates of (*R*)-sulforaphene and (*S*)-sulforaphane

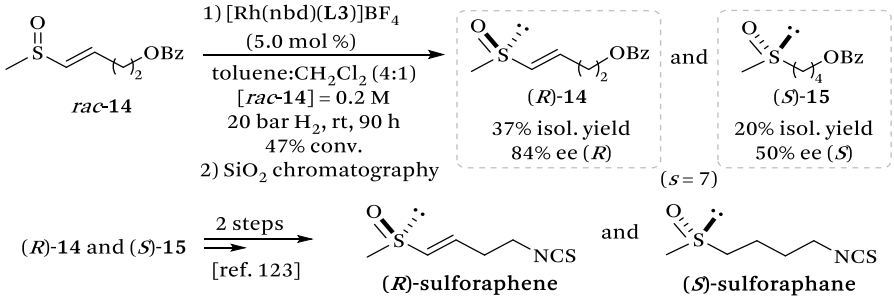

Resolution of sulfoxide *rac*-**14** furnished unreacted starting material (*R*)-**14** with high enantioselectivities (84% ee; see Scheme 8), whilst the hydrogenated product (*S*)-**15** could only be obtained with moderate enantioselectivity (50% ee; see Scheme 8). In this particular reaction, minor amounts of the over-reduced sulfide derived from product **15** were detected in the reaction crude (6%). However, this by-product could be easily separated by standard SiO_2 column chromatography. (*R*)-sulforaphene and (*S*)-sulforaphane could be easily prepared from the advanced synthetic intermediates (*R*)-**14** and (*S*)-**15** following well-established synthetic protocols.[123]

(119) The *anti*-arrangement of substituents in the hydrogenated product **13f** was established by comparison with the spectroscopic data reported in ref. 51a
(120) Shishu, A. K. Singla; Kaur, I. P. *Planta Med.* **2003**, 69, 184-186.
(121) Zhang, Y.; Talalay, P.; Cho, C. G.; Posner, G. H. *Proc. Natl. Acad. Sci. USA* **1992**, *89*, 2399-2403.
(122) This compound is currently in clinical trials. For further information, see: (a) Joel, S.; Marson, C.; Savy, P., WO2004046094A1, 2004. (b) Marson, C. M.; Savy, P.; Rioja, A. S.; Mahadevan, T.; Mikol, C.; Veerupillai, A.; Nsubuga, E.; Chahwan, A.; Joel, S. P. *J. Med. Chem.* **2006**, *49*, 800-805. (c) Paris, M.; Porcelloni, M.; Binaschi, M.; Fattori, D. *J. Med. Chem.* **2008**, *51*, 1505-1529.
(123) For the ester cleavage reaction, see: Bury, A.; Earl, H. A.; Stirling, C. J. M. *J. Chem. Soc., Perkin Trans. 2* **1987**, 1281-1287. For the conversion from –OH to –NCS group, see: Ruppenthal, S.; Brueckner, R. *J. Org. Chem.* **2015**, *80*, 897-910.

Gratifyingly, the kinetic resolution of *rac*-**16** (Scheme 9) took place in a highly chemo- and stereo-selective way and excellent values of enantioselectivity were obtained for both recovered and reduced products (99% and 94% ee for (*S*)-**16** and (*R*)-**17**, respectively; see Scheme 9).

Scheme 9. Preparation of the histone deacetylase (HDAC) inhibitor intermediate (*R*)-17

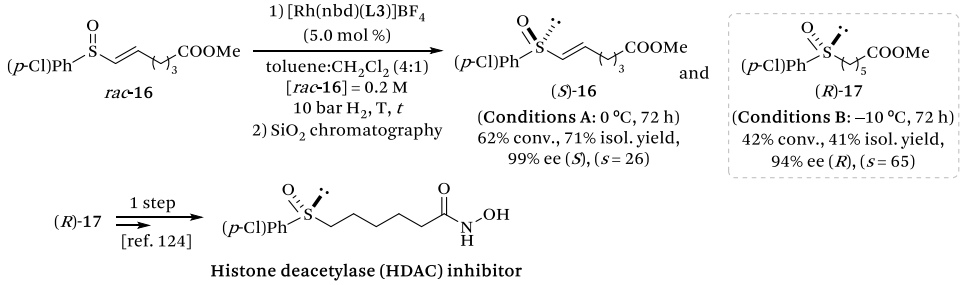

Notably, the optimized reaction for the target intermediate (*R*)-**17** (Conditions B; see Scheme 9) proceeded with a high selectivity factor ($s = 65$; see Scheme 9) and the desired sulfoxide (*R*)-**17** could be efficiently isolated in high optical purity (41% isolated yield and 94% ee; see Scheme 9). The advanced synthetic intermediate (*R*)-**17** could be transformed into the bioactive molecule following a well-established experimental procedure.[124]

3.4. CONCLUSIONS

In summary, we have exploited the potentially high structural diversity of the substrates to be hydrogenatively resolved (i.e., α,β-unsaturated sulfoxides with alkyl and aryl substituents at the α-, *E*- and *Z*-positions of the double bond) to give access to an array of new and valuable highly enantioenriched (or even enantiopure) sulfoxide-containing synthetic intermediates. We have discovered a new catalytic tool that mediates the chemo- and stereo-selective hydrogenation of an allenyl sulfoxide with the exclusive formation of the corresponding (*Z*)-configured sulfinyl alkene, opening further avenues for the (stereo)selective preparation of valuable (*Z*)-configured alkenyl sulfoxides. Moreover, we have further expanded the applicability of the enantioselective Rh-mediated hydrogenative kinetic resolution by preparing enantioenriched

(124) For the conversion of –COOMe to –CON(H)OH groups in sulfoxide **17**, see ref. 122b.

advanced synthetic intermediates of biologically active sulfoxide-containing molecules. Catalytic hydrogenative kinetic resolutions have generally proceeded with high selectivity factors and enabled the preparation of the final sulfoxides in a highly enantioenriched (or even enantiopure) form. Ongoing investigations include the extension of the application of this chemistry to other substrates, to other transition metals and study of alternative ligand designs.

3.5. EXPERIMENTAL SECTION

3.5.1. General considerations

Air- and moisture-sensitive manipulations or reactions were performed under inert atmosphere using anhydrous solvents, either in a glove box or with standard Schlenk techniques. Glassware was dried under vacuum and heated with a hot air gun before use. All solvents were dried in a Solvent Purification System (SPS). Silica gel 60 (230–400 mesh) was used for column chromatography. NMR spectra were recorded on a 400-MHz or 500-MHz UltraShield spectrometer in $CDCl_3$, unless otherwise cited. ^{1}H NMR and $^{13}C\{^{1}H\}$ NMR chemical shifts are quoted in ppm relative to the residual solvent peaks. $^{31}P\{^{1}H\}$ NMR chemical shifts are quoted in ppm relative to 85% phosphoric acid in water. High-resolution mass spectra (HRMS) were recorded using the ESI ionization method in positive mode, unless otherwise stated. Enantiomeric excesses were determined by HPLC analyses, using chiral stationary phases.

The preparation and characterization of ligand **L3** and its corresponding Rh-precatalyst [Rh(nbd)(**L3**)]BF_4 have been previously described in the literature.[46,110]

3.5.2. General synthetic procedure for sulfinyl-phosphine oxide intermediates 18–20

Intermediates **18**–**20** were prepared following previously reported methodology,[111] with slight modifications.

Ethoxydiphenylphosphine (20.2 mmol) and the corresponding α-chloro-sulfide derivative (18.5 mmol) were placed in a reaction flask equipped with a condenser under Ar atmosphere. The resulting mixture was heated at reflux (150 °C) and stirred for 2 h under the same conditions. After that time, the

crude was allowed to reach room temperature and a crystalline solid was formed in the sine of the solution. The resulting solid was washed with cold *n*-pentane (2 x 50 mL) and dried under reduced pressure to afford a pale yellow oil that was used in the next step without further purification.[125]

To a stirring solution of the crude product obtained in the previous reaction (12.6 mmol)[125] in CH_2Cl_2 (100 mL), a solution of *m*-CPBA (ca. 14.0 mmol) was slowly added at −78 °C under Ar atmosphere. The resulting solution was stirred for 1 h under the same reaction conditions. After that time, sodium metabisulfite (50 mL, sat. solution) was added and the resulting suspension was allowed to reach room temperature. The mixture was washed with an aqueous solution of sodium bicarbonate (250 mL, sat. solution), dried over anhydrous $MgSO_4$, filtered and evaporated under reduced pressure to yield a white spongy solid. The resulting solid was solubilized using a mixture of solvents (130 mL, *n*-pentane:CH_2Cl_2 = 8:5 v/v) and recrystallized by lowering the temperature of the solution to −18 °C for 18 h. The crystalline solid was filtered, washed with cold *n*-pentane (2 x 50 mL) and dried under reduced pressure to yield the desired product as white crystals (47−58% isolated yield).

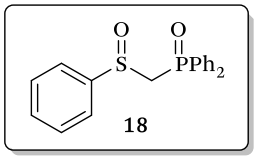

18

The general synthetic procedure was followed starting with α-chlorothioanisole (2.51 mL, 95%, 18.5 mmol) and ethoxydiphenylphosphine (4.72 mL, 93%, 20.2 mmol). Further oxidation with *m*-CPBA (3.13 g, ca. 77%, ca. 14 mmol) afforded the desired sulfinyl-phosphine oxide as a white crystalline solid (3.92 g, 58% isolated yield). The spectroscopic data were in agreement with those reported.[111]

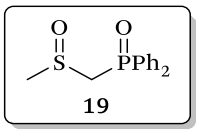

19

The general synthetic procedure was followed starting with chloromethyl methyl sulfide (1.78 mL, 95%, 20.2 mmol) and ethoxydiphenylphosphine (4.72 mL, 93%, 20.2 mmol). Further oxidation with *m*-CPBA (4.72 g, ca. 77%, ca. 21 mmol) afforded the desired sulfinyl-phosphine oxide as a white solid (2.46 g, 47% isolated yield). The spectroscopic data were in agreement with those reported.[114b]

(125) 99% of purity (regarding P-containing species) was determined by IGD $^{31}P\{^1H\}$ NMR analysis.

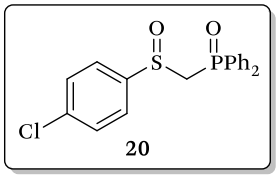

20

The general synthetic procedure was followed starting with chloromethyl 4-chlorophenyl sulfide (2.59 mL, 97%, 17.5 mmol) and ethoxy-diphenylphosphine (4.4 mL, 97%, 19.6 mmol). Further oxidation with *m*-CPBA (2.98 g, ca. 77%, ca. 13.3 mmol) afforded the desired sulfinyl-phosphine oxide as a white crystalline solid (3.3 g, 50% isolated yield). ^{1}H NMR (500 MHz, $CDCl_3$) δ 7.87–7.82 (m, 2H, CH_{Ar}), 7.70–7.40 (m, 12H, CH_{Ar}), 4.02 (dd, J = 14.3 Hz, J = 7.7 Hz, 1H, C*H*H), 3.82 (dd, J = 14.3 Hz, J = 10.2 Hz, 1H, CH*H*); ^{13}C{^{1}H} NMR (126 MHz, $CDCl_3$) δ 142.9 (d, J = 5.2 Hz, C_{Ar}), 137.8 (C_{Ar}), 132.7 (d, J = 2.8 Hz, CH_{Ar}), 132.3 (d, J = 2.9 Hz, CH_{Ar}), 131.6 (d, J = 4.6 Hz, C_{Ar}), 131.1 (d, J = 10.2 Hz, CH_{Ar}), 130.8 (d, J = 4.6 Hz, C_{Ar}), 130.7 (d, J = 10.1 Hz, CH_{Ar}), 129.5 (CH_{Ar}), 129.0 (d, J = 12.7 Hz, CH_{Ar}), 128.8 (d, J = 12.6 Hz, CH_{Ar}), 125.8 (CH_{Ar}), 59.7 (d, J = 61.0 Hz, PCH_2S); ^{31}P{^{1}H} IGD NMR (162 MHz, $CDCl_3$) δ 21.2 (s); HRMS (ESI$^+$) *m*/*z* calcd for $C_{19}H_{16}ClNaO_2PS$ $[M+Na]^+$ 397.0189, found 397.0192.

3.5.3 .Synthesis of intermediate 21

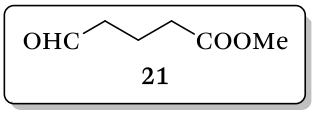

21

This product was prepared following a method reported in the literature,[126] which successfully reproduced. The spectroscopic data were in agreement with those reported.[126]

3.5.4. Synthesis of intermediate 22

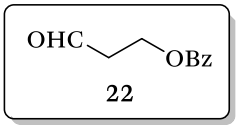

22

This product was prepared following a reported method in the literature,[127] which successfully reproduced. The spectroscopic data were in agreement with those reported.[127]

3.5.5. General synthetic procedure for sulfoxides 11a,b, 14, 16

Acetaldehyde (bp = 30 °C), benzaldehyde (bp = 53–55 °C, 12 mbar) and acrolein (bp = 53 °C) were purified by distillation under nitrogen just before

(126) Enholm, E.; Joshi, A.; Wright, D. L. *Bioorg. Med. Chem. Lett.* **2005**, *15*, 5262-5265.
(127) Nagasawa, S.; Sasano, Y.; Iwabuchi, Y. *Angew. Chem., Int. Ed.* **2016**, *55*, 13189-13194.

their use. Racemic sulfoxides **11a,b**, **14** and **16** were prepared following a reported method in the literature,[114b] with slight modifications.

To a stirring solution of the sulfinyl-phosphine oxide (28.5 mmol) in anhydrous THF (150 mL), *n*-BuLi (1.6 M solution in hexanes, 31.4 mmol) was added at –78 °C and under Ar atmosphere. The resulting solution was stirred for 30 min under the same reaction conditions. After that time, a solution of the corresponding aldehyde (31.4 mmol) in anhydrous THF (5 mL) was slowly added. Then, the reaction mixture was allowed to reach –20 °C and stirred for 18 h at that temperature. Once the reaction was complete,[128] aqueous NH_4Cl (50 mL, sat. solution) was added and the resulting suspension was extracted with Et_2O (3 x 100 mL), dried over anhydrous $MgSO_4$, and evaporated under reduced pressure to yield the crude product. Purification by silica-gel column chromatography using a solvent gradient mixture (*n*-hexane:EtOAc, *n*-pentane:EtOAc, *n*-pentane:MTBE or EtOAc:ACN) yielded the desired sulfoxide (57–79% isolated yield).

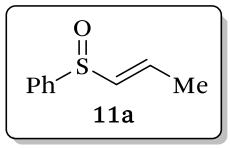

11a

The general procedure was followed starting with sulfinyl-phosphine oxide **18** (10 g, 28.5 mmol) and acetaldehyde (1.76 mL, 31.4 mmol) to yield the crude product. Purification by silica-gel column chromatography using a gradient solvent mixture (from 100% *n*-hexane to 50% EtOAc) afforded the desired sulfoxide as a colorless oil (3.75 g, 79% isolated yield). The spectroscopic data were in agreement with those reported.[114b]

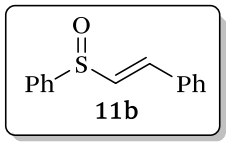

11b

The general procedure was followed starting with sulfinyl-phosphine oxide **18** (1.91 g, 5.57 mmol) and benzaldehyde (0.625 mL, 6.13 mmol) to yield the crude product. Purification by silica-gel column chromatography using a gradient solvent mixture (from 100% *n*-hexane to 40% EtOAc) afforded the desired sulfoxide as a colorless oil (940 mg, 74% isolated yield). The spectroscopic data were in agreement with those reported.[114b]

(128) The reaction progress was followed by TLC control.

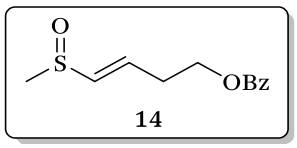

14

The general procedure was followed starting with sulfinyl-phosphine oxide **19** (2.46 g, 8.7 mmol) and aldehyde **22** (1.8 g, 10 mmol) to yield the crude product. Purification by silica-gel column chromatography using a gradient solvent mixture (from 100% EtOAc to 40% ACN) and further recrystallization of the resulting colorless oil in anhydrous Et_2O (5 mL) afforded the desired sulfoxide as a white crystalline solid (815 mg, 39% isolated yield). ^{1}H NMR (500 MHz, $CDCl_3$) δ 8.06–8.04 (m, 2H, CH_{Ar}), 7.61–7.57 (m, 1H, CH_{Ar}), 7.48–7.45 (m, 2H, CH_{Ar}), 6.61–6.55 (m, 1H, CH), 6.45 (dt, J = 15.1 Hz, J = 1.2 Hz, 1H, CH), 4.48 (t, J = 6.3 Hz, 2H, CH_2), 2.76 (m, 2H, CH_2), 2.60 (s, 3H, CH_3);^{13}C{^{1}H} NMR (126 MHz, $CDCl_3$) δ 166.3 (C=O), 136.5 (CH), 135.0 (CH), 133.1 (CH_{Ar}), 129.8 (C), 129.5 (CH_{Ar}), 128.4 (CH_{Ar}), 62.7 (CH_2), 40.6 (CH_3), 31.3 (CH_2). HRMS (ESI$^+$) m/z calcd for $C_{12}H_{14}NaO_3S$ [M+Na]$^+$ 261.0556, found 261.0552.

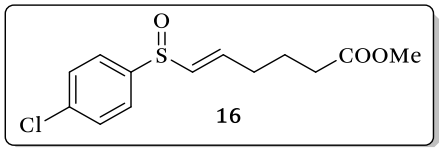

16

The general procedure was followed starting with sulfinyl-phosphine oxide **20** (3.3 g, 8.8 mmol) and aldehyde **21** (1.31 g, 10.1 mmol) to yield the crude product. Purification by silica-gel column chromatography using a gradient solvent mixture (from 100% *n*-hexane to 40% EtOAc) afforded the desired sulfoxide as a colorless oil (1.42 g, 57% isolated yield). ^{1}H NMR (500 MHz, $CDCl_3$) δ 7.57–7.49 (m, 4H, CH_{Ar}), 6.64–6.58 (m, 1H, CH), 6.25 (dt, J = 15.2 Hz, J = 1.4 Hz, CH), 3.68 (s, 3H, CH_3), 2.36–2.28 (m, 4H, CH_2), 1.85–1.79 (m, 2H, CH_2); ^{13}C{^{1}H} NMR (126 MHz, $CDCl_3$) δ 173.3 (C=O), 142.6 (C_{Ar}), 139.9 (CH), 137.1 (C_{Ar}), 135.6 (CH), 129.6 (CH_{Ar}), 125.8 (CH_{Ar}), 51.6 (CH_3), 33.0 (CH_2), 31.2 (CH_2), 23.2 (CH_2); HRMS (ESI$^+$) m/z calcd for $C_{13}H_{15}ClNaO_3S$ [M+Na]$^+$ 309.0323, found 309.0319.

3.5.6. Synthesis of sulfoxide 11c

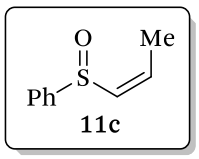

11c

By operating in a nitrogen-filled glove box, a solution of the required amount of the rhodium precatalyst [Rh(nbd)(**L4**)]BF_4 (97.1 mg, 2.5 mol % respect to the allenyl sulfoxide **17**[129], 87.7 mmol) and the corresponding allenyl-

(129) (a) Bridges, A. J. *Tetrahedron Lett.* **1980**, *21*, 4401-4404. (b) Ma, S.; Ren, H.; Wei, Q. *J. Am. Chem. Soc.* **2003**, *125*, 4817-4830.

sulfoxide **17**[129] (576 mg, 3.51 mmol) in anhydrous and degassed CH_2Cl_2 (192 mL) was placed in a glass vessel. The molar concentration of **17** was adjusted to 0.2 M by adding 770 μL of toluene (solvent ratio = CH_2Cl_2:toluene (1:4 v/v)). The reaction mixture was loaded into an autoclave reactor under N_2. The autoclave reactor was loaded with 10 bar of N_2 and slowly cooled to −10 °C. Once the temperature was stabilized (−10 °C), the reactor was depressurized, purged with H_2 gas (3 bar) and finally, pressurized at 5 bar of H_2. The reaction vessel was stirred for 42 h under the same reaction conditions. After that time, the reactor was slowly depressurized. The reaction crude was concentrated under reduced pressure and the resulting oil was purified by silica-gel column chromatography using a gradient mixture of solvent (from 100% *n*-hexane to 70% EtOAc) to afford the desired product as a pale-yellow liquid (423 mg, 76% isol. yield). The spectroscopic data were in agreement with those reported for **11c**. [114]

3.5.7. Synthesis of sulfoxide 11d

Sulfoxide **11d** was prepared following a previously reported synthetic methodology,[112] with slight modifications.

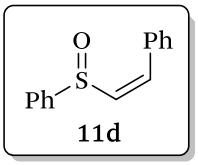

11d

To a stirring solution of phenylacetylene (6.0 mL, 53.5 mmol), CuI[130] (3 mol % with respect to phenylacetylene, 312 mg, 1.6 mmol) and Et_3N (1.49 mg, 10.7 mmol) under Ar atmosphere, thiophenol (5.52 mL, 53.5 mmol) was carefully added and the resulting solution was stirred for 4 h at 40 °C. After that time, the reaction crude was concentrated under reduced pressure and used in the next step without further purification. To a stirring solution of the crude obtained in the previous step in CH_2Cl_2 (50 mL), a solution of *m*-CPBA (1.9 g, ca. 77%, ca. 8.48 mmol) in CH_2Cl_2 (50 mL) was slowly added at −78 °C under Ar atmosphere. The resulting solution was stirred for 1 h under the same reaction conditions. After that time, aqueous Na_2SO_3 (25 mL, sat. solution) was added and the resulting suspension was allowed to reach room temperature. The mixture was washed with an aqueous solution of sodium bicarbonate (250 mL, sat. solution), dried over anhydrous $MgSO_4$, filtered and evaporated under reduced pressure to yield the crude product.

(130) Copper(I) iodide was dried in a vacuum oven at 120 °C for 24 h (1 x 10^{-1} mbar).

Purification by silica-gel column chromatography using a gradient solvent mixture (from 100% *n*-pentane to 40% EtOAc) afforded the desired sulfoxide as a white solid (885.6 mg, 52% isolated yield). The spectroscopic data were in agreement with those reported.[112]

3.5.8. General synthetic procedure for sulfoxides 11e and 11f

The synthetic procedure was based on a previously reported methodology, with slight modifications.[115a] (1-phenyl)-vinyl magnesium bromide was prepared in situ following an already reported methodology, which was efficiently reproduced.[115b]

To a stirring solution of the corresponding organomagnesium reagent (21.6 mmol) under Ar atmosphere and at –78 °C, the benzenesulfinate derivative (9.36 mmol) in anhydrous THF (100 mL) was slowly added. The resulting solution was stirred for 0.75–18 h under the same reaction conditions. The reaction crude was quenched by the addition of aqueous NH_4Cl (25 mL, sat. solution) at –78 °C, and then allowed to warm to room temperature. To the resulting suspension, water (100 mL) was added. The biphasic system was then extracted with CH_2Cl_2 (3 x 100 mL), washed with water (100 mL), dried over anhydrous $MgSO_4$, filtered and concentrated under reduced pressure to yield the crude product as a yellowish oil. Purification by silica-gel column chromatography using a solvent gradient mixture (*n*-pentane:EtOAc or *n*-hexane:EtOAc) afforded the desired sulfoxide as a colorless oil (34–93% isolated yield).

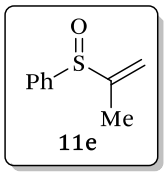

11e

The general procedure was followed starting with isoprenylmagnesium bromide (43.2 mL, 0.5 M solution in THF, 21.6 mmol) and methyl benzenesulfinate (1.25 mL, 98%, 9.36 mmol) to yield the crude product. Purification by silica-gel column chromatography using a gradient solvent mixture (from 100% *n*-pentane to 33% EtOAc) afforded the desired sulfoxide as a colorless liquid (1.45 g, 93% isolated yield). The spectroscopic data were in agreement with those reported.[131]

(131) Villar, J. M.; Delgado, A.; Llebaria, A.; Moretó, J. M.; Molins, E.; Miravitlles, C. *Tetrahedron* **1996**, *52*, 10525-10546.

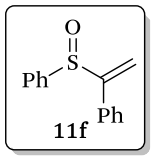

11f

The general procedure was followed starting with (1-phenyl)-vinyl magnesium (≤ 58.5 mmol in 100 mL of THF) and methyl benzenesulfinate (3.9 mL, 98%, 29.3 mmol) to yield the crude product. Purification by silica-gel column chromatography using a gradient solvent mixture (from 100% *n*-hexane to 20% EtOAc) afforded the desired sulfoxide as a colorless liquid (4.5 g, 34% isolated yield). The spectroscopic data were in agreement with those reported.[132]

3.5.9. Synthesis of allenyl sulfoxide 12

Sulfoxide **12** was prepared following a previously reported synthetic methodology, with slight modifications.[129]

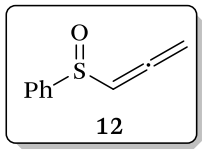

12

To a stirred solution of copper(I) thiophenolate (5.28 g, 98%, 30 mmol) in anhydrous toluene (50 mL) at 80 °C and under Ar atmosphere, trimethyl phosphite (4.29 mL, 36 mmol) was slowly added. The resulting mixture was stirred for 2.5 h under the same reaction conditions until the cuprate dissolved completely. After that time, the crude solution was filtered through Celite® and the filtrate was concentrated under reduced pressure to afford a yellow gummy solid, which was recrystallized by dissolving the crude in a mixture of Et_2O:*n*-hexane (250 mL, 50:50 v/v) and storing the resulting solution at −18 °C for 5 days. The crystalline solid was filtered and washed with cold *n*-hexane (2 x 20 mL) to yield the desired Cu(I)-complex as a pale yellow crystalline solid (6.1 g, 69% isolated yield). To a stirring solution of the Cu(I)-complex obtained in the previous step (3.44 g, 11.6 mmol) and LiBr (2.1 g, 24.2 mmol) in anhydrous THF (150 mL) under Ar atmosphere, propargyl chloride (0.952 mL, 97%, 12.8 mmol) was carefully added and the resulting reaction mixture was stirred under the same reaction conditions for 4 h. After that time, the crude was placed in a glass extraction funnel and water (200 mL) was added. The biphasic system was extracted with CH_2Cl_2 (3 x 200 mL), washed with brine (200 mL), dried over anhydrous $MgSO_4$, filtered and evaporated under reduced pressure to yield the crude product as a yellow oil. Purification by silica-gel column chromatography using a solvent gradient mixture (from 100% *n*-pentane to 5% EtOAc) yield the desired allenyl-

(132) Mancha, G.; Cuenca, A. B.; Rodríguez, N.; Medio-Simón, M.; Asensio, G. *Tetrahedron* **2010**, *66*, 6901-6905.

sulfide as a pale yellow oil. The spectroscopic data were in agreement with those reported.[129a] To a stirring solution of the allenyl-sulfide (943 mg, 6.3 mmol) in CH_2Cl_2 (50 mL) under Ar atmosphere and at −78 °C, *m*-CPBA (1.55 g, ca. 77%, ca. 6.93 mmol) in CH_2Cl_2 (50 mL) was slowly added under those conditions. The reaction mixture was stirred at −78 °C for 1.5 h. After that time, aqueous Na_2SO_3 (20 mL, sat. solution) and an additional volume of CH_2Cl_2 (200 mL) were added. To the biphasic system, aq. $NaHCO_3$ was added (200 mL) and the resulting mixture was extracted with CH_2Cl_2(3 x 200 mL), washed with brine (200 mL), dried over anhydrous $MgSO_4$, filtered and concentrated in vacuo to yield the desired product as a colorless oil (826.3 mg, 80% isolated yield). The spectroscopic data were in agreement with those reported.[129b]

3.5.10. Preparation of racemic sulfoxide *rac*-15

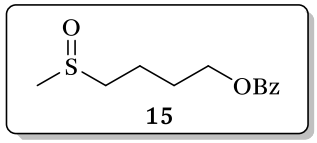

15

Operating in a nitrogen-filled glove box, a solution of the required amount of $[Rh(nbd)_2]BF_4$ (5.0 mol % with respect to the substrate, 4.26 μmol), PPh_3 (11.0 mol % with respect to the substrate, 9.37 μmol) and the corresponding sulfoxide **14** (20.5 mg, 85.1 μmol) in anhydrous and degassed CH_2Cl_2 (137 μL) was placed in a glass vessel. The molar concentration of **14** was adjusted to 0.2 M by adding 290 μL of CH_2Cl_2. The reaction mixture was loaded into an autoclave. The autoclave was purged with H_2 gas (3 bar) and finally pressurized at 8 bar of H_2. The reaction vessel was stirred for 24 h at rt. After that time, the reactor was slowly depressurized. The reaction crude was concentrated under reduced pressure and the resulting crude was filtered through a short pad of silica (ca. 2 cm of silica in a Pasteur pipette) eluting with EtOAc (2 mL) to afford a pale yellow liquid. The product was obtained as a mixture of **14**:**15** (molar ratio of **14**:**15**: 35:65), and was used without further purification for HPLC method development purposes. Complete characterization data and NMR spectrum of isolated product **15** are presented in the section 3.5.14 “Characterization of reaction products and determination of the absolute configuration”, Figure 106 and Figure 116.

3.5.11. Complete data for Table 17

Table 18. Complete data for the KR of sulfoxides *rac*-11a–f[a]

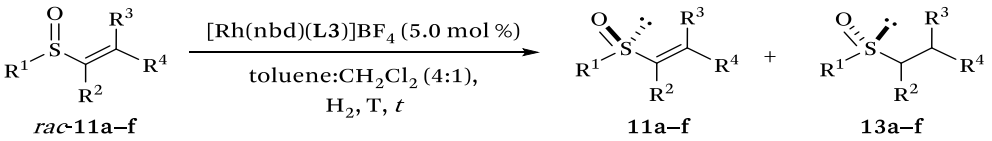

entry	R^1, R^2, R^3, R^4	P, bar	T, °C	*t*, h	conv.,[b] %	product, ee, %,[c] (*config.*)[d]	product, ee, %,[c] (*config.*)[d]	*s*[e]
1	Ph, H, H, Me (*rac*-**11a**)	10	0	66	61	**11a**, 99 (*S*)	**13a**, 63 (*R*)	51
2[f]		10	–10	20	25	**11a**, 25 (*S*)	**13a**, 90 (*R*)	23
3	Ph, H, H, Ph (*rac*-**11b**)	5	rt	48	53	**11b**, *rac*	**13b**, *rac*	–
4	Ph, H, Me, H (*rac*-**11c**)	8	rt	70	92	**11c**, 99 (*S*)	**13c**, 8 (*R*)	8
5[g]		20	0	71	63	**11c**, 83 (*S*)	**13c**, 56 (*R*)	8
6	Ph, H, Ph, H (*rac*-**11d**)	20	rt	90	75	**11d**, 62 (*S*)	**13d**, 29 (*R*)	3
7		40	0	48	24	**11d**, 15 (*S*)	**13d**, 56 (*R*)	4
8	Ph, Me, H, H (*rac*-**11e**)	5	rt	48	90	**11e**, 99 (*S*)	**13e**, 12 (*R*)	10
9		10	–10	72	21	**11e**, 24 (*S*)	**13e**, 85 (*R*)	20
10	Ph, Ph, H, H (*rac*-**11f**)	5	rt	24	54	**11f**, 99 (*R*)	**13f**, 74 (R_S,R_C)	91
11[h]		5	rt	3.5	42	**11f**, 76 (*R*)	**13f**, 93 (R_S,R_C)	60

[a,b,c,d,e]See notes *a*, *b*, *c*, *d*, and *e* in Table 17. [f]Solvent mixture = Cy:CH_2Cl_2 (4:1). [g]5% of isomerized product **11a** was detected in the reaction crude, as determined by ^{1}H NMR. [h]dr ratio of *anti*-**13f**:*syn*-**13f** ≥ 99:1, as determined by ^{1}H NMR.

3.5.12. Complete data for experiment in Scheme 9

Table 19. Kinetic resolution of substrate *rac*-16[a]

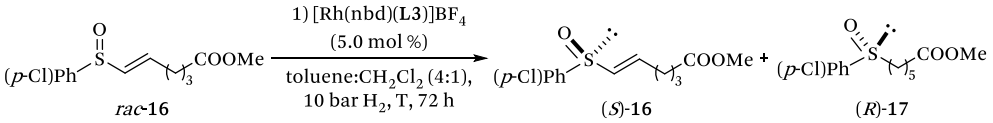

entry	T, °C	conv,[b] %	product, isol. yield,[84] %; ee, %,[c] (*config.*)[d]	product, isol. yield,[84] %; ee, %,[c] (*config.*)[d]	*s*[e]
1	0	61	**16**, 71, 99 (*S*)	**17**, 74, 69 (*R*)	26
2	–10	42	**16**, 79, 61 (*S*)	**17**, 41, 94 (*R*)	65

[a,b,c]See notes *a*, *b*, and *c* in Table 17. [d]The absolute configuration of products **16** and **17** were tentatively assigned by analogy with the results for **13d,e**. [e]See note *e* in Table 17.

3.5.13. Determination of enantiomeric excess of reaction products

HPLC conditions for 11a and 13a: Daicel Chiralcel® (25 cm x 0.46 cm) OB-H, 85:15 *n*-hexane/2-propanol, 1.0 mL/min, 254 nm. Retention times for the enantiomers: 13.7 min (*R*)-**13a**, 20.0 min (*S*)-**11a**, 28.0 min (*S*)-**13a** and 39.1 min (*R*)-**11a**.

HPLC conditions for 11b and 13b: Daicel Chiralpak® (25 cm x 0.46 cm) IA, 98:2 *n*-hexane/2-propanol, 1.0 mL/min, 254 nm. Retention times for the enantiomers: 45.9 min (*R*)-**13b**, 50.2 min (*S*)-**13b**, 59.6 min (*R*)-**11b** and 65.4 min (*S*)-**11b.**

HPLC conditions for 11c and 13c: Daicel Chiralpak® (25 cm x 0.46 cm) IC, 90:10 *n*-hexane/2-propanol, 1.0 mL/min, 254 nm. Retention times for the enantiomers: 41.5 min (*R*)-**13c**, 43.4 min (*S*)-**13c**, 74.5 min (*R*)-**11c** and 77.1 min (*S*)-**11c**.

HPLC conditions for 11d and 13d: Daicel Chiralpak® (25 cm x 0.46 cm) IC, 95:5 *n*-hexane/2-propanol, 1.0 mL/min, 254 nm. Retention times for the enantiomers: 20.1 min (*R*)-**13d**, 22.0 min (*S*)-**13d**, 26.6 min (*R*)-**11d** and 36.3 min (*S*)-**11d**.

HPLC conditions for 11e and 13e: Daicel Chiralpak® (25 cm x 0.46 cm) IC, 95:5 *n*-hexane/2-propanol, 1.0 mL/min, 230 nm. Retention times for the enantiomers: 8.5 min (*S*)-**13e**, 12.1 min (*S*)-**11e**, 14.6 (*R*)-**13e** and 18.7 min (*R*)-**11e**.

HPLC conditions for 11f and 13f: Daicel Chiralpak® (25 cm x 0.46 cm) IC, 95:5 *n*-hexane/2-propanol, 1.0 mL/min, 230 nm. Retention times for the enantiomers: 55.4 min (*R*)-**11f**, 60.0 min (*S*)-**11f**, 68.4 min (R_S,R_C)-**13f** and 90.8 min (S_S,S_C)-**13f**.

HPLC conditions for 14 and 15: Daicel Chiralpak® (25 cm x 0.46 cm) IA, 95:5 *n*-hexane/2-propanol, 1.0 mL/min, 230 nm. Retention times for the enantiomers: 52.8 min (*S*)-**14**, 58.1 min (*R*)-**14**, 63.6 min (*S*)-**15** and 73.3 min (*R*)-**15**.

HPLC conditions for 16 and 17:[101] Daicel Chiralcel® (25 cm x 0.46 cm) OB-H, 50:50 *n*-heptane/2-propanol, 0.5 mL/min, 254 nm. Retention times for the enantiomers: 20.1 min (*S*)-**17**, 22.9 min (*S*)-**16**, 44.0 min (*R*)-**16** and 50.5 min (*R*)-**17**.

3.5.14. Characterization of reaction products and determination of the absolute configuration

The absolute configurations of products **11e,f** and **13e,f** were determined by comparison with reported optical rotations for **13e,f**. The absolute configuration of products **11a–d** and **13a–d** were tentatively assigned by analogy with the results for **13e,f**.

(*S*)-(*E*)-(prop-1-en-1-ylsulfinyl)benzene (*S*)-**11a** (optimized result for product **11a**; Table 17, entry 1): 99% ee (*S*). This product was obtained as a mixture of compounds (molar ratio (**11a**:**13a**) = 39:61), which could not be purified by standard chromatographic techniques. The spectroscopic data were in agreement with those reported.[114b]

(*R*)-(propylsulfinyl)benzene (*R*)-**13a** (optimized result for product **13a**; Table 17, entry 1): 90% ee (*R*). This product was obtained as a mixture of compounds (molar ratio (**11a**:**13a**) = 75:25), which could not be purified by

standard chromatographic techniques. The spectroscopic data were in agreement with those reported.[114b]

(*E*)-(2-(phenylsulfinyl)vinyl)benzene **11b** (Table 17; entry 2): This product was obtained as a mixture of compounds (molar ratio (**11b**:**13b**) = 47:53), which could not be purified by standard chromatographic techniques. The spectroscopic data were in agreement with those reported.[114b]

(*S*)-(*Z*)-(prop-1-en-1-ylsulfinyl)benzene (*S*)-**11c**: (optimized result for product **11c**; Table 17, entry 3): 99% ee (*S*). This product was obtained as a mixture of compounds (molar ratio (**11c**:**11a**:**13c**) = 3:5:72), which could not be purified by standard chromatographic techniques. (Table 18, entry 5): 83% ee (*S*). This product was obtained as a mixture of compounds (molar ratio (**11c**:**13c**) = 37:63), which could not be purified by standard chromatographic techniques. The spectroscopic data were in agreement with those reported [114a]

(*S*)-(*Z*)-((2-phenylsulfinyl)vinyl)benzene (*S*)-**11d** (optimized result for product **11d**; Table 17, entry 4): 62% ee (*S*). This product was obtained as a mixture of compounds (molar ratio (**11d**:**13d**) = 25:75), which could not be purified by standard chromatographic techniques. The spectroscopic data were in agreement with those reported.[112]

(*R*)-(phenethylsulfinyl)benzene (*R*)-**13d** (optimized result for product **13d**; Table 17, entry 4): 56% ee (*R*). This product was obtained as a mixture of compounds (molar ratio (**11d**:**13d**) = 76:24), which could not be purified by standard chromatographic techniques. The spectroscopic data were in agreement with those reported.[133]

(*S*)-(prop-1-en-2-ylsulfinyl)benzene (*S*)-**11e** (optimized result for product **11e**; Table 17, entry 5): 99% ee (*S*). $[\alpha]^{27}_{D} = -40$ (*c* 1.17, $CHCl_3$). The spectroscopic data were in agreement with those reported.[131]

(*R*)-(isopropylsulfinyl)benzene (*R*)-**13e** (optimized result for product **13e**; Table 17, entry 5): 85% ee (*R*). $[\alpha]^{27}_{D} = +126$ (*c* 0.31, $CHCl_3$) for

(133) Fabretti, A.; Ghelfi, F.; Grandi, R.; Pagnoni, U. M. *Synth. Commun.* **1994**, *24*, 2393-2398.

85% ee (*R*) [Lit:[134] $[\alpha]^{20}_D$ = −146.9 (*c* 0.42, $CHCl_3$) for 72% ee (*S*)]. The spectroscopic data were in agreement with those reported.[134]

(*R*)-(1-(phenylsulfinyl)vinyl)benzene (*R*)-**11f** (optimized result for product **11f**; Table 17, entry 6): 99% ee (*R*). $[\alpha]^{24}_D$ = −53.1 (*c* 0.28, acetone) for 99% ee (*R*). The spectroscopic data were in agreement with those reported.[132]

(((*R*$_S$,*R*$_C$)-1-phenylethyl)sulfinyl)benzene (*R*$_S$,*R*$_C$)-**13f** (optimized result for product **13f**; Table 17, entry 6): 93% ee (*R*$_S$,*R*$_C$). $[\alpha]^{24}_D$ = +122.3 (*c* 0.42, acetone) for 93% ee (*R*$_S$,*R*$_C$) [Lit$[\alpha]^{25}_D$ = +204.2 (*c* 1.5, acetone) for 99% ee (*R*$_S$,*R*$_C$)]. The spectroscopic data were in agreement with those reported for *anti*-**13f**.[135]

(*R*)-(*E*)-4-(methylsulfinyl)but-3-en-1-yl benzoate (*R*)-**14**: New compound. 84% ee (*R*). $[\alpha]^{26}_D$ = −43 (*c* 0.28, CH_2Cl_2). The spectroscopic data were in agreement with those obtained for product **14**.

(*S*)-4-(methylsulfinyl)butyl benzoate (*S*)-**15**: New compound. 50% ee (*S*). $[\alpha]^{26}_D$ = +10 (*c* 0.15, CH_2Cl_2). The spectroscopic data were in agreement with those obtained for **15**. ^{1}H NMR (400 MHz, $CDCl_3$) δ 8.06–8.04 (m, 2H, CH_{Ar}), 7.60–7.44 (m, 3H, CH_{Ar}), 4.40 (bs, 2H, CH_2), 2.84–2.73 (m, 2H, CH_2), 2.61 (s, 3H, CH_3), 2.01–1.96 (m, 4H, CH_2); $^{13}C\{^1H\}$ NMR (100 MHz, $CDCl_3$) δ 166.5 (C=O), 133.0 (CH_{Ar}), 130.0 (C_q), 129.5 (CH_{Ar}), 128.4 (CH_{Ar}), 64.0 (CH_2), 54.1 (CH_2), 38.6 (CH_3), 27.9 (CH_2), 19.5 (CH_2); HRMS (ESI^+) *m*/*z* calcd for $C_{12}H_{16}NaO_3S$ $[M+Na]^+$ 263.0712, found 263.0721.

(*S*)-methyl-(*E*)-6-((4-chlorophenyl)sulfinyl)hex-5-enoate (*S*)-**16**: New compound. 99% ee (*S*). $[\alpha]^{25}_D$ = −78.8 (*c* 0.64, $CHCl_3$) for 99% ee (*S*). The spectroscopic data were in agreement with those obtained for product **16**.

(134) Hampel, T.; Ruppenthal, S.; Saelinger, D.; Brueckner, R. *Chem. – Eur. J.* **2012**, *18*, 3136-3140.
(135) Sato, T.; Otera, J. *Synlett* **1995**, 365-366.

(*R*)-methyl-6-((4-chlorophenyl)sulfinyl)hexanoate (*R*)-**17:** 93% of ee (*R*). $[\alpha]^{25}_{D}$ = +64 (*c* 0.60, $CHCl_3$).[136] The spectroscopic data were in agreement with those reported.[101]

3.5.15. Selected NMR data from catalytic experiments

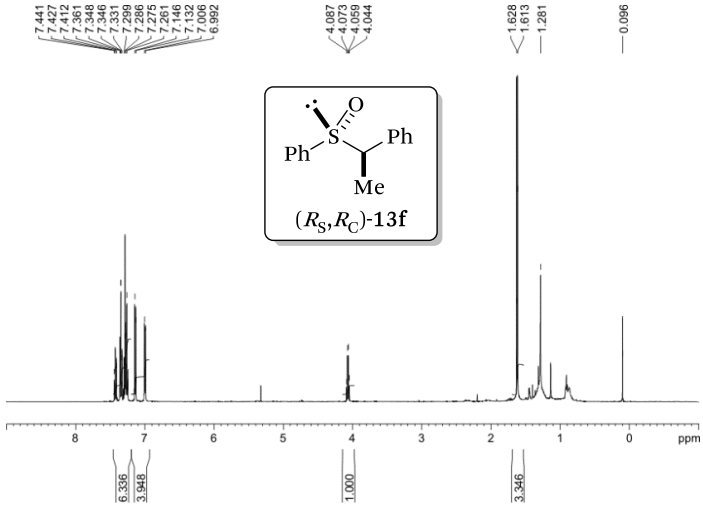

Figure 103. ^{1}H NMR (500 MHz, $CDCl_3$) of isolated (R_S,R_C)-**13f** (Table 17, entry 10).

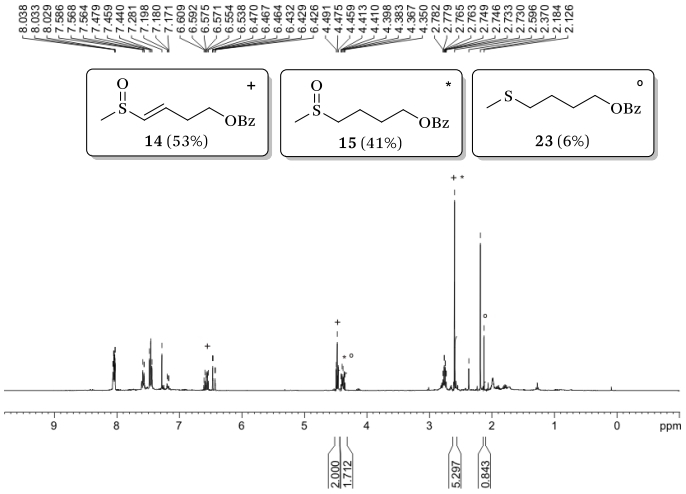

Figure 104. ^{1}H NMR (400 MHz, $CDCl_3$) of the reaction crude from Scheme 8.[137]

(136) Although there are reports where product **17** is obtained in an enantiomerically enriched form, see for example ref. 101; the value of the specific rotation for product **17** is not provided.

(137) Product **23** is a known product in the literature: Mamalis, P.; Rydon, H. N. *J. Chem. Soc.* **1955**, 1049-1065.

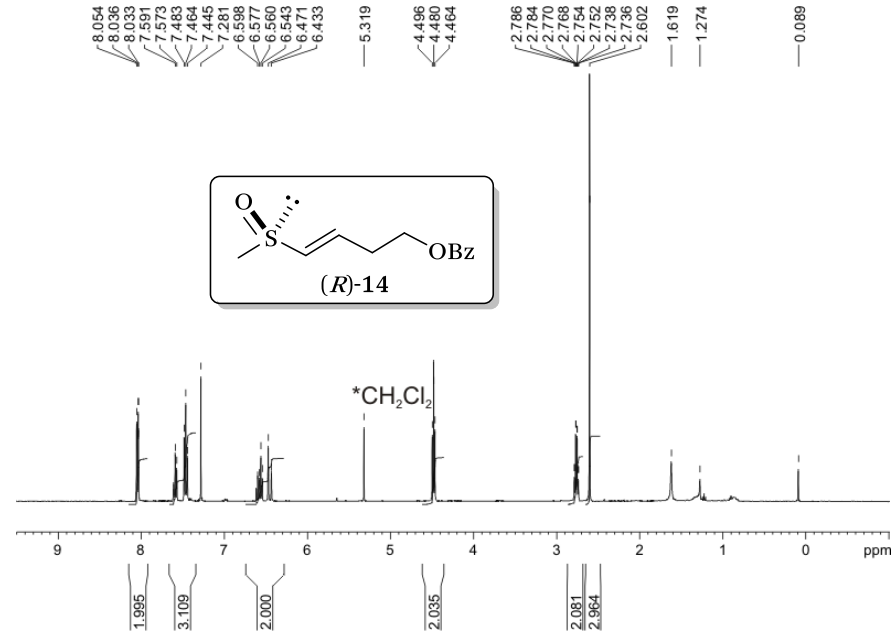

Figure 105. ^{1}H NMR (400 MHz, $CDCl_3$) of isolated (*R*)-**14** (Scheme 8).

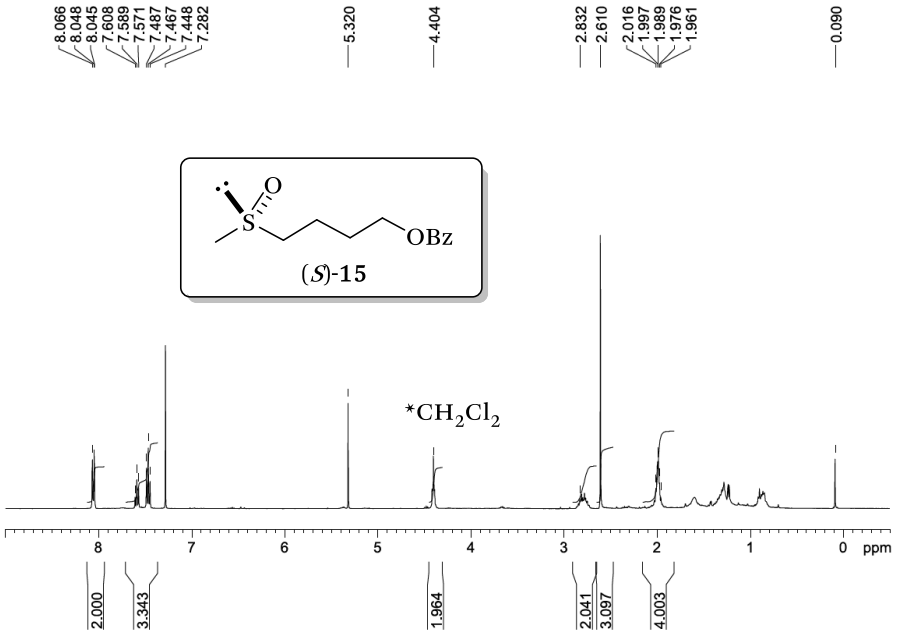

Figure 106. ^{1}H NMR (400 MHz, $CDCl_3$) of isolated of (*S*)-**15** (Scheme 8).

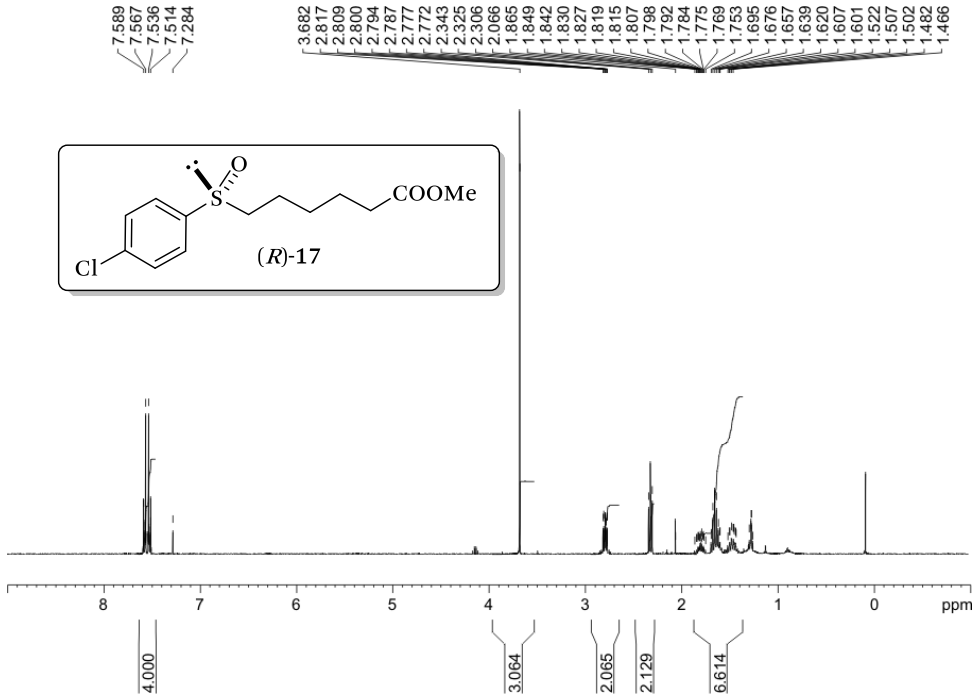

Figure 107. ^{1}H NMR (400 MHz, $CDCl_3$) of isolated (*R*)-**17** (Scheme 9).

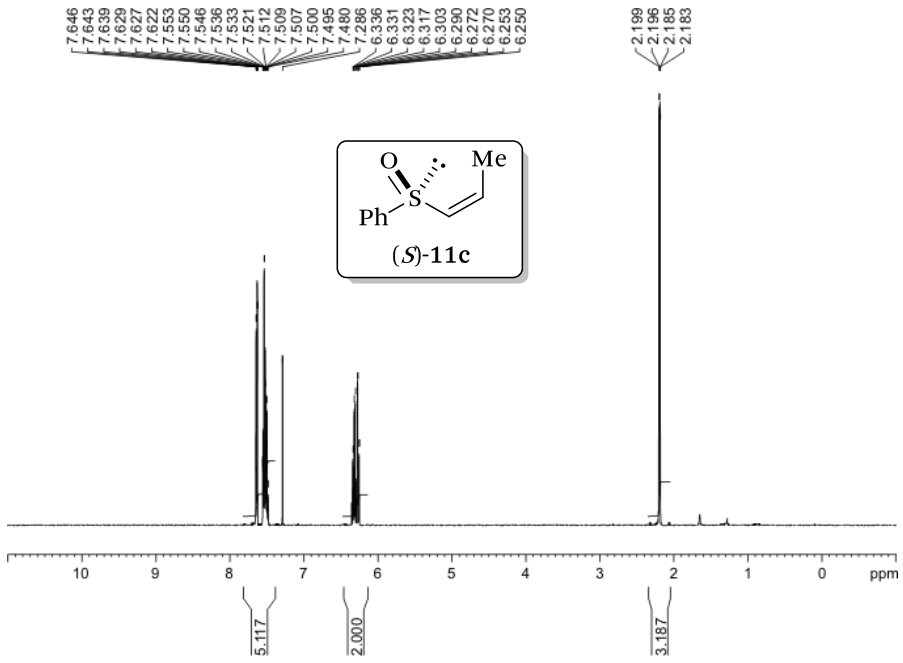

Figure 108. ^{1}H NMR (500 MHz, $CDCl_3$) of reaction product *rac*-**11c** from **12** (Figure 102).

3.5.16. NMR of new compounds

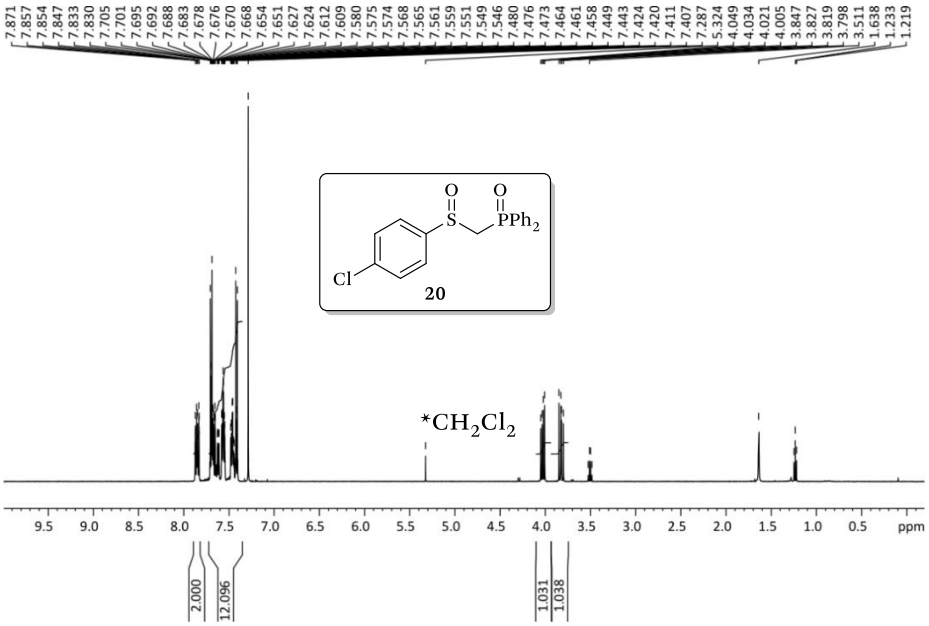

Figure 109. ^{1}H NMR (500 MHz, $CDCl_3$) of **20**.

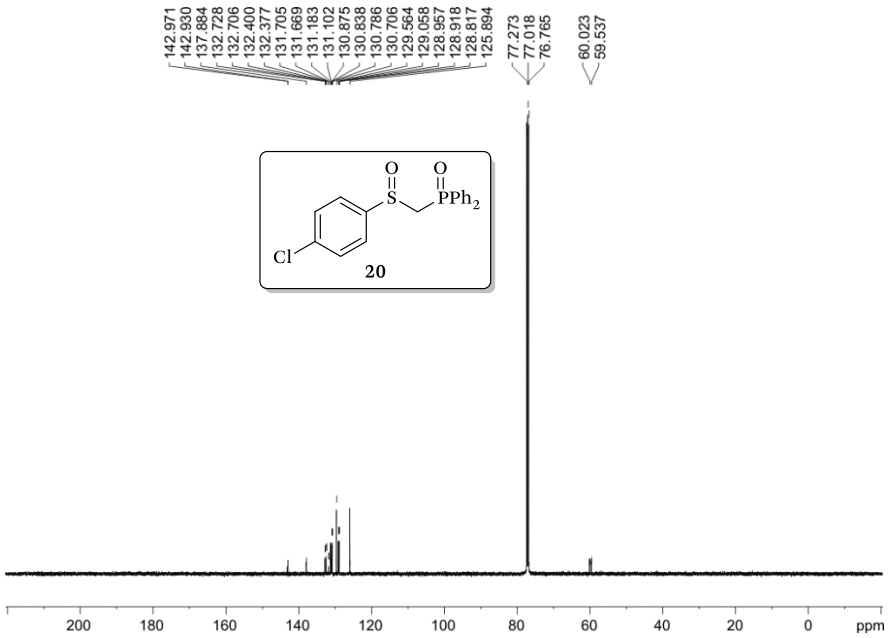

Figure 110. $^{13}C\{^{1}H\}$ NMR (126 MHz, $CDCl_3$) of **20**.

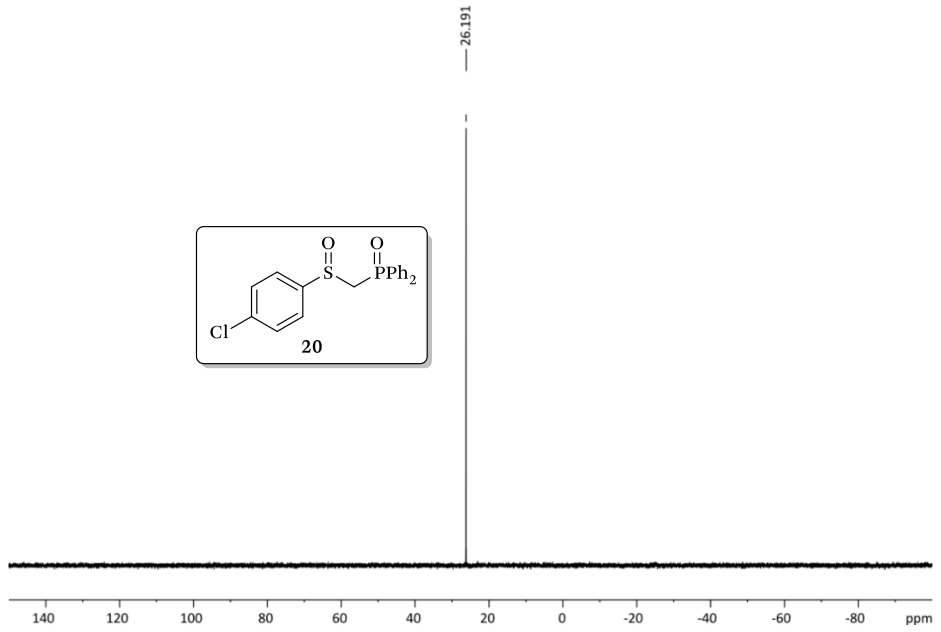

Figure 111. $^{31}P\{^{1}H\}$ NMR (162 MHz, $CDCl_3$) of **20**.

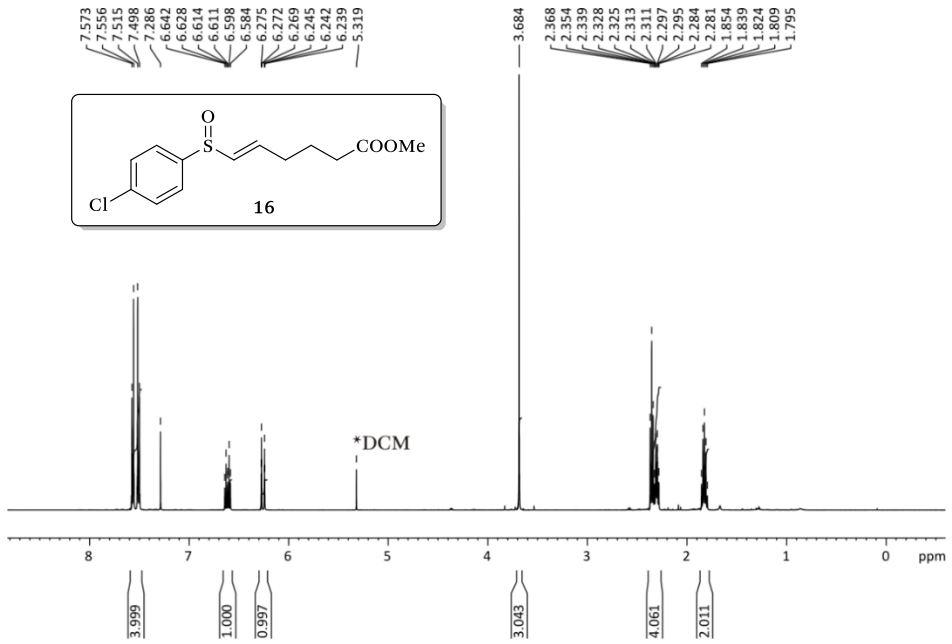

Figure 112. ^{1}H NMR (500 MHz, $CDCl_3$) of **16**.

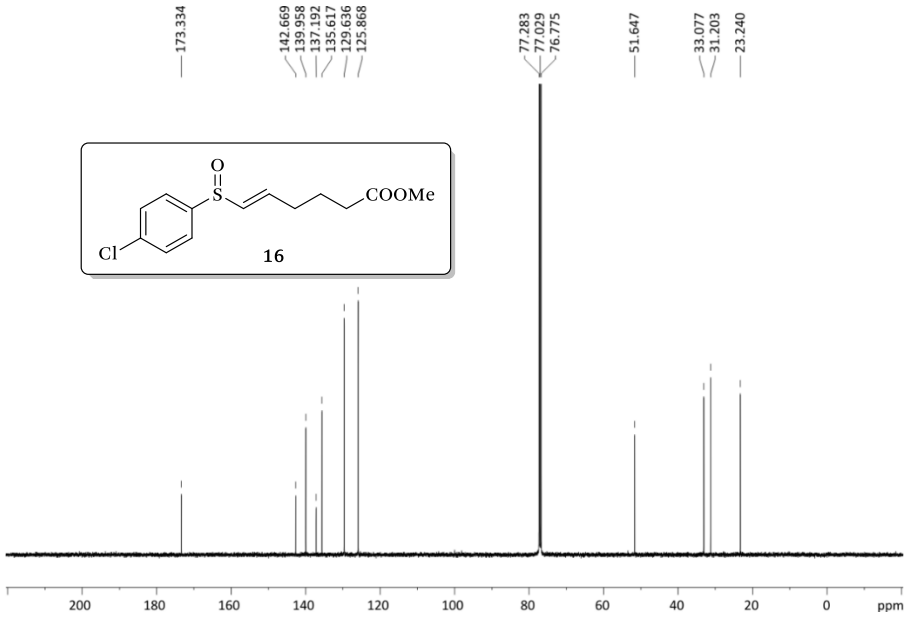

Figure 113. $^{13}C\{^{1}H\}$ NMR (126 MHz, $CDCl_3$) of **16**.

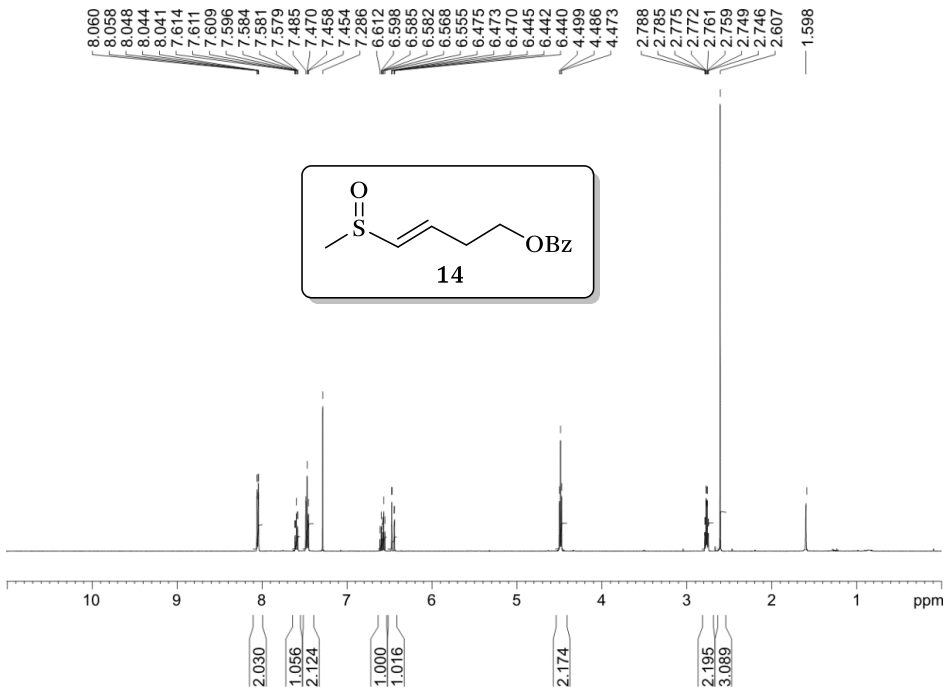

Figure 114. ^{1}H NMR (500 MHz, $CDCl_3$) of **14**.

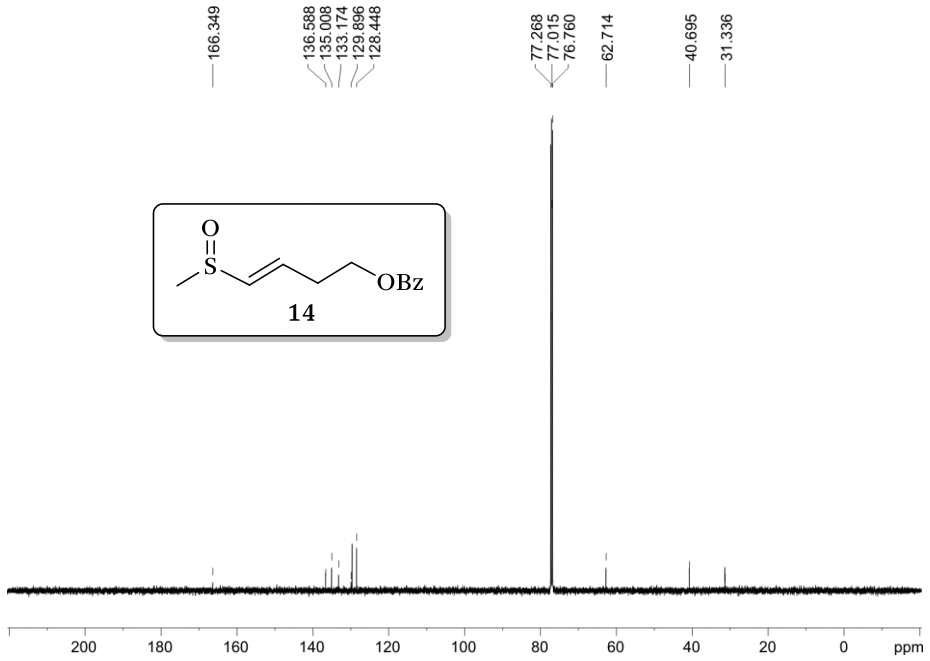

Figure 115. $^{13}C\{^{1}H\}$ NMR (126 MHz, $CDCl_3$) of **14**.

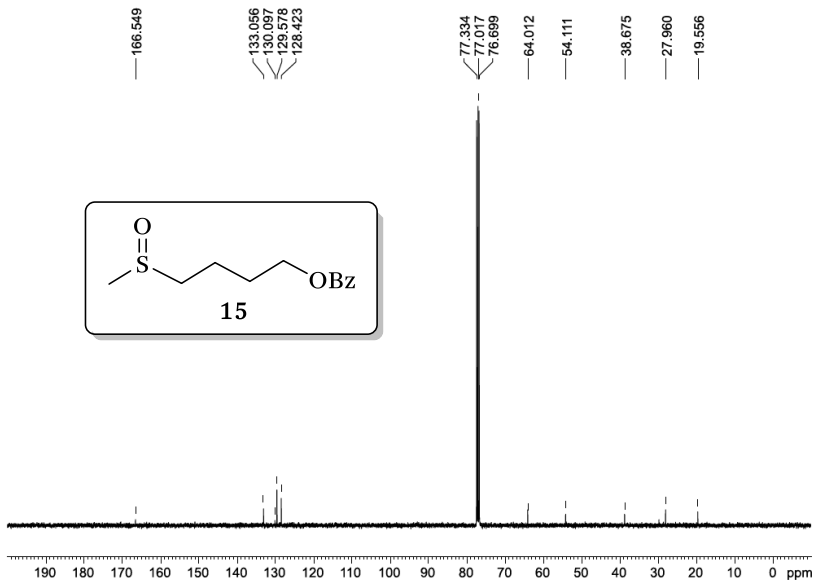

Figure 116. $^{13}C\{^{1}H\}$ (100 MHz, $CDCl_3$) of **15**.[138]

(138) The ^{1}H NMR data of new compound **15** has been already presented in Figure 106.

3.5.17. Selected HPLC data from catalytic experiments

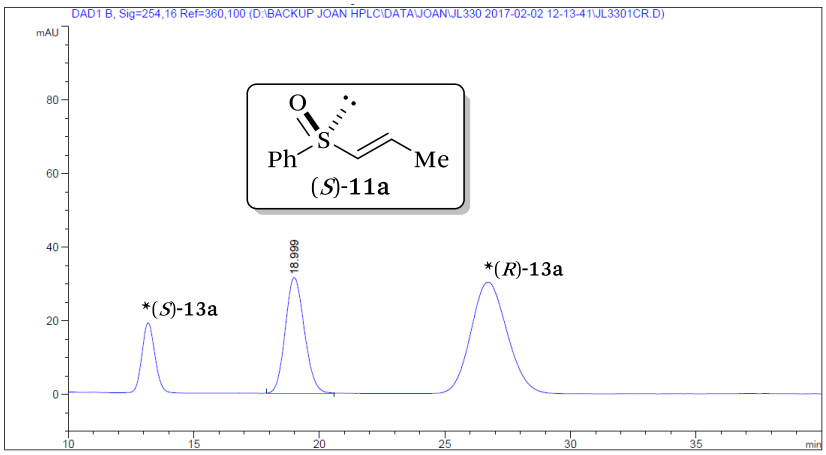

Peak #	RetTime [min]	Type	Width [min]	Area [mAU*s]	Height [mAU]	Area %
1	18.999	BB	0.8236	1663.47559	31.42296	100.0000

Figure 117. Chiral HPLC trace of (*S*)-**11a** (optimized conditions for **11a**, Table 17, entry 1).

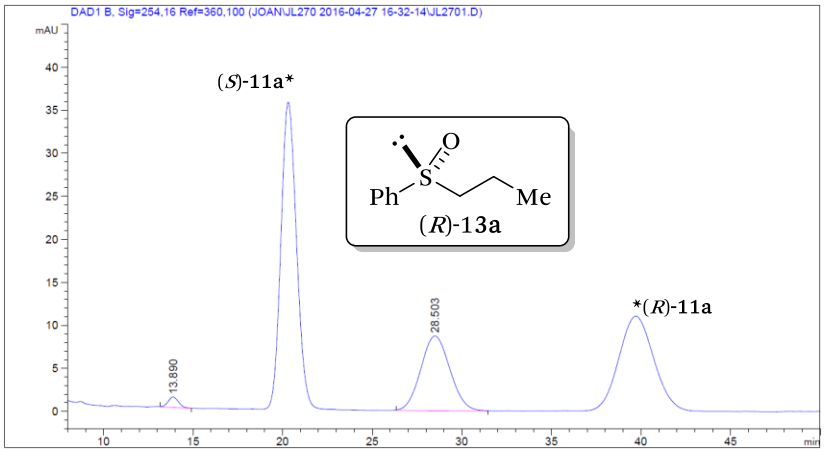

Peak #	RetTime [min]	Type	Width [min]	Area [mAU*s]	Height [mAU]	Area %
1	13.890	BB	0.5966	48.06209	1.20695	4.6804
2	28.503	BB	1.5840	978.80750	8.67751	95.3196

Figure 118. Chiral HPLC trace of (*R*)-**13a** (optimized conditions for **13a**, Table 17, entry 1)

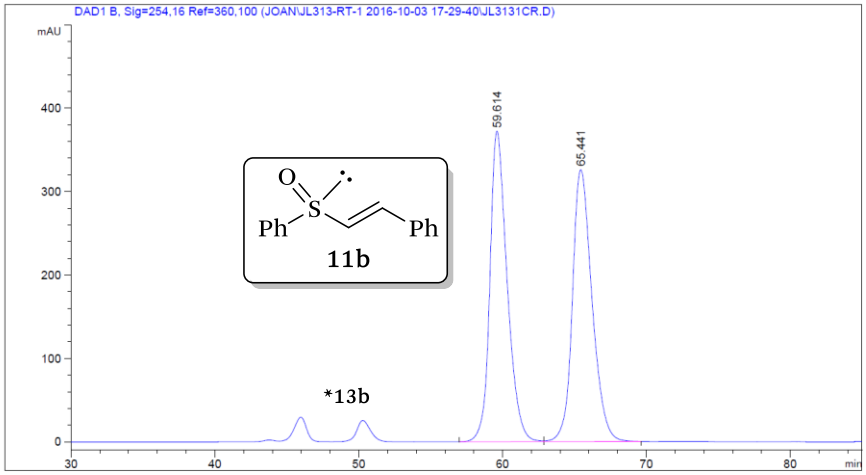

Peak #	RetTime [min]	Type	Width [min]	Area [mAU*s]	Height [mAU]	Area %
1	59.614	BV	1.2582	3.10205e4	372.23880	50.1202
2	65.441	VB	1.4317	3.08717e4	325.73401	49.8798

Figure 119. Chiral HPLC trace of **11b** (Table 17, entry 2).

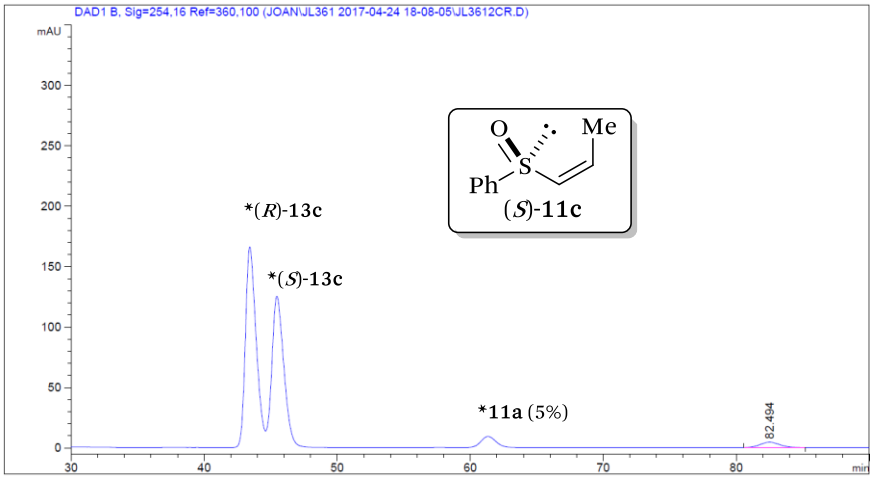

Peak #	RetTime [min]	Type	Width [min]	Area [mAU*s]	Height [mAU]	Area %
1	82.494	BB	1.4881	443.93030	4.33012	100.0000

Figure 120. Chiral HPLC trace of (*S*)-**11c** (optimized conditions for product **11c**; Table 17, entry 3).

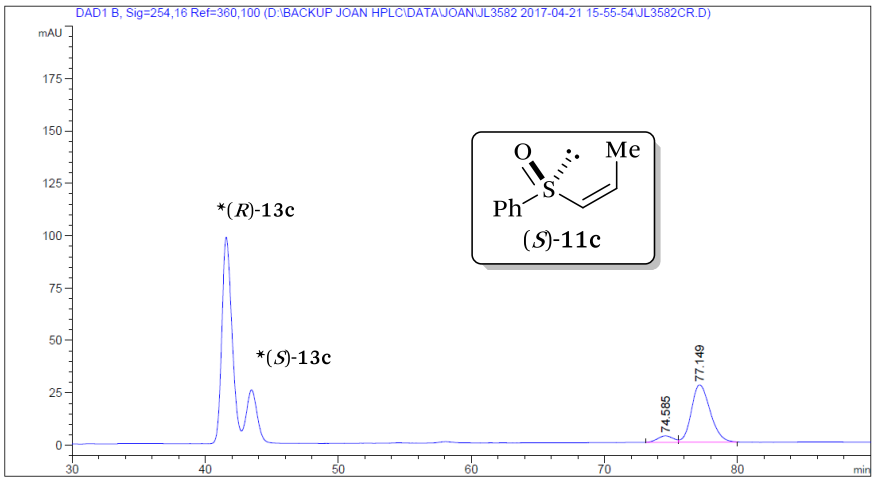

Peak #	RetTime [min]	Type	Width [min]	Area [mAU*s]	Height [mAU]	Area %
1	74.585	BV	1.0960	252.32649	3.06002	8.5817
2	77.149	VB	1.4795	2687.96509	27.37716	91.4183

Figure 121. Chiral HPLC trace of (*S*)-**11c** (Table 18, entry 5).

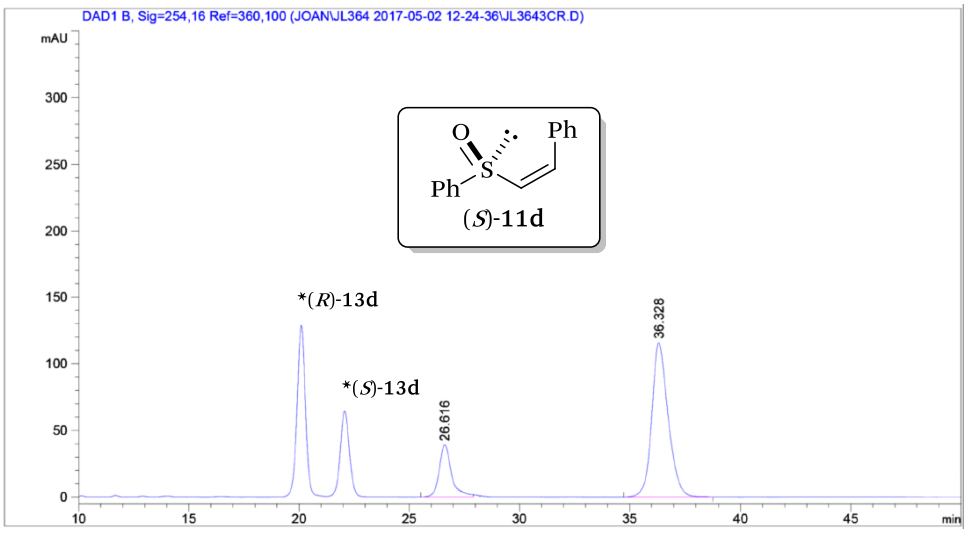

Peak #	RetTime [min]	Type	Width [min]	Area [mAU*s]	Height [mAU]	Area %
1	26.616	BV	0.5477	1405.38037	39.06830	19.0391
2	36.328	BB	0.7711	5976.18359	115.60921	80.9609

Figure 122. Chiral HPLC trace of (*S*)-**11d** (optimized conditions for **11d**, Table 17, entry 4).

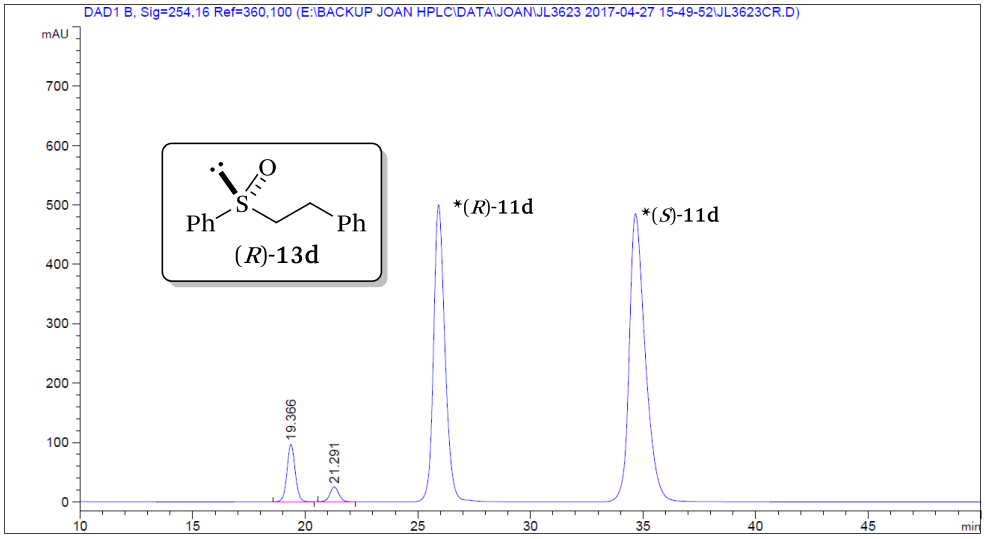

Peak #	RetTime [min]	Type	Width [min]	Area [mAU*s]	Height [mAU]	Area %
1	19.366	BB	0.3906	2460.13086	96.75608	77.8947
2	21.291	BB	0.4265	698.14801	25.10010	22.1053

Figure 123. Chiral HPLC trace of (*R*)-**13d** (optimized conditions for **13d**, Table 17, entry 4).

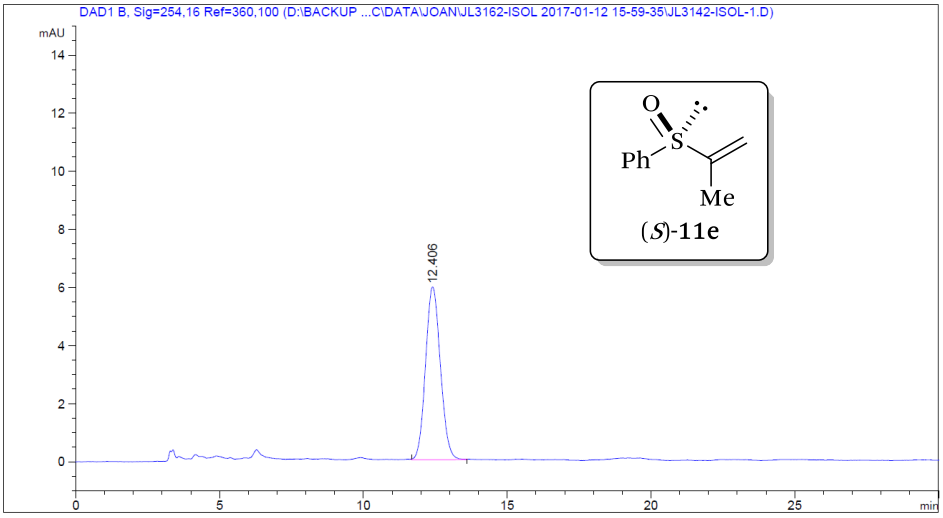

Peak #	RetTime [min]	Type	Width [min]	Area [mAU*s]	Height [mAU]	Area %
1	12.406	BB	0.5585	213.44536	5.95013	100.0000

Figure 124. Chiral HPLC trace of (*S*)-**11e** (optimized conditions for **11e**; Table 17, entry 5).

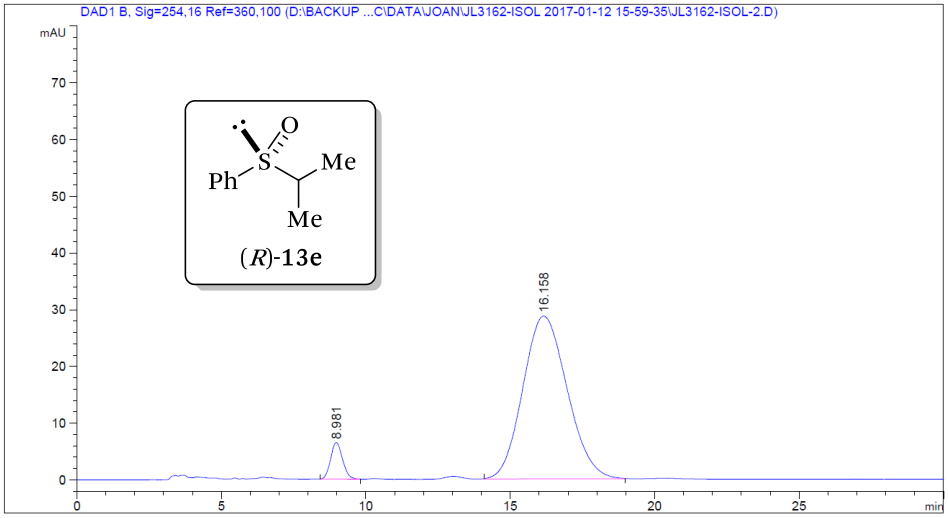

Peak #	RetTime [min]	Type	Width [min]	Area [mAU*s]	Height [mAU]	Area %
1	8.981	BB	0.4460	184.18587	6.43312	5.6866
2	16.158	BB	1.6015	3054.74805	28.70584	94.3134

Figure 125. Chiral HPLC trace of (*R*)-**13e** (optimized conditions for **13e**; Table 17, entry 5).

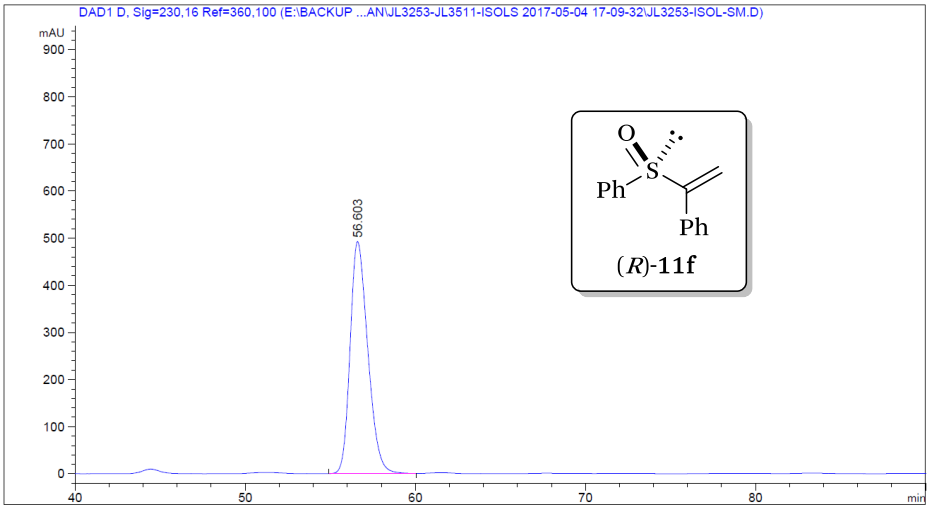

Peak #	RetTime [min]	Type	Width [min]	Area [mAU*s]	Height [mAU]	Area %
1	56.603	BB	1.1187	3.55694e4	492.45944	100.0000

Figure 126. Chiral HPLC trace of (*R*)-**11f** (optimized conditions for **11f**; Table 17, entry 6).

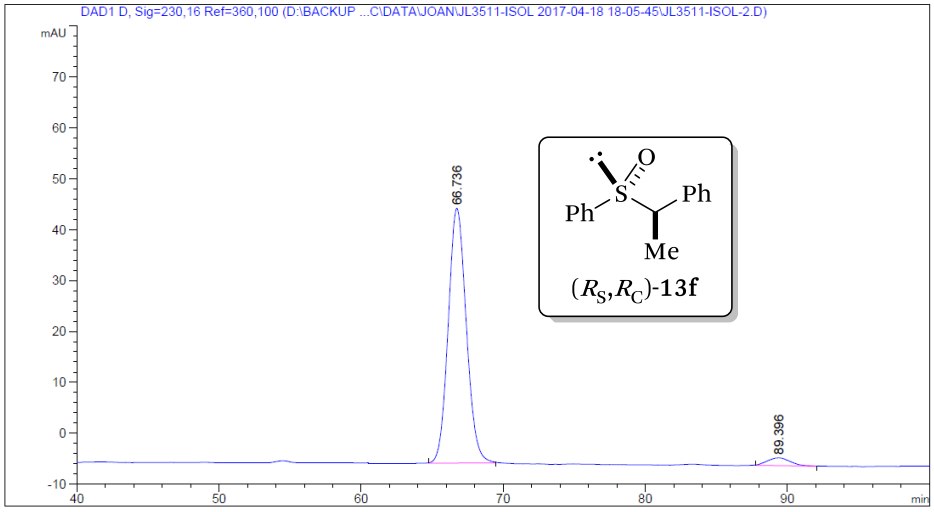

Peak #	RetTime [min]	Type	Width [min]	Area [mAU*s]	Height [mAU]	Area %
1	66.736	BB	1.3804	4426.55957	50.02383	96.3834
2	89.396	BB	1.3152	166.09923	1.53160	3.6166

Figure 127. Chiral HPLC trace of (R_S,R_C)-**13f** (optimized conditions for **13f**; Table 17, entry 6).

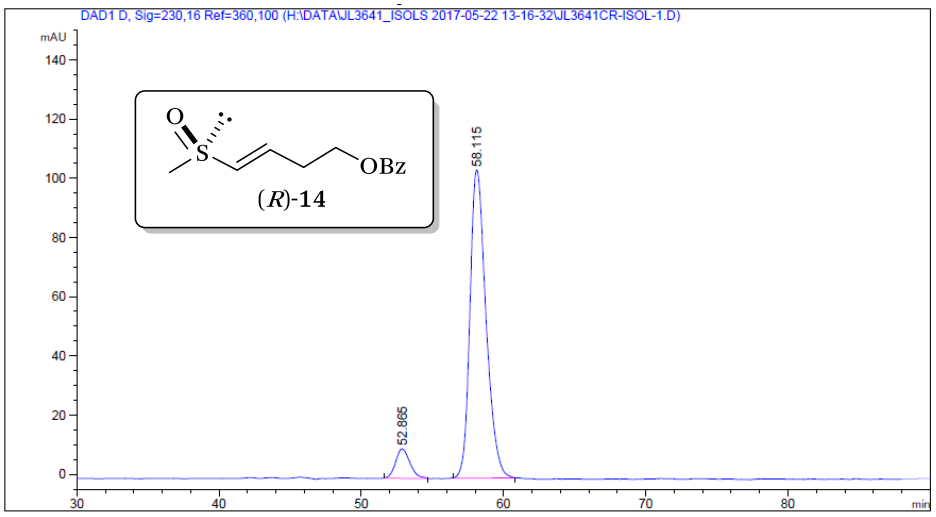

Peak #	RetTime [min]	Type	Width [min]	Area [mAU*s]	Height [mAU]	Area %
1	52.865	BB	1.0422	698.62750	9.93738	7.8757
2	58.115	BB	1.1816	8172.03467	104.13175	92.1243

Figure 128. Chiral HPLC trace of (*R*)-**14** (Scheme 8).

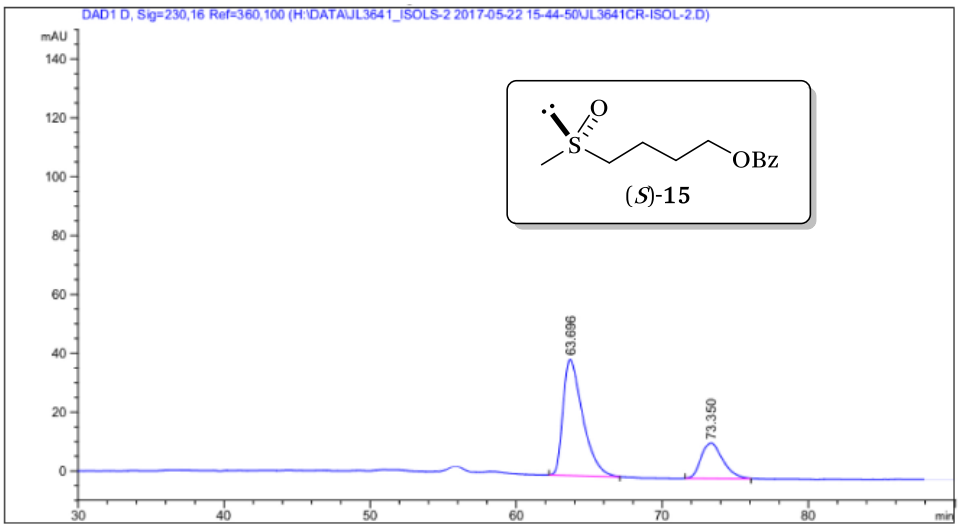

Peak #	RetTime [min]	Type	Width [min]	Area [mAU*s]	Height [mAU]	Area %
1	63.696	BB	1.3822	3714.12012	39.45780	74.9243
2	73.350	BB	1.3358	1243.04089	12.02677	25.0757

Figure 129. Chiral HPLC trace of (*S*)-**15** (Scheme 8).

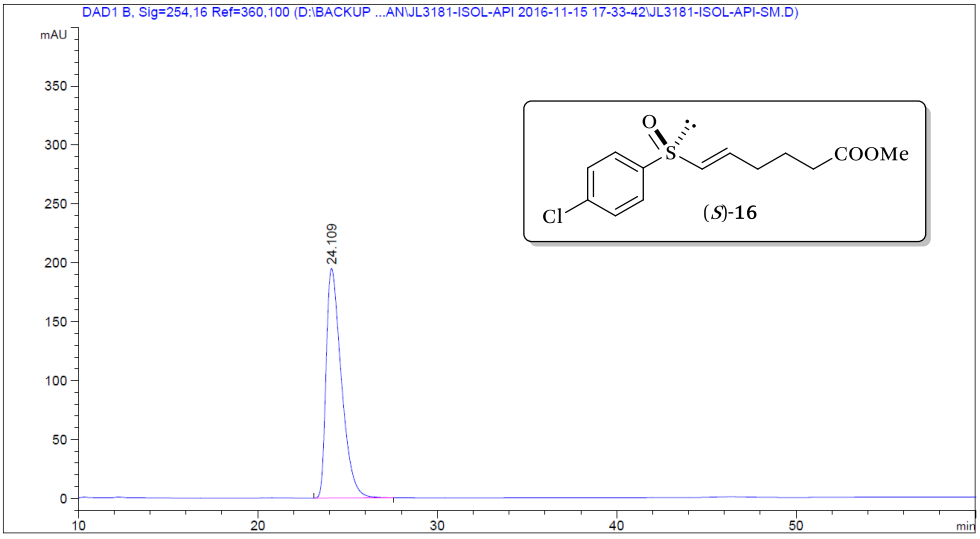

Peak #	RetTime [min]	Type	Width [min]	Area [mAU*s]	Height [mAU]	Area %
1	24.109	BB	0.8966	1.15057e4	194.93532	100.0000

Figure 130. Chiral HPLC trace of (*S*)-**16** (Scheme 9, **conditions A**).

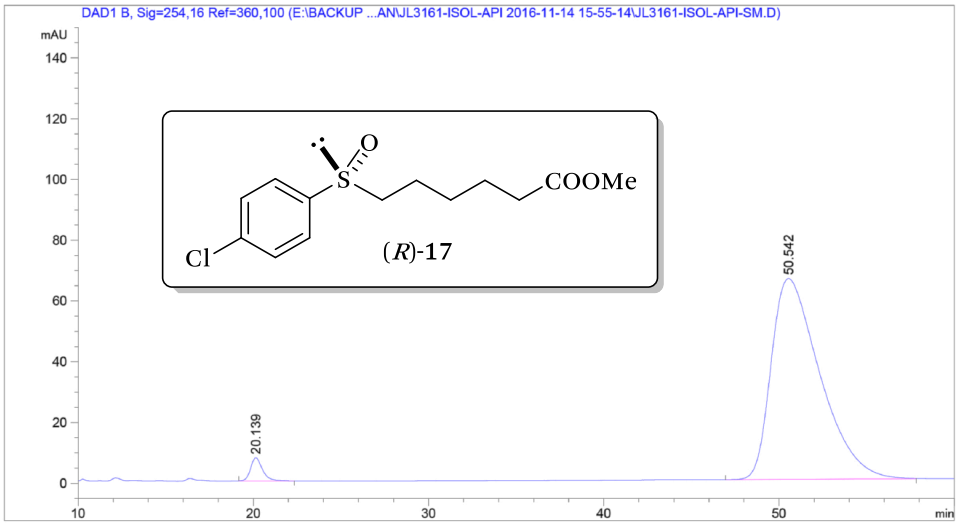

Peak #	RetTime [min]	Type	Width [min]	Area [mAU*s]	Height [mAU]	Area %
1	20.139	BB	0.7169	364.36972	7.63302	2.7718
2	50.542	VB	2.9435	1.27811e4	66.11130	97.2282

Figure 131. Chiral HPLC trace of (*R*)-**17** (Scheme 9, **conditions B**).

UNIVERSITAT ROVIRA I VIRGILI
RHODIUM CATALYSIS IN ENANTIOSELECTIVE HYDROGENATIVE TRANSFORMATIONS: FROM THE DESIGN OF NEW LIGANDS TO REACTIONS OF ATYPICAL SUBSTRATES
Joan Ramon Lao Mulinari

CHAPTER IV

Stereoselective Rh-Catalyzed Hydrogenative Desymmetrization of Achiral Substituted 1,4-Dienes

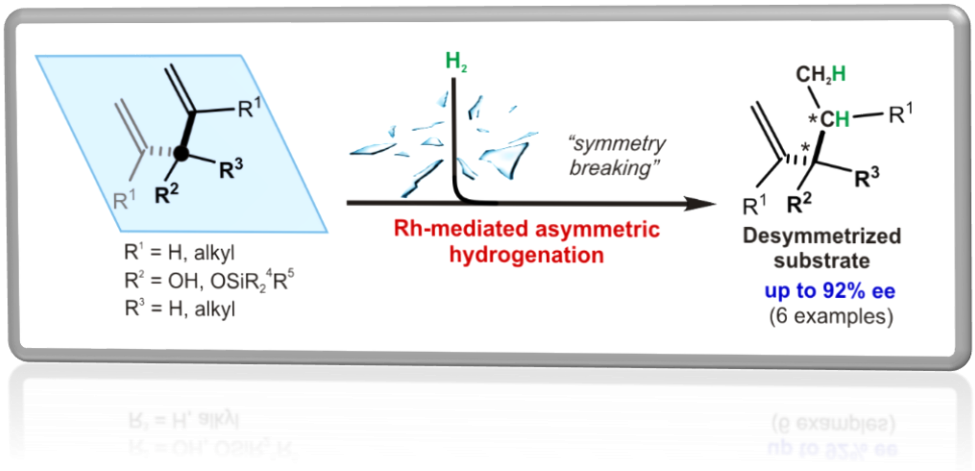

UNIVERSITAT ROVIRA I VIRGILI
RHODIUM CATALYSIS IN ENANTIOSELECTIVE HYDROGENATIVE TRANSFORMATIONS: FROM THE DESIGN OF NEW LIGANDS TO REACTIONS OF ATYPICAL SUBSTRATES
Joan Ramon Lao Mulinari

Stereoselective Rh-Catalyzed Hydrogenative Desymmetrization of Achiral Substituted 1,4-Dienes

4.1. ABSTRACT

Highly efficient catalytic stereoselective hydrogenative desymmetrization reactions mediated by rhodium complexes derived from enantiopure phosphine–phosphite (P–OP) ligands are described. The highest performing ligand, which contains a TADDOL-derived phosphite fragment, presented excellent catalytic properties for the desymmetrization of a set of achiral 1,4-dienes, providing access to the selective formation of a variety of enantioenriched secondary and tertiary alcohols (six examples, up to 92% ee).

4.2. INTRODUCTION

The stereoselective desymmetrization of achiral and *meso* compounds has proved to be a powerful synthetic entry for the preparation of more elaborate optically enriched molecules.[139] This transformation implies breaking the symmetry of the molecule by a synthetic operation, in which two enantiotopic groups of an achiral or *meso* compound are differentiated: the choice of one enantiotopic group (or face) over the other is provided by a chiral reagent or an enantioselective catalyst. Compared to other asymmetric catalytic methodologies, desymmetrization offers several advantages,[140] such as allowing for the concurrent generation of multiple stereogenic centers in a single synthetic step.[141] The potential of this synthetic method has been demonstrated by its application in a wide range of catalytic asymmetric transformations.[139]

(139) For selected reviews on this topic, see: (a) Willis, M. C. *J. Chem. Soc., Perkin Trans. 1* **1999**, 1765-1784. (b) Rovis, T. In *New Frontiers in Asymmetric Catalysis*; Mikami, K., Lautens, M., Eds.; John Wiley & Sons, Inc., 2007; p. 275., ref. 26a, and the references cited therein.
(140) For example, see: (a) *Comprehensive Chirality*; Carreira, E. M., Yamamoto, H., Eds.; Elsevier Science: Oxford, 2012; Vols. *1–9*. (b) Rachwalski, M.; Vermue, N.; Rutjes, F. P. J. T. *Chem. Soc. Rev.* **2013**, *42*, 9268-9282.
(141) For a representative book about the classical synthetic methodologies for preparing of enantioenriched all-carbon quaternary centers and their applicability, see: *Quaternary Stereocenters: Challenges and Solutions for Organic Synthesis*; Christoffers, J., Baro, A., Eds.; Wiley–VCH: Weinheim, 2006.

However, catalytic stereoselective desymmetrizations by reductive methods have been less studied,[139c] and for certain transformations, no satisfactory solution in terms of efficiency or chemo- and stereoselectivity has yet been developed.[142] For instance, the catalytic hydrogenative desymmetrization of achiral 1,4-dienes (Scheme 10) can be considered an example of understudied desymmetrization.

Scheme 10. Stereoselective hydrogenative desymmetrization of a general achiral 1,4-diene

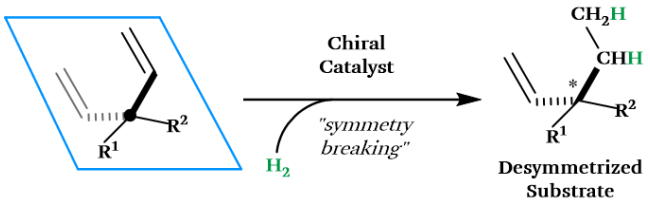

Several challenges need to be addressed when developing efficient stereoselective catalysts for this transformation: (i) selectivity control in terms of obtaining the monohydrogenation product of the achiral 1,4-diene and (ii) the ability of the catalyst to differentiate two enantiotopic vinyl groups. Notable progress in this topic was made by Brown et al., who paved the way for desymmetrizing a set of achiral 1,4-dienes through enantioselective hydrogenation. These authors used enantiopure Rh-bisphosphine complexes as catalysts and demonstrated the feasibility of this hydrogenative desymmetrization, though without complete control of the chemoselectivity of the reaction and with only moderate enantioselectivities (up to 53% ee).[53]

Following our efforts in developing highly efficient catalytic systems derived from phosphine–phosphite (P–OP) ligands for asymmetric hydrogenations[143] and kinetic resolutions,[143] we became interested in developing enantioselective catalysts for the hydrogenative desymmetrization of achiral 1,4-dienes (Table 20 and Table 22), as the resulting products can be considered versatile building blocks for the construction of more complex molecules. Herein, we describe the optimization studies toward the identification of the lead enantioselective catalyst and development of

(142) For selected understudied examples of catalytic reductive desymmetrizations, see ref 139c and references cited therein.
(143) For the efficient application of P–OP ligands in Rh- and Ir-mediated asymmetric hydrogenations, see: refs. 43, 44, 80 and 110.

optimal reaction conditions, together with their application in the desymmetrization of a set of structurally diverse achiral 1,4-dienes.

4.3. RESULTS AND DISCUSSION

Compounds **24a–c** were selected for the initial studies, as these substrates had already been hydrogenatively desymmetrized by Brown et al.[53] After some experimentation, efficient desymmetrization conditions involving low temperature (–40 °C), 1 bar of H_2 in CH_2Cl_2, and the Rh-complex derived from ligand **L2** as the catalyst were identified (Table 20).[144]

Table 20. Preliminary studies of the desymmetrization of substrates 24a–c[a]

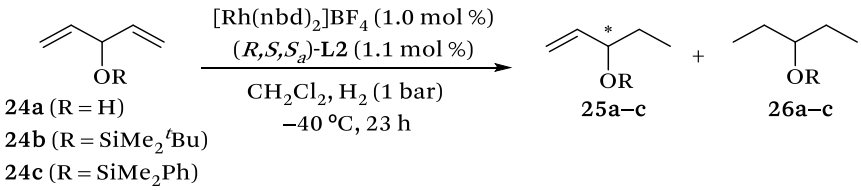

entry	substrate	conv., %[b]	25:26[b]	ee of 25, %;[c] (*S*)[d]
1	**24a**	>99	>99:1	46
2	**24b**	>99	>99:1	62
3	**24c**	>99	>99:1	66

[a][Substrate] = 0.1 M. [b]Determined by ^{1}H NMR. [c]Determined by chiral HPLC analysis after derivatization into the corresponding benzoyl derivatives **27**.[145] [d]The absolute configuration of **25a** was established by comparison with reported optical rotation values for **27a**. The absolute configuration of **25b** and **25c** was tentatively assigned by analogy with the stereochemical outcome of the reaction leading to **25a**.

As summarized in Table 20, the rhodium complex derived from ligand **L2** afforded products **25a–c** with full conversion and perfect chemoselectivity (**25:26** ratio >99:1) in the three substrates assessed (entries 1–3, Table 20). Moreover, products **25a–c** were obtained with moderate ee values (from 46 to 66% of ee; entries 1–3, Table 20). The best result in this screening was achieved for substrate **24c**, where the desymmetrized product **25c** was

(144) Ligand **L2** was selected for the initial studies due to its high catalytic performance in Rh-mediated asymmetric hydrogenations; see refs. 42b,d.
(145) Determination of the enantiomeric excess of products **25** by chiral GC or HPLC analysis proved to be difficult. For this reason, products **25** were transformed into their benzoate esters **27** to facilitate the analysis (see the Experimental Section for details).

selectively obtained with complete conversion and with 66% ee (entry 3 in Table 20). Further studies were aimed at improving the enantioselectivity of the desymmetrization of **24c** by screening a library of structurally diverse P–OP ligands (Figure 132). The assayed conditions and results are listed in Table 21.

In general, and regardless of the nature of the set of P–OP ligands tested in these screening studies (**L1**–**L8** and **L11**–**L16**; see (Figure 132), their derived Rh-catalysts efficiently mediated the desymmetrization of **24c** with excellent values of activity (from 74 to 99% of conversion), perfect chemoselectivity (**25c**:**26c** ratios >99:1), and variable enantioselectivities, which strongly depended on the type of ligand used (see entries 1–14; see Table 21).

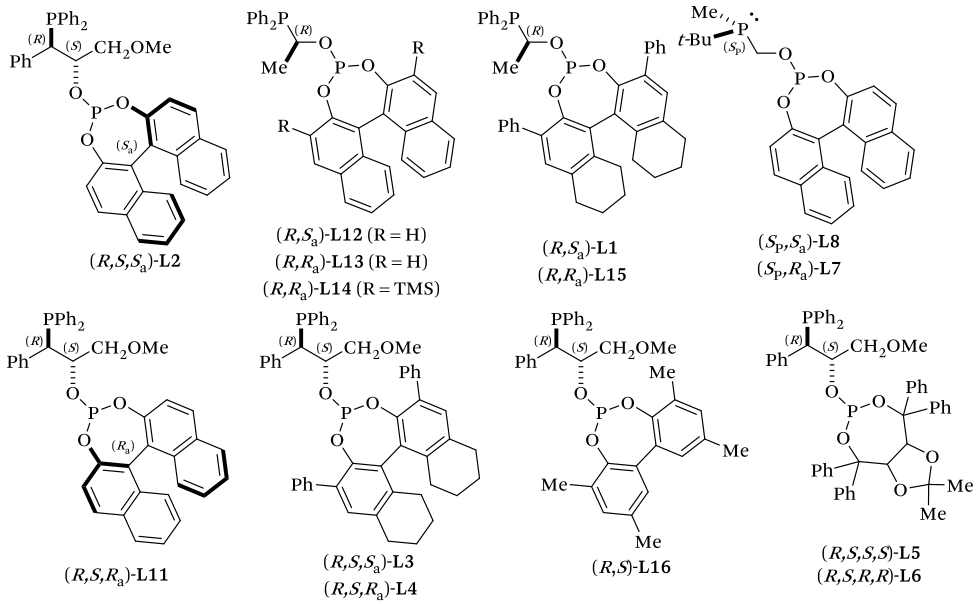

Figure 132. Library of P–OP ligands[146] screened in the hydrogenative desymmetrization of substrate **24c**.

(146) The P–OP ligands presented in Figure 132 can be categorized in two principal groups: (i) geminal ligands **L1**, **L7**, **L8** and **L12–L15** (phosphine and phosphite groups bound to the same carbon) incorporating a stereogenic axis and further stereogenic carbon or phosphorus centers (the Rh-complexes derived from these ligands present strained asymmetric environments around the metal center; P–Rh–PO angle of ca. 80°; see refs. 38b and 143a); (ii) vicinal ligands **L2–L6** and **L11** (phosphine and phosphite groups bound to vicinal carbons) containing two consecutive stereogenic C-atoms (these ligands also incorporate enantiopure BINOL- or TADDOL-derived phosphites).

In a first series of experiments, geminal P–OP ligands **L1**, **L7**, **L8** and **L12–L15** (Figure 132) were tested. These narrow bite angle ligands[146] proved to be effective in the desymmetrization of **24c** in terms of activity (conversion >99%) and chemoselectivity (**24c**:**25c** ratio >99:1), but not in terms of enantioselectivity (from null to 34% ee, entries 1–7, see Table 21).

Table 21. Ligand screening for substrate 24c[a]

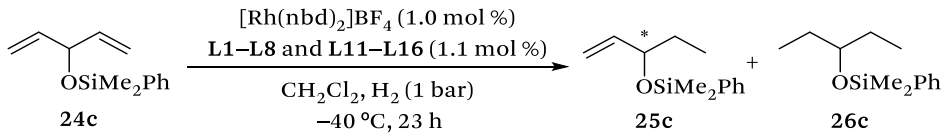

entry	ligand	25c:26c[b]	ee of 25c, %;[c] *(config.)*[d]
1	**L12**	>99:1	*rac*
2	**L13**	>99:1	*rac*
3	**L14**	>99:1	17 (*R*)
4	**L1**	>99:1	16 (*S*)
5	**L15**	>99:1	27 (*R*)
6	**L8**	>99:1	33 (*S*)
7	**L7**	>99:1	34 (*S*)
8[e]	**L11**	>99:1	18 (*S*)
9[f]	**L2**	>99:1	66 (*S*)
10	**L3**	>99:1	36 (*S*)
11	**L4**	>99:1	33 (*R*)
12	**L16**	>99:1	49 (*S*)
13	**L5**	>99:1	80 (*S*)
14	**L6**	>99:1	77 (*S*)

[a,b,c,d]See footnotes *a*, *b*, *c* and *d* in Table 20. Full conversions were achieved, unless otherwise stated. [e]74% of conversion was obtained. [f]This result has been already shown in Table 20.

Vicinal P–OP ligands[146] **L2–L6**, **L11** and **L16** were subsequently studied (Figure 132). The phosphite group in the ligand played a crucial role in the enantioselectivity of the reaction. As regards P–OP ligands with [1,1′-biaryl]-2,2′-diol-derived phosphite groups (i.e., **L2**, **L3**, **L11**, **L4** and **L16**), as already discussed, ligand **L2** containing a (S_a)-BINOL-derived phosphite fragment mediated the desymmetrization of **24c** with moderately high ee (66% ee, entry 3 in Table 20). An inversion of the configuration of the phosphite fragment (ligand **L11** with a (R_a)-BINOL group) was detrimental both for the catalytic activity and enantioselectivity (74% of conversion and 18% ee; entry 8

in Table 21). Ligands bearing substituents at the 3 and 3′ positions of the [1,1′-biaryl]-2,2′-diol unit (**L3** and **L4**; see Figure 132) were also assessed in the desymmetrization of **24c**. Although complete conversions and chemoselectivities were observed with ligands **L3** and **L4** (entries 10 and 11; Table 21), no improvement on enantioselectivity was achieved with this modification in the ligand backbone (up to 36% ee; entries 10 and 11, Table 21). Ligand **L16**, which incorporates the 3,3′,5,5′-tetramethyl-[1,1′-biphenyl]-2,2′-diol-derived phosphite group, was also assessed in this transformation in order to study whether a conformationally adaptive biaryl group could be beneficial for the stereoselectivity of the reaction. As with the other ligands studied, this new ligand mediated the desymmetrization of **24c** with perfect conversion and chemoselectivity but moderated enantioselectivity (49% ee; entry 12 in Table 21). In order to broaden the structural diversity of the catalyst, ligands containing the TADDOL-derived phosphite fragment were included in this study (**L5** and **L6**; see Figure 132).[147,148] The use of these ligands in the desymmetrization of **24c** resulted in a considerable improvement in the enantioselectivities of **25c** (ranging from 77 to 80% ee; entries 13 and 14, Table 21) compared to the other ligands assessed in this study (Table 21). Interestingly, the sense of stereoinduction in the desymmetrization of **24c** mediated by **L5** and **L6** is mainly dictated by the stereocenters of the ligand backbone, as the (*S*,*S*)- and (*R*,*R*)-TADDOL-containing ligands (**L5** and **L6**, respectively) led to product **25c** having the same absolute configuration.

With an optimal catalyst for desymmetrizing **24c** in hand, the desymmetrization of **24a** and **24b** with the optimal TADDOL containing ligand **L5** was then studied. The substrate scope of the reaction was also expanded to structurally diverse 1,4-dienes **24d–f** using the optimal ligand **L5**. The optimized reaction conditions and the best results obtained in this study are listed in Table 22. Substrate **24a** and its *O*-silylated analogue **24b** were

(147) For selected examples on the efficient application of P–OP ligands bearing the TADDOL-derived phosphite in asymmetric catalysis, see: (a) Falk, A.; Fiebig, L.; Neudoerfl, J.-M.; Adler, A.; Schmalz, H.-G. *Adv. Synth. Catal.* **2011**, *353*, 3357-3362. (b) Naeemi, Q.; Dindaroglu, M.; Kranz, D. P.; Velder, J.; Schmalz, H.-G. *Eur. J. Org. Chem.* **2012**, 1179-1185. (c) Dindaroglu, M.; Akyol, S.; Simsir, H.; Neudorfl, J.-M.; Burke, A.; Schmalz, H.-G. *Tetrahedron: Asymmetry* **2013**, *24*, 657-662. (d) Falk, A.; Goederz, A.-L.; Schmalz, H.-G. *Angew. Chem., Int. Ed.* **2013**, *52*, 1576-1580. (e) Falk, A.; Cavalieri, A.; Nichol, G. S.; Vogt, D.; Schmalz, H.-G. *Adv. Synth. Catal.* **2015**, *357*, 3317-3320.
(148) For the preparation of ligands **L5** and **L6**, see refs. 46 and 43d.

efficiently desymmetrized by the Rh-catalyst derived from **L5** with perfect chemoselectivities (**25:26** ratio >99:1) and with high enantioselectivities (84 and 87% ee; entries 1 and 2 in Table 22).

Table 22. Substrate scope for the desymmetrization of substrates 24a–f[a]

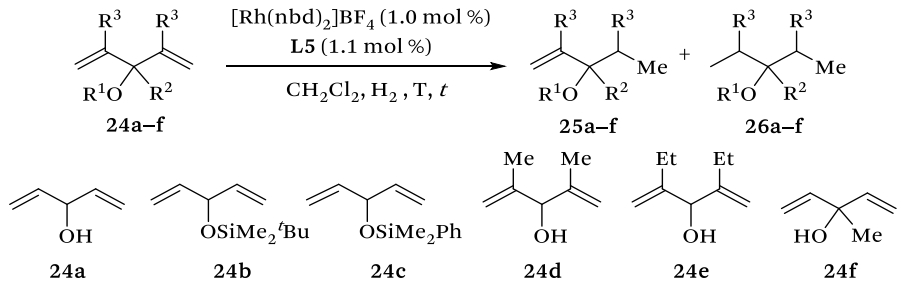

entry	substrate	P, bar	T, °C	*t*	25:26[b]	ee of 25, %;[c] (*config.*)[d]
1	**24a**	1	–40	23 h	>99:1	84 (*S*)
2[e]	**24b**	1	–40	23 h	>99:1	87 (*S*)
3[f]	**24c**	1	–40	23 h	>99:1	80 (*S*)
4	**24d**	5	–20	5 d	>98:2	59 (*S*)
5	**24e**	5	–20	5 d	>92:8[g]	70 (3*R*,4*S*)
6	**24f**	1	–40	23 h	>99:1	92 (*S*)

[a,b,c]See footnotes *a*, *b*, *c* in Table 20. Full conversion were achieved, unless otherwise stated. [d]The absolute configuration of products **25d–f** was tentatively assigned by analogy with the stereochemical outcome of the reaction leading to **25a**. [e]64% of conversion was obtained. [f]This result has been shown in Table 21. [g]dr of *syn*-**25e** >99:1, as determined by ^{1}H NMR.[149]

Switching from a hydroxyl group (in **24a**) to bulkier silyl ether groups (in **24b** and **24c**) was well tolerated by the catalyst and did not greatly affect the outcome of the reaction in terms of chemo- and enantioselectivity. Substrates **24d** and **24e** were studied in order to assess the influence of substituents at the 2 and 4 positions of the 1,4-diene. The presence of these substituents made necessary the use of higher H_2 pressure (5 bar instead of 1 bar of H_2), higher temperatures (–20 °C instead of –40 °C), and extended reaction times (5 days instead of 23 h). Enantioselectivities of the desymmetrized products **25d** and **25e** were lower (59 and 70% ee, respectively; entries 4 and 5, Table 22) than those observed for the unsubstituted products **24a–c** (compare entries 4 and 5 with entries 1–3 and 6; Table 22).

Interestingly, a slight increase in the bulkiness of the substituents at the 2 and 4 positions (from methyl in **24d** to ethyl in **24e**) translated into an increase in the enantioselectivity of up to 11% (from 59 to 70% of ee; compare entries 4 and 5, Table 22). Furthermore, the desymmetrization of **24e** led exclusively to the formation of the *syn*-**25e** diastereoisomer (dr or *syn*:*anti* ratio >99:1; entry 5 in Table 22).[149,150]

Derivatization of the reaction product *syn*-**25e** into the 1-naphthylurethane derivative **28** (Scheme 11) was efficiently performed, and the relative stereochemistry of product *syn*-**25e** was unequivocally established from the crystalline derivative **28** by single-crystal X-ray analysis (Figure 133).[149]

Scheme 11. Derivatization of Product *syn*-25e to 28[149]

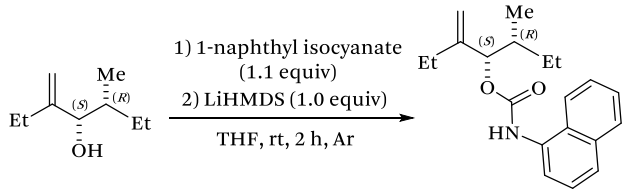

(3*R*,4*S*)-**25e** or *syn*-**25e** (3*R*,4*S*)-**28** or *syn*-**28**

Encouraged by these results, the desymmetrization of substrates leading to enantioenriched dialkyl vinyl tertiary alcohols was pursued. This type of compounds cannot be prepared by asymmetric hydrogenation of carbonyl precursors, and the proposed desymmetrization strategy is an interesting variant to the classical C–C bond forming approach (enantioselective alkylation of a ketone with an organometallic derivative) toward enantioenriched dialkyl vinyl tertiary alcohols.[151]

Substrate **24f** was therefore subjected to desymmetrization conditions (entry 6 in Table 22). The desired product **25f** was obtained with complete

(149) See the Experimental Section for further details.
(150) The *anti*-diastereoisomer was not detected by ^{1}H NMR analysis of the reaction crude.
(151) For reviews regarding this topic, see: (a) Betancort, J. M.; García, C.; Walsh, P. J. *Synlett* **2004**, 749-760. (b) Kanai, M. C–C Bond Formation (1,2-Alkenylation). In *Comprehensive Chirality*; Carreira, E. M., Yamamoto, H., Eds.; Elsevier Science: Oxford, 2012; Vol. *4*, pp 343–354. (c) Madduri, A. V. R.; Harutyunyan, S. R.; Minnaard, A. J. *Drug Discovery Today: Technol.* 2013, 10, e21–e27. (d) Rong, J.; Pellegrini, T.; Harutyunyan, S. R. *Chem. – Eur. J.* **2016**, *22*, 3558-3570. For selected examples, see: (e) García, C.; LaRochelle, L. K.; Walsh, P. J. *J. Am. Chem. Soc.* **2002**, *124*, 10970-10971. (f) Li, H.; Walsh, P. J. *J. Am. Chem. Soc.* **2005**, *127*, 8355-8361. (g) Jeon, S.-J.; Li, H.; García, C.; LaRochelle, L. K.; Walsh, P. J. *J. Org. Chem.* **2005**, *70*, 448-455.

conversion, perfect chemoselectivity (**25f**:**26f** ratio >99:1), and very high enantioselectivity (92% ee; entry 6 in Table 22).

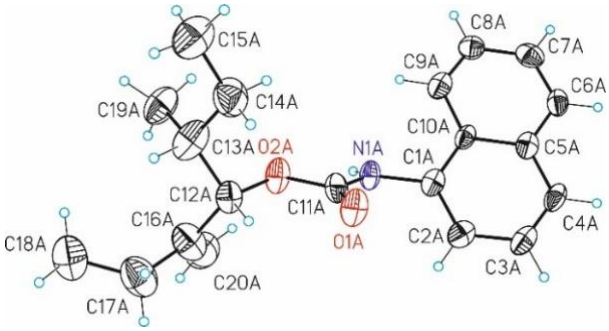

Figure 133. ORTEP Plot (thermal ellipsoids shown at 50% of probability level) of *syn*-**28**.

4.4. CONCLUSIONS

In short, a highly stereoselective catalytic hydrogenative desymmetrization based on Rh-complexes derived from phosphine–phosphite ligands has been developed. The lead enantioselective catalyst, derived from the TADDOL-containing ligand **L5**, has given access to a set of highly enantioenriched secondary and tertiary alcohols (up to 92% ee). The presented results demonstrate the ability of the lead catalyst to differentiate between the two enantiotopic vinyl groups from the substrates. Moreover, the desymmetrization of a substrate containing two pro-stereogenic carbons (**24e**) proceeded with complete diastereoselectivity. Investigations to gain deeper insight in the reaction mechanism are currently underway.

4.5. EXPERIMENTAL SECTION

4.5.1. General considerations

Air- and moisture-sensitive manipulations or reactions were carried out in an inert atmosphere using anhydrous solvents (Solvent Purification System), either in a glove box or with standard Schlenk techniques. Glassware was dried under vacuum and was heated with a hot air gun before use. Silica gel 60 (230–400 mesh) was used for column chromatography. NMR spectra were recorded on 400 MHz or 500 MHz spectrometers in $CDCl_3$, unless otherwise cited. ^{1}H NMR and $^{13}C\{^{1}H\}$ NMR chemical shifts are quoted in ppm relative to the residual solvent peaks. High-resolution mass spectra (HRMS) were recorded using the ESI or EI ionization method in positive mode, unless

otherwise cited. HPLC analyses were performed using a chromatograph equipped with a diode array UV detector (DAD). Melting points were determined by DSC. IR spectra were recorded using Attenuated Total Reflection (ATR) technique. Optical rotations were measured on a polarimeter.

4.5.2. Preparation of substrates 24b–f and *rac*-25d,e

Dienes **24d**,[152] **24e**,[115] **24f**,[153] and silyl-ether derivatives **24b**[53] and **24c**[53] were prepared following an already reported synthetic methodology, which was efficiently reproduced. The spectroscopic data was consistent with the reported data.

General procedure for *rac*-25d and *rac*-25e: Products *rac*-**25d** and *rac*-**25e** were prepared following a method previously reported in the literature,[154] with the following modifications: Under inert conditions, the corresponding aldehyde (5.98 mmol) was added to a stirring solution of the organomagnesium bromide (ca. 7.18 mmol) in anhydrous THF (25 mL) at 0 °C. Stirring was continued for 1 h at 0 °C and the reaction mixture was then allowed to reach rt, and stirred for additional 18 h. The reaction was quenched at 0 °C by the slow addition of ca. 20 mL of a saturated aqueous solution of NH_4Cl. The resulting crude was then extracted with Et_2O (3 x 80 mL), dried over anhydrous $MgSO_4$, filtered and concentrated in vacuo to afford the crude as a yellowish oil. Further purification by silica gel column chromatography yielded the desired product as a colorless liquid.

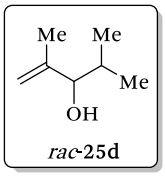

rac-25d

***rac*-2,4-dimethylpenten-1-en-3-ol[154] (*rac*-25d):** The general procedure was efficiently applied starting from isopropylmagnesium bromide and methacrolein to afford the desired product as a colorless liquid (1.77 g, 22% isol. yield). The spectral data were consistent with those reported.[154]

(152) Boccara, N.; Maitte, P. *Bull. Soc. Chim. Fr.* **1972**, 1448-1462.
(153) Shing, T. K. M.; Zhu, X. Y.; Yeung, Y. Y. *Chem. – Eur. J.* **2003**, *9*, 5489-5500.
(154) Bassetti, M.; D'Annibale, A.; Fanfoni, A.; Minissi, F. *Org. Lett.* **2005**, *7*, 1805-1808.

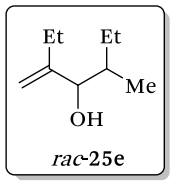

rac-25e

***rac*-3-methyleneheptan-4-ol (*rac*-25e):** The general procedure was efficiently applied, starting from 2-butenyl-magnesium bromide[155] and 2-methylbutyraldehyde to afford the desired product (0.41 g, 40% isol. yield) as a colorless liquid. The isolated product was obtained as a mixture of ***syn*-25e** and ***anti*-25e** diastereoisomers in a *syn:anti* 60:40 ratio. ^{1}H NMR (400 MHz, $CDCl_3$) ***syn*-25e**: δ 5.01–5.00 (m, 1H, C*H*H), 4.90–4.89 (m, 1H, CH*H*), 3.94 (d, *J* = 5.2 Hz, 1H, CH), 2.17–1.89 (m, 2H, CH_2), 1.59–1.51 (m, 1H, CH), 1.47–1.37 (m, 1H, C*H*H), 1.25–1.14 (m, 1H, CH*H*), 1.07 (t, *J* = 7.4 Hz, 3H, CH_3), 0.92 (t, *J* = 7.4 Hz, 3H, CH_3), 0.86 (d, *J* = 6.7 Hz, 3H, CH_3); ***anti*-25e**: δ 4.98–4.97 (m, 1H, C*H*H), 4.89–4.88 (m, 1H, CH*H*), 3.82 (d, *J* = 7.3 Hz, 1H, CH), 2.17–1.89 (m, 2H, CH_2), 1.72–1.63 (m, 1H, C*H*H), 1.59–1.51 (m, 1H, CH), 1.14–1.10 (m, 1H, CH*H*), 1.07 (t, *J* = 7.4 Hz, 3H, CH_3), 0.90 (t, *J* = 7.4 Hz, 3H, CH_3), 0.82 (d, *J* = 6.8 Hz, 3H, CH_3); $^{13}C\{^1H\}$ NMR (100 MHz, $CDCl_3$) ***syn*-25e**: δ 152.7 (C), 108.7 (CH_2), 78.5 (CH), 37.5 (CH), 26.5 (CH_2), 24.5 (CH_2), 13.3 (CH_3), 12.2 (CH_3), 11.8 (CH_3); ***anti*-25e**: δ 152.6 (C), 109.7 (CH_2), 80.6 (CH), 37.7 (CH), 24.2 (CH_2), 23.6 (CH_2), 15.7 (CH_3), 12.1 (CH_3), 11.3 (CH_3); HRMS (EI^+) *m/z* calcd for C_9H_{17} $[M–OH]^+$ 125.1330, found 125.1331; IR (neat, cm^{-1}) υ 3392 ($O–H_{st}$), 1646 ($C=C_{st}$).

4.5.3. General procedure for catalytic hydrogenative desymmetrizations

The following procedure was performed inside a nitrogen filled dry box: A solution of the Rh-precursor $[Rh(nbd)_2]BF_4$ (2 μmol), the P–OP ligand (2.2 μmol) and the 1,4-diene (0.2 mmol) in anhydrous and degassed CH_2Cl_2 were placed in a glass vessel. In all cases the molar concentration of a given substrate was adjusted to 0.1 M by adding the required amount of CH_2Cl_2. The reaction mixtures were loaded under N_2 into an autoclave reactor or in a sealed glass vessel equipped with septa. The autoclave was pressurized with N_2 gas (10 bar) without stirring, and the reaction mixtures were placed into a precooled bath (at the required temperature) and were allowed to equilibrate for ca. 20 min. In the case 1 bar experiments, an atmosphere of N_2 was maintained during the temperature equilibration. The autoclave was then slowly depressurized, purged three times with H_2 gas (3 bar) or with a balloon

(155) 2-Butenyl-magnesium bromide was prepared following the procedure reported in ref. 115b.

filled with H_2 (for low pressure experiments) and finally pressurized at the required pressure of H_2 gas. The general work-up was: rapid filtration on a short pad of silica gel, elution with EtOAc (1.5 mL) and solvent removal in vacuo. Conversions, chemo- and diastereo-selectivities were determined by ^{1}H NMR from the reaction crude. The enantiomeric excesses were determined by chiral HPLC after derivatization into the corresponding benzoate derivatives **27**.

4.5.4. General procedure for derivatization of compounds 25 into benzoate ester derivatives 27

Reaction products bearing silyl-ether groups (**25b** and **25c**) were subjected to desilylation prior to the benzoylation step.[53]

Method A: Under inert conditions, Et_3N (3.92 mmol) was slowly added to a stirring solution of the corresponding alkene (3.27 mmol), DMAP (0.16 mmol) and Bz_2O (3.94 mmol) in anhydrous CH_2Cl_2 (20 mL). The resulting solution was stirred for 18 h under the same conditions. After that time, the reaction crude was directly concentrated in vacuo to afford the crude product as a yellowish oil. Further purification by silica gel column chromatography (using a solvent mixture of *n*-hexane:EtOAc or *n*-pentane:MTBE) yielded the desired product as a colorless liquid.

Method B: Under inert conditions, LiHMDS (2.94 mmol) was carefully added to a stirring solution of the corresponding alkene (1.96 mmol) in anhydrous THF (1.6 mL) at rt. The reaction mixture was stirred for 30 min and BzCl (2.94 mmol) was then added, and the resulting solution was stirred for 16 h under the same conditions. After that time, the reaction was quenched by the addition of water (5.0 mL) and extracted with EtOAc (3 x 5 mL), washed with brine (10 mL), dried over anhydrous $MgSO_4$, filtered and concentrated in vacuo. Further purification by silica gel column chromatography (using a solvent mixture of Cy:EtOAc) yielded the desired product.

The racemic and/or enantiopure benzoate ester derivatives **27a**, **27d**, and **27e** were prepared following *Method A*. On the other hand, the racemic and/or enantiopure benzoate ester derivative **27f** was prepared following *Method B*.

4.5.5. Characterization and determination of the enantiomeric excess of reaction products 27

(*S*)-pent-1-en-3-yl benzoate[156] (**27a**; entries 1–3, Table 22): The spectral data were consistent with those reported. [Lit:[156] $[\alpha]^{27}_D$ = +43.8 (*c* 1.5, $CHCl_3$) for 98% ee (*S*)]. Product **27a** (from **24a**; entry 1, Table 3): 84% ee (*S*), $[\alpha]^{27}_D$ = +31.8 (*c* 0.28, $CHCl_3$); product **27a** (from **24b**; entry 2, Table 3): 87% ee (*S*); product **27a** (from **24c**; entry 3, Table 3): 80% ee (*S*). HPLC conditions for the enantiomers:[156] Daicel Chiralcel® (25 cm x 0.46 cm) OB-H, 99.5:0.5 *n*-heptane/2-propanol, 0.5 mL/min, 210 nm. Retention times for the enantiomers: 11.9 min (*S*)-**27a** and 13.3 min (*R*)-**27a**.

(*S*)-2,4-dimethylpent-1-en-3-yl benzoate (**27d**; entry 4, Table 22): 59% ee (*S*), $[\alpha]^{28}_D$ = +18.3 (*c* 0.84, $CHCl_3$). HPLC conditions: Daicel Chiralpak® (25 cm x 0.46 cm) IA, 100% *n*-pentane, 1.0 mL/min, 210 nm. Retention times for the enantiomers: 10.0 min (*R*)-**27d** and 10.8 min (*S*)-**27d**. ^{1}H NMR (400 MHz, $CDCl_3$) δ 8.11–8.08 (m, 2H, CH), 7.60–7.56 (m, 1H, CH), 7.49–7.45 (m, 2H, CH), 5.18 (d, *J* = 7.2 Hz, 1H, CH), 5.03–5.02 (m, 1H, CH), 4.98–4.97 (m, 1H, CH), 2.15–2.07 (m, 1H, CH), 1.80–1.79 (m, 3H, CH_3), 1.00 (dd, *J* = 20.9 Hz, *J* = 6.7 Hz, 6H, CH_3); $^{13}C\{^1H\}$ NMR (100 MHz, $CDCl_3$) δ 165.8 (C=O), 142.2 (C), 132.8 (CH), 130.6 (C), 129.5 (CH), 128.3 (CH), 113.7 (CH_2), 82.8 (CH–OBz), 29.9 (CH), 19.1 (CH_3), 18.5 (CH_3), 17.8 (CH_3); HRMS (ESI^+) *m/z* calcd for $C_{14}H_{18}NaO_2$ $[M+Na]^+$ 241.1199, found 241.1203; IR (neat, cm^{-1}) υ 1719 ($C{=}O_{st}$), 1286 ($C{-}O_{st}$).

(3*R*,4*S*)-3-methyl-5-methyleneheptan-4-yl benzoate (**27e**; entry 5, Table 22): 70% ee (+), $[\alpha]^{27}_D$ = +32.5 (*c* 0.43, $CHCl_3$). HPLC conditions: Daicel Chiralcel® (25 cm x 0.46 cm) OD-H, 100% *n*-pentane, 1.0 mL/min, 210 nm. Retention times for the *syn*-enantiomers: 8.8 min (3*S*,4*R*)-**27e** and 9.4 min (3*R*,4*S*)-**27e**. ^{1}H NMR (400 MHz, $CDCl_3$) δ 8.09–8.06 (m, 2H, CH), 7.58–7.54 (m, 1H, CH), 7.47–7.43 (m, 2H, CH), 5.38 (d, *J* = 5.4 Hz, 1H, CH), 5.02–5.01 (m, 1H, C*H*H), 4.94–4.93 (m, 1H, CH*H*), 2.14–2.07 (m, 2H, CH_2), 1.91–1.77 (m, 1H, CH), 1.51–1.41 (m, 1H, C*H*H), 1.30–1.18 (m, 1H, CH*H*), 1.10 (t, *J* = 7.4 Hz, 3H, CH_3), 0.99 (d, *J* = 6.8 Hz, 3H, CH_3), 0.95 (t, *J* = 7.3 Hz, 3H, CH_3); $^{13}C\{^1H\}$ NMR

(156) Geurts, K.; Fletcher, S. P.; Feringa, B. L. *J. Am. Chem. Soc.* **2006**, *128*, 15572-15573.

(100 MHz, $CDCl_3$) δ 165.79 (C=O), 148.1 (C), 132.82 (CH), 130.69 (C), 129.6 (CH), 128.38 (CH), 110.1 (CH_2), 80.0 (CH), 36.7 (CH), 26.3 (CH_2), 25.0 (CH_2), 14.0 (CH_3), 12.0 (CH_3), 11.7 (CH_3); HRMS (ESI^+) *m*/*z* calcd for $C_{16}H_{22}NaO_2$ $[M+Na]^+$ 269.1512, found 269.1500; IR (neat, cm^{-1}) υ 1718 ($C=O_{st}$), 1649 ($C=C_{st}$).

(*S*)-3-methylpent-1-en-3-yl benzoate (**27f**; entry 6, Table 22): 92% ee (*S*), $[\alpha]^{27}_D$ = +15.8 (*c* 0.24, $CHCl_3$). HPLC conditions: Daicel Chiralcel® (25 cm x 0.46 cm) OD-H, 100% *n*-pentane, 1.0 mL/min, 210 nm. Retention times for the enantiomers: 14.4 min (*R*)-**27f** and 15.5 min (*S*)-**27f**. ^1H NMR (500 MHz, $CDCl_3$) δ 8.04–8.01 (m, 2H, CH), 7.56–7.52 (m, 1H, CH), 7.44–7.41 (m, 2H, CH), 6.08 (dd, *J* = 17.5 Hz, *J* = 11.0 Hz, 1H, CH), 5.26 (dd, *J* = 17.5 Hz, *J* = 0.9 Hz, 1H, C*H*H), 5.19 (dd, *J* = 11.0 Hz, *J* = 0.9 Hz, 1H, CH*H*), 2.05–1.91 (m, 2H, CH_2), 1.67 (s, 3H, CH_3), 0.96 (t, *J* = 14.8 Hz, 3H, CH_3); $^{13}C\{^1H\}$ NMR (125 MHz, $CDCl_3$) δ 165.3 (C=O), 141.7 (CH), 132.6 (CH), 131.7 (C), 129.5 (CH), 128.3 (CH), 113.4 (CH_2), 84.0 (C), 32.4 (CH_2), 23.2 (CH_3), 8.0 (CH_3); HRMS (ESI^+) *m*/*z* calcd for $C_{13}H_{16}NaO_2$ $[M+Na]^+$ 227.1043, found 227.1039; IR (neat, cm^{-1}) υ 1714 ($C=O_{st}$), 1644 ($C=C_{st}$).

4.5.6. Preparation of 1-naphthyl urethane derivative 28

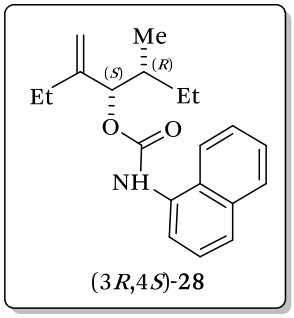

(3*R*,4*S*)-**28**

(3*R*,4*S*)-3-methyl-5-methyleneheptan-4-yl-1-naphthyl urethane (28): Under inert conditions, LiHMDS (117 μL, 1 M, 0.117 mmol) was carefully added to a stirring solution of the enantioenriched (70% ee; entry 5, Table 3) *syn*-**25e** (16.6 mg, 0.117 mmol) and 1-naphthyl isocyanate (18.8 μL, 98%, 0.129 mmol) in THF (1.5 mL), at rt. Stirring was continued for 2 h and the resulting suspension was evaporated under reduced pressure to yield a yellowish oil. Further purification by silica gel column chromatography (using a solvent mixture of *n*-pentane:MTBE) afforded the desired product as a white solid (22.6 mg, 62% isol. yield), mp = 56–57 °C; ^1H NMR (300 MHz, $CDCl_3$) δ 7.92–7.87 (m, 3H, CH), 7.69–7.66 (m, 1H, CH), 7.58–7.45 (m, 3H, CH), 6.97 (bs, 1H, NH), 5.18 (d, *J* = 5.8 Hz, 1H, CH), 5.06 (s, 1H, C*H*H), 4.98 (s, 1H, CH*H*), 2.11–2.04 (m, 2H, CH_2), 1.76–1.72 (m, 1H, C*H*H), 1.50–1.43 (m, 1H, CH*H*), 1.28–1.09 (m, 5H, CH_2

and CH_3), 0.99–0.74 (m, 6H, CH_3); $^{13}C\{^1H\}$ NMR (75 MHz, $CDCl_3$) δ 154.1 (C=O), 148.4 (C), 134.0 (C), 132.6 (C), 128.8 (CH), 126.1 (CH), 125.9 (CH), 125.8 (CH), 124.9 (C), 120.4 (C),110.2 (CH_2), 81.0 (CH), 36.6 (CH), 26.1 (CH_2), 24.9 (CH_2), 14.0 (CH_3), 11.9 (CH_3), 11.6 (CH_3); HRMS (ESI^+) *m/z* calcd for $C_{20}H_{25}NNaO_2$ $[M+Na]^+$ 334.1777, found 334.1771; $[\alpha]_{25}^{D}$ = +15.8 (*c* 0.03, $CHCl_3$); IR (neat, cm^{-1}) υ 3283 (N–H_{st}), 3053 (C=–H_{st}), 1693 (C=O_{st}), 1529 (C_{Ar}–$C_{Ar,st}$).

4.5.7. Single crystal X-ray structure determination of product 28

The ORTEP Plot of product **28** is presented in Figure 133.

Crystal preparation: Single crystals of compound **28** were grown by melting the product (50–60 °C) followed by seeding when cooled at 45 °C. The crystals were allowed to grow under these conditions for 18 h. The resulted crystals were immersed in perfluoropolyether oil for manipulation.

Data collection: Crystal structure determination for **28** was carried out using a Apex DUO diffractometer equipped with a Kappa 4-axis goniometer, an APEX II 4K CCD area detector, a Microfocus Source E025 IuS using MoKα radiation, Quazar MX multilayer Optics as monochromator and an Oxford Cryosystems low temperature device Cryostream 700 plus (T = –173 °C). Full-sphere data collection was used with *ω* and *φ* scans. *Programs used:* Data collection APEX-2,[157] data reduction Bruker Saint[158] V/.60A and absorption correction SADABS.[159]

Structure Solution and Refinement: Crystal structure solution was achieved using the computer program SHELXTL.[160] Visualization was performed with

(157) Data collection with APEX II version v2013.4-1. Bruker (2007). Bruker AXS Inc., Madison, Wisconsin, USA.
(158) Data reduction with Bruker SAINT version V8.30c. Bruker (2007). Bruker AXS Inc., Madison, Wisconsin, USA.
(159) SADABS: V2012/1 Bruker (2001). Bruker AXS Inc., Madison, Wisconsin, USA. Blessing, R. H. Acta Crystallogr., Sect. A: Found. Crystallogr. 1995, A51, 33-38.
(160) SHELXT: Sheldrick, G. M. Acta Crystallogr., Sect. A: Found. Crystallogr. 2015, 71, 3-8.

the program SHELXle.[161] Missing atoms were subsequently located from difference Fourier synthesis and added to the atom list. Least-squares refinement on F^2 using all measured intensities was carried out using the program SHELXL 2015.[160,162] All non-hydrogen atoms were refined including anisotropic displacement parameters.

Comments to the structure of 28: The asymmetric unit contains two independent molecules of the same compound with the same relative stereochemistry. Due to the low quality of the crystals obtained it was not possible to determine the absolute configuration of this molecule using anomalous dispersion effects.

Table 23. Crystal data and structural parameters for 28

compound	**28**		
Formula	$C_{20}H_{25}N_1O_2$	**Z**	4
Formula weight	311.41	**ρ (g/cm^3)**	1.189
Crystal size (mm^3)	0.25 x 0.06 x 0.02	**μ (mm^{-1})**	0.076
Crystal colour	colourless	**θ_{max} (°)**	26.15
Temp (K)	100	**Reflec. measured**	21143
Crystal system	Monoclinic	**Unique reflections**	4734 [R_{int} = 0.0796]
Space group	$P2_1$	**Absorpt. correct.**	SADABS
A (Å)	9.3889(11)	**Trans. min/max**	0.998/0.665
B (Å)	11.6277(14)	**Parameters/Restrains**	426/3
C (Å)	16.0269(18)	**R1/wR2 [I>2σ(I)]**	0.0903/0.2405
α (deg)	90	**R1/wR2 [all data]**	0.1277/0.2703
β (deg)	96.069(4)	**Goodness-of-fit (F^2)**	1.035
γ (deg)	90	**Peak/hole (e/Å^{-3})**	0.552/−0.320
V (Å^3)	1739.9(4)	**Absolute Structure Determination**	Not possible

(161) SHELXle: Huebschle, C. B.; Sheldrick, G. M.; Dittrich, B. J. Appl. Crystallogr. 2011, 44, 1281-1284.
(162) SHELXL: Sheldrick, G. M. Acta Crystallogr., Sect. C: Struct. Chem. 2015, 71, 3-8.

Table 24. Bond lengths [Å] and angles [°] for 28

Bond lengths [Å]			
N1A-C11A	1.355(9)	N1B-C11B	1.356(9)
N1A-C1A	1.430(8)	N1B-C1B	1.421(8)
O1A-C11A	1.200(8)	O1B-C11B	1.206(8)
O2A-C11A	1.355(8)	O2B-C11B	1.359(8)
O2A-C12A	1.434(8)	O2B-C12B	1.468(8)
C1A-C2A	1.375(9)	C1B-C2B	1.388(10)
C1A-C10A	1.406(10)	C1B-C10B	1.398(10)
C2A-C3A	1.397(10)	C2B-C3B	1.411(10)
C3A-C4A	1.343(10)	C3B-C4B	1.334(12)
C4A-C5A	1.412(10)	C4B-C5B	1.436(11)
C5A-C6A	1.405(10)	C5B-C6B	1.391(11)
C5A-C10A	1.441(9)	C5B-C10B	1.438(9)
C6A-C7A	1.381(10)	C6B-C7B	1.363(12)
C7A-C8A	1.407(10)	C7B-C8B	1.411(11)
C8A-C9A	1.339(11)	C8B-C9B	1.360(11)
C9A-C10A	1.433(9)	C9B-C10B	1.419(10)
C12A-C16A	1.536(11)	C12B-C16B	1.503(10)
C12A-C13A	1.537(12)	C12B-C13B	1.515(9)
C13A-C14A	1.486(13)	C13B-C19B	1.499(10)
C13A-C19A	1.538(12)	C13B-C14B	1.550(10)
C14A-C15A	1.525(13)	C14B-C15B	1.499(10)
C16A-C20A	1.358(14)	C16B-C20B	1.342(10)
C16A-C17A	1.463(12)	C16B-C17B	1.485(11)
C17A-C18A	1.552(14)	C17B-C18B	1.532(12)
Bond angles [°]			
C11A-N1A-C1A	123.4(5)	C4A-C3A-C2A	121.7(6)
C11A-O2A-C12A	116.8(5)	C3A-C4A-C5A	120.6(6)
C2A-C1A-C10A	121.0(6)	C6A-C5A-C4A	122.4(6)
C2A-C1A-N1A	120.9(6)	C6A-C5A-C10A	118.9(6)
C10A-C1A-N1A	118.2(6)	C4A-C5A-C10A	118.7(6)
C1A-C2A-C3A	119.7(7)	C7A-C6A-C5A	121.2(6)

C6A-C7A-C8A	119.7(7)	C4B-C3B-C2B	121.0(7)
C9A-C8A-C7A	121.0(7)	C3B-C4B-C5B	121.6(7)
C8A-C9A-C10A	121.7(6)	C6B-C5B-C4B	122.8(7)
C1A-C10A-C9A	124.3(6)	C6B-C5B-C10B	119.6(7)
C1A-C10A-C5A	118.2(6)	C4B-C5B-C10B	117.6(7)
C9A-C10A-C5A	117.5(6)	C7B-C6B-C5B	121.6(7)
O1A-C11A-O2A	124.7(6)	C6B-C7B-C8B	119.3(7)
O1A-C11A-N1A	127.4(6)	C9B-C8B-C7B	121.1(7)
O2A-C11A-N1A	107.9(5)	C8B-C9B-C10B	120.9(6)
O2A-C12A-C16A	108.2(6)	C1B-C10B-C9B	123.4(6)
O2A-C12A-C13A	110.5(6)	C1B-C10B-C5B	119.1(6)
C16A-C12A-C13A	112.7(7)	C9B-C10B-C5B	117.5(6)
C14A-C13A-C12A	111.5(7)	O1B-C11B-N1B	126.0(6)
C14A-C13A-C19A	113.7(8)	O1B-C11B-O2B	123.8(6)
C12A-C13A-C19A	110.9(7)	N1B-C11B-O2B	110.1(5)
C13A-C14A-C15A	115.3(8)	O2B-C12B-C16B	107.4(5)
C20A-C16A-C17A	122.6(8)	O2B-C12B-C13B	107.7(5)
C20A-C16A-C12A	121.0(8)	C16B-C12B-C13B	117.6(6)
C17A-C16A-C12A	116.4(7)	C19B-C13B-C12B	113.2(6)
C16A-C17A-C18A	118.0(8)	C19B-C13B-C14B	113.0(6)
C11B-N1B-C1B	122.9(5)	C12B-C13B-C14B	108.6(5)
C11B-O2B-C12B	115.1(5)	C15B-C14B-C13B	115.6(6)
C2B-C1B-C10B	121.0(6)	C20B-C16B-C17B	123.5(7)
C2B-C1B-N1B	119.9(6)	C20B-C16B-C12B	118.8(7)
C10B-C1B-N1B	119.2(6)	C17B-C16B-C12B	117.7(6)
C1B-C2B-C3B	119.7(7)	C16B-C17B-C18B	114.1(7)

Table 25. Torsion angles [°] for 28

Torsion angles [°]			
C11A-N1A-C1A-C2A	45.3(9)	C1A-C2A-C3A-C4A	–0.7(10)
C11A-N1A-C1A-C10A	–134.9(7)	C2A-C3A-C4A-C5A	0.1(10)
C10A-C1A-C2A-C3A	–0.4(9)	C3A-C4A-C5A-C6A	–179.7(6)
N1A-C1A-C2A-C3A	179.3(6)	C3A-C4A-C5A-C10A	1.5(9)

C4A-C5A-C6A-C7A	179.3(6)	C13A-C12A-C16A-C17A	–64.9(10)
C10A-C5A-C6A-C7A	–1.8(9)	C20A-C16A-C17A-C18A	–75.2(14)
C5A-C6A-C7A-C8A	2.5(10)	C12A-C16A-C17A-C18A	108.8(10)
C6A-C7A-C8A-C9A	–2.2(10)	C11B-N1B-C1B-C2B	–44.4(9)
C7A-C8A-C9A-C10A	1.4(10)	C11B-N1B-C1B-C10B	136.1(7)
C2A-C1A-C10A-C9A	179.5(6)	C10B-C1B-C2B-C3B	–0.3(10)
N1A-C1A-C10A-C9A	–0.3(9)	N1B-C1B-C2B-C3B	–179.8(6)
C2A-C1A-C10A-C5A	2.0(9)	C1B-C2B-C3B-C4B	–1.2(11)
N1A-C1A-C10A-C5A	–177.7(5)	C2B-C3B-C4B-C5B	2.7(11)
C8A-C9A-C10A-C1A	–178.2(6)	C3B-C4B-C5B-C6B	176.4(7)
C8A-C9A-C10A-C5A	–0.7(9)	C3B-C4B-C5B-C10B	–2.5(10)
C6A-C5A-C10A-C1A	178.6(6)	C4B-C5B-C6B-C7B	–179.0(7)
C4A-C5A-C10A-C1A	–2.5(8)	C10B-C5B-C6B-C7B	–0.1(10)
C6A-C5A-C10A-C9A	0.9(8)	C5B-C6B-C7B-C8B	–0.9(11)
C4A-C5A-C10A-C9A	179.8(6)	C6B-C7B-C8B-C9B	0.7(11)
C12A-O2A-C11A-O1A	–11.7(10)	C7B-C8B-C9B-C10B	0.7(10)
C12A-O2A-C11A-N1A	169.0(6)	C2B-C1B-C10B-C9B	–178.9(6)
C1A-N1A-C11A-O1A	0.7(12)	N1B-C1B-C10B-C9B	0.5(9)
C1A-N1A-C11A-O2A	180.0(6)	C2B-C1B-C10B-C5B	0.4(9)
C11A-O2A-C12A-C16A	–119.3(7)	N1B-C1B-C10B-C5B	179.9(5)
C11A-O2A-C12A-C13A	116.9(7)	C8B-C9B-C10B-C1B	177.7(6)
O2A-C12A-C13A-C14A	–65.2(8)	C8B-C9B-C10B-C5B	–1.7(9)
C16A-C12A-C13A-C14A	173.6(7)	C6B-C5B-C10B-C1B	–177.9(6)
O2A-C12A-C13A-C19A	62.6(9)	C4B-C5B-C10B-C1B	1.0(9)
C16A-C12A-C13A-C19A	–58.6(9)	C6B-C5B-C10B-C9B	1.4(9)
C12A-C13A-C14A-C15A	–175.3(8)	C4B-C5B-C10B-C9B	–179.7(6)
C19A-C13A-C14A-C15A	58.4(12)	C1B-N1B-C11B-O1B	–6.1(11)
O2A-C12A-C16A-C20A	–3.5(11)	C1B-N1B-C11B-O2B	175.6(6)
C13A-C12A-C16A-C20A	119.0(10)	C12B-O2B-C11B-O1B	0.9(9)
O2A-C12A-C16A-C17A	172.6(7)	C12B-O2B-C11B-N1B	179.3(5)

C11B-O2B-C12B-C16B	–87.5(7)	C12B-C13B-C14B-C15B	–168.5(6)
C11B-O2B-C12B-C13B	145.0(6)	O2B-C12B-C16B-C20B	108.5(7)
O2B-C12B-C13B-C19B	–46.7(7)	C13B-C12B-C16B-C20B	–130.0(7)
C16B-C12B-C13B-C19B	–168.1(6)	O2B-C12B-C16B-C17B	–70.3(7)
O2B-C12B-C13B-C14B	–173.0(5)	C13B-C12B-C16B-C17B	51.2(9)
C16B-C12B-C13B-C14B	65.6(8)	C20B-C16B-C17B-C18B	–8.3(11)
C19B-C13B-C14B-C15B	65.1(8)	C12B-C16B-C17B-C18B	170.5(7)

4.5.8. NMR spectra of desymmetrized products 25

4.5.8.1. Catalytic hydrogenative desymmetrization of substrate 24a

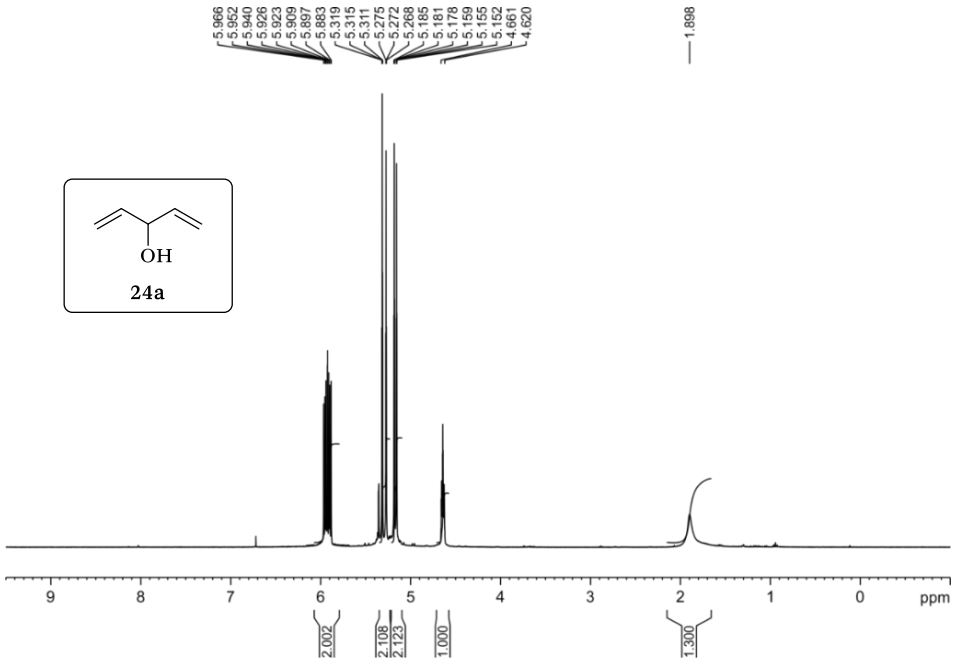

Figure 134. ^{1}H NMR (400 MHz, CD_2Cl_2) of **24a**.

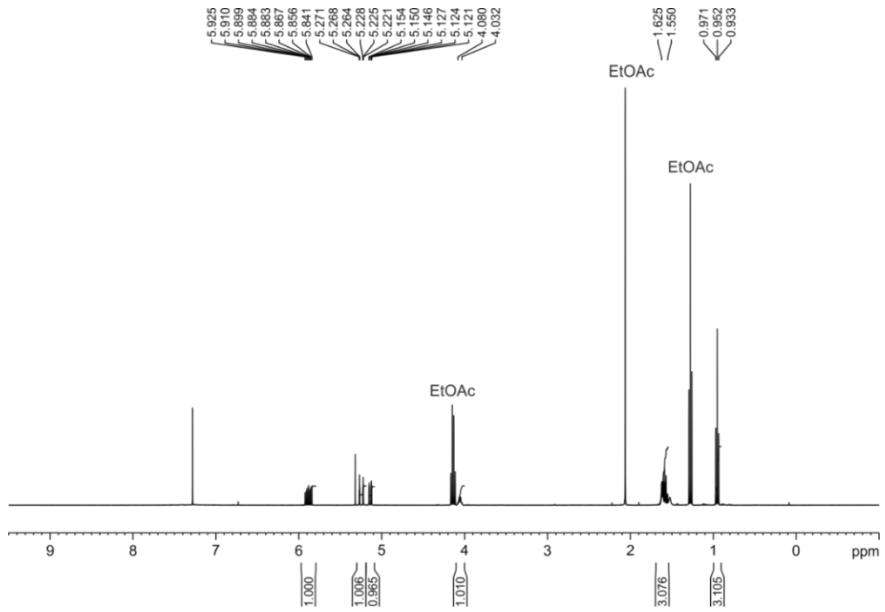

Figure 135. ^{1}H NMR (400 MHz, $CDCl_3$) of the crude mixture for the desymmetrization of **24a** (Table 22, entry 1).

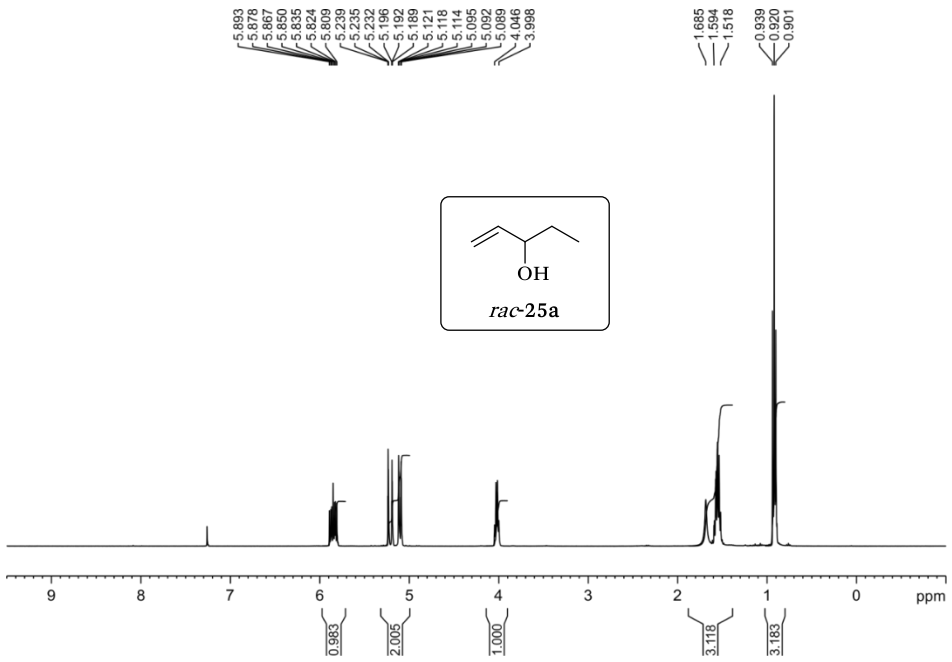

Figure 136. ^{1}H NMR (400 MHz, $CDCl_3$) of *rac*-**25a**.

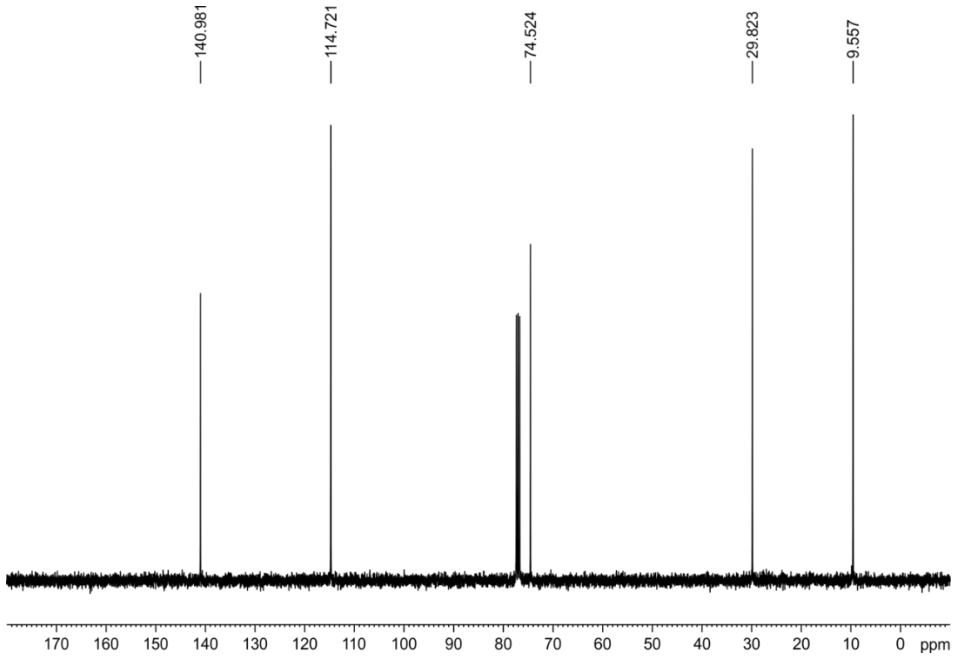

Figure 137. $^{13}C\{^{1}H\}$ NMR (100 MHz, $CDCl_3$) of *rac*-**25a**.

4.5.8.2. Catalytic hydrogenative desymmetrization of substrate 24b

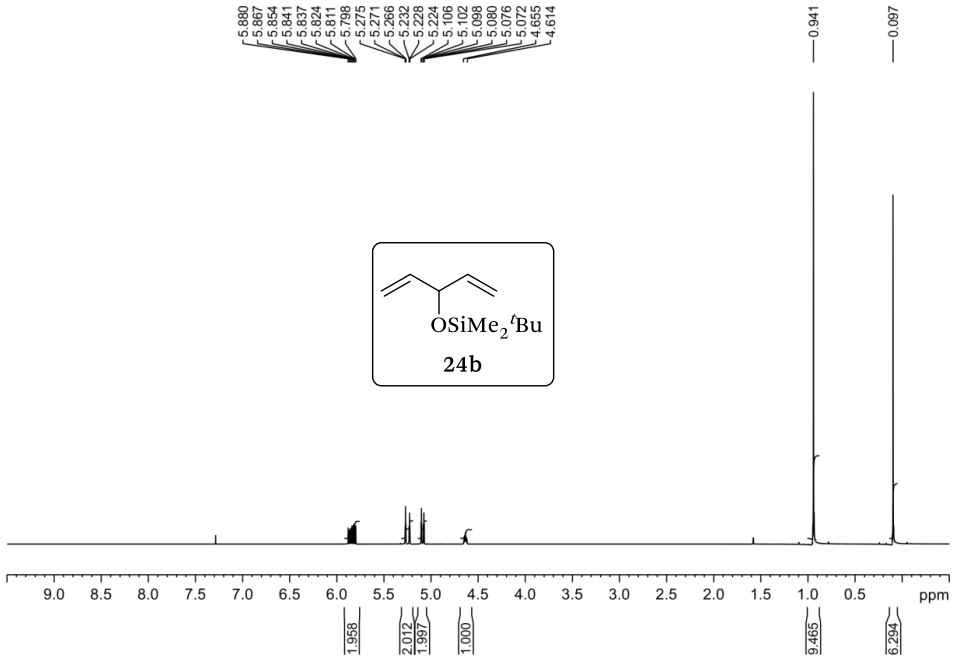

Figure 138. ^{1}H NMR (400 MHz, $CDCl_3$) of **24b**.

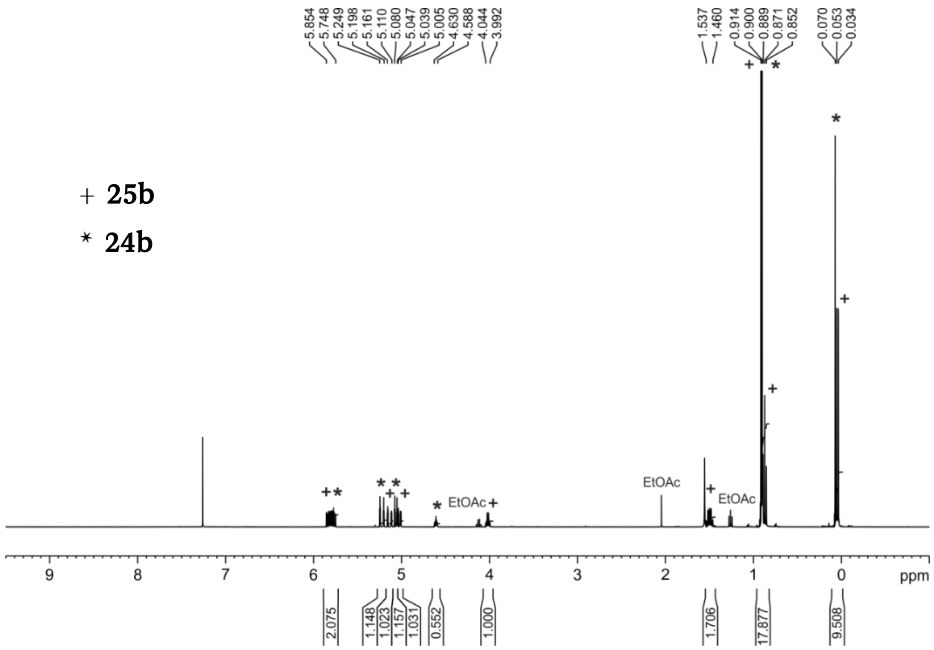

Figure 139. ^{1}H NMR (400 MHz, $CDCl_3$) of the crude mixture for the desymmetrization of **24b** (Table 22, entry 2).

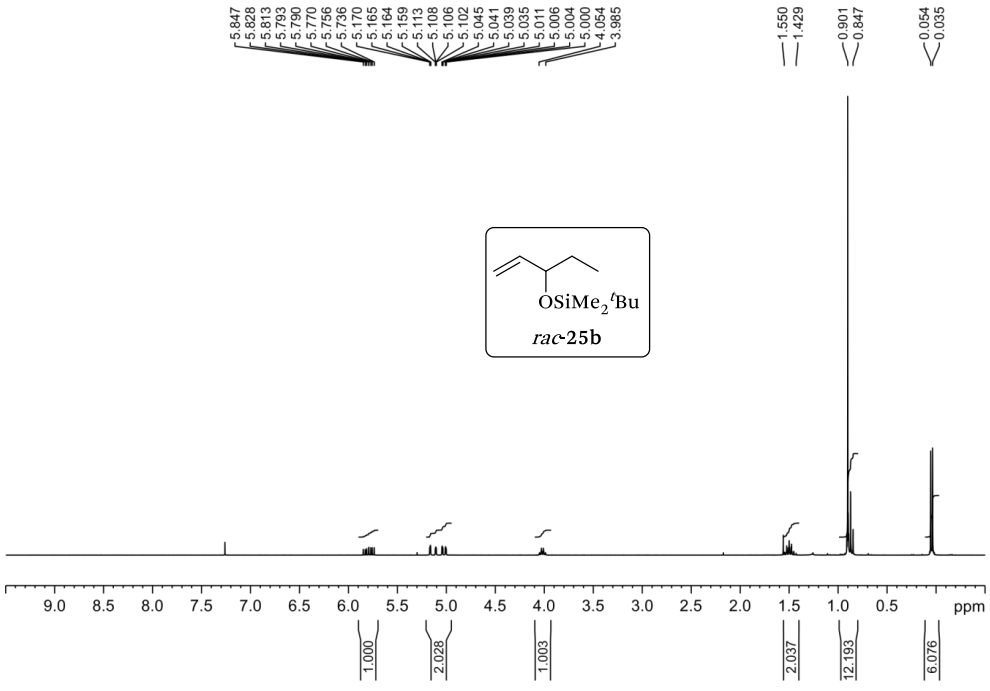

Figure 140. ^{1}H NMR (300 MHz, $CDCl_3$) of *rac*-**25b**.

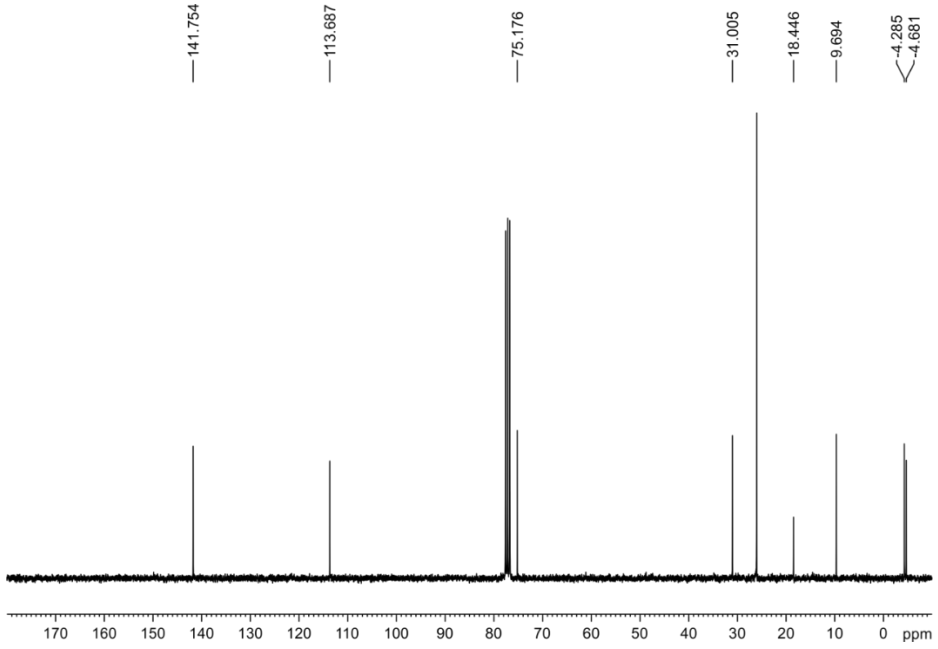

Figure 141. $^{13}C\{^{1}H\}$ NMR (75 MHz, $CDCl_3$) of *rac*-**25b**.

4.5.8.3. Catalytic hydrogenative desymmetrization of substrate 24c

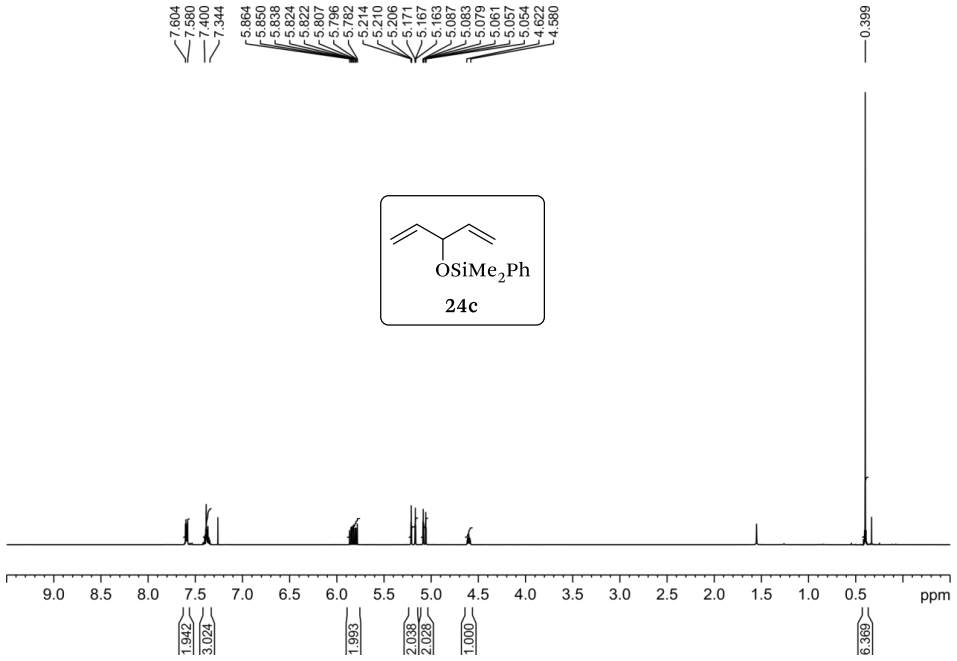

Figure 142. ^{1}H NMR (400 MHz, $CDCl_3$) of **24c**.

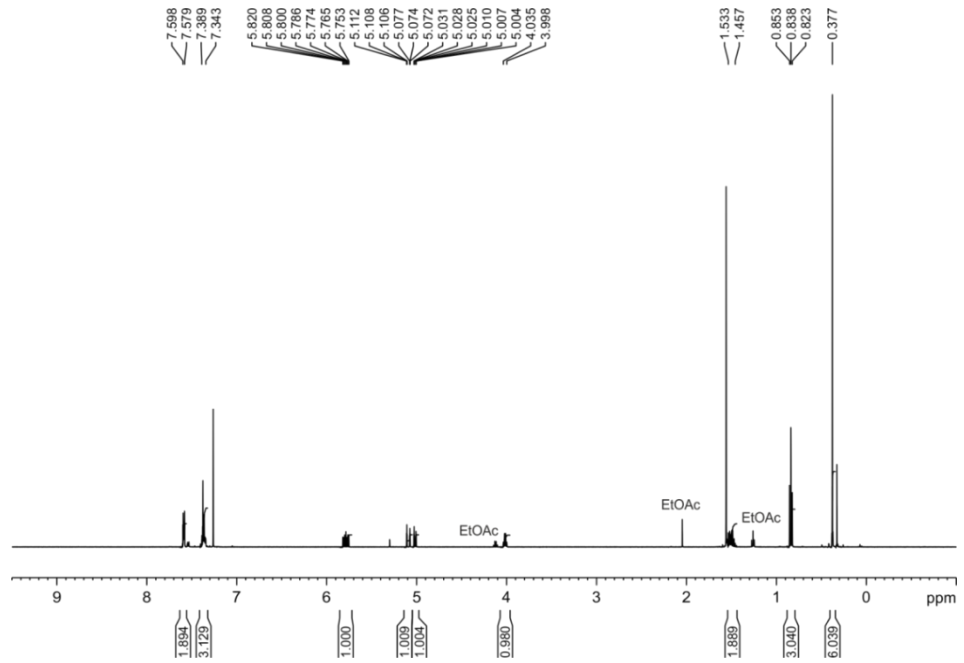

Figure 143. ^{1}H NMR (400 MHz, $CDCl_3$) of the crude mixture for the desymmetrization of **24c** (Table 22, entry 3).

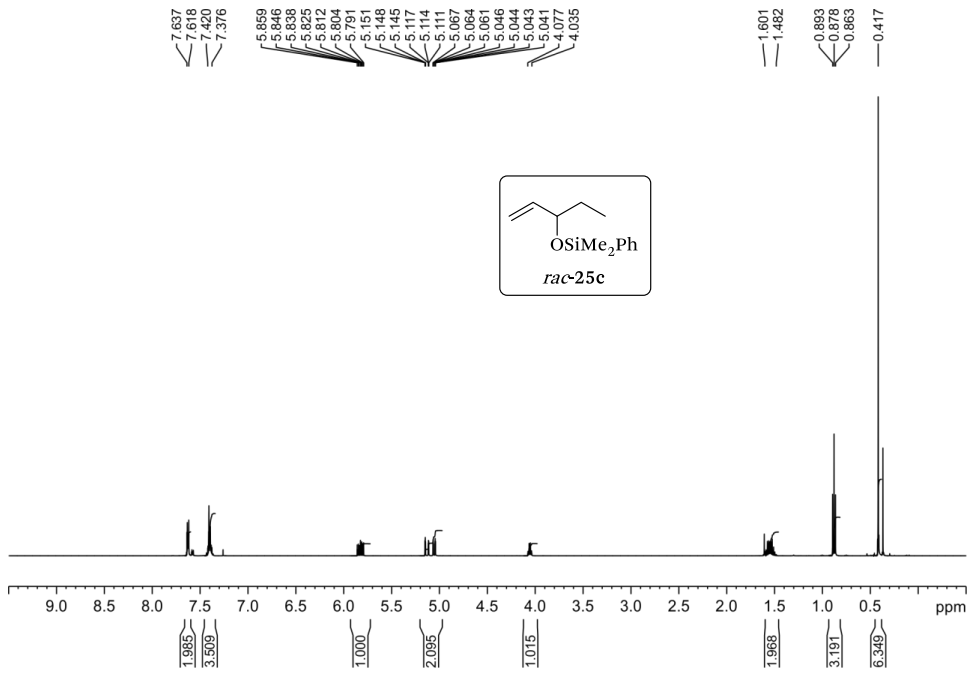

Figure 144. ^{1}H NMR (500 MHz, $CDCl_3$) of *rac*-**25c**.

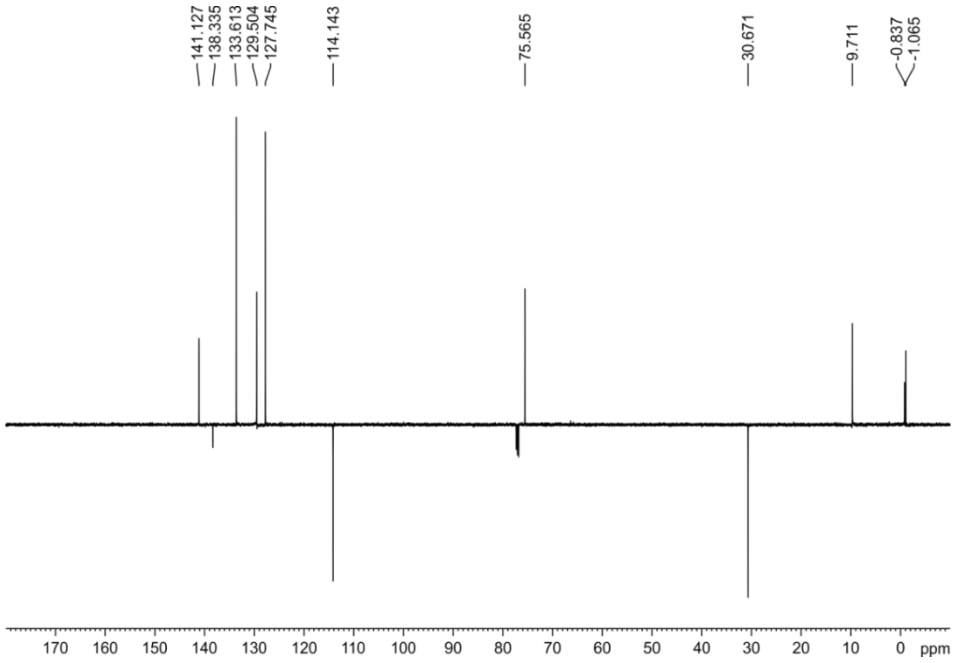

Figure 145. $^{13}C\{^{1}H\}$ NMR as DEPTQ135 (125 MHz, $CDCl_3$) of *rac*-**25c**.

4.5.8.4. Catalytic hydrogenative desymmetrization of substrate 24d

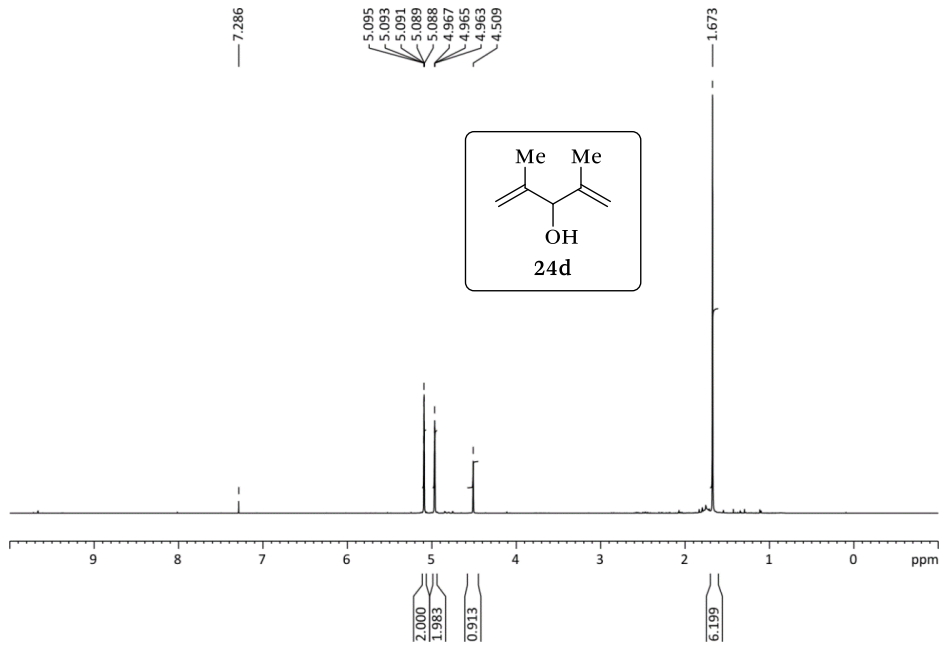

Figure 146. ^{1}H NMR (500 MHz, $CDCl_3$) of **24d**.

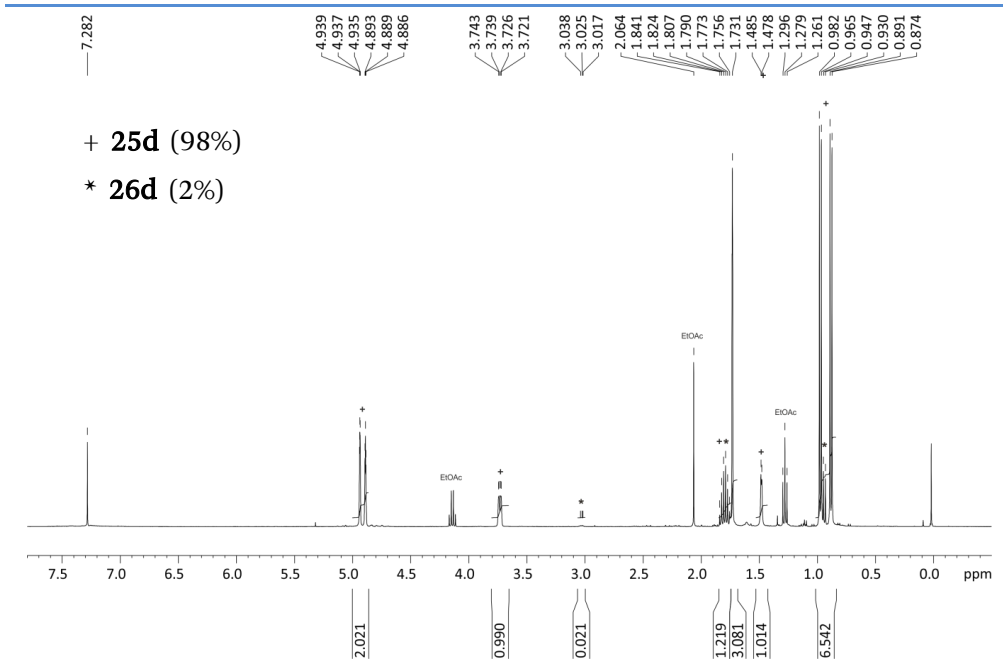

Figure 147. ^{1}H NMR (400 MHz, $CDCl_3$) of the crude mixture for the desymmetrization of **24d** (Table 22, entry 4).

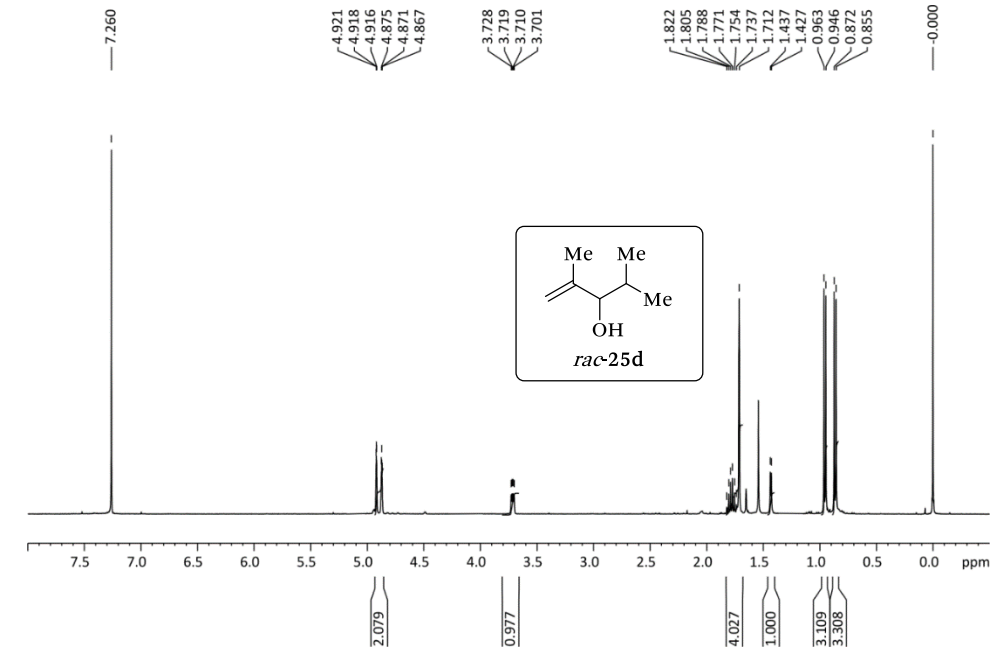

Figure 148. ^{1}H NMR (400 MHz, $CDCl_3$) of *rac*-**25d**.

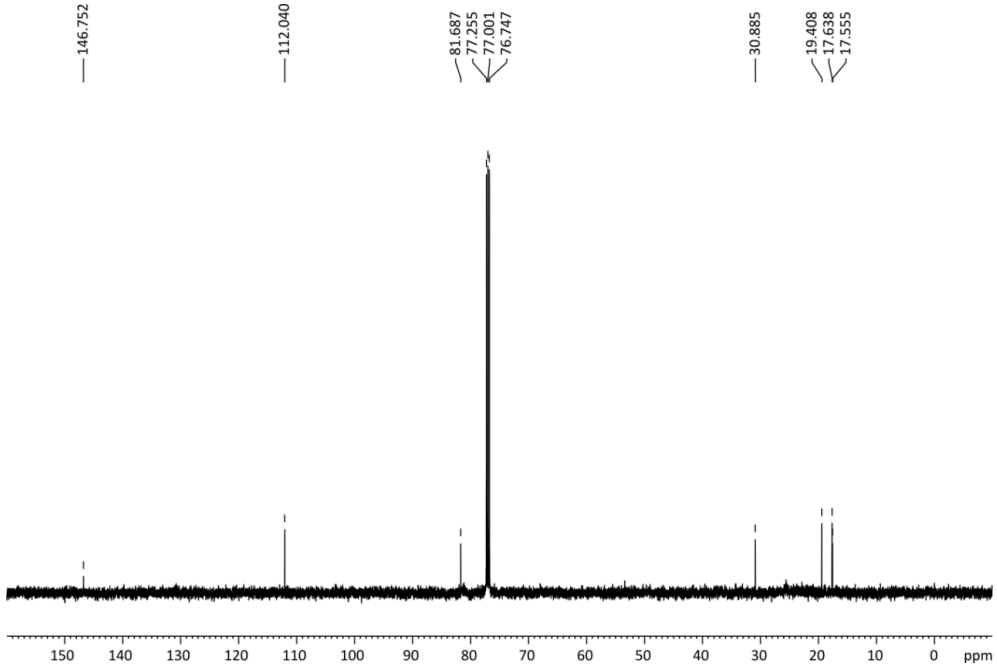

Figure 149. $^{13}C\{^{1}H\}$ NMR (100 MHz, $CDCl_3$) of *rac*-**25d**.

4.5.8.5. Catalytic hydrogenative desymmetrization of substrate 24e

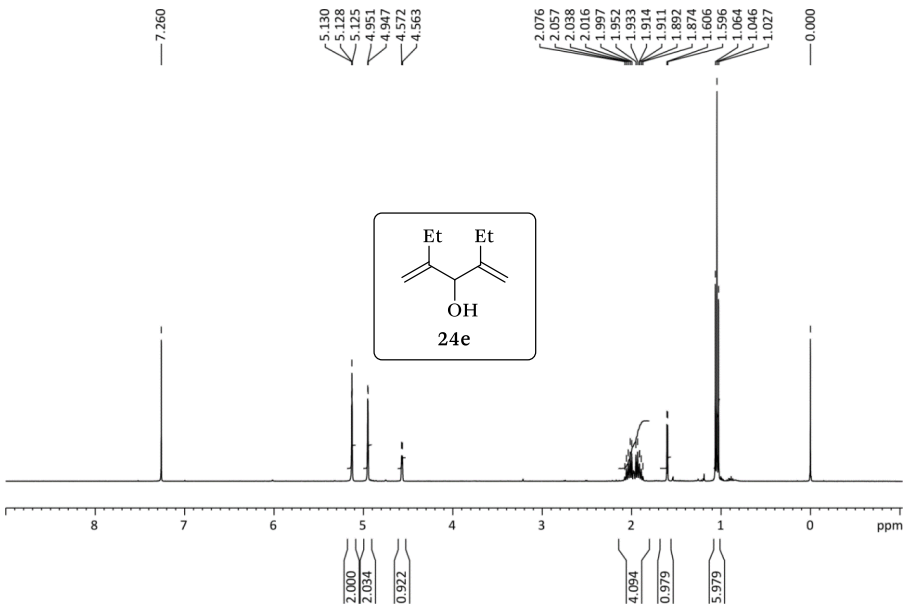

Figure 150. ^{1}H NMR (400 MHz, $CDCl_3$) of **24e**.

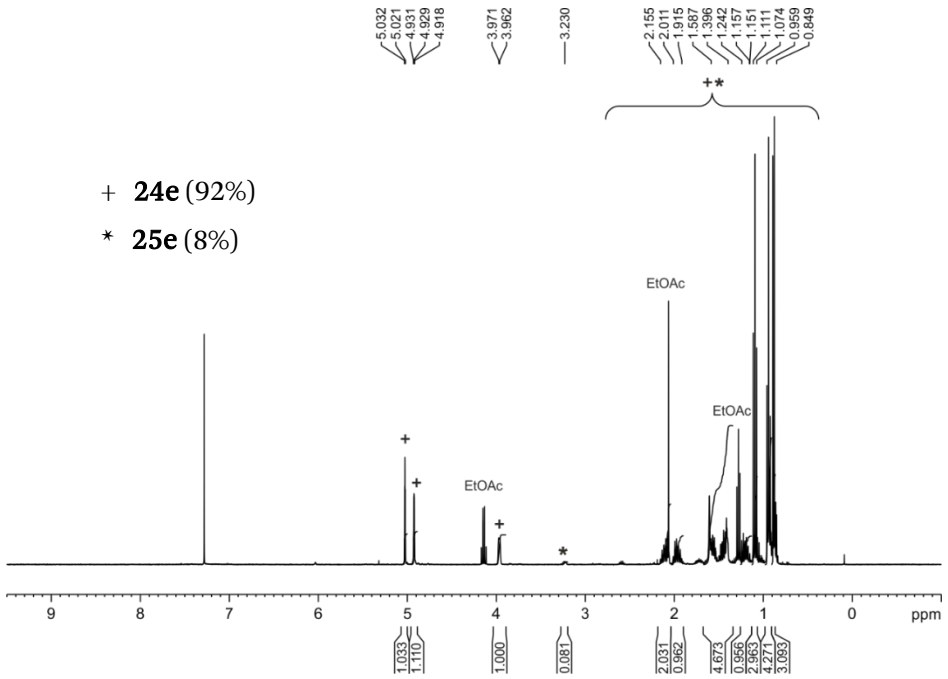

Figure 151. ^{1}H NMR (400 MHz, $CDCl_3$) of the crude mixture for the desymmetrization of **24e** (Table 22, entry 5).

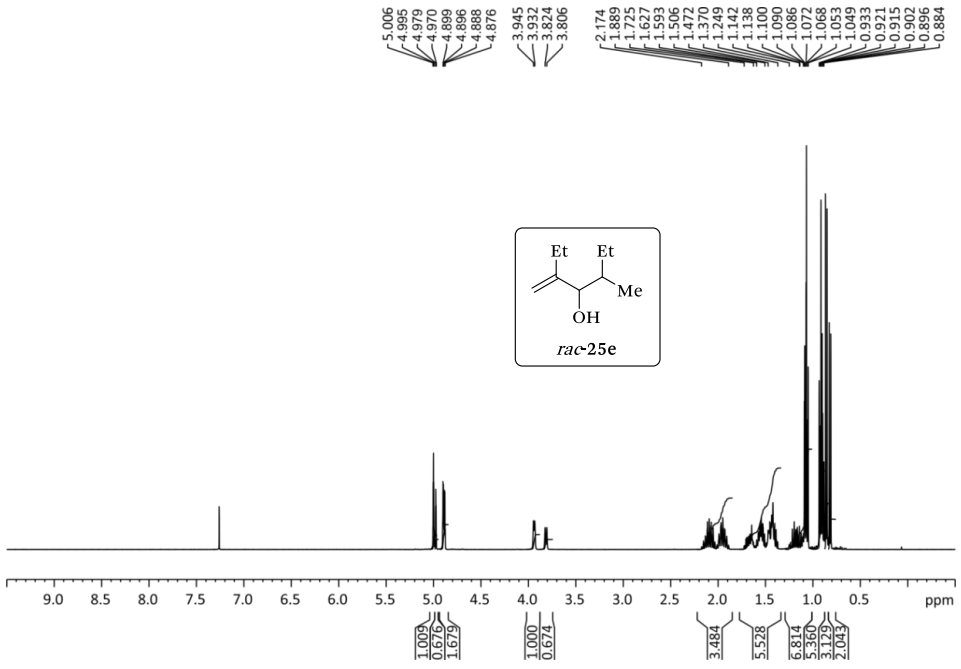

Figure 152. ^{1}H NMR (400 MHz, $CDCl_3$) of *rac*-**25e**.

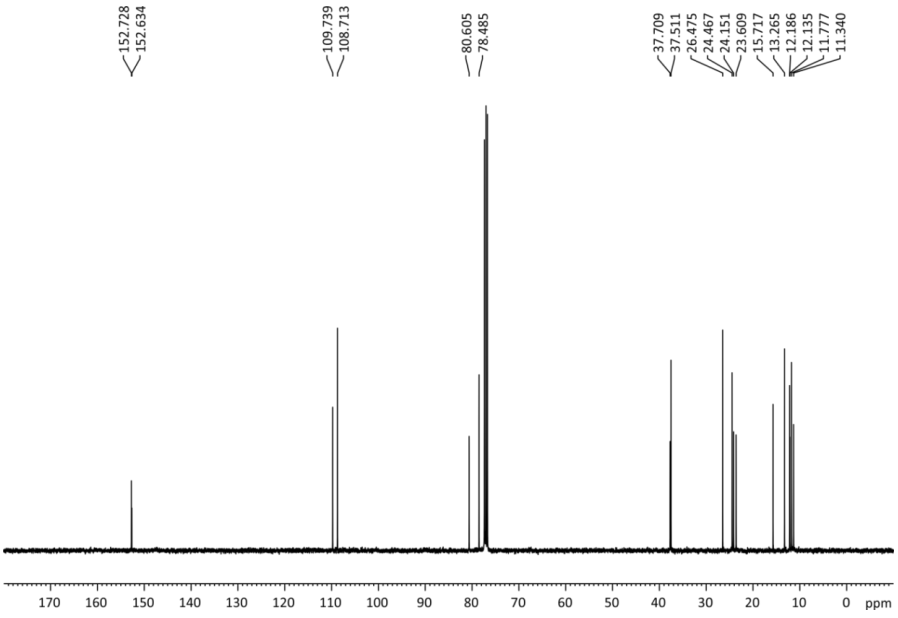

Figure 153. $^{13}C\{^{1}H\}$ NMR (100 MHz, $CDCl_3$) of *rac*-**25e**.

4.5.8.6. Catalytic hydrogenative desymmetrization of substrate 24f

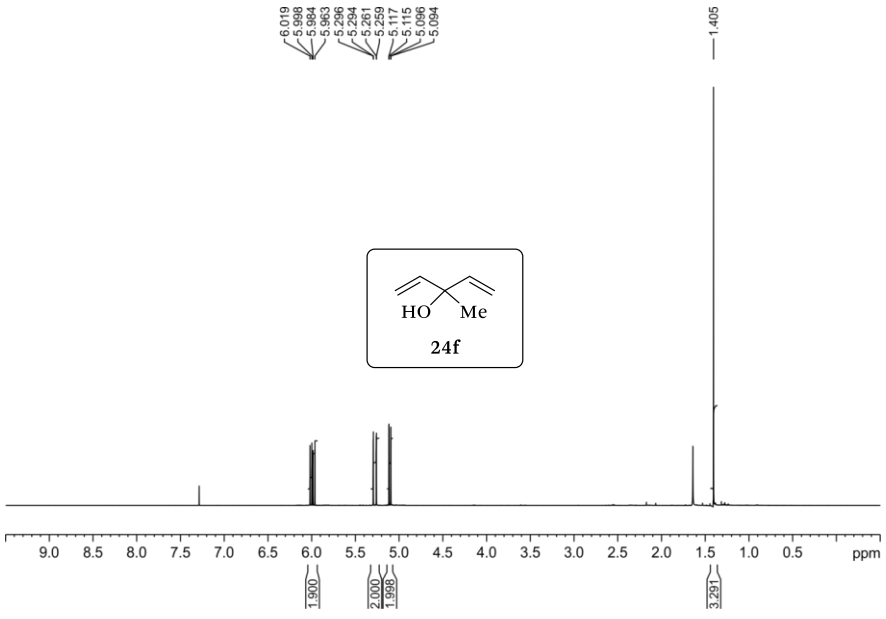

Figure 154. ^{1}H NMR (500 MHz, $CDCl_3$) of **24f**.

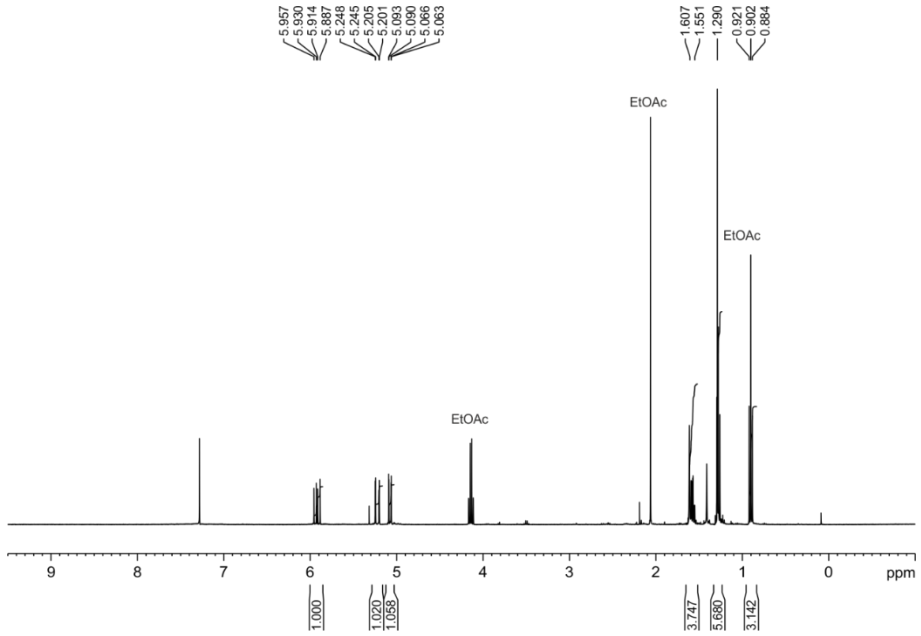

Figure 155. ^{1}H NMR (400 MHz, $CDCl_3$) of the crude mixture for the desymmetrization of **24f** (Table 22, entry 6).

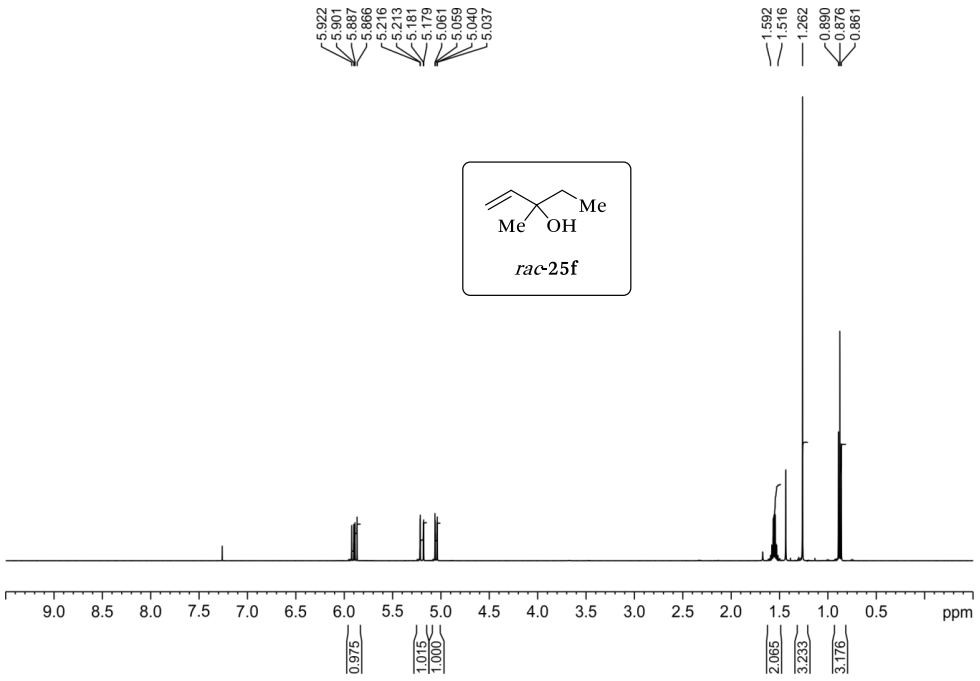

Figure 156. ^{1}H NMR (500 MHz, $CDCl_3$) of *rac*-**25f**.

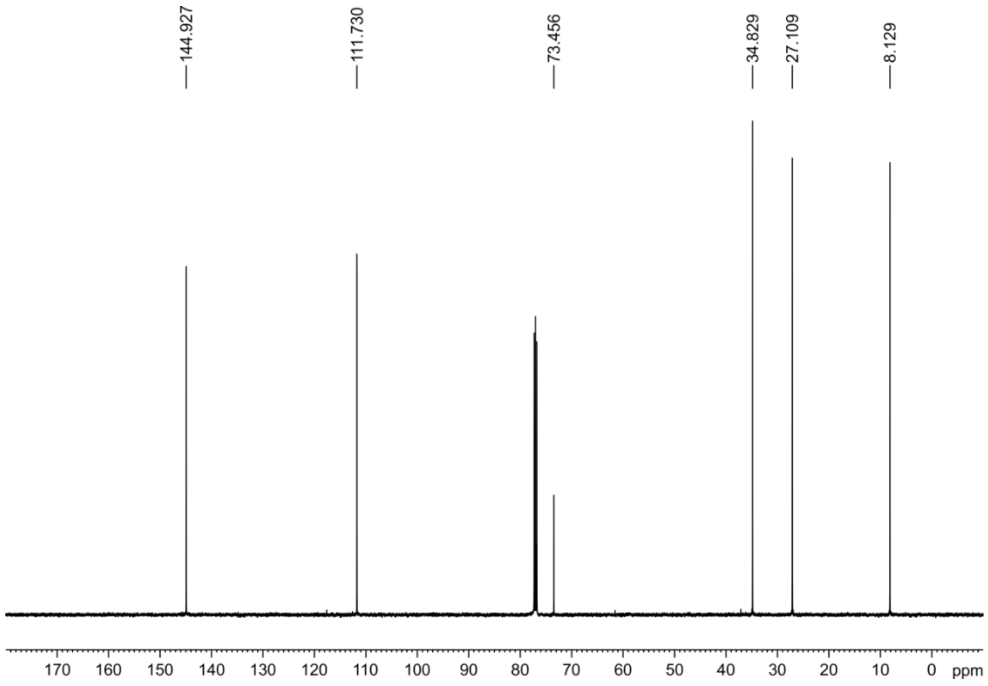

Figure 157. $^{13}C\{^{1}H\}$ NMR (125 MHz, $CDCl_3$) of *rac*-**25f**.

4.5.9. NMR spectra of benzoate ester derivatives 27 and derivative 28

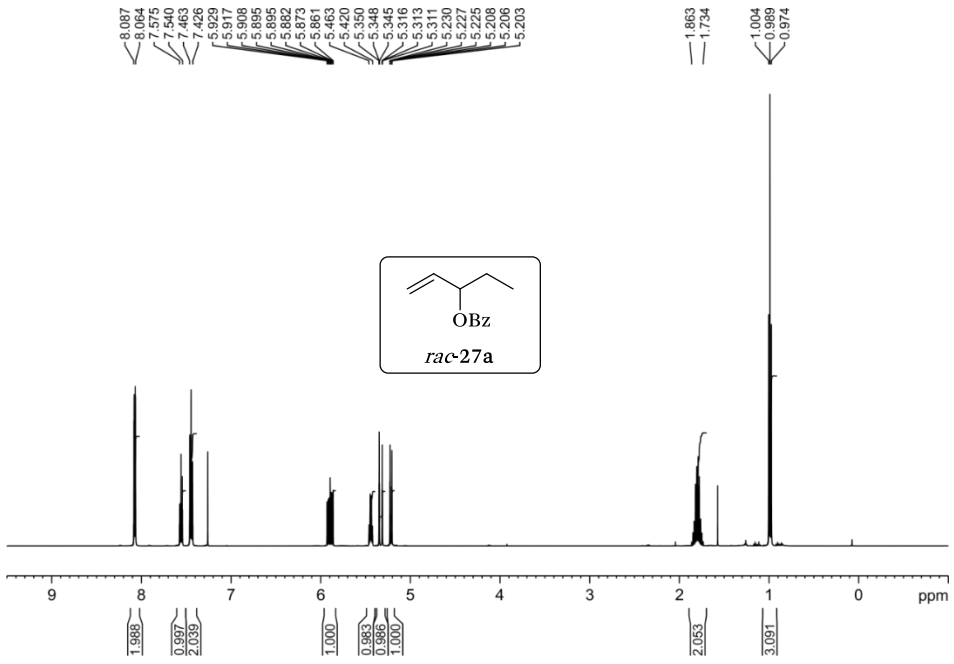

Figure 158. ^{1}H NMR (500 MHz, $CDCl_3$) of *rac*-**27a**.

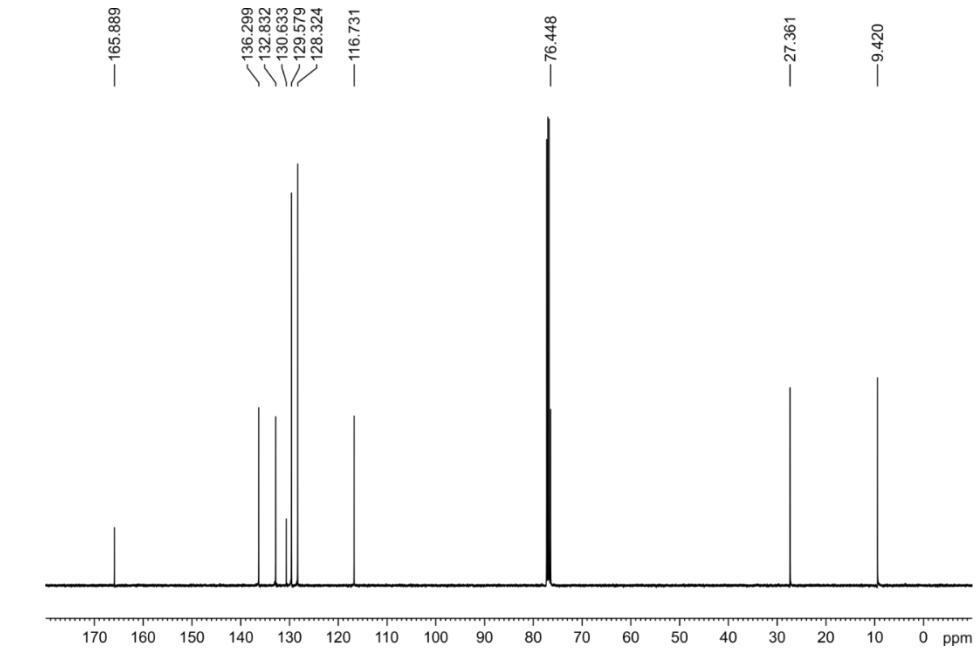

Figure 159. $^{13}C\{^{1}H\}$ NMR (125 MHz, $CDCl_3$) of *rac*-**27a**.

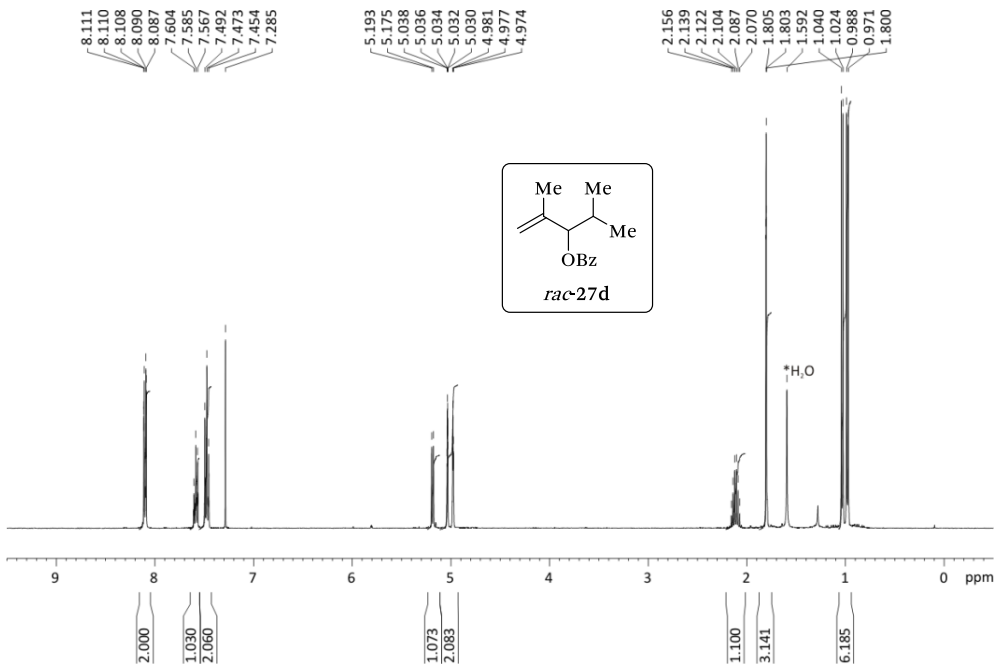

Figure 160. ^{1}H NMR (400 MHz, $CDCl_3$) of *rac*-**27d**.

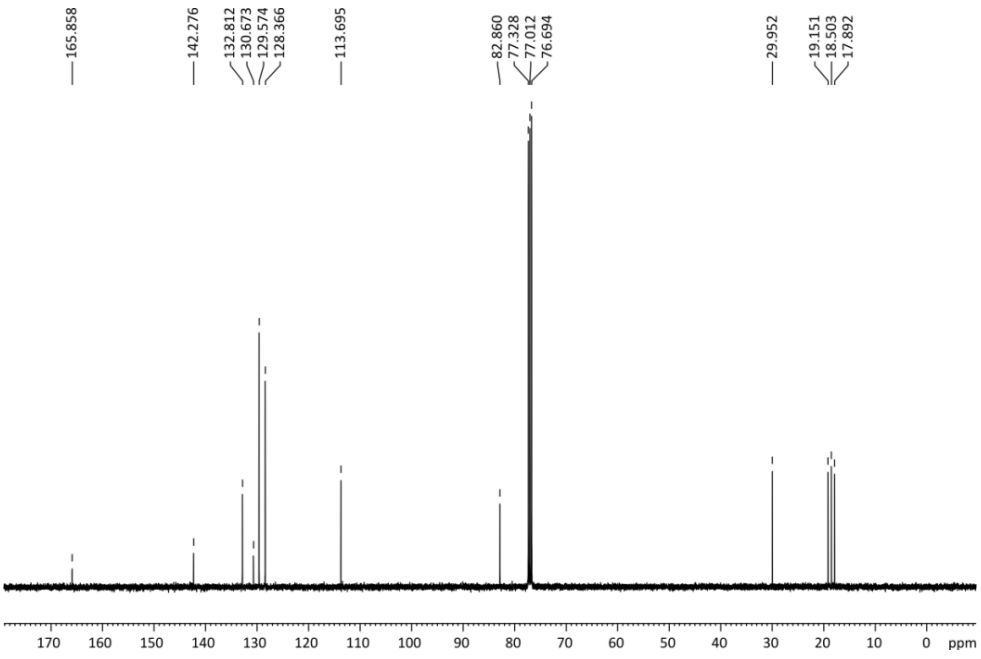

Figure 161. $^{13}C\{^{1}H\}$ NMR (100 MHz, $CDCl_3$) of *rac*-**27d**.

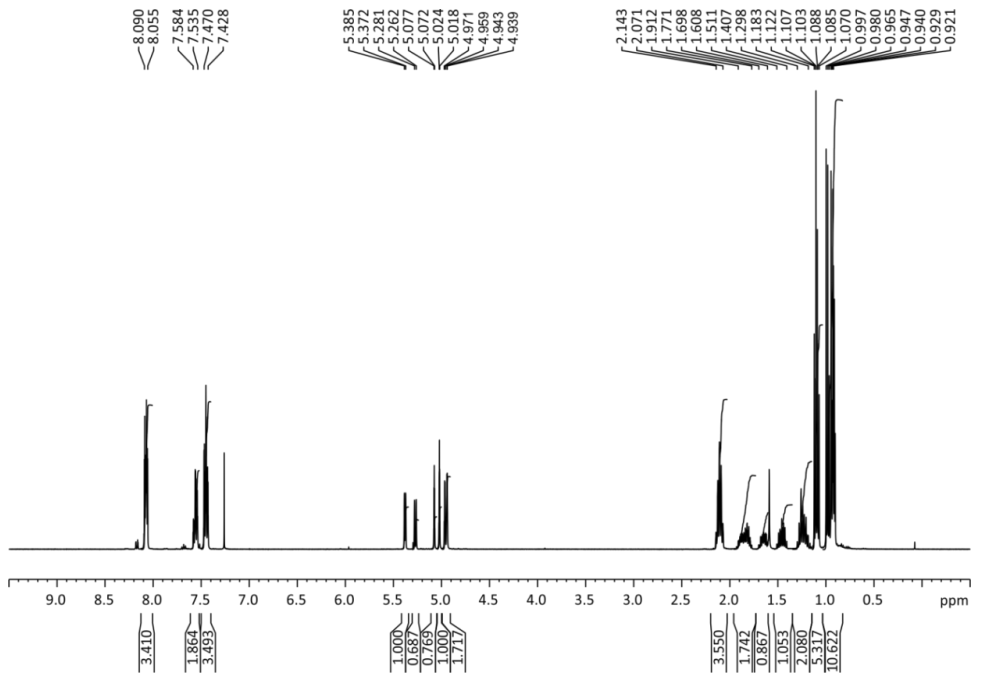

Figure 162. ^{1}H NMR (400 MHz, $CDCl_3$) of *rac*-**27e**.

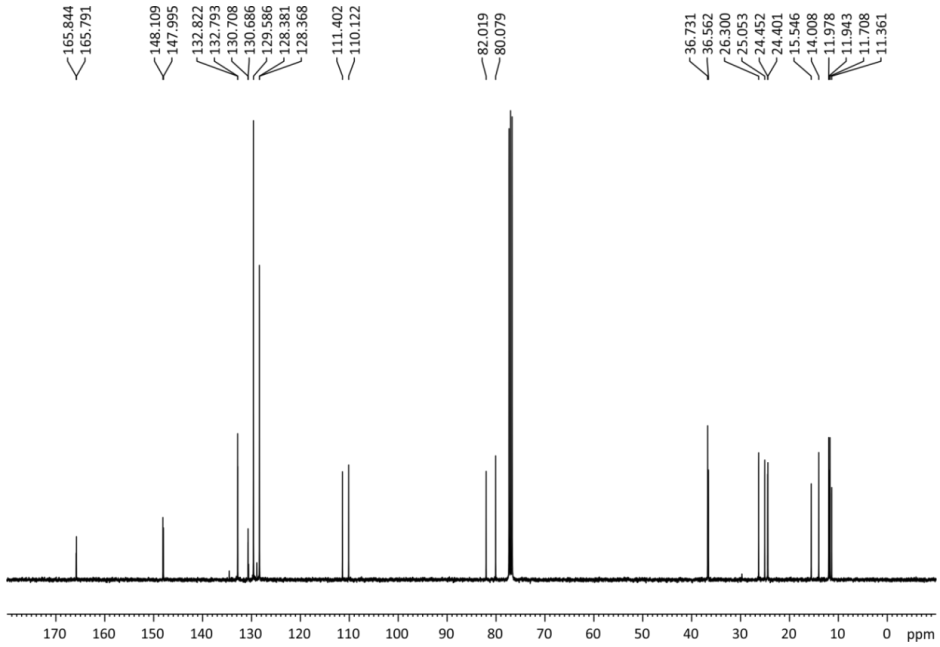

Figure 163. $^{13}C\{^{1}H\}$ NMR (100 MHz, $CDCl_3$) of *rac*-**27e**.

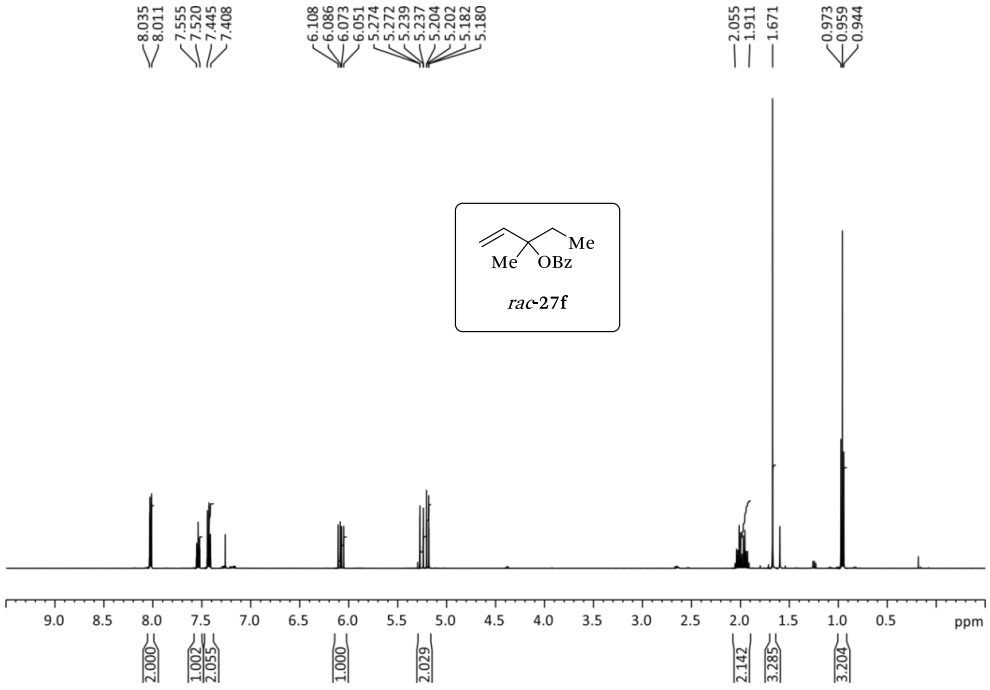

Figure 164. ^{1}H NMR (500 MHz, $CDCl_3$) of *rac*-**27f**.

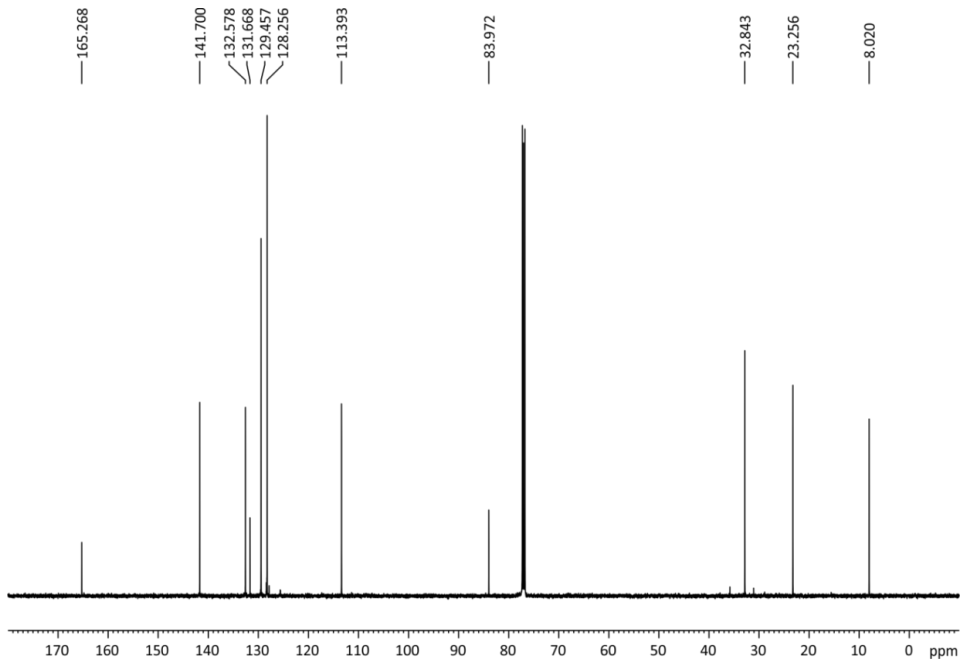

Figure 165. $^{13}C\{^{1}H\}$ NMR (125 MHz, $CDCl_3$) of *rac*-**27f**.

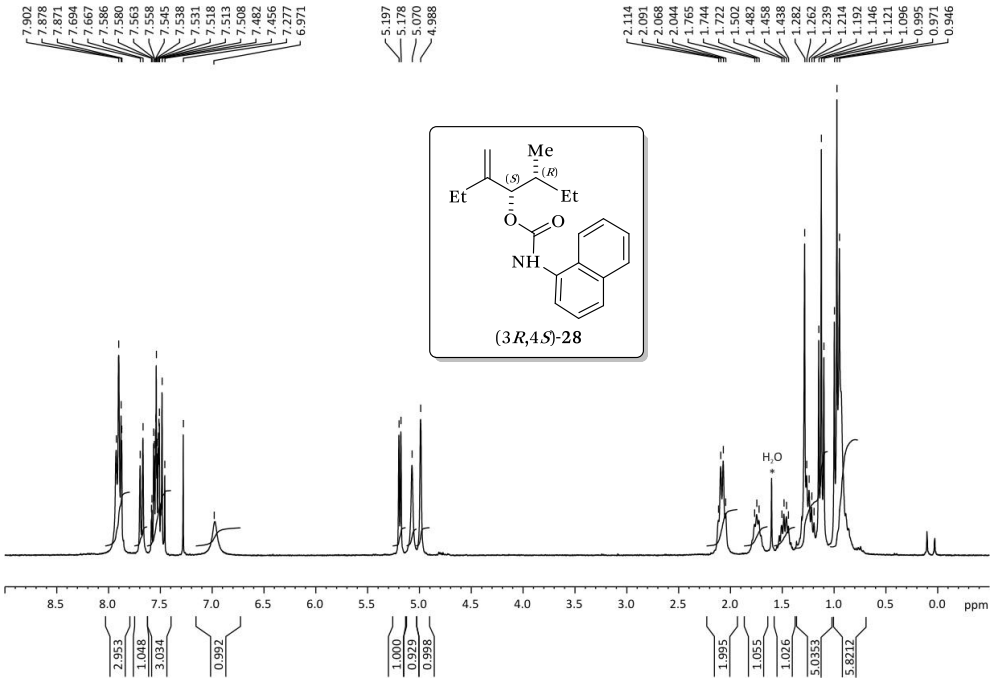

Figure 166. ^{1}H NMR (300 MHz, $CDCl_3$) of (3*R*,4*S*)-**28**.

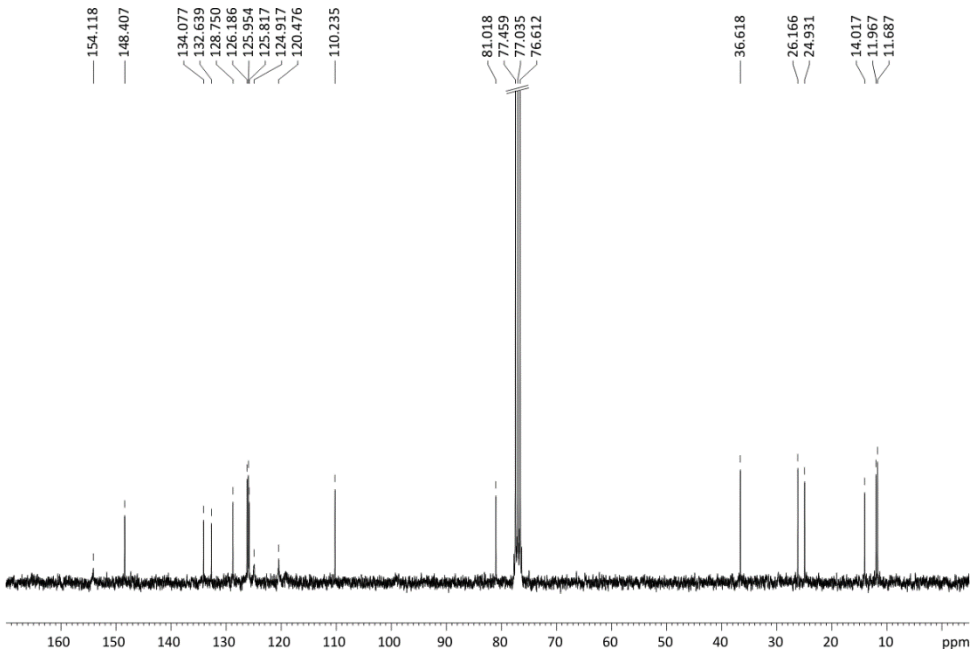

Figure 167. $^{13}C\{^{1}H\}$ NMR (75 MHz, $CDCl_3$) of (3*R*,4*S*)-**28**.

4.5.10. HPLC chromatograms of racemic compounds *rac*-27a and *rac*-27d–f

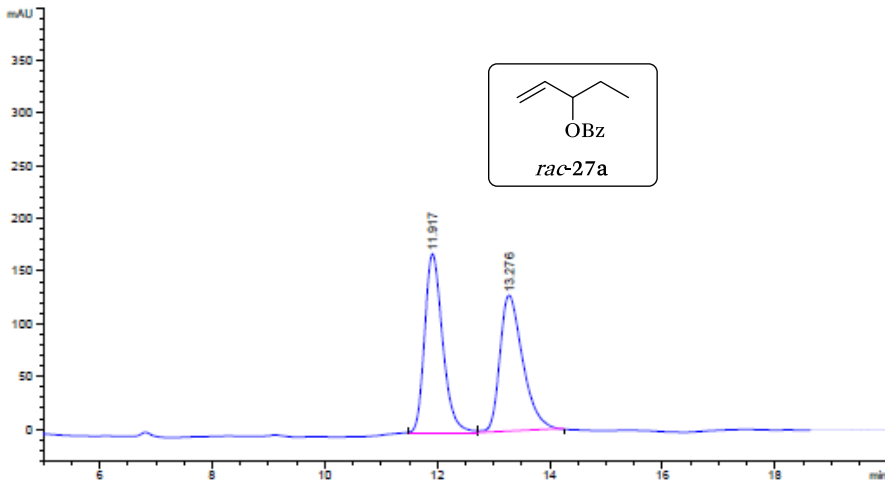

Peak #	RetTime [min]	Type	Width [min]	Area [mAU*s]	Height [mAU]	Area %
1	11.917	MM	0.3701	3768.15015	169.70535	50.8865
2	13.276	MM	0.4701	3636.85303	128.95157	49.1135

Figure 168. Chiral HPLC trace for *rac*-**27a**.

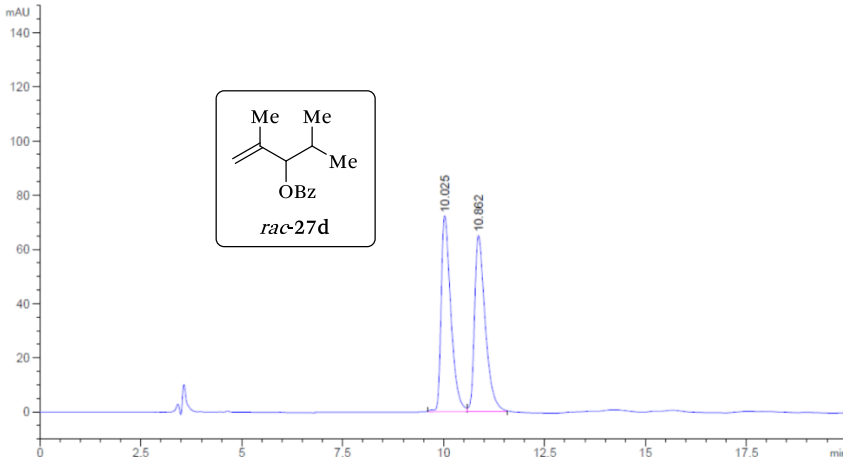

Peak #	RetTime [min]	Type	Width [min]	Area [mAU*s]	Height [mAU]	Area %
1	10.025	BV	0.2530	1208.76453	72.30396	50.1591
2	10.862	VB	0.2793	1201.09509	65.08539	49.8409

Figure 169. Chiral HPLC trace for *rac*-**27d**.

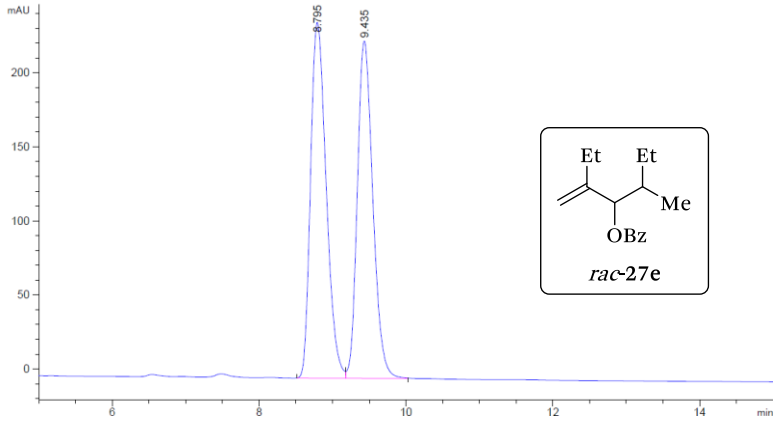

Peak #	RetTime [min]	Type	Width [min]	Area [mAU*s]	Height [mAU]	Area %
1	8.795	BV	0.2303	3548.33374	240.21742	51.4648
2	9.435	VB	0.2294	3346.34399	227.82498	48.5352

Figure 170. Chiral HPLC trace for *rac*-**27e**.[163]

(163) The corresponding enantiomers of the *syn*- and *anti*-diastereoisomers coelute under the chromatographic conditions.

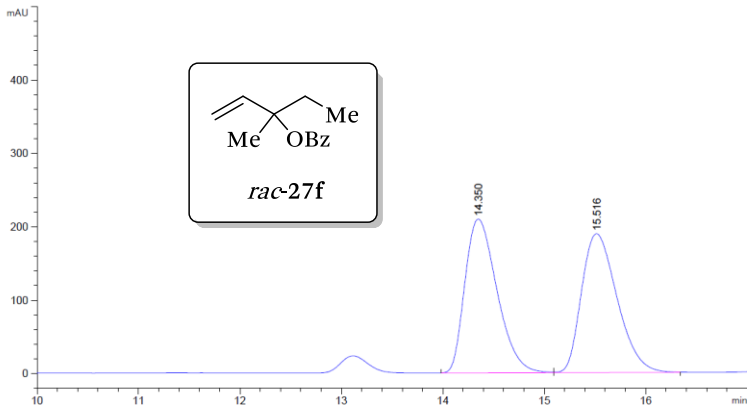

Peak #	RetTime [min]	Type	Width [min]	Area [mAU*s]	Height [mAU]	Area %
1	14.350	BV	0.3449	4617.93945	209.69554	50.0042
2	15.516	VB	0.3825	4617.15918	189.37022	49.9958

Figure 171. Chiral HPLC trace for *rac*-**27f**.

4.5.11. Selected HPLC data from catalytic experiments

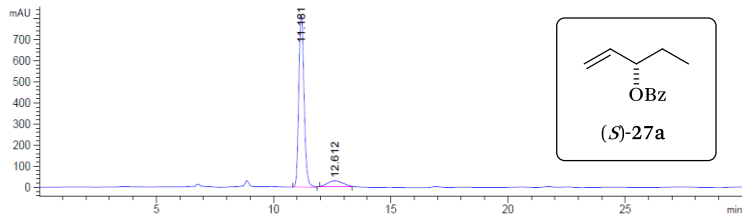

Peak #	RetTime [min]	Type	Width [min]	Area [mAU*s]	Height [mAU]	Area %
1	11.181	BB	0.2469	1.27657e4	814.22974	91.8225
2	12.612	MM	0.7285	1136.88062	26.01112	8.1775

Figure 172. Chiral HPLC trace for the desymmetrization of **24a**, product (*S*)-**27a** (Table 22, entry 1).

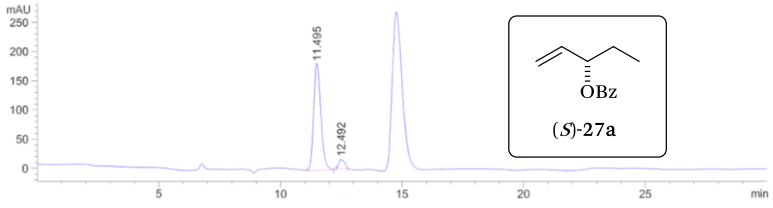

Peak #	RetTime [min]	Type	Width [min]	Area [mAU*s]	Height [mAU]	Area %
1	11.495	MM	0.3430	3766.34741	182.99191	93.7435
2	12.492	MM	0.2424	251.36679	17.28370	6.2565

Figure 173. Chiral HPLC trace for the desymmetrization of **24b**, product (*S*)-**27a** (Table 22, entry 2).

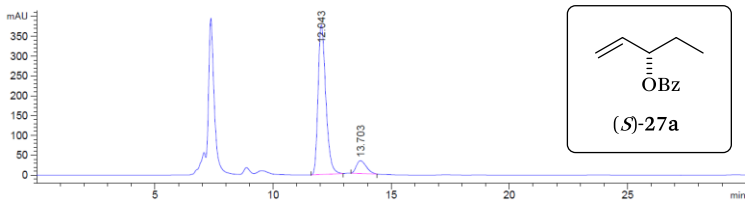

Peak #	RetTime [min]	Type	Width [min]	Area [mAU*s]	Height [mAU]	Area %
1	12.043	MM	0.3811	8625.76563	377.21033	90.1547
2	13.703	MM	0.4810	941.96759	32.63612	9.8453

Figure 174. Chiral HPLC trace for the desymmetrization of **24c**, product (*S*)-**27a** (Table 22, entry 3).

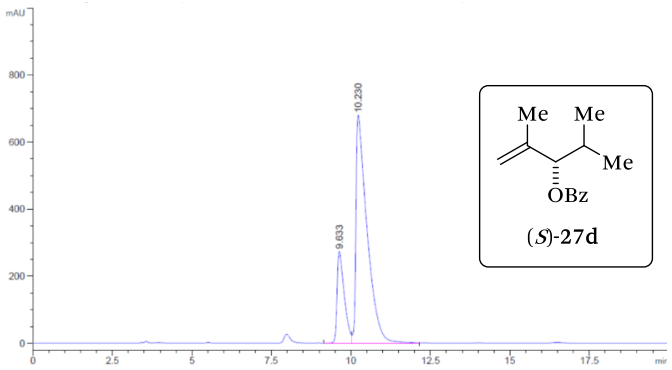

Peak #	RetTime [min]	Type	Width [min]	Area [mAU*s]	Height [mAU]	Area %
1	9.633	BV	0.2336	4302.76465	273.36188	20.7061
2	10.230	VV	0.3410	1.64774e4	679.16290	79.2939

Figure 175. Chiral HPLC trace for the desymmetrization of **24d**, product (*S*)-**27d** (Table 22, entry 4).

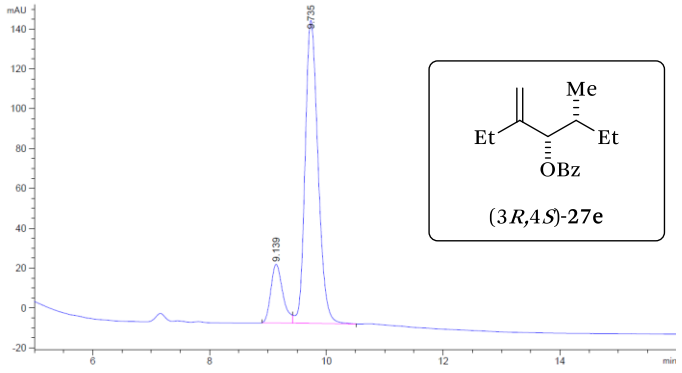

Peak #	RetTime [min]	Type	Width [min]	Area [mAU*s]	Height [mAU]	Area %
1	9.139	MF	0.2376	420.01080	29.46686	15.2261
2	9.735	FM	0.2562	2338.48926	152.15088	84.7739

Figure 176. Chiral HPLC trace for the desymmetrization of **24e**, product (3*R*,4*S*)-**27e** (Table 22, entry 5).

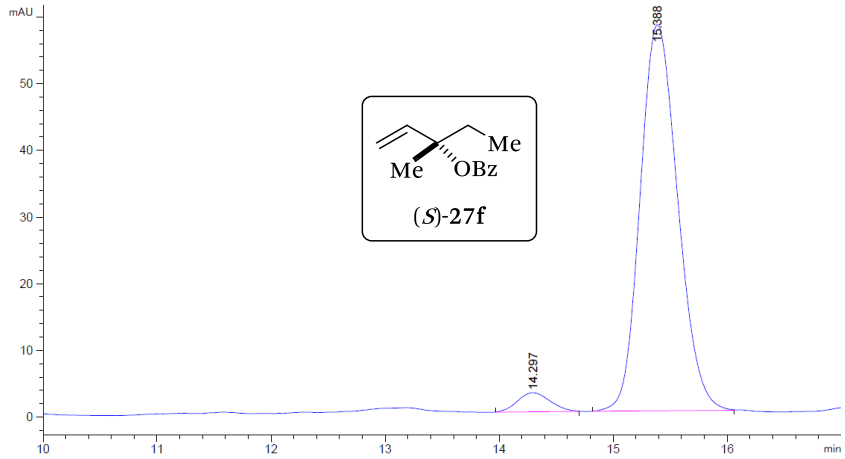

Peak #	RetTime [min]	Type	Width [min]	Area [mAU*s]	Height [mAU]	Area %
1	14.297	MM	0.3314	56.95283	2.86452	4.1137
2	15.388	MM	0.3821	1327.50537	57.90999	95.8863

Figure 177. Chiral HPLC trace for the desymmetrization of **24f**, product (*S*)-**27f** (Table 22, entry 6).

UNIVERSITAT ROVIRA I VIRGILI
RHODIUM CATALYSIS IN ENANTIOSELECTIVE HYDROGENATIVE TRANSFORMATIONS: FROM THE DESIGN OF NEW LIGANDS TO REACTIONS OF ATYPICAL SUBSTRATES
Joan Ramon Lao Mulinari

CONCLUSIONS

1. A new synthetic strategy for the preparation of a set of narrow bite angle phosphine-phosphite ligands has been developed. These ligands have proved to generate stereoselective efficient catalysts with typical Rh-precursors for asymmetric hydrogenations and hydroformylations (i.e., $[Rh(nbd)_2]BF_4$ and $[Rh(\kappa^2O,O'\text{-acac})(CO)_2]$, respectively). The resulting Rh-complexes provided high enantioselectivities (up to 99% ee) in the asymmetric hydrogenation of structurally diverse functionalized alkenes. Moreover, the Rh-complexes derived from those narrow bite angle ligands were very active (up to 99% conversion) and regioselective (branched/linear product ratios up to 97/3) in the asymmetric hydroformylation of terminal olefins providing moderate enantioselectivities (up to 64% ee).

2. An efficient catalytic methodology based on hydrogenative kinetic resolutions of racemic vinyl-substituted sulfoxides has been developed for the preparation of highly enantioenriched (or even enantiopure) sulfoxide-containing compounds. A sufficient differentiation in the reaction rate of the hydrogenation of the two enantiomers of the starting materials provided by cationic Rh-complex derived from a phosphine-phosphite ligand containing the enantiopure 3,3'-diphenyl-substituted H_8-BINOL phosphite-derived fragment allowed for high enantioselectivities in this hydrogenative transformation. After catalyst and reaction optimization, efficient conditions for the kinetic resolution of a set of aryl- and aralkyl-substituted sulfoxides were developed and allowed for the isolation of both recovered and hydrogenated products (54–80% of isolated yields referred to half the amount of starting material) in very high optical purities (up to 99% and up to 97% ee for the unreacted and hydrogenated enantiomers of the starting material, respectively) and with high selectivity factors (*s* values up to ca. 150).

3. Substrate diversity has been exploited for preparing synthetically valuable sulfoxides in highly enantioenriched (or even enantiopure) form. The scope of the hydrogenative kinetic resolution has been broadened to a set of structurally diverse α,β-unsaturated sulfoxides incorporating alkyl- and aryl- substituents at the alpha, *E*- and

Z-positions of the C=C double bond: This synthetic method has allowed for the selective preparation and isolation (up to 76% of isolated yield referred to half the amount of starting material) of highly enantioenriched (or even enantiopure) (un)saturated sulfoxides in a single synthetic step (up to 99% ee) and with high selectivity factors (*s* values up to ca. 90). Moreover, the synthetic applicability of this method has been demonstrated by preparing a number of valuable synthetic intermediates of biologically active sulfoxides in an enantioenriched form ((*R*)-sulforaphene, (*S*)-sulforaphane and a histone deacetylase inhibitor).

4. An efficient hydrogenative catalytic desymmetrization methodology of achiral 1,4-dienes mediated by Rh-complexes derived from phosphine-phosphite ligands has been developed. After ligand and reaction condition optimization studies, the highest performing ligand for this transformation (in terms of chemo- and stereo-selectivity of the reaction), which contains an enantiopure TADDOL-derived phosphite fragment (TADDOL: (2,2-dimethyl-1,3-dioxolane-4,5-diyl)bis-(diphenyl-methanol)), exhibited excellent catalytic properties in the desymmetrization of a set of structurally diverse achiral 1,4-dienes. This synthetic methodology gave access to highly enantioenriched secondary and tertiary alcohols (up to 92% ee).

SUMMARY OF THE THESIS

The present doctoral thesis encompasses the design and synthesis of new enantiopure phosphine-phosphite (P–OP) ligands and the further application of the new and previously discovered P–OP ligands in the development of efficient catalytic systems for different enantioselective transformations that could be used for the preparation of synthetically relevant molecules with pharmaceutical, biological or agrochemical interest.

In this context, we first directed our efforts to the preparation of new narrow bite angle phosphine-phosphite ligands incorporating a stereogenic phosphino group (the *S*$_P$-*tert*-butyl(methyl)phosphino motif) and a spacer between the phosphino and phosphite groups containing only one carbon atom. We envisaged that such ligands would provide an asymmetric and rigid environment around the metal center (Figure 178).

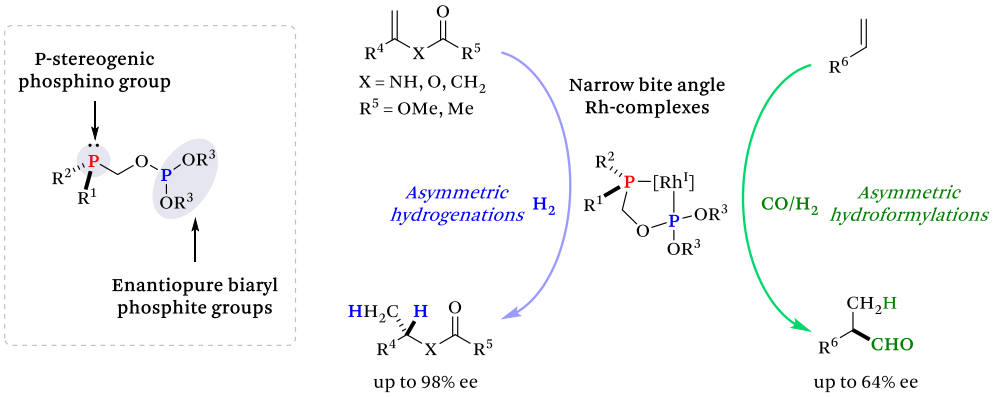

Figure 178. General structures of narrow bite angle ligands containing P-stereogenic phosphino groups and the corresponding Rh^I-complexes for asymmetric hydrogenations and hydroformylations.

The synthetic strategy for preparing these ligands consisted of the base-mediated *O*-phosphorylation of an enantiomerically pure phosphino alcohol borane complex with enantiopure chlorophosphites derived from BINOL (i.e., 1,1'-bi-2-naphthol) or 3,3'-diphenyl-substituted H_8-BINOL (i.e., octahydro-1,1'-binaphtalene-2,2'-diol) followed by cleavage of the borane protecting groups (overall isolated yields ranging from 28 to 44%). Furthermore, the ability of these ligands to form stable metal-complexes with the typical Rh-precursors for asymmetric hydrogenations and hydroformylations was as well studied. In this context, cationic rhodium(I) complexes with the formula

[Rh(nbd)(P–OP)]BF_4 could be efficiently prepared and isolated by reacting stoichiometric amounts of the ligand and [$Rh(nbd)_2$]BF_4.

Regarding the coordination with typical rhodium(I) precursors for asymmetric hydroformylations (i.e., [Rh(κ^2O,O'–acac)$(CO)_2$]), the formation of the expected metal complexes with formula [Rh(κ^2O,O'–acac)(P–OP)] was confirmed by standard spectroscopic techniques. The catalytic performance of the rhodium complexes in asymmetric hydrogenations was evaluated in a set of structurally diverse functionalized alkenes: high catalytic activities (up to >99% conversion) and enantioselectivities (up to 98% ee) were achieved. The ligand that provided the best results in terms of enantioselectivity in asymmetric hydrogenations was the one that incorporated an (*S*)-configured phosphino group and the sterically hindered 3,3'-diphenyl substituted (*R*)-H_8-BINOL phosphite fragment. The new narrow bite angle P–OP ligands were also screened in the asymmetric hydroformylation of a set of structurally diverse terminal alkenes. In this particular reaction, moderate to high values of activity and regioselectivity were generally obtained (up to 99% conversion and branched to linear product ratios up to 97/3) though the enantioselectivities of the resulting branched aldehydes were only moderate (up to 64% ee).

Coinciding with the main aim of developing efficient catalytic systems for hydrogenative asymmetric transformations and considering the excellent catalytic properties achieved by the Rh-complexes derived from phosphine-phosphite ligands developed by the group in asymmetric hydrogenations of standard functionalized alkenes, we then directed our investigations toward the development of new asymmetric hydrogenative transformations with the objective of preparing synthetically relevant products.

In this context, optically pure sulfoxides represent a valuable class of optically active compounds that have broad applicability in several areas such as in asymmetric synthesis (as chiral auxiliaries or ligands) and in biologically related sciences (as natural or synthetic bioactive compounds). Among the approaches that asymmetric catalysis offers, kinetic resolution of racemic sulfoxides can be considered an appealing method for the preparation of two optically active sulfoxides in only one synthetic step. For that purpose, we focused our studies in developing a catalytic methodology for hydrogenatively resolving racemic α,β-unsaturated sulfoxides by asymmetric hydrogenations using Rh-complexes derived from P–OP ligands (Figure 179). After ligand and reaction condition optimization, we found that the P–OP ligand that

incorporated the 3,3'-diphenyl-substituted (*S*)-H_8-BINOL fragment was the optimal ligand for this transformation (ligand **L3** in Figure 179).

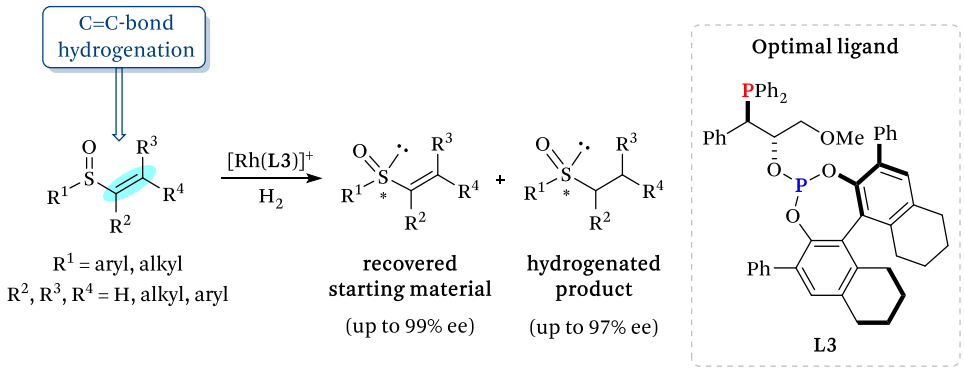

Figure 179. Hydrogenative kinetic resolution of α,β-unsaturated sulfoxides by Rh-mediated asymmetric hydrogenations.

With the optimal catalyst in hand, we optimized specific reaction conditions for obtaining the recovered starting material and hydrogenated product with the highest possible yield and enantioselectivity. In general, regardless of the nature of the substrate, both recovered and hydrogenated products were isolated in notable yields (up to 80% isolated yields for recovered and resolved products referred to half the amount of starting material), with high enantioselectivities (up to 99% and 97% of ee for recovered and resolved products, respectively) and with remarkably high selectivity factors (*s* values up to 148). Moreover, coordination studies between the Rh-precatalyst and both racemic and enantiopure vinyl sulfoxides were performed in solution. The NMR data obtained from those studies gave us some insight about the favored stereodifferentiating routes of the catalytic reaction and we could tentatively propose a plausible reaction pathway for the hydrogenative kinetic resolution of vinyl sulfoxides using Rh-(P–OP)$^+$ complexes. Further studies on this catalytic methodology were performed in order to study the effects of precisely positioning alkyl or aryl substituents at the α-, *E*- and *Z*-positions of the double bond in the (stereo)chemical outcome of the reactions. As the selective synthesis of some of racemic α,β-unsaturated sulfoxides constituted a challenge, we also developed interesting synthetic protocols for the preparation of α,β-unsaturated sulfoxides that can be useful for the synthetic community (i.e. (*Z*)-selective hydrogenations of allenyl sulfoxide derivatives). After some experimentation, efficient and selective catalytic conditions were identified. The presence of substituents at the vinyl moiety was well tolerated, and moderate to excellent enantioselectivities were observed for both

recovered and resolved products (up to 99% and 93% of ee for recovered and resolved products, respectively) with high selectivity factors (*s* up to 91). Moreover, the practicality of this kinetic resolution methodology was further demonstrated by preparing a number of advanced synthetic intermediates of biologically active molecules containing sulfoxide groups ((*R*)-sulforaphene, (*S*)-sulforaphane and a histone deacetylase inhibitor), which could be efficiently obtained and isolated with moderate to high values of enantioselectivity (50–94% of ee).

Following our efforts in developing highly efficient catalytic systems derived from phosphine-phosphite ligands, we became interested in developing enantioselective catalysts for the hydrogenative desymmetrization of achiral 1,4-dienes, as the resulting products can be considered versatile building blocks for the construction of more complex molecules (Figure 180).

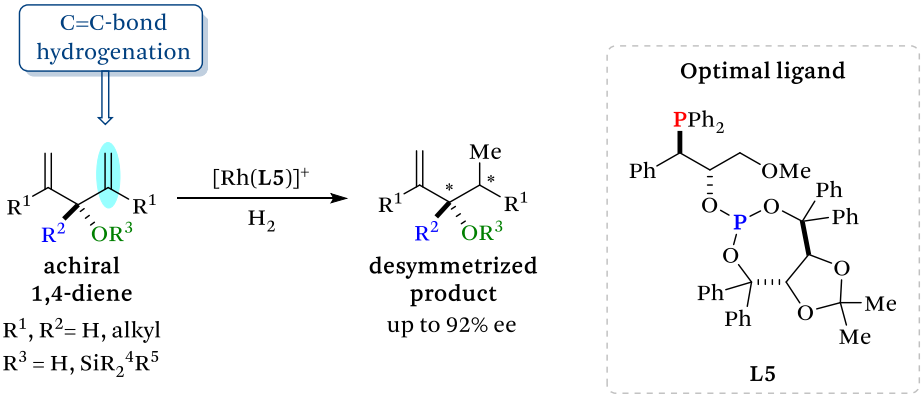

Figure 180. Hydrogenative desymmetrization of achiral 1,4-dienes and the optimal P–OP ligand for this transformation.

After reaction condition optimization and further ligand screening, we observed that the use of a ligand incorporating the (*S*,*S*)-TADDOL (i.e. ((2,2-dimethyl-1,3-dioxolane-4,5-diyl)bis-(diphenylmethanol)) moiety provided the best results in terms of activity, chemo- and enantio-selectivity, so that was selected as the optimal ligand for this transformation (see **L5** in Figure 180). With the optimal catalyst in hand, the scope of the reaction was expanded to a set of structurally diverse 1,4-dienes. The presence of substituents at the 2 and 4 positions, or even the presence of disubstitution at the 3 position of the 1,4-diene, did not produce detrimental effects in the outcome of the catalytic reaction, and the reaction products could be selectively obtained (selectivity >92%) with high values of enantioselectivity (up to 92% ee).

UNIVERSITAT ROVIRA I VIRGILI
RHODIUM CATALYSIS IN ENANTIOSELECTIVE HYDROGENATIVE TRANSFORMATIONS: FROM THE DESIGN OF NEW LIGANDS TO REACTIONS OF ATYPICAL SUBSTRATES
Joan Ramon Lao Mulinari

UNIVERSITAT ROVIRA I VIRGILI
RHODIUM CATALYSIS IN ENANTIOSELECTIVE HYDROGENATIVE TRANSFORMATIONS: FROM THE DESIGN OF NEW LIGANDS TO REACTIONS OF ATYPICAL SUBSTRATES
Joan Ramon Lao Mulinari

UNIVERSITAT ROVIRA I VIRGILI
RHODIUM CATALYSIS IN ENANTIOSELECTIVE HYDROGENATIVE TRANSFORMATIONS: FROM THE DESIGN OF NEW LIGANDS TO REACTIONS OF ATYPICAL SUBSTRATES
Joan Ramon Lao Mulinari

UNIVERSITAT ROVIRA I VIRGILI
RHODIUM CATALYSIS IN ENANTIOSELECTIVE HYDROGENATIVE TRANSFORMATIONS: FROM THE DESIGN OF NEW LIGANDS TO REACTIONS OF ATYPICAL SUBSTRATES
Joan Ramon Lao Mulinari

UNIVERSITAT
ROVIRA i VIRGILI